Genome engineering of the magnetosome island in *Magnetospirillum gryphiswaldense*

Dissertation zur Erlangung des Doktorgrades
der Fakultät für Biologie
der Ludwig-Maximilians-Universität München

vorgelegt von

Anna Lohße
aus Schlema, Deutschland

2014

Erklärung

Diese Dissertation wurde im Sinne von § 12 der Promotionsordnung vom 27. November 1991, in der Fassung der 3. Änderungssatzung vom 05. Oktober 2011, von Herrn Professor Dr. Dirk Schüler betreut.

Eidesstattliche Versicherung

Ich versichere hiermit an Eides statt, dass die vorgelegte Dissertation von mir selbständig und ohne unerlaubte Hilfe angefertigt ist. Des Weiteren erkläre ich, dass ich nicht anderweitig ohne Erfolg versucht habe, eine Dissertation einzureichen oder mich einer Doktorprüfung zu unterziehen. Die vorliegende Dissertation liegt weder ganz, noch in wesentlichen Teilen einer anderen Prüfungskommission vor.

München, ...

.....
Anna Lohße

Dissertation eingereicht am .....

1. Gutachterin/ 1. Gutachter: Professor Dr. Dirk Schüler

2. Gutachterin/ 2. Gutachter: Professor Dr. Heinrich Jung

Mündliche Prüfung am 02.09.2014

Publications

Parts of this work contributed to following publications or are in the process of being published:

Lohße A, Ullrich S, Katzmann E, Borg S, Wanner G, Richter M, Voigt B, Schweder T, Schüler D. Functional Analysis of the Magnetosome Island in *Magnetospirillum gryphiswaldense*: The *mamAB* Operon is Sufficient for Magnetite Biomineralization. PLoS One. 2011; 6(10):e25561.

A.L., S.U. and D.S. conceived and designed the study. A.L. and S.U. established protocols and planned experiments. A.L., S.U., E.K., S.B., G.W., M.R., B.V. and T.S. performed experiments. E.K. and S.B. made TEM pictures. A.L., S.U., E.K., S.B., M.R., B.V., T.S. and D.S. analyzed the data. M.R., G.W., T.S. and D.S. provided reagents/materials/analysis tools. A.L. and D.S. wrote the manuscript with input from all authors. D.S. supervised the work.

Kolinko I, **Lohße A**, Borg S, Raschdorf O, Jogler C, Tu Q, Pósfai M, Tompa É, Plitzko JM, Brachmann A, Wanner G, Müller R, Zhang Y, Schüler D. Biosynthesis of magnetic nanostructures in a foreign organism by transfer of bacterial magnetosome gene clusters. Nature Nanotechnology. 2014 Mar; 9(3):193-7.

I.K., D.S., Y.Z., Q.T., C.J. and R.M. planned and performed cloning experiments. I.K. and A.L. performed genetic transfers and cultivation experiments. G.W. prepared cryo- and chemically fixed cells. S.B., O.R. and G.W. performed TEM and I.K. analyzed the data. J.P. and O.R. performed cryo-electron tomography experiments. E.T. and M.P. took highresolution TEM micrographs and analyzed the data. I.K. and A.L. took fluorescence micrographs and performed phenotypization experiments. I.K. performed western blot experiments and analyzed proteomic data. A.B. performed Illumina genome sequencing and I.K. analyzed the data. I.K. and D.S. designed the study and wrote the paper. All authors discussed the results and commented on the manuscript.

Lohße A, Borg S, Raschdorf O, Kolinko I, Tompa É, Pósfai M, Faivre D, Baumgartner J, Schüler D. Genetic dissection of the *mamAB* and *mms6* operons reveals a gene set essential for magnetosome biogenesis in *Magnetospirillum gryphiswaldense*. Journal of Bacteriology. *Published ahead of print 9 May 2014*.

A.L. and D.S. conceived and designed the study. A.L. established protocols and planned experiments. A.L., O.R., I.K., E.T., M.P., D.F. and J.B. performed experiments. S.B. performed TEM analyses. O.R. performed deletion analysis of Δ*mamL*. I.K. complemented Δ*mamA*. E.T. and M.P. performed HRTEM. D.F. and J.B. performed XANES experiments. A.L. and D.S. wrote the manuscript with input from all authors. D.S. supervised the work.

Lohße A*, Kolinko I*, Borg S, Uebe R, Raschdorf O, Brachmann A, Schüler D. Genome engineering of *Magnetospirillum gryphiswaldense* improves magnetosome yield by overexpression of magnetosome operons. *In preparation*. [* These authors contribute equally to this work.]

A.L., I.K. and D.S. conceived and designed the study. A.L. and I.K. established protocols and planned experiments. I.K. designed ΔRecA+*mamAB* 1x, ΔRecA+*mamAB* 2x, ΔRecA+*ABG6X* and ΔRecA+-*ABG6X*+*feo* and A.L. constructed ΔRecA+*mms6* 1x, 2x, 3, 4x, ΔRecA+*GFDC* and ΔRecA+*GFDC/mms6*. A.L and I.K. performed phenotypic characterization experiments. A.L. measured particle number and size of all mutants except of ΔRecA+*ABG6X*+*feo*. A.L. performed ferrozine assay for all mutants except of ΔRecA+*mms6* 4x, ΔRecA+*ABG6X*, and ΔRecA+*ABG6X*+*feo*. A.L. meassured cell length of all mutants except of ΔRecA+*ABG6X* and ΔRecA+*ABG6X*+*feo*. I.K. performed SDS analysis and quantitative Western Blot of ΔRecA+*mamAB*. S.B. performed TEM analyses. R.U. performed mass cultivation. O.R. performed CET. A.B. performed Illumina sequencing. A.L. and I.K. performed data analysis. A.L., I.K. and D.S. wrote the manuscript. D.S. supervised the work.

München, ...

.....	.....	.....
Anna Lohße	Isabel Kolinko	Prof. Dirk Schüler

Table of Contents

List of Figures

List of Tables

List of Abbreviations

aa ..... amino acid
ABC ..... ATP-binding cassette
BAR ..... Protein domain also found in the proteins Bin-Amphiphysin-Rvs
bp ..... base pair
CDF ..... cation-diffusion facilitator
CET ..... cryo-electron tomography
CL ..... cell lysate
CM ..... cytoplasmic membrane
Cre ..... causes recombination
E. coli ..... *Escherichia coli*
EFC ..... extended Fes and CIP4 homology
fla ..... flagellin
Fos ..... fosmid
FSM ..... flask standard medium
FtsZ ..... filamenting temperature-sensitive mutant Z
FUR ..... ferric uptake regulator
GalK ..... galaktokinase
GFP ..... green fluorescent protein
Gm ..... gentamicin
HRTEM ..... high-resolution transmission electron microscopy
HtrA ..... high temperature requirement
Kan ..... kanamycin
kb ..... kilobase pair
LC-MS ..... liquid chromatography-mass spectrometry
LG ..... lysin glycine
lox ..... locus of X-over
loxP ..... locus of X-over P1
MAI ..... magnetosome island
MALDI-TOF ..... matrix-assisted laser desorption ionization time-of-flight
mam ..... magnetosome membrane
MM ..... magnetosome membrane
mme ..... magnetosome membrane
mms ..... magnetic particle membrane-specific
MP ..... membrane protein

mRNA ..... messenger ribonucleic acid

MSR ..... *Magnetospirillum gryphiswaldense*

MTB ..... magnetotactic bacteria

mtx ..... magnetotaxis

Nap ..... nitrate reductase, periplasmic

NF ..... non-magnetic fraction

Nir ..... nitrite reductase

OATZ ..... oxic-anoxic transition zone

OM ..... outer membrane

OP3 ..... obsidian pool 3

ORF ..... open reading frame

oriT ..... origin of transfer

P ..... promoter

PDZ ..... protein domain also found in the proteins PSD95, DlgA and Zo-1

RecA ..... recombination protein A

rRNA ..... ribosomal ribonucleic acid

SDS-PAGE ..... sodium dodecyl sulphate - polyacrylamide gel electrophoresis

TEM ..... transmission electron microscopy

Tet ..... tetracycline

Tn ..... transposase

TPR ..... tetra tricopeptid repeat

Tps ..... transposon

TRIS ..... Tris(hydroxymethyl)aminomethane

tRNA ..... transfer ribonucleic acid

WT ..... wildtype

X-Gluc 5-bromo-4-chloro-3-indoxyl-D-glucuronidase

XANES ..... X-ray absorption near edge structure

Xis ..... excisionases

Summary

The ability of *Magnetospirillum gryphiswaldense* to orient along the earth's magnetic field lines is based on specific organelles, the magnetosomes, which are membrane-enveloped, nanometer-sized crystals of magnetite (Fe_3O_4). The biosynthesis of functional magnetosomes depends on several steps including the (i) invagination of magnetosome vesicles, (ii) protein sorting, (iii) iron transport and crystallization of magnetite minerals, (iv) crystal maturation, and (v) assembly into linear chains. Each step is under strict genetic control, and genes encoding the magnetosome proteins were identified within the *mms6*, *mamGFDC*, *mamAB*, and *mamXY* operons that are located within a conserved genomic region referred to as magnetosome island (MAI). The MAI further contains a number of genes with unknown functions and numerous transposase genes that account for more than 20% of the coding region. It has mostly remained unknown, which genes within the MAI are important for magnetosome biomineralization and resemble the minimal essential gene set for biosynthesis. In this thesis the MAI of *M. gryphiswaldense* has been analyzed by mutagenesis to reveal the function and relevance for magnetosome biosynthesis of encoded proteins. An improved Cre-*lox*-based technique was used for introducing several large deletions covering the entire MAI. While genes flanking the identified magnetosome operons have no functional relevance for biosynthesis, less than 25% of the region comprising the *mms6*, *mamGFDC*, *mamAB*, and *mamXY* operons could be associated with magnetite biomineralization. Whereas only deletion of the *mamAB* operon resulted in the complete loss of magnetic particles, deletion of the *mms6*, *mamGFDC*, and *mamXY* operons led to severe defects in biomineralization. However, strains in which these operons were eliminated together retained the ability to synthesize small, irregular crystallites, demonstrating that the *mamAB* operon is the only region of the MAI, which is necessary and sufficient for magnetosome biosynthesis in *M. gryphiswaldense*. The genetic dissection of the *mamAB* operon revealed that while deletions of *mamI*, *N*, *A*, *R*, *S*, *T*, and *mamU*, which have functions in magnetite crystal nucleation and crystal maturation, did not abolish magnetosome formation, elimination of *mamE*, *L*, *M*, *O*, *Q*, and *mamB* fully inhibited magnetosome compartment and/or crystal formation and thus are essential for magnetosome biosynthesis. Single gene deletion of the *mms6* operon revealed two further important regulators for magnetosome biomineralization, namely Mms36 and Mms48. Finally, overexpression of the magnetosome operons alone or in various combinations was used to enhance particle synthesis in *M. gryphiswaldense*. While overexpression of the *mamGFDC* and the *mamAB* operon alone did not resulted in adequate improvements in magnetosome biomineralization, the overexpression of the *mms6* operon significantly increased both the crystal size and the amount of crystals per cell. The altogether insertions of the *mms6*, *mamGFDC*, *mamAB*, and *mamXY* operon further enhanced magnetosome formation by increasing particle number about 117% compared to the wildtype. Based on results obtained in this study, combined with previous investigations of magnetosome genes and proteins, an extended model for magnetosome biomineralization in *M. gryphiswaldense* is proposed.

Zusammenfassung

Magnetospirillum gryphiswaldense synthetisiert membranumschlossene Magnetitkristalle (Fe_3O_4), so genannte Magnetosomen. Der komplexe Prozess der Biosynthese von Magnetosomen umfasst verschiedene Abläufe: (i) die Biogenese von Magnetosomenvesikeln, (ii) das Proteinrekruitment, (iii) den Eisentransport und die Kristallisation des Magnetits, (iv) die Kristallreifung sowie (v) die lineare Anordnung der Magnetosomen. Die Synthese von Magnetosomen ist genetisch determiniert und wichtige Magnetosomengene wurden innerhalb der *mms6*, *mamGFDC*, *mamAB* und *mamXY* Operons detektiert, welche in einer so genannten genomischen Magnetosomeninsel (MAI) konserviert vorliegen. Diese beinhaltet weiterhin eine Vielzahl von Genen mit bisher unbekannter Funktion sowie Transposasengene, welche über 20% der MAI ausmachen. Die Bedeutung der Magnetosomengene sowie der übrigen Gene innerhalb der MAI speziell für die Biosynthese von magnetischen Partikeln und der minimale Gensatz zur Bildung von Magnetosomen ist weitestgehend unbekannt. In der vorliegenden Arbeit wurde eine verbesserte Cre-*lox*-basierte Technik zur Deletion verschiedener Regionen der MAI eingesetzt. Während die Gene, welche die Magnetosomenoperons flankieren, keine entscheidenden Funktionen für die Biomineralisation besitzen, haben ausschließlich die Magnetosomenoperons eine funktionale Relevanz. Im Unterschied zur Deletion des *mamAB* Operons, welche einen vollständigen Verlust der Magnetosomenbiomineralisation bewirkt, führen die Deletionen des *mms6*, *mamGFDC* oder des *mamXY* Operons zu verschiedenen Defekten in der Partikelsynthese. Zellen, in welchen diese drei Operons gemeinsam deletiert wurden, sind weiterhin in der Lage, kleine, irreguläre Partikel zu synthetisieren. Dies demonstriert, dass ausschließlich das *mamAB* Operon innerhalb der MAI in *M. gryphiswaldense* essentiell und ausreichend zur Biosynthese von Magnetosomen ist. Die genetische Untersuchung des *mamAB* Operons zeigt, dass die Gene *mamI*, *N*, *A*, *R*, *S*, *T* und *mamU*, welche entscheidende Rollen in der Kristallnukleation und -reifung haben, nicht essentiell für die Biosynthese von Magnetosomen sind. Ausschließlich die Deletionen der Gene *mamE*, *L*, *M*, *O*, *Q* und *mamB* inhibieren vollständig die Bildung von Magnetosomenkompartimenten und/oder -kristallen und stellen somit den potentiellen, minimalen Gensatz der Biomineralisation in *M. gryphiswaldense* dar. Durch Einzelgenanalysen des *mms6* Operons wurden zwei weitere entscheidende Regulatoren der Biomineralisation von Magnetosomen, Mms36 und Mms48, identifiziert. Die Überexpression der Magnetosomenoperons wurde verwendet um die Partikelsynthese in *M. gryphiswaldense* zu optimieren. Während kaum signifikante Verbesserung der Magnetosomenbildung durch die Überexpression des *mamGFDC* oder des *mamAB* Operons beobachtet werden konnte, ist die Anzahl und Größe der Magnetosomen entscheidend durch die Überexpression des *mms6* Operons erhöht wurden. Die Insertion aller Magnetosomenoperons führte im Vergleich zum Wildtyp zu einem Anstieg der Magnetosomenanzahl um 117%. Basierend auf den Ergebnissen dieser Arbeit sowie vorhergehender Untersuchungen zu Magnetosomenproteinen ist ein umfassendes Model der Magnetosomenbiosynthese in *M. gryphiswaldense* entworfen worden.

Aims

Although the functional significance of the MAI in *M. gryphiswaldense* for magnetosome biomineralization was predicted, the experimental evidence and characterization of most magnetosome genes as well as regions flanking the magnetosome operons have been lacking behind. Thus, the first part of this thesis includes a comprehensive bioinformatic, proteomic and genetic analysis of all MAI genes in *M. gryphiswaldense*, to finally detect proteins involved in magnetosome formation. By modification of the previously described Cre-*loxP* method all magnetosome operons independently or in various combinations as well as the remaining parts of the MAI were analyzed by deletion to confirm their functional relevance for the biomineralization process. The stepwise removal of unnecessary or problematic genomic regions was realized to engineer strains of *M. gryphiswaldense*, which may exhibit increased genetic stability due to the elimination of repeats and transposases, or might show improved growth as well as increased magnetosome yields because of reduced gene content.

Whereas deletion of the *mamGFDC* operon led to severe defects in morphology, size and organization of magnetite crystals, only loss of the *mamAB* operon resulted in cells entirely devoid of magnetite crystals. This suggests that only the *mamAB* operon may contain genes that are absolutely essential for magnetosome biosynthesis. However, only a minor number of genes within the highly conserved *mamAB* operon (*mamH*, *E*, *J*, *K*, *M*, *O*, and *mamB*) was analyzed in detail so far and individual functions of the *mms6* operon genes in *M. gryphiswaldense* have remained unknown as well.

Therefore, the second part of this thesis is based on genetic dissection of the *mms6* and *mamAB* operons to reveal the importance of *mgr4074*, *mms6*, *mmsF*, *mms36* (alias *mgr4071*) and *mms48* (alias *mgr4070*) as well as *mamI*, *L*, *N*, *P*, *A*, *Q*, *R*, *S*, *T*, and *mamU* in magnetosome biosynthesis and to analyze whether these genes have functions similar or distinct from those of their corresponding orthologues in the related strain *M. magneticum*. Additionally, these results were crucial to determine the potential minimal set of essential genes and proteins for magnetosome biomineralization.

As previously reported, the expression of the *mamGFDC* operon genes under control of the strong P_{mamDC} promotor increased biomineralization even beyond wildtype levels resulting in cells synthesizing larger and more magnetosomes. This prompted us within the third part of this thesis to systematically investigate the effect of controlled overexpression of the *mms6*, *mamGFDC*, *mamAB* and *mamXY* operons in various combinations to potentially enhance magnetosome yields by modulating the magnetic phenotype of *M. gryphiswaldense*.

1 Chapter I

Introduction

1.1 Magnetotactic bacteria and magnetosome biosynthesis

The ability to sense and move along magnetic fields, referred to as magnetotaxis, is linked to the capability of biomineralization of intracellular magnetic organelles termed magnetosomes [1]. It is assumed that the combination of magneto-, aero-, chemo-, and probably phototaxis is employed to find the preferred low-oxygen environment within the oxic-anoxic-transition zone (OATZ; Figure 1.1A) [1]. The biosynthesis of magnetosomes is spread among a wide range of bacterial lineages with respect to phylogeny, physiology, and morphology. First discovered by Salvatore Bellini in the late 1950s, the magnetic prokaryotes are nowadays referred to as magnetotactic bacteria (MTB) [2].

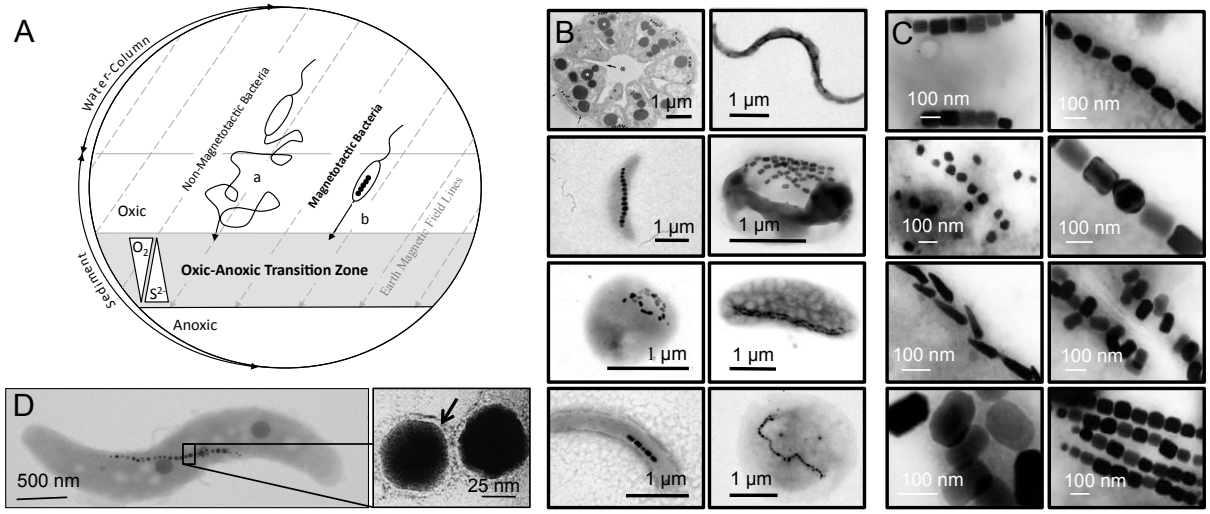

Figure 1.1: **Magnetosome formation in magnetotactic bacteria (MTB)**. A: Magnetic alignment along the earth's magnetic field lines of MTB impaired by magnetosomes reduces a three-dimensional search problem (a) to a one-dimensional search (b) to find the growth favoring oxic-anoxic-transition zone. B: TEM micrographs reflecting the high morphological diversity of magnetotactic bacteria. Modified according to [3,4,5]. C: Transmission electron micrographs (TEM) of the magnetosome diversity found in various MTB. Modified according to [6]. Scale bar: 100 nm. D: Electron micrographs of a *M. gryphiswaldense* cell and its magnetosome chain. The inset shows a micrograph of isolated magnetosomes enclosed by the magnetosome membrane (arrow) [7].

All MTB analyzed so far belong to the α-, γ- and δ- subgroups of Proteobacteria as well as the deep branching *Nitrospirae*-phylum and the candidate division OP3 [8,9,10,11]. Beside magnetotactic cocci, rods, spirilla, vibrios, and ovoid cells, even multicellular aggregates of MTB have been observed (Figure 1.1B), synthesizing numerous crystalline structures composed of magnetite (Fe_3O_4) and/or greigite (Fe_3S_4; Figure 1.1C) [8,12,13,14,15].

Therefore, a large quantity of iron is required and its intracellular accumulation leads to a tremendous iron content of 2-4% (dry weight) in MTB in comparison to 0.027% in *Escherichia coli* [16,17,18].

Although the mechanism of iron accumulation in MTB is so far not completely understood in detail, several recent studies revealed that the formation of functional magnetosomes depends on several steps: the (i) magnetosome membrane formation [19], (ii) magnetosome protein sorting [20], (iii) iron transport and crystallization [21], (iv) particle maturation [20] and (v) assembly as well as positioning of mature crystals [22,23,24,25].

The magnetosome membrane, which envelops the magnetosome minerals (Figure 1.1D) is formed prior to crystal formation. Based on biochemical analyses of isolated magnetosomes it was shown that the magnetosome membrane originates as an invagination of the cytoplasmic membrane [25,26,27].

The biogenesis of the magnetosome vesicles occurs independently and before the targeting of at least a subset of magnetosome proteins to this compartment begins. This was suggested to be important for proper biomineralization of minerals and was detected by localization studies of various magnetosome proteins [20,28].

Early studies of iron uptake within *Magnetospirillum gryphiswaldense*, the model organism of this thesis (Figure 1.1D), demonstrated that ferrous iron uptake proceeds at low rates by a diffusion-like process and ferric iron is taken up by a fast, energy-dependent mechanism [17,29]. Within the draft genome assembly of *M. gryphiswaldense* common iron uptake systems are encoded, including FeoB ferrous iron uptake systems, a putative ATP-binding-cassette (ABC) ferric iron transporter and a putative ABC-type ferric siderophore transporter. Whereas the ferrous iron transporters FeoB1 and FeoB2 play an accessory role in magnetite biomineralization [30] or function in magnetosome biomineralization and oxidative stress protection [31], no evidence for siderophores was found in *M. gryphiswaldense* as described for the related strains *M. magnetotacticum*, *M. magneticum* and *Magnetovibrio blakemorei* [16,29,32,33,34]. The ferric uptake regulator Fur regulates global iron homeostasis in *M. gryphiswaldense*, which also affects magnetite formation, probably by balancing the competing demand of biochemical iron supply and magnetosome biomineralization [35,36].

Several hypotheses have been proposed for the nucleation process within magnetite-containing MTB. Historically, based on Mössbauer spectroscopy on *M. magnetotacticum* cells, it was suggested that three different phases in the magnetite crystallization process are involved: (i) low-density, non-magnetic hydrous ferric oxides followed by the (ii) high-density-hydrous ferric oxide (ferrihydrite), which is produced by dehydration and then transformed by partial reduction to (iii) magnetite [37]. However, a Mössbauer study in *M. gryphiswaldense*, did not observe any precursors apart from ferritin, from which, in combination with ferrous iron, magnetite is supposed to be co-precipitated within the magnetosome compartments [38,39]. In contrast, by X-ray circular magnetic dichroism in the same bacterial strain, hematite (α-Fe_2O_3) is suggested as a precursor to magnetite and to form an outer layer around the nascent magnetite phase [40]. A more recent and detailed study of the related strain *M. magneticum* shows that magnetite synthesis proceeds through phase transformation: a highly disordered phosphate-rich ferric

hydroxide phase, consistent with prokaryotic ferritin, is transfered via transient, short-lived and poorly crystalline ferric (oxyhydr)oxide intermediates, such as ferrihydrite, poorly crystalline iron oxyhydroxydes and nanometric hematite to magnetite. This partially combines and extents all previous described observations [41]. Subsequently, particle maturation leads to formation of 35 and 120 nm crystals, which is for magnetite within a permanent, single magnetic domain size range and sufficient for a functioning interaction with the weak geomagnetic field [42,43,44]. Finally, for the proper assembly of magnetosomes, single crystals were aligned into linear chains along a filamentous cytoskeletal structure and positioned at midcell [24].

1.2 Genetics of magnetosome biosynthesis

1.2.1 *Magnetospirillum gryphiswaldense* and identification of its magnetosome genes

The model organism *M. gryphiswaldense* (Figure 1.1D) was isolated from sediments of the river Ryck near Greifswald (Germany) and synthesizes cubooctahedral crystals composed of magnetite. The 3-5 μm long and helically shaped gram-negative bacterium belongs to the α-Proteobacteria and is bipolar monotrichous flagellated. The microaerophilic strain is chemo-organoheterotroph utilizing different organic acids with oxygen or nitrogen as terminal electron acceptor [45]. Magnetosomes of *M. gryphiswaldense* are commonly aligned in a chain-like structure containing up to 60 particles with an average crystal diameter of 35 to 40 nm that are surrounded by the magnetosome membrane [26,44,46,47]. Within the magnetosome membrane a specific set of more than 30 proteins direct the biomineralization of highly crystalline particles with unique characteristics, which make them attractive for use in a broad range of biomedical and biotechnological applications [48,49,50].

The biosynthesis of magnetosomes is not understood in detail, but it is known that both the biomineralization of inorganic magnetite crystals and their assembly into highly ordered chains are under strict genetic control. However, the number and identity of magnetosome genes and their precise functions in magnetosome biosynthesis have mostly remained unknown. Several methods were applied to identify genes involved in this process, and the magnetosome genes were named "*magnetosome membrane*" (*mam*), "*magnetic particle membrane-specific*" (*mms*), "*magnetotaxis*" (*mtx*) or "*magnetosome membrane genes*" (*mme*), respectively [51,52,53]. Historically, the first magnetosome-associated proteins were detected by proteomic analysis using one or two dimensional gel electrophoresis of membrane and soluble fractions of *M. gryphiswaldense*. By reverse genetics the corresponding genes *mamA*, *B*, *C*, *D*, *E*, *F*, *G*, *J*, *M*, *N*, *O*, *Q*, *R*, *S*, *T*, *W*, *Y*, and *mamX*, *mmsF*, *mms6*, *mme22*, *mmeA*, as well as *mtxA* were revealed [46,51,54]. It was shown that the genes *mamA* and *mamB* as well as *mamD* and *mamC* are located within two different clusters, termed as *mamAB* and *mamDC* clusters [51].

First experimental indications for their functional significance in magnetosome formation came from the isolation of a non-magnetic mutant strain, which had lost almost 80 kb by a spontaneous deletion that included all known magnetosome genes as well as further unidentified genes [54,55]. It became obvious that the magnetosome genes are located within a single genomic region, described as putative magnetosome island (MAI) within *M. gryphiswaldense* and a further magnetosome cluster, termed as *mms6* cluster was detected [54,55]. The functional significance of the MAI was confirmed by a comparative genomics approach based on the growing number of sequenced MTB genomes, which revealed that magnetotaxis signature genes are predominantly located within this region. Furthermore, the highly conserved *mamXY* cluster within the MAI of *M. gryphiswaldense* was identified [53]. Because of the detection of the MAI genes also in other cultivated and uncultivated α-proteobacterial MTB (conservation) it has been suggested that the MAI was transferred horizontally [53,54,56,57]. This was further corroborated by the discovery of homologous gene clusters in all tested MTB so far, such as the δ-Proteobacteria *Desulfovibrio magneticus* RS-1 [58] and the multicellular magnetotactic prokaryote [59], as well as in the deep-branching *Nitrospirae*-phylum [56]. Alternatively, it was discussed that the origin of magnetotaxis might be rather monophyletic, whereas magnetosome formation was developed in a common ancestor of all MTB and horizontal gene transfer appears to play a role in their distribution [59,60].

In *M. gryphiswaldense*, the MAI was shown to encompass 130 kb, comprising the *mms6*, *mamGFDC*, *mamAB*, and *mamXY* operons (Figure 1.2) [54]. These operons are transcribed as single polycistronic messengers under control of the P_{mms6}, P_{mamDC}, P_{mamH}, and P_{mamXY} promoters [61,62]. In addition to genes implicated in magnetosome biomineralization, the MAI contains a number of genes with unknown functions and numerous transposase genes that account for more than 20% of the coding region (Figure 1.2.). Owing to frequent homologous recombinations between the numerous direct or inverted repeats associated with transposase genes, the MAI is genetically unstable, resulting in frequent spontaneous loss of the magnetic phenotype [54,63].

With the identification of the MAI, forward genetics based on mutagenesis by targeted or random base pair substitution, insertion, or deletion became a powerful tool to reveal the genetic importance of genes or regions for magnetosome biosynthesis by comparing phenotypic changes with the unmodified wildtype. Beside MAI genes, also genes outside of the MAI became targets for mutational analyses. For example, deletions of *nap* and *nir* genes, whose products catalyze the reduction of nitrate (NO_3^-) to nitrite (NO_2^-) and nitrite to nitric oxide (NO), respectively, resulted in biomineralization defects. This indicates that magnetite biomineralization is linked to dissimilatory nitrate reduction potentially by participation of Nap and Nir in redox reactions required for magnetite biomineralization or even oxidize ferrous iron directly for magnetosome formation [64,65]. Further, enzymes participating in denitrification (nitrite reductase Cd_1), and in aerobic respiration (cytochrome c oxidase Cbb_3), as well as the oxygen sensor Fnr have been found to poise optimal redox conditions during magnetite biomineralization, as indicated by mutagenesis and cultivation experiments [64,66]. Inactivation of the flagellin gene *flaA* caused non-

magnetotactic cells lacking flagellar filaments [67] and deletion of the genes, encoding the iron uptake regulator Fur [34] and the ferrous iron transporter FeoB1 and FeoB2 [30,31] (described above) leads to reduction of magnetosome size and number, indicating their role in magnetosome biomineralization.

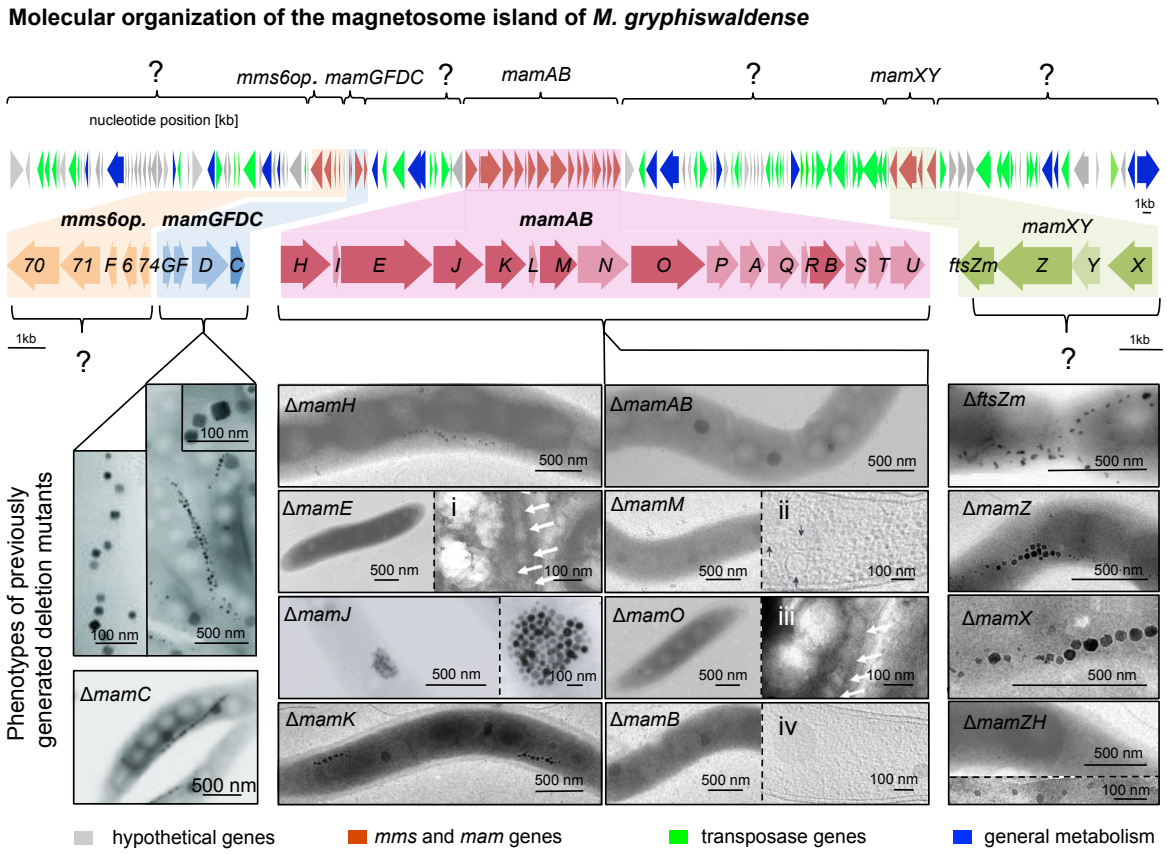

Figure 1.2: **Molecular organization and deletion analysis of the magnetosome island of *M. gryphiswaldense***. Schematic representation of the magnetosome island of *M. gryphiswaldense* that contains several *mam* and *mms* genes within the *mms6*, *mamGFDC*, *mamAB* and *mamXY* operons, several transposase genes, genes encoding other assigned functions and a high number of hypothetical genes with unknown functions indicated by different colors. Whereas the *mamGFDC* and *mamAB* operon were genetically analyzed by targeted mutagenesis, functions of regions flanking the magnetosome clusters as well as of the *mms6* and *mamXY* operons have remained unknown (labeled by a question mark). Brighter colored genes within the magnetosome operons were not investigated by single gene deletion so far. Transmission electron micrographs demonstrate phenotypes of previously generated deletion mutants. Whereas Δ*mamGFDC* [69], Δ*mamC* [69], Δ*mamH* [62], Δ*mamJ* [23], Δ*mamK* [70], Δ*ftsZm* [71], Δ*mamZ* [62], Δ*mamX* and Δ*mamHZ* [62] display various biomineralization defects, *mamE* [72], *mamM* [35], *mamO* [72] and *mamB* [35] were described to be essential for magnetosome biosynthesis, as indicated by the absence of electron dense crystals. Cryo electron micrograms and Cryo-ultrathin sections demonstrate the presence of magnetosome membranes in Δ*mamE*, Δ*mamM*, and Δ*mamO* (i-iii; arrows) or the absence of compartments in Δ*mamB* (vi) [72,73]. The MAI is modified according to [53,54,68].

1.2.2 The genetic toolset for analysis of magnetosome biosynthesis in *M. gryphiswaldense*

Magnetosome formation is one of the most structurally and genetically complex processes within prokaryotic organism, including several proteins with so far unknown functions. Genetic analyses to study underlying mechanisms have been hindered for a long time by the lack of appropriate methodologies

and tools for genetic manipulation. Technical requirements, such as techniques for clonal selection on agar plates [74], availability of suitable selection markers [74], gene transfer [74], GFP fusions [75,76] as well as techniques for site-directed and random mutagenesis [67,68,69,77,78] became available for *M. gryphiswaldense* only at the beginning of this work. Whereas techniques like the transfer of genes through electroporation or by chemical methods are not efficient or applicable for *M. gryphiswaldense*, plasmidal transfer became possible by conjugation [74]. Tools for site-directed mutagenesis, including allelic replacement by double-cross-over or insertion-duplication mutagenesis mediated by RecA were established [67,69,77]. This includes a counter-selection method based on SacB, which confers sensitivity to sucrose, but was applied only in few cases for *M. gryphiswaldense* due to unstable *sacB* expression [69]. Furthermore, a Cre-*loxP* mediated excision system was used to routinely mutate the genome of *M. gryphiswaldense* for large-scale deletions up to 67 kb [68].

However, several rounds of screening for mutants are necessary, and especially methods based on allelic replacement bear the high risk for detection of false positive deletions, which make the tools inefficient and time-consuming. Only recently a more efficient counter-selection method mediated by galactokinase (GalK), which induces sensitivity to galactose or 2-deoxygalactose in the absence of a galactose metabolizing pathway, was established [79]. Furthermore, construction of transposable expression vectors comprising the MycoMar or Tn5 transposase genes enabled the single copy insertion into random chromosomal sites for stable magnetosome gene expression and transfer into foreign hosts [67,78]. New inducible and efficient vector systems based on optimization of the Tet-inducible system and the previously identified P_{mamDC} promoter, enable high-level and tunable expression after induction [76]. Although successful procedures became available, isolation of deletion mutants is still a highly tedious and time-consuming task due to the slow growth of *M. gryphiswaldense* with its high doubling time of three to seven hours and strategies depend on sequential rounds of insertions and excisions. As a consequence, although several candidate magnetosome genes of the MAI were predicted, only few of them (*mamGFDC* operon, *mamC*, *mamJ*, and *mamAB* operon) had been experimentally confirmed at the beginning of this work (Figure 1.2).

1.2.3 Detailed genetic analyses of the magnetosome island in *M. gryphiswaldense*

Deletion of the whole 2.071 kb *mamGFDC* operon of *M. gryphiswaldense*, which contains the genes *mamG*, *F*, *D*, and *mamC* resulted in the formation of smaller and less regular magnetosomes, indicating that the most abundant magnetosome proteins MamG, F, D, and MamC, with over 35% of all magnetosome-associated proteins, did not inhibit crystal nucleation or prevented MM vesicle synthesis and thus, are not essential for magnetosome biomineralization [69]. Loss of *mamC* only had a minor impact on magnetite crystal formation and cells produce magnetosomes that were on average slightly smaller than wildtype crystals (Figure 1.2) [69].

The ~5 kb large *mamXY* operon is conserved in all cultivated magnetospirilla strains and encodes MamY, MamX, MamZ (previously referred to as MamH-like) and the tubulin-like FtsZm protein (previously referred to as FtsZ-like) [80], for which a key role was predicted mainly based on comparative genome analyses [81]. Previously, single gene deletions of *mamX* and *mamZ* resulted in very similar mutant phenotypes and strains formed regularly shaped and sized magnetite particles flanked by a variable number of small, irregularly shaped particles (Figure 1.2) [62]. Both proteins, MamX and MamZ are likely involved in redox control to maintain optimal conditions for magnetite formation. These functions depend on the two putative haem c binding "magnetochrome" domains of MamX as well as the ferric reductase-like transmembrane component of MamZ [62]. The mutant Δ*ftsZm* of *M. gryphiswaldense* only displayed a magnetosome phenotype, when the cells were grown in medium with ammonium instead of nitrate, resulting in cells with many small, poorly crystalline needle-like crystals, which indicates a functional link to denitrification, redox control, and magnetosomal iron homeostasis (Figure 1.2) [71].

The ~6.6 kb *mms6* operon comprises the genes *mgr4074*, *mms6*, *mmsF*, *mms36* (alias *mgr4071*) and *mms48* (alias *mgr4070*), but their individual functions remained unknown (Figure 1.2). In the highly related strain *M. magneticum*, the *mms6* cluster was described to comprise only *amb0955* (*mgr4074*), *amb0956* (*mms6*), *amb0967* (*mmsF*), but lacks homologues of *mms36* and *mms48* [82]. Whereas deletion of *amb0955* resulted in no obvious magnetosome phenotype, single gene deletions of *mms6* in *M. magneticum* performed by different research groups revealed inconsistent phenotypes. While Tanaka *et al*. [83], reported an important regulatory function of Mms6 for magnetosome morphology, Murat *et al*., only observed minor effects on magnetosome biosynthesis after deletion of *mms6 in vivo* in *M. magneticum* [82]. *In vitro*, the small (12.76 kDa in *M. gryphiswaldense* and 14.69 kDa in *M. magneticum*) Mms6 protein was shown to be tightly bound to isolated bacterial magnetite crystals as visualized by atomic force microscopy and TEM [84,85]. *In vitro* crystallization experiments suggested that Mms6 and peptides mimicking it have iron-binding activity and affected the formation of cubo-octahedral crystal morphologies [86,87]. However, it remains to be shown, if the *mms6* operon genes have functions similar or distinct from those of their corresponding orthologues in *M. magneticum*.

In contrast to the smaller operons, the large *mamAB* operon was found to contain genes absolutely essential for magnetosome biosynthesis in *M. gryphiswaldense* and also *M. magneticum*, as its deletion resulted in the complete loss of magnetic particles [20,68]. A recent comprehensive genetic dissection of the *mamAB* operon in *M. magneticum* revealed that *mamH*, *P*, *R*, *S*, and *mamT* encode accessory functions for magnetosome synthesis, since mutants display various biomineralization defects, whereas *mamU* and *mamV* had no obvious magnetosome phenotype [20]. As in *M. gryphiswaldense* (see below), *mamK* and *mamJ* were implicated in magnetosome chain assembly, but their loss did not affect biomineralization [25,88]. However, gene deletions of *mamI*, *E*, *L*, *M*, *N*, *O*, and *mamQ* as well as *mamB* (co-deleted with their respective orthologs) fully abolished magnetosome synthesis in *M. magneticum* [20,28]. Whereas MamI, L, Q and MamB were suggested to be essential for vesicle genesis, MamE, O, M, and MamN were classified to be mainly required for magnetite crystallization [20].

The discovery of a small ”magnetosome islet” in the genome of *M. magneticum* with further copies of *mamE*, *J*, *K*, *L*, *M*, *F* as well as *mamD* suggested genetic redundancy that remains to be clarified with respect to determination of the minimal essential gene set [89].

In *M. gryphiswaldense* the ~16.4 kb *mamAB* operon contains 17 genes (*mamH*, *I*, *E*, *J*, *K*, *L*, *M*, *N*, *O*, *P*, *A*, *Q*, *R*, *B*, *S*, *T* and *mamU*; Figure 1.2). Only a few genes of the *mamAB* operon were analyzed individually in this organism so far (Figure 1.3). Deletion of *mamH* caused a moderate decrease of magnetosome number and size. Co-deletion with its partial homologue *mamZ* had a considerably stronger effect with only very few or no regular crystals detectable in the cells, suggesting that MamH is involved in redox control like its homologue MamZ (Figure 1.3) [62]. The actin-like protein MamK forms a filamentous structure for magnetosome assembly and interacts with the acidic protein MamJ that is involved in connecting magnetosomes to the filament (Figure 1.3). Both proteins, however, have no or only minor effects on biomineralization, as deletion mutants Δ*mamK* formed shorter and fragmented chains and deletion of *mamJ* led to detached particles of the magnetosome filament, resulting in particle agglomeration without any chain formation (Figure 1.2) [23,24]. Deletion of *mamE*, *O*, *M* and *mamB* resulted in either a total inhibition of crystal nucleation or prevented MM vesicle synthesis, indicating that these genes are essential for magnetosome biosynthesis [72,73,90].

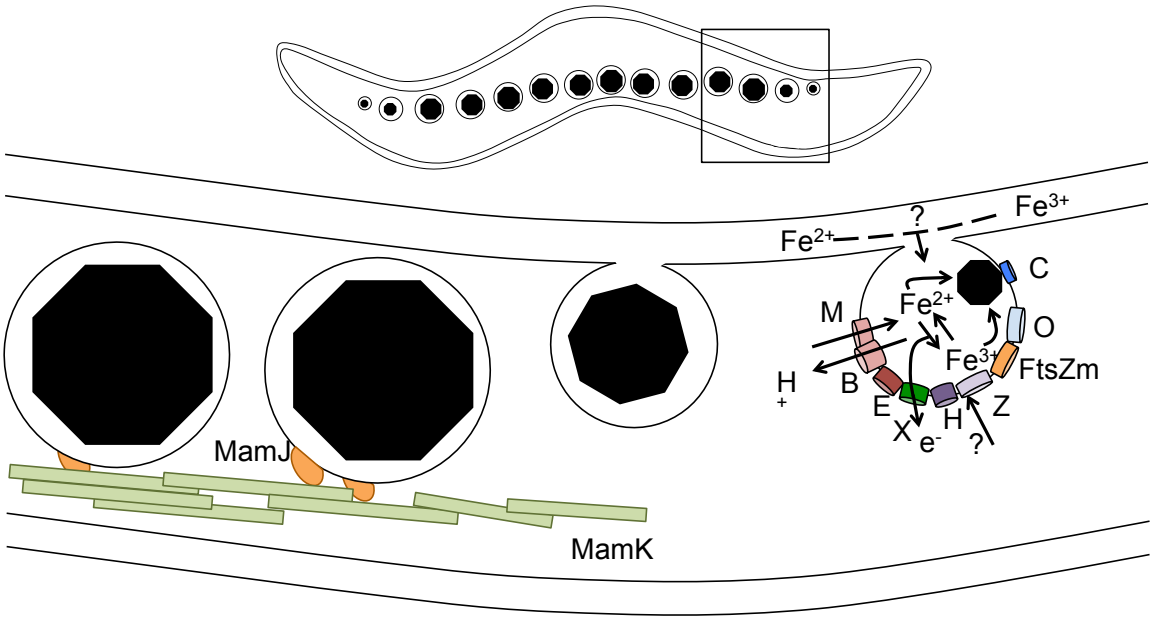

Figure 1.3: **Overview about previously analyzed magnetosome proteins, encoded by the MAI of *M. gryphiswaldense***. Corresponding genes were analyzed by mutagenesis in addition to further molecular analyses to determine protein functions. MamH, MamZ and MamX functionally interact to balance the redox state of iron within the magnetosome compartment. FtsZm is likely involved in denitrification, redox control, and/or magnetosomal iron homeostasis. The actin-like protein MamK interacts with the acidic protein MamJ to align the magnetosomes into chain-like structures. MamC is important for crystal maturation. Whereas MamB was suggested to be essential for vesicle genesis, MamE, MamO, and MamM were classified to be mainly required for magnetite crystallization. Detailed genetic analyses of remaining proteins, encoded by the *mms6*, *mamGFDC*, *mamAB* and *mamXY* operons as well as flanking regions of the MAI were previously not implemented.

1.3 References

1. Bazylinski D, Lefèvre C, Schüler D (2013) Magnetotactic Bacteria. In: Rosenberg E, DeLong E, Lory S, Stackebrandt E, Thompson F, editors. The Prokaryotes: Springer Berlin Heidelberg. pp. 453-494.
2. Bellini C, Di Battista E, Boccardo F, Campisi C, Villa G, *et al.* (2009) The role of lymphoscintigraphy in the diagnosis of lymphedema in Turner syndrome. Lymphology 42: 123-129.
3. Keim CN, Abreu F, Lins U, Lins de Barros H, Farina M (2004) Cell organization and ultrastructure of a magnetotactic multicellular organism. J Struct Biol 145: 254-262.
4. Lin W, Wang Y, Gorby Y, Nealson K, Pan Y (2013) Integrating niche-based process and spatial process in biogeography of magnetotactic bacteria. Sci Rep 3.
5. Lin W, Li J, Schüler D, Jogler C, Pan Y (2009) Diversity analysis of magnetotactic bacteria in Lake Miyun, northern China, by restriction fragment length polymorphism. Sys Appl Microbiol 32: 342-350.
6. Schüler D (1999) Formation of magnetosomes in magnetotactic bacteria. J Mol Microbiol Biotechnol 1: 79-86.
7. Schüler D (2008) Genetics and cell biology of magnetosome formation in magnetotactic bacteria. FEMS Microbiol Rev 32: 654-672.
8. Spring S, Amann R, Ludwig W, Schleifer KH, van Gemerden H, *et al.* (1993) Dominating role of an unusual magnetotactic bacterium in the microaerobic zone of a freshwater sediment. Appl Environ Microbiol 59: 2397-2403.
9. Jogler C, Lin W, Meyerdierks A, Kube M, Katzmann E, *et al.* (2009) Toward Cloning of the Magnetotactic Metagenome: Identification of Magnetosome Island Gene Clusters in Uncultivated Magnetotactic Bacteria from Different Aquatic Sediments. Appli Environ Microbiol 75: 3972-3979.
10. Kolinko S, Jogler C, Katzmann E, Wanner G, Peplies J, *et al.* (2012) Single-cell analysis reveals a novel uncultivated magnetotactic bacterium within the candidate division OP3. Environ Microbiol 14: 1709-1721.
11. Lefèvre CT, Frankel RB, Abreu F, Lins U, Bazylinski DA (2011) Culture-independent characterization of a novel, uncultivated magnetotactic member of the *Nitrospirae* phylum. Environ Microbiol 13: 538-549.
12. Delong EF, Frankel RB, Bazylinski DA (1993) Multiple evolutionary origins of magnetotaxis in bacteria. Science 259: 803-806.
13. Flies CB, Jonkers HM, de Beer D, Bosselmann K, Böttcher ME, *et al.* (2005) Diversity and vertical distribution of magnetotactic bacteria along chemical gradients in freshwater microcosms. FEMS Microbiol Ecol 52: 185-195.

14. Amann R, Peplies Jr, Schüler D (2007) Diversity and Taxonomy of Magnetotactic Bacteria. In: Schüler D, editor. Magnetoreception and Magnetosomes in Bacteria: Springer Berlin Heidelberg. pp. 25-36.
15. Lefèvre CT, Bernadac A, Yu-Zhang K, Pradel N, Wu LF (2009) Isolation and characterization of a magnetotactic bacterial culture from the Mediterranean Sea. Environ Microbiol 11: 1646-1657.
16. Paoletti LC, Blakemore RP (1986) Hydroxamate production by *Aquaspirillum magnetotacticum*. J Bacteriol 167: 73-76.
17. Schüler D, Baeuerlein E (1998) Dynamics of iron uptake and Fe_3O_4 biomineralization during aerobic and microaerobic growth of *Magnetospirillum gryphiswaldense*. J Bacteriol 180: 159-162.
18. Abdul-Tehrani H, Hudson AJ, Chang YS, Timms AR, Hawkins C, *et al*. (1999) Ferritin mutants of *Escherichia coli* are iron deficient and growth impaired, and fur mutants are iron deficient. J Bacteriol 181: 1415-1428.
19. Komeili A, Vali H, Beveridge TJ, Newman DK (2004) Magnetosome vesicles are present before magnetite formation, and MamA is required for their activation. Proc Natl Acad Sci U S A 101: 3839-3844.
20. Murat D, Quinlan A, Vali H, Komeili A (2010) Comprehensive genetic dissection of the magnetosome gene island reveals the step-wise assembly of a prokaryotic organelle. Proc Natl Acad Sci U S A 107: 5593-5598.
21. Faivre D, Bottger LH, Matzanke BF, Schüler D (2007) Intracellular magnetite biomineralization in bacteria proceeds by a distinct pathway involving membrane-bound ferritin and an iron(II) species. Angew Chem Int Ed Engl 46: 8495-8499.
22. Frankel RB, Bazylinski DA (2006) How magnetotactic bacteria make magnetosomes queue up. Trends Microbiol 14: 329-331.
23. Scheffel A, Gruska M, Faivre D, Linaroudis A, Plitzko JM, *et al*. (2006) An acidic protein aligns magnetosomes along a filamentous structure in magnetotactic bacteria. Nature 440: 110-114.
24. Katzmann E, Scheffel A, Gruska M, Plitzko JM, Schüler D (2010) Loss of the actin-like protein MamK has pleiotropic effects on magnetosome formation and chain assembly in *Magnetospirillum gryphiswaldense*. Mol Microbiol 77: 208-224.
25. Komeili A, Li Z, Newman DK, Jensen GJ (2006) Magnetosomes are cell membrane invaginations organized by the actin-like protein MamK. Science 311: 242-245.
26. Schüler D (2004) Molecular analysis of a subcellular compartment: the magnetosome membrane in *Magnetospirillum gryphiswaldense*. Arch Microbiol 181: 1-7.
27. Gorby YA, Beveridge TJ, Blakemore RP (1988) Characterization of the bacterial magnetosome membrane. J Bacteriol 170: 834-841.

28. Quinlan A, Murat D, Vali H, Komeili A (2011) The HtrA/DegP family protease MamE is a bifunctional protein with roles in magnetosome protein localization and magnetite biomineralization. Mol Microbiol 80: 1075-1087.
29. Schüler D, Baeuerlein E (1996) Iron-limited growth and kinetics of iron uptake in *Magnetospirillum gryphiswaldense*. Arch Microbiol 166: 301-307.
30. Rong C, Huang Y, Zhang W, Jiang W, Li Y, *et al*. (2008) Ferrous iron transport protein FeoB1 gene (*feoB1*) plays an accessory role in magnetosome formation in *Magnetospirillum gryphiswaldense* strain MSR-1. Res Microbiol 159: 530-536.
31. Rong C, Zhang C, Zhang Y, Qi L, Yang J, *et al*. (2012) FeoB2 Functions in magnetosome formation and oxidative stress protection in *Magnetospirillum gryphiswaldense* strain MSR-1. J Bacteriol 194: 3972-3976.
32. Calugay RJ, Okamura Y, Wahyudi AT, Takeyama H, Matsunaga T (2004) Siderophore production of a periplasmic transport binding protein kinase gene defective mutant of *Magnetospirillum magneticum* AMB-1. Biochem Biophys Res Commun 323: 852-857.
33. Calugay RJ, Takeyama H, Mukoyama D, Fukuda Y, Suzuki T, *et al*. (2006) Catechol siderophore excretion by magnetotactic bacterium *Magnetospirillum magneticum* AMB-1. J Biosci Bioeng 101: 445-447.
34. Uebe R, Voigt B, Schweder T, Albrecht D, Katzmann E, *et al*. (2010) Deletion of a *fur-like* gene affects iron homeostasis and magnetosome formation in *Magnetospirillum gryphiswaldense*. J Bacteriol 192: 4192-4204.
35. Uebe RJ, K. Henn, V. Poxleitner, G. Katzmann, E. Plitzko, J.M. Zarivach, R. Kasama, T. Wanner, G. Pósfai, M. Böttger, L. Matzanke, B. Schüler, D. (2011) The cation diffusion facilitator proteins MamB and MamM of *Magnetospirillum gryphiswaldense* have distinct and complex functions, and are involved in magnetite biomineralization and magnetosome membrane assembly. Mol Microbiol 82: 818Ð835.
36. Huang Y, Zhang W, Jiang W, Rong C, Li Y (2007) Disruption of a *fur-like* gene inhibits magnetosome formation in *Magnetospirillum gryphiswaldense* MSR-1. Biochem (Moscow) 72: 1247-1253.
37. Frankel RB, Papaefthymiou GC, Blakemore RP, O'Brien W (1983) Fe_3O_4 precipitation in magnetotactic bacteria. Biochimica et Biophysica Acta (BBA) - Mol Cell Res 763: 147-159.
38. Faivre D, Böttger LH, Matzanke BF, Schüler D (2007) Intracellular magnetite biomineralization in bacteria proceeds by a distinct pathway involving membrane-bound ferritin and an iron(II) species. Angew Chem Int Ed Engl 46: 8495-8499.
39. Fdez-Gubieda ML, Muela A, Alonso J, Garcia-Prieto A, Olivi L, *et al*. (2013) Magnetite biomineralization in *Magnetospirillum gryphiswaldense*: time-resolved magnetic and structural studies. ACS Nano 7: 3297-3305.

40. Staniland S, Ward B, Harrison A, van der Laan G, Telling N (2007) Rapid magnetosome formation shown by real-time x-ray magnetic circular dichroism. PNAS 104: 19524-19528.
41. Baumgartner J, Morin G, Menguy N, Perez Gonzalez T, Widdrat M, *et al*. (2013) Magnetotactic bacteria form magnetite from a phosphate-rich ferric hydroxide via nanometric ferric (oxyhydr)oxide intermediates. Proc Natl Acad Sci U S A 110: 14883-14888.
42. Moskowitz BM (1995) Biomineralization of magnetic minerals. Reviews Geophy 33: 123-128.
43. Dunin-Borkowski RE, McCartney MR, Pósfai MI, Frankel RB, Bazylinski DA, *et al*. (2001) Off-axis electron holography of magnetotactic bacteria: magnetic microstructure of strains MV-1 and MS-1. Europ J Microbiol 13: 671-684.
44. Schüler D, Frankel RB (1999) Bacterial magnetosomes: microbiology, biomineralization and biotechnological applications. Appl Microbiol Biotech 52: 464-473.
45. Schüler D, Köhler M (1992) The isolation of a new magnetic spirillum. Zentralblatt für Mikrobiologie 147: 150-151.
46. Grünberg K, Müller EC, Otto A, Reszka R, Linder D, *et al*. (2004) Biochemical and proteomic analysis of the magnetosome membrane in *Magnetospirillum gryphiswaldense*. Appl Environ Microbiol 70: 1040-1050.
47. Schüler D (2002) The biomineralization of magnetosomes in *Magnetospirillum gryphiswaldense*. Int Microbiol 5: 209-214.
48. Faivre D, Schüler D (2008) Magnetotactic bacteria and magnetosomes. Chem Rev 108: 4875-4898.
49. Lang C, Schüler D (2006) Microbial Bionanotechnology: Biological Self-Assembly Systems and Biopolymer- Based Nanostructures. In: Rehm B, editor. Microbial Bionanotechnology: Biological Self-Assembly Systems and Biopolymer- Based Nanostructures. Wymondham: Horizon Scientific Press. pp. 107.
50. Lang C, Schüler D, Faivre D (2007) Synthesis of magnetite nanoparticles for bio- and nanotechnology: genetic engineering and biomimetics of bacterial magnetosomes. Macromol Biosci 7: 144-151.
51. Grünberg K, Wawer C, Tebo BM, Schüler D (2001) A large gene cluster encoding several magnetosome proteins is conserved in different species of magnetotactic bacteria. Appl Environ Microbiol 67: 4573-4582.
52. Tanaka M, Okamura Y, Arakaki A, Tanaka T, Takeyama H, *et al*. (2006) Origin of magnetosome membrane: Proteomic analysis of magnetosome membrane and comparison with cytoplasmic membrane. Proteomics 6: 5234-5247.
53. Richter M, Kube M, Bazylinski DA, Lombardot T, Glockner FO, *et al*. (2007) Comparative genome analysis of four magnetotactic bacteria reveals a complex set of group-specific genes implicated in magnetosome biomineralization and function. J Bacteriol 189: 4899-4910.

54. Ullrich S, Kube M, Schübbe S, Reinhardt R, Schüler D (2005) A hypervariable 130-kilobase genomic region of *Magnetospirillum gryphiswaldense* comprises a magnetosome island which undergoes frequent rearrangements during stationary growth. J Bacteriol 187: 7176-7184.
55. Schübbe S, Kube M, Scheffel A, Wawer C, Heyen U, *et al*. (2003) Characterization of a spontaneous nonmagnetic mutant of *Magnetospirillum gryphiswaldense* reveals a large deletion comprising a putative magnetosome island. J Bacteriol 185: 5779-5790.
56. Jogler C, Wanner G, Kolinko S, Niebler M, Amann R, *et al*. (2011) Conservation of proteobacterial magnetosome genes and structures in an uncultivated member of the deep-branching *Nitrospira* phylum. Proc Natl Acad Sci U S A 108: 1134-1139.
57. Jogler C, Lin W, Meyerdierks A, Kube M, Katzmann E, *et al*. (2009) Toward cloning of the magnetotactic metagenome: identification of magnetosome island gene clusters in uncultivated magnetotactic bacteria from different aquatic sediments. Appl Environ Microbiol 75: 3972-3979.
58. Nakazawa H, Arakaki A, Narita-Yamada S, Yashiro I, Jinno K, *et al*. (2009) Whole genome sequence of *Desulfovibrio magneticus* strain RS-1 revealed common gene clusters in magnetotactic bacteria. Genome Res 19: 1801-1808.
59. Abreu F, Cantao ME, Nicolas MF, Barcellos FG, Morillo V, *et al*. (2011) Common ancestry of iron oxide- and iron-sulfide-based biomineralization in magnetotactic bacteria. ISME J.
60. Lefèvre CT, Trubitsyn D, Abreu F, Kolinko S, de Almeida LGP, *et al*. (2013) Monophyletic origin of magnetotaxis and the first magnetosomes. Environ Microbiol 15: 2267-2274.
61. Schübbe S, Wurdemann C, Peplies J, Heyen U, Wawer C, *et al*. (2006) Transcriptional organization and regulation of magnetosome operons in *Magnetospirillum gryphiswaldense*. Appl Environ Microbiol 72: 5757-5765.
62. Raschdorf O, Müller FD, Pósfai M, Plitzko JM, Schüler D (2013) The magnetosome proteins MamX, MamZ and MamH are involved in redox control of magnetite biomineralization in *Magnetospirillum gryphiswaldense*. Mol Microbiol 89: 872-886.
63. Kolinko I, Jogler C, Katzmann E, Schüler D (2011) Frequent mutations within the genomic magnetosome island of *Magnetospirillum gryphiswaldense* are mediated by RecA.
J Bacteriol. 193(19): 5328-34.
64. Li Y, Bali S, Borg S, Katzmann E, Ferguson SJ, *et al*. (2013) Cytochrome cd1 Nitrite Reductase NirS Is Involved in Anaerobic Magnetite Biomineralization in *Magnetospirillum gryphiswaldense* and Requires NirN for Proper d1 Heme Assembly. J Bacteriol 195: 4297-4309.
65. Li Y, Katzmann E, Borg S, Schüler D (2012) The Periplasmic Nitrate Reductase Nap Is Required for Anaerobic Growth and Involved in Redox Control of Magnetite Biomineralization in *Magnetospirillum gryphiswaldense*. J Bacteriol 194: 4847-4856.

66. Li Y, Raschdorf O, Silva KT, Schüler D (2014) The terminal oxidase Cbb3 functions in redox control of magnetite biomineralization in *Magnetospirillum gryphiswaldense*. J Bacteriol.
67. Schultheiss D, Kube M, Schüler D (2004) Inactivation of the flagellin gene *flaA* in *Magnetospirillum gryphiswaldense* results in nonmagnetotactic mutants lacking flagellar filaments. Appl Environ Microbiol 70: 3624-3631.
68. Ullrich S, Schüler D (2010) Cre-*lox*-based method for generation of large deletions within the genomic magnetosome island of *Magnetospirillum gryphiswaldense*. Appl Environ Microbiol 76: 2439-2444.
69. Scheffel A, Gardes A, Grünberg K, Wanner G, Schüler D (2008) The major magnetosome proteins MamGFDC are not essential for magnetite biomineralization in *Magnetospirillum gryphiswaldense* but regulate the size of magnetosome crystals. J Bacteriol 190: 377-386.
70. Katzmann E, Scheffel A, Gruska M, Plitzko JM, Schüler D (2010) Loss of the actin-like protein MamK has pleiotropic effects on magnetosome formation and chain assembly in *Magnetospirillum gryphiswaldense*. Mol Microbiol 77: 208-224.
71. Müller FD, Raschdorf O, Nudelman H, Messerer M, Katzmann E, *et al*. (2014) The FtsZ-like protein FtsZm of *Magnetospirillum gryphiswaldense* likely interacts with its generic homolog and is required for biomineralization under nitrate deprivation. J Bacteriol 196: 650-659.
72. Yang W, Li R, Peng T, Zhang Y, Jiang W, *et al*. (2010) *mamO* and *mamE* genes are essential for magnetosome crystal biomineralization in *Magnetospirillum gryphiswaldense* MSR-1. Res Microbiol 161: 701-705.
73. Uebe R, Junge K, Henn V, Poxleitner G, Katzmann E, *et al*. (2011) The cation diffusion facilitator proteins MamB and MamM of *Magnetospirillum gryphiswaldense* have distinct and complex functions, and are involved in magnetite biomineralization and magnetosome membrane assembly. Mol Microbiol 82: 818-835.
74. Schultheiss D, Schüler D (2003) Development of a genetic system for *Magnetospirillum gryphiswaldense*. Arch Microbiol 179: 89-94.
75. Lang C, Schüler D (2008) Expression of green fluorescent protein fused to magnetosome proteins in microaerophilic magnetotactic bacteria. Appl Environ Microbiol 74: 4944-4953.
76. Borg S, Hofmann J, Pollithy A, Lang C, Schüler D (2014) New vectors for chromosomal integration enable high-level constitutive or inducible magnetosome expression of fusion proteins in *Magnetospirillum gryphiswaldense*. Appl Environ Microbiol. doi: 10.1128/AEM.00192-14
77. Schultheiss D, Handrick R, Jendrossek D, Hanzlik M, Schüler D (2005) The Presumptive Magnetosome Protein Mms16 Is a Poly(3-Hydroxybutyrate) Granule-Bound Protein (Phasin) in *Magnetospirillum gryphiswaldense*. J Bacteriol 187: 2416-2425.
78. Kolinko I, Lohße A, Borg S, Raschdorf O, Jogler C, *et al*. (2014) Biosynthesis of magnetic nanostructures in a foreign organism by transfer of bacterial magnetosome gene clusters. Nat Nano 9: 193-197.

79. Raschdorf O, Plitzko JrM, Schüler D, Müller FD (2014) A tailored *galK* counterselection system for efficient markerless gene deletion and chromosomal tagging in *Magnetospirillum gryphiswaldense*. Appl Environ Microbiol. doi: 10.1128/AEM.00588-14.
80. Ding Y, Li J, Liu J, Yang J, Jiang W, *et al*. (2010) Deletion of the *ftsZ-like* gene results in the production of superparamagnetic magnetite magnetosomes in *Magnetospirillum gryphiswaldense*. J Bacteriol 192: 1097-1105.
81. Richter M, Kube M, Bazylinski DA, Lombardot T, Glockner FO, *et al*. (2007) Comparative genome analysis of four magnetotactic bacteria reveals a complex set of group-specific genes implicated in magnetosome biomineralization and function. J Bacteriol 189: 4899-4910.
82. Murat D, Falahati V, Bertinetti L, Csencsits R, Krnig A, *et al*. (2012) The magnetosome membrane protein, MmsF, is a major regulator of magnetite biomineralization in *Magnetospirillum magneticum* AMB-1. Mol Microbiol 85: 684-699.
83. Tanaka M, Arakaki A, Matsunaga T (2010) Identification and functional characterization of liposome tubulation protein from magnetotactic bacteria. Mol Microbiol 76: 480-488.
84. Arakaki A, Webb J, Matsunaga T (2003) A novel protein tightly bound to bacterial magnetic particles in *Magnetospirillum magneticum* strain AMB-1. J Biol Chem 278: 8745-8750.
85. Oestreicher Z, Valverde-Tercedor C, Chen L, Jimenez-Lopez C, Bazylinski DA, *et al*. (2012) Magnetosomes and magnetite crystals produced by magnetotactic bacteria as resolved by atomic force microscopy and transmission electron microscopy. Micron 43: 1331-1335.
86. Amemiya Y, Arakaki A, Staniland SS, Tanaka T, Matsunaga T (2007) Controlled formation of magnetite crystal by partial oxidation of ferrous hydroxide in the presence of recombinant magnetotactic bacterial protein Mms6. Biomat 28: 5381-5389.
87. Arakaki A, Masuda F, Amemiya Y, Tanaka T, Matsunaga T (2010) Control of the morphology and size of magnetite particles with peptides mimicking the Mms6 protein from magnetotactic bacteria. J Colloid Interface Sci 343: 65-70.
88. Draper O, Byrne ME, Li Z, Keyhani S, Barrozo JC, *et al*. (2011) MamK, a bacterial actin, forms dynamic filaments in vivo that are regulated by the acidic proteins MamJ and LimJ. Mol Microbiol 82: 342-354.
89. Rioux JB, Philippe N, Pereira S, Pignol D, Wu LF, *et al*. (2010) A second actin-like MamK protein in *Magnetospirillum magneticum* AMB-1 encoded outside the genomic magnetosome island. PLoS One 5: e9151.
90. Lohße A, Ullrich S, Katzmann E, Borg S, Wanner G, *et al*. (2011) Functional analysis of the magnetosome island in *Magnetospirillum gryphiswaldense*: the *mamAB* operon is sufficient for magnetite biomineralization. PLoS One 6: e25561.

2 Chapter II

1st Publication

Functional Analysis of the Magnetosome Island in *Magnetospirillum gryphiswaldense*: The *mamAB* Operon is Sufficient for Magnetite Biomineralization.

Publication state: published in PLoS One. 2011;6(10):e25561.

Abstract

Bacterial magnetosomes are membrane-enveloped, nanometer-sized crystals of magnetite, which serve for magnetotactic navigation. All genes implicated in the synthesis of these organelles are located in a conserved genomic magnetosome island (MAI). We performed a comprehensive bioinformatic, proteomic and genetic analysis of the MAI in *Magnetospirillum gryphiswaldense*. By the construction of large deletion mutants we demonstrate that the entire region is dispensable for growth, and the majority of MAI genes have no detectable function in magnetosome formation and could be eliminated without any effect. Only <25% of the region comprising four major operons could be associated with magnetite biomineralization, which correlated with high expression of these genes and their conservation among magnetotactic bacteria. Whereas only deletion of the *mamAB* operon resulted in the complete loss of magnetic particles, deletion of the conserved *mms6*, *mamGFDC*, and *mamXY* operons led to severe defects in morphology, size and organization of magnetite crystals. However, strains, in which these operons were eliminated together retained the ability to synthesize small irregular crystallites, and weakly aligned in magnetic fields. This demonstrates that whereas the *mamGFDC*, *mms6* and *mamXY* operons have crucial and partially overlapping functions for the formation of functional magnetosomes, the *mamAB* operon is the only region of the MAI, which is necessary and sufficient for magnetite biomineralization. Our data further reduce the known minimal gene set required for magnetosome formation and will be useful for future genome engineering approaches.

Introduction

The ability of magnetotactic bacteria (MTB) to orient in the earth's magnetic field is based on specific organelles, the magnetosomes. In the α-proteobacterium *Magnetospirillum gryphiswaldense* and related MTB, magnetosomes consist of magnetite (Fe_3O_4) crystals enclosed by a phospholipid membrane.

This magnetosome membrane (MM) contains a specific set of >20 proteins, which direct the biomineralization of highly ordered crystals [1,2,3]. Synthesis of magnetosomes has recently emerged as a model for prokaryotic organelle formation and biomineralization [4,5]. In addition, magnetosomes represent biogenic magnetic nanoparticles with unique characteristics, which make them attractive for use in a wide range of biomedical and biotechnological applications [4,6,7].

Although the mechanism of magnetosome synthesis is not understood in detail, several recent studies revealed that the formation of functional magnetosomes depends on several steps, which include the invagination of MM vesicles from the inner membrane [8,9], the transport of iron and crystallization of magnetite within these vesicles [10], and the assembly of mature crystals into a linear chain along a filamentous cytoskeletal structure [9,11,12,13]. It has been also become clear that each of these steps is under strict genetic control. By proteomic analysis of *M. gryphiswaldense* (in the following referred to as MSR), genes encoding the MM-specific proteins were identified within a single genomic magnetosome island (MAI) [14,15]. The functional significance of this region was confirmed by a comparative genomics approach, which revealed that magnetotaxis signature genes are predominantly located within the MAI [16]. Because of their general conservation in other cultivated and uncultivated α-proteobacterial MTB [3,17,18,19] it has been suggested that the MAI was transferred horizontally [15,16,18,20,21]. This was further corroborated by the recent discovery of homologous gene clusters in the δ-proteobacteria *Desulfovibrio magneticus* RS-1 [22] and the multicellular magnetotactic prokaryote (MMP) [23], as well as in the deep-branching *Nitrospirae*-phylum [21].

In addition to all genes, so far implicated in magnetosome biomineralization, the MAI of MSR contains a number of genes with unknown functions and numerous transposase genes that account for >20% of the coding region [14]. Owing to frequent homologous recombinations between the numerous direct or inverted repeats associated with transposase genes, the MAI is genetically unstable, resulting in frequent spontaneous loss of the magnetic phenotype [15,24]. In MSR all known magnetosome genes are comprised within four gene clusters known as *mms6*, *mamGFDC*, *mamAB*, and *mamXY* operons. First experimental indications for their functional significance in magnetosome formation came from the isolation of a non-magnetic mutant strain, which had lost 80 kb of the MAI by a spontaneous deletion that included the *mamAB*, *mms6* and *mamGFDC* operons [25].

Targeted deletion of the entire *mamGFDC* operon revealed that the small MamGFDC proteins, which account for >35% of all magnetosome-associated proteins, are not essential, but involved in size control, since mutant cells formed smaller and less regular magnetite crystals [26]. In a recent study by Murat *et al*. deletion analysis of the MAI in *M. magneticum* (referred to as AMB) revealed three regions, which are crucial for magnetite crystal formation [27]. Whereas the deletion of the R2 and R3 regions including parts of the *mamGFDC* and *mms6* operons led to severe defects in the size and morphology of the crystals, loss of the *mamAB* operon resulted in cells entirely devoid of magnetite crystals [27]. Only the deletion of *mamE*, *M*, *N*, *O*, *L*, *I*, and also of *mamQ* and *mamB*, if co-deleted with their respective duplicates outside the *mamAB* operon, entirely abolished magnetite synthesis. Non-magnetic cells were also

observed upon deletion of this operon in MSR [25]. This suggested that only the *mamAB* operon may contains genes that are absolutely essential [27]. However, it has remained unknown whether this region is also sufficient for magnetosome biomineralization in the absence of other magnetosome genes, since possible genetic redundancy was suggested by the identification of genes, which are identical or similar to genes from *mamAB* operon and partially encoded within a ”magnetosome islet” located elsewhere in the genome of AMB [28].

Despite morphological similarities between the strains AMB and MSR, previous studies suggested that function of orthologous genes might be somewhat distinct in these organisms depending on their different genetic context [8], since only about 50% of all genes are shared by the genomes of these two strains [16]. In particular, the MAI regions flanking the magnetosome operons show a divergent organization, gene content and were speculated to possibly harbor additional determinants for magnetosome formation [16,18].

Here, we show that highly expressed and conserved genes within the MAI of MSR are mostly confined to the *mms6*, *mamGFDC*, *mamXY*, and *mamAB* operons. By deletion of these operons, either independently or in combination, we demonstrate that all four of them have crucial and partially overlapping functions in the synthesis of functional magnetosomes, whereas only the *mamAB* operon is absolutely essential for magnetite biomineralization. Intriguingly, even in the absence of all other three operons as well of further parts of the MAI, the *mamAB* operon proved sufficient to maintain synthesis of small magnetite crystals. A further motivation for this study was to explore the potential for reduction of dispensable or instable gene content from the residual MAI. By using an improved Cre-*lox*-based technique, we demonstrate that 115 kb of the MAI can be deleted without any consequences for growth, while 59 kb have no obvious function in magnetosome synthesis.

Results

Expression of MAI genes coincides with their conservation and operon localization

Besides numerous (>50) transposase and phage related genes, the *mam* and *mms* operons within the MAI are flanked by a number of ORFs, mostly annotated as hypothetical genes, which may represent either unrecognized determinants for magnetosome formation, genes with unknown different functions, or simply pseudogenes or misannotations. To tentatively distinguish between regions of predicted relevance and those not likely involved in magnetotaxis, we reasoned that putative magnetosome genes are expected (I) to lack strong prediction of other cellular functions, (II) to be highly conserved among MTB, and (III) to be expressed during magnetosome synthesis. We therefore reassessed functional annotation of the MAI against current databases. Only 12 of the MAI genes have functionally predicted homologs outside MTB (Fig. 2.1), which encode three hemerythrin-like proteins, putative regulatory pro-

teins, secretion components, a sensory transduction histidine kinase, a partition-related protein, and an IdiA fragment (Tab. S1). To identify conserved genes, we tested by blastp analysis the presence of all genes from the MAI of MSR against all genomic information available from cultivated MTB (Fig. 2.1, Tab. S2.1). Genes that are highly conserved between several MTB were found mostly confined to the *mam* and *mms* operons, where ten ORFs (*mamE*, *K*, *M*, *O*, *A*, *Q*, *B*, *T*, and with lower similarity *mamI* and *mamP*) are conserved in all analyzed strains including MSR, AMB, *Desulfovibrio magneticus* RS-1, *M. magnetotacticum* MS-1, *Magnetococcus marinus* MC-1, and *Magnetovibrio blakemorei* MV-1. *MamE*, *I*, *K*, *M*, *O*, *P*, *A*, *Q*, *B* genes were also detected in the metagenomic MAI fragment Fos001, whereas a second metagenomic clone Fos002 lacks mamI but contains *mamT* [20]. *MamE*, *I*, *M*, *P*, *A*, *B*, and two *mamQ* homologs were also found in the incomplete MAI sequence of "*Candidatus* Magnetobacterium bavaricum" [21]. Nine ORFs have homologs in only one other MTB (Fig. 2.1), and 41 genes are shared by at least all magnetospirilla (Fig. 2.1).

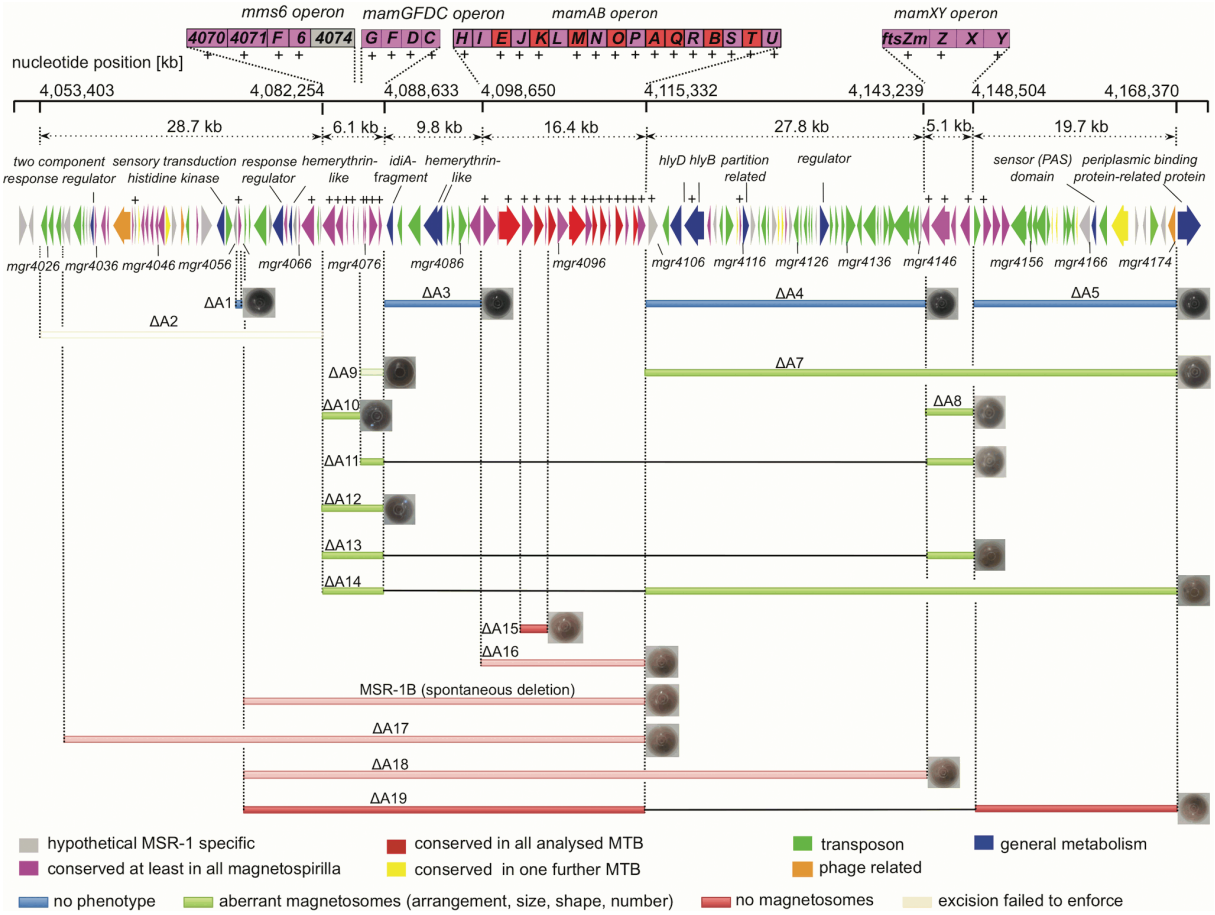

Figure 2.1: **Molecular organization and characteristics of the MAI of *M. gryphiswaldense***. Extensions of deletions are shown by bars of different colors indicating the general phenotype. For overview, strains generated in previous studies are shown in semi-transparent color. The magnetite content of mutant strains is illustrated by the color of corresponding cell pellet. Degree of gene conservation is highlighted by different colors. Genes found expressed by proteomic analysis are indicated by "+".

However, only 7 of these genes show positional conservation within the MAI of AMB, whereas the rest is located elsewhere in the genome in the latter strain. Twenty-two genes, which are mostly confined to

larger regions close to the putative boundaries of the MAI, are specific for MSR (i. e., have no homolog in any other organism), and appear less likely to represent determinants required for magnetosome formation. Thus, hypothetical genes outside the *mam* and *mms* operons are poorly conserved, with none of them found shared by all sequenced MTB. To identify expressed products of ORFs encoded within the MAI, we performed proteomic analyses of magnetosomes, as well as intracellular soluble and membrane-enriched protein fractions of cells grown under magnetite forming conditions. In total, 923 proteins were identified by 1D LC-MS/MS analysis, or from spots detected on 2D gels. In summary, only 33 proteins encoded within the MAI were found expressed in the membrane or magnetosome fraction of MSR. These for instance include, with the exception of Mgr4074, MamI, MamL, and MamX, all proteins encoded by the *mamAB*, *mamGFDC*, *mms6*, and *mamXY* operons, whereas only seven genes outside the *mam* and *mms* operons were found expressed (*mgr4041*, *mamW*, *mgr4067*, *mgr4106*, *mgr4109*, *mgr4115*; *mgr4152*, Fig. 2.1; Tab. S2.1) as well as one gene barely inside the boundaries of the 130 kb region (*mgr4022*) [29]. With the exception of MamK, none of the MAI proteins was detected within the soluble protein fraction among the analyzed spots.

Mutagenesis of MAI genes

By excluding putatively essential genes such as tRNA and rRNA genes, we predicted a core region of 115 kb from *mgr4026* to *mgr4174*, comprising 149 ORFs that are probably not important for central metabolic functions and including all so far known magnetosome genes. According to bioinformatic prediction and expression data, this region was divided into partially overlapping target regions for mutagenesis (Fig. 2.1). We constructed 13 mutant strains, in which single or several of these targets were excised, resulting in deletions between 400 bp and 61 kb. Shorter deletions (up to 7 kb) were generated by allelic replacement (double crossover mediated by homologous recombination, Fig. S2.1A) [30], whereas Cre-*lox* excision (Fig. S2.1B; Fig. S2.2) [25,31], was used for the construction of larger deletions between 5 and 53 kb.

We noticed that success of deletion mutagenesis was not fully predictable. For instance, whereas we previously generated the ΔA17 deletion in the MSR-1B background [25], we failed to enforce deletion of parts of that region (ΔA2) in the WT background despite of repeated attempts. With few exceptions described below, all mutants including the longest deletion (ΔA14) extending over 58.9 kb exhibited WT-like growth, indicating that no central metabolic functions are encoded by deleted MAI genes. However, Cmag measurements and TEM of mutant strains revealed three different classes of phenotypes with respect to magnetosome formation: (I) Mutants that were unaffected in magnetosome formation, i. e. cells were virtually WT-like with respect to crystal appearance (shape, size, number per cell and alignment) including the long deletions ΔA3 (9.8 kb), ΔA4 (27.8 kb), and ΔA5 (19.7 kb), as well as Δ*mamW* (411 bp), eliminating a protein that was previously identified as associated with magnetosomes in MSR [15,16]. (II) Mutants, in which magnetosome formation was entirely abolished, as indicated by a pale pink to orange cell pellet (in contrast to the black appearance of the WT), lack of a magnetic response

(Cmag=0) and the absence of any electron dense particles. The non-magnetic mutants ΔA19, in which an additional 19.7 kb fragment was excised in the background of deletion mutant MSR-1B, and ΔA15 comprising the *mamJKL* genes, had in common a deletion of either the entire *mamAB* operon or parts of it, similar to strains MSR-1B, ΔA16, ΔA17 and ΔA18, which had been generated in previous studies [15,25]. (III) A third class of mutant strains still exhibited a magnetic response, but cells were gradually affected in magnetosome biomineralization or assembly, resulting in fewer, smaller and irregular crystals or distorted chains (Fig. 2.2).

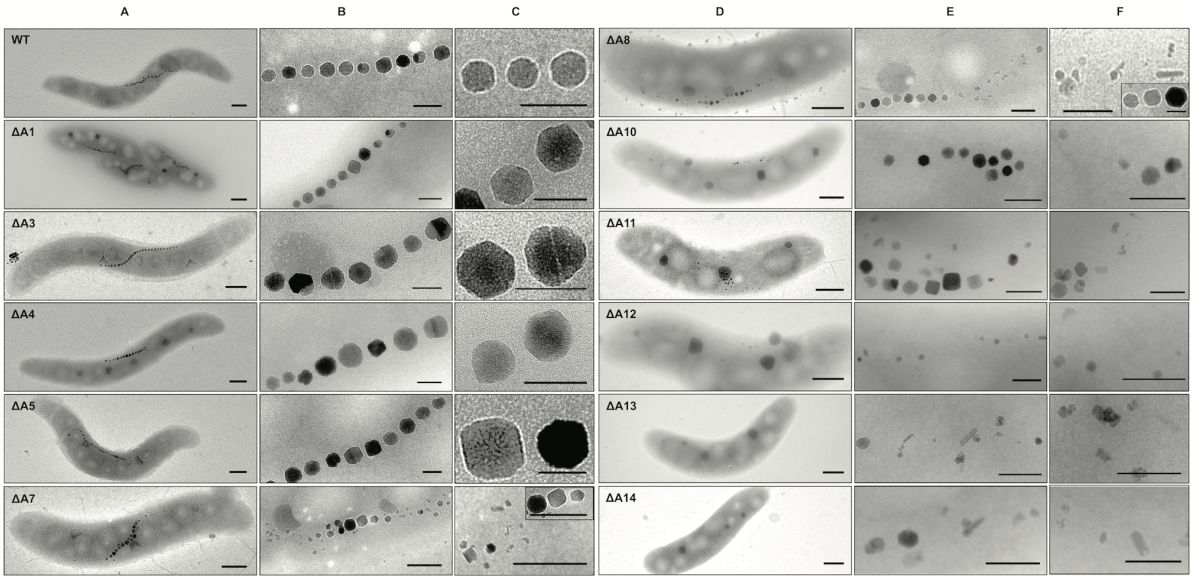

Figure 2.2: **TEM micrographs of cells (A, D) and magnetosome morphologies (B, C, E, F) observed within the generated deletion mutants**. Scale bar: 400 nm in A and D; 50 nm in B and C; 100 nm in E and F.

Mutants of this class could be recognized by variable intensities of brownish color of colonies and cell pellets (Fig. 2.1). Single-operon deletions of *mms6* (ΔA10) and *mamXY* (ΔA8) showed a significantly reduced magnetic response, but still contained electron-dense particles with different sizes and shapes (Tab. 2.1). Strain ΔA10 had smaller crystals (Tab. 2.1) that were scattered throughout the cell or aligned in irregular, widely spaced ”pseudo-chains” (i. e. with <10 crystals per chain; Fig. 2.2). Crystals between 25 and 30 nm were predominant, whereas particles larger than 50 nm were not observed, unlike WT crystals that were most frequently between 40 and 50 nm with a maximum size up to 70 nm (data not shown). Besides cubo-octahedral crystals also heterogeneous crystal shapes were observed (Fig. 2.2). Complementation with fragments comprising genes *mgr4072*, *mgr4073*, and *mgr4074* restored size, shape and alignment of crystals to WT range within about one third of the cells (data not shown).

Strain ΔA8 had an inconsistent phenotype. TEM revealed a variety of magnetosome appearances between different cells, including those lacking any electron-dense particles (Fig. 2.3 A), and those with non-uniform, small crystals lacking any chain configuration (Fig. 2.3 B-F). Remarkably, many cells contained two distinct types of crystals: short chains of almost regular (i.e. cubicle-shaped) crystals, which were flanked by irregular particles with poorly defined morphologies (Fig. 2.3 G-K). Analysis of

about 350 crystals from cells of the latter phenotype revealed that approximately 66% of the crystals were irregular and less electron dense, slightly elongate and poorly crystalline particles (Fig. 2.2). The different particles had distinct size distributions: Among irregular particles, sizes between 15 and 25 nm were most abundant, whereas the regular-shaped crystals had a maximum size of 60 nm, and diameters between 35 to 45 nm were most frequent among them (Fig. 2.3).

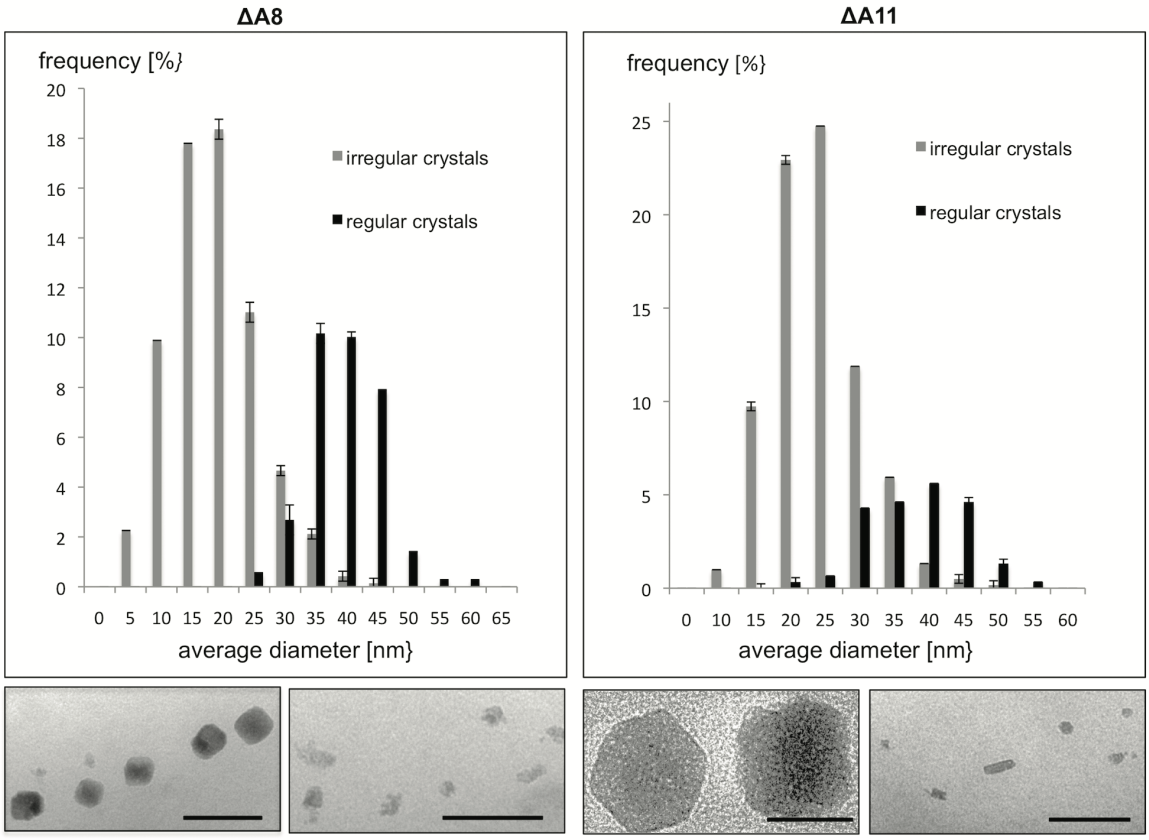

Figure 2.3: **Magnetosome size distributions of electron dense particles within the mutants ΔA8 and ΔA11**. Representative micrographs of corresponding crystal morphologies are shown. Scale bar: 100 nm.

The WT-like phenotype could be restored by transcomplementation with plasmid pmamXY containing the entire *mamXY* cluster (*mgr4147* to *mgr4150*; data not shown). A similar phenotype was observed for the mutant ΔA7 (Fig. 2), in which the deletion included the regions A4 and A5 in addition to the *mamXY* operon (Fig. 2.1; Tab. 2.1), resulting in an average crystal size of 23.5 nm. Crystal number per cell was not significantly affected in comparison to WT (Tab. 2.1).

Operons whose single deletions had magnetosome phenotypes were also deleted in combination with each other. This was also achieved by modification of the previously described Cre-*lox* method [25] by using altered *lox* sequences [32] that enabled the construction of strains bearing multiple unmarked deletions by sequential rounds of insertions and excisions (Fig. S2.1). In strain ΔA12 the entire *mms6* operon was deleted in addition to the adjacent *mamGFDC* operon. This resulted in a stronger phenotype compared to its parent strain Δ*GFDC* [26], i. e. it formed even fewer and smaller magnetosomes that were aberrantly shaped and less regularly aligned (Fig. 2.2). The deletion of both operons also resulted in a particle size reduction of 52% compared to the WT, although crystals were only slightly

smaller than in a deletion of *mms6* operon alone (Tab. 2.1). While crystal numbers per cell were only slightly reduced in comparison to the *mms6* operon mutant, the magnetic response of ΔA12 culture was markedly weaker ($Cmag_{[\Delta A12]}$=0.6; Tab. 2.1).

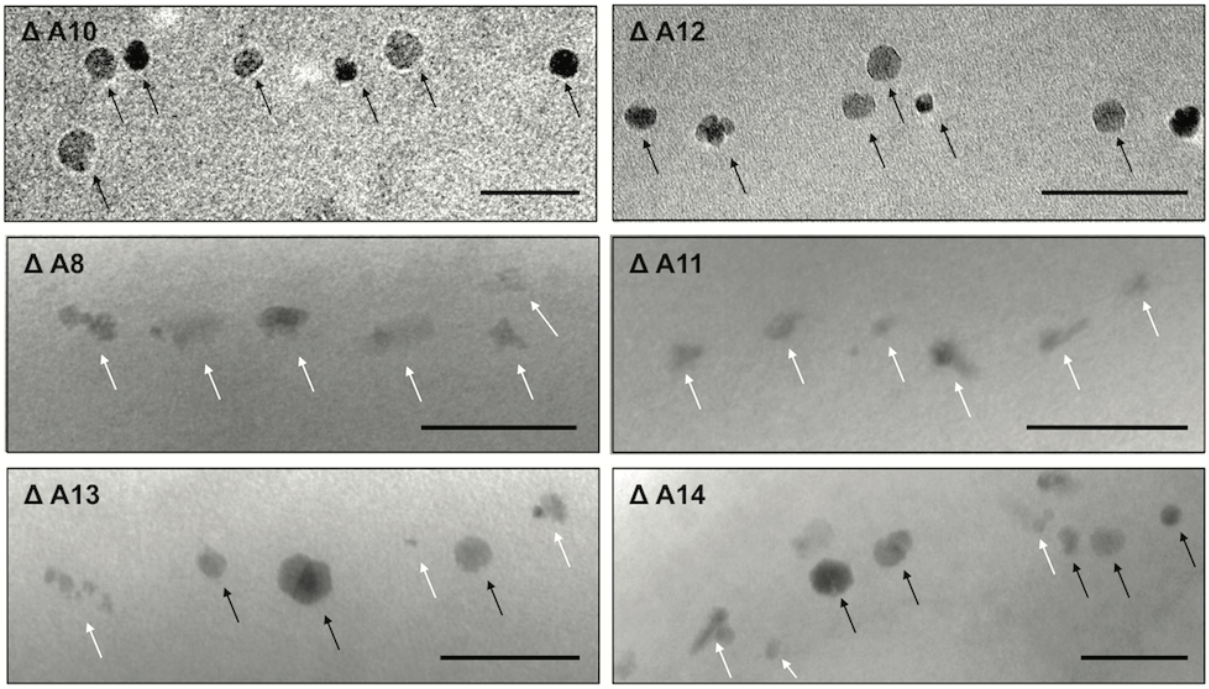

Figure 2.4: **Comparison of magnetosome morphologies within several mutant strains of *M. gryphiswaldense***. Illustration of the combined effect on crystal morphology caused by stepwise excision of *mms6*, *mamGFDC* and *mamXY* operons. Micrographs show various distinct crystal morphologies within strains ΔA10 and ΔA12 (cubicle-shaped, black arrows) and ΔA8 and ΔA11 (elongate shaped, white arrows) that are coexistent within the mutants ΔA13 and ΔA14. Scale bar: 100 nm.

The ΔA11 double deletion mutant of *mamXY* and *mamGFDC* operons showed a reduced Cmag ($Cmag_{[\Delta A11]}$=1.2; Tab. 2.1) and a phenotype as inconsistent as strain ΔA8 (Fig. 2.3). Compared to ΔA8, particles were smaller (Fig. 2.4), fewer per cell and less frequently aligned in chain-like structures (Fig. 2.2). Also, the number of crystals with regular morphology was reduced to 21.8%. We also eliminated *mms6*, *mamGFDC*, and *mamXY* operons altogether using two approaches: While sequential triple deletion by allelic replacement of the three regions resulted in strain ΔA13, deletion of the *mamGFDC* and *mms6* operons in a parental background (ΔA7) that already lacked the entire right arm of the MAI (about 53 kb) containing the *mamXY* operon resulted in strain ΔA14 (Fig. 2.1). Remarkably, both strains still displayed a detectable, although weak magnetic response ($Cmag_{[\Delta A13]}$=0.3; $Cmag_{[\Delta A14]}$=0.5) and contained tiny misshapen electron dense crystallites (Fig. 2.2; Tab. 2.1). Crystal sizes were decreased to 54.8% of WT size and 84.8% of ΔA8 size, but were identical between ΔA13 and ΔA14 strains (Tab. 2.1). From all mutants, both strains ΔA13 and ΔA14 contained the fewest magnetosome number per cell (12-13 in average) and crystal shapes resembled the irregular morphologies found in strains ΔA7, ΔA8, ΔA10, ΔA11, and ΔA12. Thus, the phenotype of ΔA13 and ΔA14 is characterized by the coexistence of distinct particle morphologies found in the respective single operon deletion mutants (Fig. 2.5).

Table 2.1: **Characteristics of MAI deletion mutants.**

Name of the strain	Deleted genes	Method of deletion	Extend of deletion	Phenotypic characteristics		
				Cmag[a]	Average magnetosome size [nm]	Number of magnetosomes per cell
Wild type [53]	/	/	/	2.0±0.1	47.8-35.6[b]	34.3±8.4
ΔA1 (ΔmamW)	*mgr4057*	allelic replacement	411 bp	WT	WT (37.2±10.7)	WT (28.8±4.3)
ΔA2	*mgr4026* to *mgr4069*	Cre-*lox* two vectors	28,728 bp	/	/	/
ΔA3	*mgr4079* to *mgr4088*	Cre-*lox* two vectors	9,828 bp	WT	WT (41.2±13.7)	WT (27.8±4.7)
ΔA4	*mgr4106* to *mgr4146*	Cre-*lox* two vectors	27,795 bp	WT	WT (39.7±15.5)	WT (28.5±8.2)
ΔA5	*mgr4151* to *mgr4174*	Cre-*lox* two vectors	19,651 bp	WT	WT (35.0±14.2)	WT (29.9±8.6)
ΔA7	*mgr4106 to mgr4174*	Cre-*lox* two vectors	52,823 bp	Intermediate	Intermediate (23.5±15.9)	WT (35.0±8.2)
ΔA8 (ΔmamXY)	*mgr4147* to *mgr4150*	allelic replacement	5,077 bp	Intermediate	Intermediate (23.0±11.5)	WT (32.2±11.4)
ΔA9 (ΔGFDC) [26]	*mgr4075 to mgr4078*	allelic replacement	2,071 bp	Intermediate [26]	Intermediate [26]	WT [26]
ΔA10 (Δmms6 op)	*mgr4070* to *mgr4074*	allelic replacement	3,632 bp	Intermediate	Intermediate (19.7±6.9)	Intermediate (16.8±6.2)
ΔA11 (ΔmamGFDC_ ΔmamXY)	*mgr4075* to *mgr4078*; *mgr4147* to *mgr4150*	allelic replacement	7,148 bp	Intermediate	Intermediate (20.7±10.3)	Intermediate (25.3±6.0)
ΔA12 (Δmms6 op_ ΔmamGFDC)	*mgr4070* to *mgr4078*	allelic replacement	6,070 bp	Weak	Intermediate (18.4±6.0)	Intermediate (15.3±5.6)

ΔA13 (Δmms6 op_ ΔmamGFDC_ ΔmamXY)	*mgr4070* to *mgr4078*; *mgr4147* to *mgr4150*	allelic replacement	11,050 bp	Weak	Intermediate (19.3±8.1)	Weak (13.0±4.3)
ΔA14 (ΔA7_ Δmms6op_ ΔmamGFDC)	*mgr4106 to mgr4174; mgr4070 to mgr4078*	Cre-*lox* two vectors and allelic replacement	58,893 bp	Weak	Intermediate (19.7±7.7)	Weak (12.1±3.4)
ΔA15 (ΔmamJKL)	*mgr4092* to *mgr4094*	allelic replacement	2,656 bp	non magnetic	0	0
ΔA16 (mamAB#K7) [25]	*mgr4089* to *mgr4105*	Cre-*loxP* two vectors	16,362 bp	non magnetic	0	0
ΔA17 (MSR-1_SU12) [25]	*mgr4029* to *mgr4105*	Cre-*loxP* two vectors	61,000 bp	non magnetic	0	0
ΔA18 (MSR-1B mgr4058 to mgr4146) [25]	*mgr4058* to *mgr4146*	Cre-*loxP* two vectors	67,345 bp	non magnetic	0	0
ΔA19	*mgr4058 to mgr4105; mgr4151* to *mgr4175*	Cre-*loxP* two vectors	60,033 bp	non magnetic	0	0

[a] WT: no signiffcant difference to WT cells; Intermediate: 80-40% of WT characteristic; Weak: less than 40% of WT characteristic

[b] Mean sizes were found slightly variable within a range between 48-35 nm due to minor variations of cultivation conditions and growth phase

Discussion

We performed a comprehensive investigation of the MAI in MSR by combined bioinformatic, proteomic and genetic analysis. With the exception of *mgr4041* and *mgr4106*, which are MSR-specific, all other genes from the 115 kb core region that were found expressed are also highly conserved in magnetospirilla or even all MTB. The majority of expressed genes (26 of 33) were localized within the *mms6*, *mamGFDC*, *mamAB*, and *mamXY* operons [25,27]. These were also the only regions, which displayed a magnetosome phenotype upon their deletion. Thus, in contrast to previous observations in AMB [27], conservation and expression of MAI genes showed a strong correlation with a function in magnetosome formation. We used a Cre-*lox* based method [25,31], which allows the efficient excision of large fragments. The largest single deletion obtained by this method comprised 53 kb in strain ΔA7. Using modified *lox*-sites enabled multiple sequential rounds of marker-less deletions. This resulted in strains, in which up to 59 kb were deleted, comprising about 50% of the MAI and encoding 78 ORFs.

Despite of repeated attempts, no deletion of the A2 region (Fig. 2.1) was obtained. Whereas the ΔA17 (MSR_SU12) deletion was straightforwardly generated in the MSR-1B background in a previous approach [25], we failed to partially delete this region (ΔA2) in the WT background. It remains to be shown whether this was due to low efficiency, or if deletion of this region would be lethal only in the presence of the residual MAI genes. The absence of detectable phenotypes apart from magnetosome formation in the deletion strains indicates that the MAI encodes no important functions for growth under laboratory conditions. Whereas less than 25% of the MAI region could be associated with magnetosome formation, more than 50% of the MAI seems to have no obvious functions.

Remarkably, among the genes with no phenotype are several of the magnetospirilla-specific genes, such as *mgr4067*, *mgr4109*, *mgr4115*, *mgr4152*, and *mgr4057* (*mamW*), which had been previously implicated in magnetite synthesis because of its magnetosome expression [16]. We also failed to detect a phenotype for the two hemerythrin-like genes harbored within the deleted A3 region. Because of their MAI localization and the known functions of hemerythrins from other organisms in the sensing or transport of oxygen and iron, it was speculated that these proteins may play a role in magneto-aerotaxis and magnetosome formation [33,34]. However, it cannot be excluded that their loss can be compensated by the numerous (i. e. 23) homologs encoded elsewhere in the genome. Taken together, although it remains possible that some deletion strains could show a phenotype under different growth conditions, or only in combination with other deletions, most of the genes flanking the identified magnetosome operons have no functional relevance and might just represent genetic ”junk” or remnants from previous transfer events of the MAI.

Our deletion analysis confirmed several results of previous studies, in which the functional significance of several regions, such as *mamAB*, *mms6*, and *mamGFDC* were shown for AMB [27], and partially for MSR [25,26]. However, despite of the high similarity of targeted genes, we also found several striking differences between the two organisms. One example is the conserved *mamXY* operon, which contains

several magnetotaxis signature genes, and for which a key role was predicted mostly based on comparative genome analysis [16]. While MamY was recently implicated in MM biogenesis in AMB [35], MamX has similarity to the serine like proteases MamE and MamS, whereas MamZ is an ortholog of MamH and resembles permeases of the major facilitator superfamily. The FtsZ-like gene has homology to the tubulin-like protein, which is involved in cell division in many bacteria [36]. In contrast to the *mamXY* operon deletion in AMB, which did not show a strong effect [27], we found that *mamXY* genes have a crucial function in magnetite biomineralization of MSR. This is consistent with the results obtained by Ding *et al*., who reported that the deletion of the *ftsZ-like* gene alone already resulted in the synthesis of smaller, predominantly superparamagnetic particles [37].

The deletion of all *mamXY* genes had an even stronger effect, which is different from all previously reported magnetosome phenotypes. Strikingly, all deletions including this operon had an inconsistent phenotype, which varied between different cells. In addition to size reduction, this was characterized by the co-existence of various distinct magnetosome morphologies within many single cells.

The deletion of genes from the *mms6* operon had slightly different effects in AMB and MSR too. Single deletion of the *mms6* gene in AMB already caused smaller and elongated crystals [38], thus resembling the R3 mutant constructed by Murat *et al*. [27], which comprised deletion of genes from both the *mms6* and *mamGFDC* operons. In contrast, 58% of crystals within cells of the single operon deletion mutant in MSR (strain ΔA10) still had cubicle-shaped appearance, whereas elongate crystals were absent from the mutants ΔA10 and ΔA12. Although the phenotypes cannot be directly compared, since the extents of deletions are not fully congruent, this might point towards slightly distinct functions of the homologous regions in AMB and MSR. In MSR co-deletion of the *mms6* operon together with *mamGFDC* in strain ΔA12 resulted in a further reduction of shape regularity and alignment of crystals, but only in a slight decrease of size, whereas the number of particles per cell was similar to strain ΔA10 (Δ*mms6*). This argues for a certain functional overlap between the two operons, which is consistent with the high similarity between some of the encoded proteins, such as MmsF and MamF, which share 61% identity, and Mms6, which shares a conspicuous LG-rich motif with MamG and MamD [2,39]. However, single operon mutant phenotypes suggest that genes of the *mms6* operon have a more pronounced effect on crystal size, number and alignment than *mamGFDC*, perhaps by direct binding to the surface of nascent crystallites through hydrophilic domains [40], or by enlarging the surface and curvature of MM vesicles, which spatially constrain the growth of magnetite crystals [26].

Intriguingly, even in the ΔA14 and ΔA13 strains, in which the *mms6*, *mamGFDC*, and *mamXY* operons were deleted in triple, magnetite formation was not entirely abolished and cells still weakly aligned in magnetic fields, although crystal sizes were further decreased and elongate crystals were present. Despite of a functional overlap in size control of magnetite crystals, the roles of the *mms6*, *mamGFDC*, and *mamXY* genes are not fully redundant, as indicated by the distinct morphologies found in their respective single operon deletions. While simultaneous excision of the *mamGFDC* and *mms6* operon lead to heterogeneous cubicle-shaped crystals, loss of *mamXY* operon lead to poorly crystalline and elon-

gate crystals, which were also detected within the double deletion mutant of *mamXY* and *mamGFDC*. Interestingly, these effects are superimposed in the *mamGFDC*, *mms6*, *mamXY* triple deletion strains (ΔA13 and ΔA14), in which crystallites of both morphologies are present. Altogether, these observations indicate that the *mamGFDC*, *mms6* and *mamXY* operons have important and additive functions for the formation of regularly shaped crystals that are sufficiently large to be functional for interaction with the weak geomagnetic field [39,41].

Consistent with observations for AMB [27], only the *mamAB* operon contains genes, which are essential for magnetosome formation. However, our data for the first time demonstrate that the *mamAB* operon is the only region of the MAI, which is necessary and sufficient to maintain magnetite biomineralization even in the absence of the *mamGFDC*, *mms6*, and *mamXY* clusters. Although it cannot be precluded that additional, so far unrecognized determinants might be encoded outside the MAI, this further reduces the minimal gene set, which is likely required for biomineralization. As the MamJ and MamK proteins were already shown to have roles in magnetosome chain assembly rather than in biomineralization [8,42], the core set of MAI genes essential for magnetite biomineralization in MSR can be expected to be less than 15, and according to the identification of further non-essential genes in the *mamAB* operon of AMB (*mamA*, *H*, *U*, *V*, *P*, *T*, *R*, *S*) [27] this number is likely to shrink further.

Our results will be also useful for future genome reduction approaches. Comparable experiments in other bacteria have shown that large-scale deletions of target sequences are extremely powerful in engineering of strains optimized for biotechnological processes [43,44,45]. By stepwise removal of unnecessary or problematic genomic regions, in future approaches also strains of MSR can be engineered for the production of magnetosome particles, which may exhibit increased genetic stability due to the elimination of repeats and transposases, or might show improved growth or increased magnetosome yields because of reduced gene content. In summary, deletion analysis of MAI indicates that whereas only the *mamAB* operon is essential, different regions have important functions in control of size and morphology of magnetosomes. Thus, modular deletion or expression of various magnetosome genes and operons could be used for the production of engineered magnetic nanoparticles with tailored properties.

Materials and Methods

Bacterial strains, plasmids, and culture conditions

Bacterial strains and plasmids used in this study are listed in Table S2.2. *M. gryphiswaldense* strains were grown microaerobically in modified flask standard medium (FSM) at 30°C [46] and moderate agitation (120 rpm). *E. coli* strains were cultivated as previously described [47] and 1 mM DL-α, ε-diaminopimelic acid (DAP) was added to lysogeny broth media growing *E. coli* BW29427 (K. Datsenko and B. L. Wanner, unpublished data). Strains were routinely cultured on dishes with 1.5% (w/v) agar.

For strains carrying recombinant plasmids, media were supplemented with 25 g/ml kanamycin (Km), 12 g/ml tetracycline (Tet), and 15 g/ml gentamicin (Gm) for *E. coli* strains, and 5 g/ml kanamycin, 5 g/ml tetracycline, and 20 g/ml gentamicin for *M. gryphiswaldense* strains, respectively. Blue-white screening was performed by adding 50 μg/ml X-Gluc (5-bromo-4-chloro-3-indoxyl-D-glucuronidase; AppliChem, Darmstadt, Germany) to FSM.

Molecular and genetic techniques

The working draft of *M. gryphiswaldense* genome sequence (GenBank accession number No. CU459003) was used for primer design. Oligonucleotids (Tab. S2.3) were purchased from Sigma-Aldrich (Steinheim, Germany). Chromosomal DNA of *M. gryphiswaldense* was isolated as described previously [3]. Plasmids were constructed by standard recombinant techniques as described in detail in the supplemental data. All constructs were sequenced on an ABI 3700 capillary sequencer (Applied Biosystems, Darmstadt, Germany), utilizing BigDye Terminator v3.1. Sequence data were analyzed with Software Vector NTI Advance® 11.5 (Invitrogen, Darmstadt, Germany).

Analytical methods

Magnetic reaction of cells was checked by light microscopy applying a bar magnet. Optical density and magnetic response (Cmag) of exponentially growing cells were measured photometrical at 565 nm as previously reported [48]. For Cmag messurement a magnetic field of approximately 70 millitesla was used [48]. As this field can possibly magnetize small magnetosomes in the superparamagnetic size range and cause artificially high Cmag readings, all putative magnetosome phenotypes were verified by transmission electron microscopy (TEM). For TEM analysis, exponential cells were 10-fold concentrated and adsorbed onto carbon-coated copper grids. Samples were viewed and recorded with a TECNAI FEI20 microscope (FEI, Eindhoven, Netherlands). Magnetosome crystals were analyzed with respect to size, shape and numbers per cell. Magnetosome crystals were scored for chain formation as described by [8]. For pictures of cell pellets, cells were cultivated anaerobic in FSM and 10^9 cells were concentrated by centrifugation.

Cell fractionation, protein digestion, mass spectrometry, and data analysis

For proteomic analysis *M. gryphiswaldense* WT was grown in microaerobic 1-liter batch cultures and cell fractions (membrane-enriched, soluble, and magnetosomes) were prepared as previously described [2,29]. Soluble proteins were separated in 2D PAGE (pH 4-7 and 3-10). Analysis of 2D gels including relative quantification was done with the Delta2D software (Decodon, Greifswald, Germany). Protein spots were cut from 2D gels, transferred into microtiter plates, and tryptically digested using the Ettan Spot Handling Workstation (GE Healthcare, Munich, Germany). Mass spectra of protein fragments were measured by MALDI-TOF-MS/MS using a Proteome Analyzer 4800 (Applied Biosystems, Munich,

Germany). The parameters for measurements were set as described in [49]. The spectra were searched against the published genome sequence from *M. gryphiswaldense* by using the JCoast 1.6 software [50], and proteins were identified using the Mascot search engine. For analysis of magnetosomes and membrane proteins, gel lanes obtained from 1D-SDS-PAGE were cut into 10 equal slices. Gel slices were digested manually with trypsin and analysed by LC coupled mass spectrometry performed as described by [51]. Relative quantification of membrane proteins was based on spectral counting using Scaffold [52].

Acknowledgement

AL was supported by the Konrad-Adenauer-Stiftung. We are thankful to Dr. D. Albrecht for measurement of mass spectra of protein fragments by MALDI-TOF-MS/MS and Dr. D. Becher for LC-MS/MS analysis (Ernst Moritz Arndt University, Greifswald).

References

1. Schüler D (2004) Molecular analysis of a subcellular compartment: the magnetosome membrane in *Magnetospirillum gryphiswaldense*. Arch Microbiol 181: 1-7.
2. Grünberg K, Müller EC, Otto A, Reszka R, Linder D, *et al*. (2004) Biochemical and proteomic analysis of the magnetosome membrane in *Magnetospirillum gryphiswaldense*. Appl Environ Microbiol 70: 1040-1050.
3. Grünberg K, Wawer C, Tebo BM, Schüler D (2001) A large gene cluster encoding several magnetosome proteins is conserved in different species of magnetotactic bacteria. Appl Environ Microbiol 67: 4573-4582.
4. Faivre D, Schüler D (2008) Magnetotactic bacteria and magnetosomes. Chem Rev 108: 4875-4898.
5. Murat D, Byrne M, Komeili A (2010) Cell biology of prokaryotic organelles. Cold Spring Harb Perspect Biol 2: a000422.
6. Lang C, Schüler D (2006) Biogenic nanoparticles: production, characterization, and application of bacterial magnetosomes. J Phys: Condens Matter 18: 2815-2828.
7. Lang C, Schüler D, Faivre D (2007) Synthesis of magnetite nanoparticles for bio- and nanotechnology: genetic engineering and biomimetics of bacterial magnetosomes. Macromol Biosci 7: 144-151.
8. Katzmann E, Scheffel A, Gruska M, Plitzko JM, Schüler D (2010) Loss of the actin-like protein MamK has pleiotropic effects on magnetosome formation and chain assembly in *Magnetospirillum gryphiswaldense*. Mol Microbiol 77: 208-224.

9. Komeili A, Li Z, Newman DK, Jensen GJ (2006) Magnetosomes are cell membrane invaginations organized by the actin-like protein MamK. Science 311: 242-245.
10. Faivre D, Bottger LH, Matzanke BF, Schüler D (2007) Intracellular magnetite biomineralization in bacteria proceeds by a distinct pathway involving membrane-bound ferritin and an iron(II) species. Angew Chem Int Ed Engl 46: 8495-8499.
11. Frankel RB, Bazylinski DA (2006) How magnetotactic bacteria make magnetosomes queue up. T Microbiol 14: 329-331.
12. Scheffel A, Gruska M, Faivre D, Linaroudis A, Plitzko JM, *et al*. (2006) An acidic protein aligns magnetosomes along a filamentous structure in magnetotactic bacteria. Nature 440: 110-114.
13. Faivre D, Fischer A, Garcia-Rubio I, Mastrogiacomo G, Gehring AU (2010) Development of cellular magnetic dipoles in magnetotactic bacteria. Biophys J 99: 1268-1273.
14. Schübbe S, Kube M, Scheffel A, Wawer C, Heyen U, *et al*. (2003) Characterization of a spontaneous nonmagnetic mutant of *Magnetospirillum gryphiswaldense* reveals a large deletion comprising a putative magnetosome island. J Bacteriol 185: 5779-5790.
15. Ullrich S, Kube M, Schübbe S, Reinhardt R, Schüler D (2005) A hypervariable 130-kilobase genomic region of *Magnetospirillum gryphiswaldense* comprises a magnetosome island which undergoes frequent rearrangements during stationary growth. J Bacteriol 187: 7176-7184.
16. Richter M, Kube M, Bazylinski DA, Lombardot T, Glockner FO, *et al*. (2007) Comparative genome analysis of four magnetotactic bacteria reveals a complex set of group-specific genes implicated in magnetosome biomineralization and function. J Bacteriol 189: 4899-4910.
17. Schübbe S, Williams TJ, Xie G, Kiss HE, Brettin TS, *et al*. (2009) Complete genome sequence of the chemolithoautotrophic marine magnetotactic coccus strain MC-1. Appl Environ Microbiol 75: 4835-4852.
18. Jogler C, Kube M, Schübbe S, Ullrich S, Teeling H, *et al*. (2009) Comparative analysis of magnetosome gene clusters in magnetotactic bacteria provides further evidence for horizontal gene transfer. Environ Microbiol 11: 1267-1277.
19. Matsunaga T, Okamura Y, Fukuda Y, Wahyudi AT, Murase Y, *et al*. (2005) Complete genome sequence of the facultative anaerobic magnetotactic bacterium Magnetospirillum sp. strain AMB-1. DNA Res 12: 157-166.
20. Jogler C, Lin W, Meyerdierks A, Kube M, Katzmann E, *et al*. (2009) Toward cloning of the magnetotactic metagenome: identification of magnetosome island gene clusters in uncultivated magnetotactic bacteria from different aquatic sediments. Appl Environ Microbiol 75: 3972-3979.

21. Jogler C, Wanner G, Kolinko S, Niebler M, Amann R, et al. (2011) Conservation of proteobacterial magnetosome genes and structures in an uncultivated member of the deep-branching *Nitrospira* phylum. Proc Natl Acad Sci U S A 108: 1134-1139.
22. Nakazawa H, Arakaki A, Narita-Yamada S, Yashiro I, Jinno K, *et al*. (2009) Whole genome sequence of *Desulfovibrio magneticus* strain RS-1 revealed common gene clusters in magnetotactic bacteria. Genome Res 19: 1801-1808.
23. Abreu F, Cantao ME, Nicolas MF, Barcellos FG, Morillo V, *et al*. (2011) Common ancestry of iron oxide- and iron-sulfide-based biomineralization in magnetotactic bacteria. ISME J 1-7.
24. Kolinko I, Jogler C, Katzmann E, Schüler D (2011) Frequent mutations within the genomic magnetosome island of *Magnetospirillum gryphiswaldense* are mediated by RecA. J Bacteriol 193(19): 5328-34.
25. Ullrich S, Schüler D (2010) Cre-*lox*-based method for generation of large deletions within the genomic magnetosome island of *Magnetospirillum gryphiswaldense*. Appl Environ Microbiol 76: 2439-2444.
26. Scheffel A, Gardes A, Grünberg K, Wanner G, Schüler D (2008) The major magnetosome proteins MamGFDC are not essential for magnetite biomineralization in *Magnetospirillum gryphiswaldense* but regulate the size of magnetosome crystals. J Bacteriol 190: 377-386.
27. Murat D, Quinlan A, Vali H, Komeili A (2010) Comprehensive genetic dissection of the magnetosome gene island reveals the step-wise assembly of a prokaryotic organelle. Proc Natl Acad Sci U S A 107: 5593-5598.
28. Rioux JB, Philippe N, Pereira S, Pignol D, Wu LF, *et al*. (2010) A second actin-like MamK protein in *Magnetospirillum magneticum* AMB-1 encoded outside the genomic magnetosome island. PLoS One 5: e9151.
29. Uebe R, Voigt B, Schweder T, Albrecht D, Katzmann E, *et al*. (2010) Deletion of a *fur-like* gene affects iron homeostasis and magnetosome formation in *Magnetospirillum gryphiswaldense*. J Bacteriol 192: 4192-4204.
30. Schultheiss D, Kube M, Schüler D (2004) Inactivation of the flagellin gene *flaA* in *Magnetospirillum gryphiswaldense* results in nonmagnetotactic mutants lacking flagellar filaments. Appl Environ Microbiol 70: 3624-3631.
31. Marx CJ, Lidstrom ME (2002) Broad-host-range *cre-lox* system for antibiotic marker recycling in gram-negative bacteria. Biotechniques 33: 1062-1067.
32. Suzuki N, Nonaka H, Tsuge Y, Inui M, Yukawa H (2005) New multiple-deletion method for the *Corynebacterium glutamicum* genome, using a mutant lox sequence. Appl Environ Microbiol 71: 8472-8480.
33. Frankel RB, Williams TJ, Bazylinski DA (2006) Magneto-Aerotaxis. In: Schüler D, editor. In Magnetosomes and Magnetoreception in Bacteria. Heidelberg, Germany: Springer Verlag. pp. 1-24.

34. French CE, Bell JM, Ward FB (2008) Diversity and distribution of hemerythrin-like proteins in prokaryotes. FEMS Microbiol Lett 279: 131-145.
35. Tanaka M, Arakaki A, Matsunaga T (2010) Identification and functional characterization of liposome tubulation protein from magnetotactic bacteria. Mol Microbiol 76: 480-488.
36. Erickson HP, Anderson DE, Osawa M (2010) FtsZ in bacterial cytokinesis: cytoskeleton and force generator all in one. Microbiol Mol Biol Rev 74: 504-528.
37. Ding Y, Li J, Liu J, Yang J, Jiang W, *et al*. (2010) Deletion of the *ftsZ-like* gene results in the production of superparamagnetic magnetite magnetosomes in *Magnetospirillum gryphiswaldense*. J Bacteriol 192: 1097-1105.
38. Tanaka M, Mazuyama E, Arakaki A, Matsunaga T (2011) MMS6 protein regulates crystal morphology during nano-sized magnetite biomineralization in vivo. J Biol Chem 286: 6386-6392.
39. Jogler C, Schüler D (2009) Genomics, genetics, and cell biology of magnetosome formation. Annu Rev Microbiol 63: 501-521.
40. Arakaki A, Masuda F, Amemiya Y, Tanaka T, Matsunaga T (2010) Control of the morphology and size of magnetite particles with peptides mimicking the Mms6 protein from magnetotactic bacteria. J Colloid Interface Sci 343: 65-70.
41. Bazylinski DA, Frankel RB (2004) Magnetosome formation in prokaryotes. Nat Rev Microbiol 2: 217-230.
42. Scheffel A, Schüler D (2007) The acidic repetitive domain of the *Magnetospirillum gryphiswaldense* MamJ protein displays hypervariability but is not required for magnetosome chain assembly. J Bacteriol 189: 6437-6446.
43. Komatsu M, Uchiyama T, Omura S, Cane DE, Ikeda H (2010) Genome-minimized Streptomyces host for the heterologous expression of secondary metabolism. Proc Natl Acad Sci U S A 107: 2646-2651.
44. Yu BJ, Sung BH, Koob MD, Lee CH, Lee JH, *et al*. (2002) Minimization of the *Escherichia coli* genome using a Tn5-targeted Cre/*loxP* excision system. Nat Biotechnol 20: 1018-1023.
45. Suzuki N, Okayama S, Nonaka H, Tsuge Y, Inui M, *et al*. (2005) Large-scale engineering of the *Corynebacterium glutamicum* genome. Appl Environ Microbiol 71: 3369-3372.
46. Heyen U, Schüler D (2003) Growth and magnetosome formation by microaerophilic Magnetospirillum strains in an oxygen-controlled fermentor. Appl Microbiol Biotechnol 61: 536-544.
47. Sambrook J, Russell DW (2001) Molecular cloning: a laboratory manual. New York: Cold Spring Harbor Laboratory Press. pp. 1-44
48. Schüler D, Uhl R, Baeuerlein E (1995) A simple light-scattering method to assay magnetism in *Magnetospirillum gryphiswaldense* FEMS Microbiol Lett 132: 139-145.
49. Voigt B, Schweder T, Sibbald MJJ, Albrecht D, Ehrenreich A, *et al*. (2006) The extracellular proteome of *Bacillus licheniformis* grown in different media and under different nutrient starvation conditions. Proteomics 6: 268-281.

50. Richter M, Lombardot T, Kostadinov I, Kottmann R, Duhaime MB, *et al*. (2008) JCoast - a biologist-centric software tool for data mining and comparison of prokaryotic (meta)genomes. BMC Bioinformatics 9: 177.
51. Wolff S, Hahne H, Hecker M, Becher D (2008) Complementary Analysis of the Vegetative Membrane Proteome of the Human Pathogen *Staphylococcus aureus*. Molecular & Cel Proteomics 7: 1460-1468.
52. Stevenson SE, Chu Y, Ozias-Akins P, Thelen JJ (2009) Validation of gel-free, label-free quantitative proteomics approaches: applications for seed allergen profiling. J Proteomics 72: 555-566.
53. Schultheiss D, Schüler D (2003) Development of a genetic system for *Magnetospirillum gryphiswaldense*. Arch Microbiol 179: 89-94.

3 Chapter III

2nd Publication

Biosynthesis of magnetic nanostructures in a foreign organism by transfer of bacterial magnetosome gene clusters.

Publication state: published in Nature Nanotechnology. 2014 Mar;9(3):193-7.

Abstract

The synthetic production of monodisperse single magnetic domain nanoparticles at ambient temperature is challenging[1,2]. In nature, magnetosomes - membrane-bound magnetic nanocrystals with unprecedented magnetic properties - can be biomineralized by magnetotactic bacteria[3]. However, these microbes are difficult to handle. Expression of the underlying biosynthetic pathway from these fastidious microorganisms within other organisms could therefore greatly expand their nanotechnological and biomedical applications[4,5]. So far, this has been hindered by the structural and genetic complexity of the magnetosome organelle and insufficient knowledge of the biosynthetic functions involved. Here, we show that the ability to biomineralize highly ordered magnetic nanostructures can be transferred to a foreign recipient. Expression of a minimal set of genes from the magnetotactic bacterium *Magnetospirillum gryphiswaldense* resulted in magnetosome biosynthesis within the photosynthetic model organism *Rhodospirillum rubrum*. Our findings will enable the sustainable production of tailored magnetic nanostructures in biotechnologically relevant hosts and represent a step towards the endogenous magnetization of various organisms by synthetic biology.

Results and Discussion

The alphaproteobacterium *M. gryphiswaldense* produces uniform nanosized crystals of magnetite (Fe_3O_4), which can be engineered by genetic[6,7] and metabolic means[8] and are inherently biocompatible. The stepwise biogenesis of magnetosomes involves the invagination of vesicles from the cytoplasmic membrane, magnetosomal uptake of iron, and redox-controlled biomineralization of magnetite crystals, as well as their self-assembly into nanochains along a dedicated cytoskeletal structure to achieve one of the highest structural levels in a prokaryotic cell[3,9]. We recently discovered genes controlling magnetosome synthesis to be clustered within a larger (115 kb) genomic magnetosome island, in which they are interspersed by numerous genes of unrelated or unknown functions[6,10]. Although the smaller *mamGFDC*,

mms6 and *mamXY* operons have accessory roles in the biomineralization of properly sized and shaped crystals[6,11], only the large *mamAB* operon encodes factors essential for iron transport, magnetosome membrane (MM) biogenesis, and crystallization of magnetite particles, as well as their chain-like organization and intracellular positioning[6,10,12].

However, it has been unknown whether this gene set is sufficient for autonomous expression of magnetosome biosynthesis. Using recombineering (recombinogenic engineering) based on phage-derived Red-ET homologous recombination, we stitched together several modular expression cassettes comprising all 29 genes (26 kb in total) of the four operons in various combinations (Supplementary Fig. 3.1), but lacking the tubulin-like *ftsZm*. This gene was omitted from its native *mamXY* operon because of its known interference with cell division during cloning. Regions 200-400 bp upstream of all operons were retained to ensure transcription from native promoters[13].

Transposable expression cassettes comprising the MycoMar (*tps*) or Tn5 transposase gene, two corresponding inverted repeats, the origin of transfer *oriT*, and an antibiotic resistance gene were utilized to enable transfer and random chromosomal integration in single copy[14,15] (Supplementary Tables 3.3 and 3.4). Chromosomal reintegration of all cassettes into different non-magnetic single-gene and operon deletion strains of *M. gryphiswaldense* resulted in stable wild type-like restoration of magnetosome biomineralization, indicating that transferred operons maintained functionality upon cloning and transfer (Supplementary Fig. 3.2). We next attempted the transfer of expression cassettes to a foreign non-magnetic host organism (Fig. 3.1).

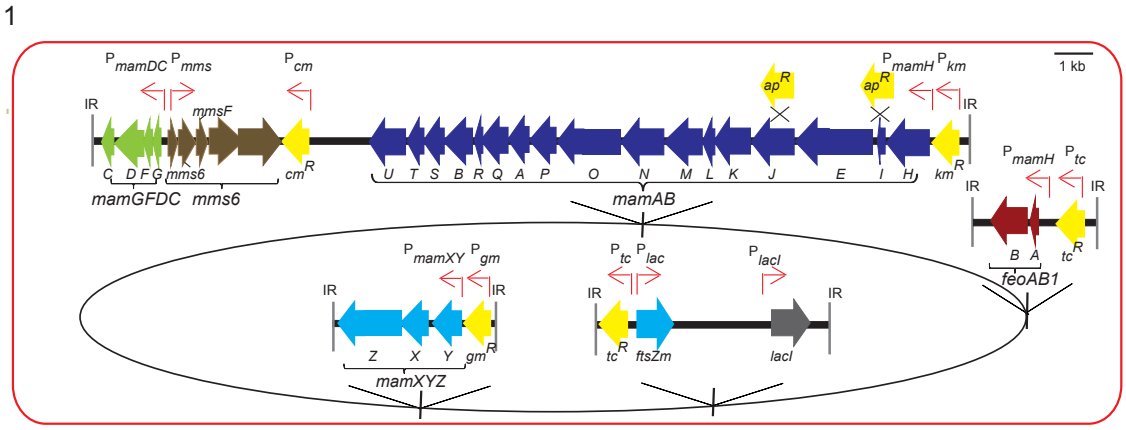

Figure 3.1: **Schematic representation of molecular organization of gene cassettes inserted into the chromosome of *R. rubrum* in a stepwise manner.** Broad arrows indicate the extensions and transcriptional directions of individual genes. Different colours illustrate the cassettes inserted into the chromosome (oval shape, not to scale) as indicated by their gene names in the figure. Shown in yellow are antibiotic resistance genes (km^R, kanamycin resistance; tc^R, tetracycline resistance; ap^R, ampicillin resistance; gm^R, gentamicin resistance). Thin red arrows indicate different promoters (P) driving transcription of inserted genes (P_{km}, P_{gm}, P_{tc}, promoters of antibiotic resistance cassettes; P_{lacI} promoter, *lac* repressor; P_{mms}, P_{mamDC}, P_{mamH}, P_{mamXY}, native promoters of the respective gene clusters from *M. gryphiswaldense*; P_{lac}, *lac* promoter). Crossed lines indicate sites of gene deletions of *mamI* and *mamJ* in strains *R. rubrum_ABG6X_dI* and *R. rubrum_ABG6X_dJ*, respectively. IR, inverted repeat defining the boundaries of the sequence inserted by the transposase.

We chose the photosynthetic alphaproteobacterium *R. rubrum* as a first model because of its biotechnological relevance and relatively close relationship to *M. gryphiswaldense*[16–18] (16S rRNA similarity to *M. gryphiwaldense*=90%). Although the *mamAB* operon alone has been shown to support some rudimentary biomineralization in *M. gryphiswaldense*[6], neither genomic insertion of the *mamAB* operon alone (pTps_*AB*) nor in combination with the accessory *mamGFDC* genes (pTps_*ABG*) had any detectable phenotypic effect (Supplementary Table 3.1). We also failed to detect a magnetic response (C_{mag}) in the classical light scattering assay[19] after insertion of pTps_*ABG6* (*mamAB*+*mamGFDC*+*mms6*). However, the cellular iron content of *R. rubrum_ABG6* increased 2.4-fold compared with the untransformed wild type (Supplementary Table 3.1). Transmission electron microscopy (TEM) revealed a loose chain of small (~12 nm) irregularly shaped electron-dense particles (Fig. 3.2a,ii), identified as poorly crystalline hematite (Fe_2O_3) by analysis of the lattice spacings in high-resolution TEM images (Supplementary Fig. 3.3), much as in the hematite particles previously identified in *M. gryphiswaldense* mutants affected in crystal formation[11,20]. To further enhance biomineralization, we next transferred pTps_*XYZ*, an insertional plasmid harbouring *mamX*, *Y* and *Z* from the *mamXY* operon, into *R. rubrum_ABG6* (Supplementary Fig. 3.1).

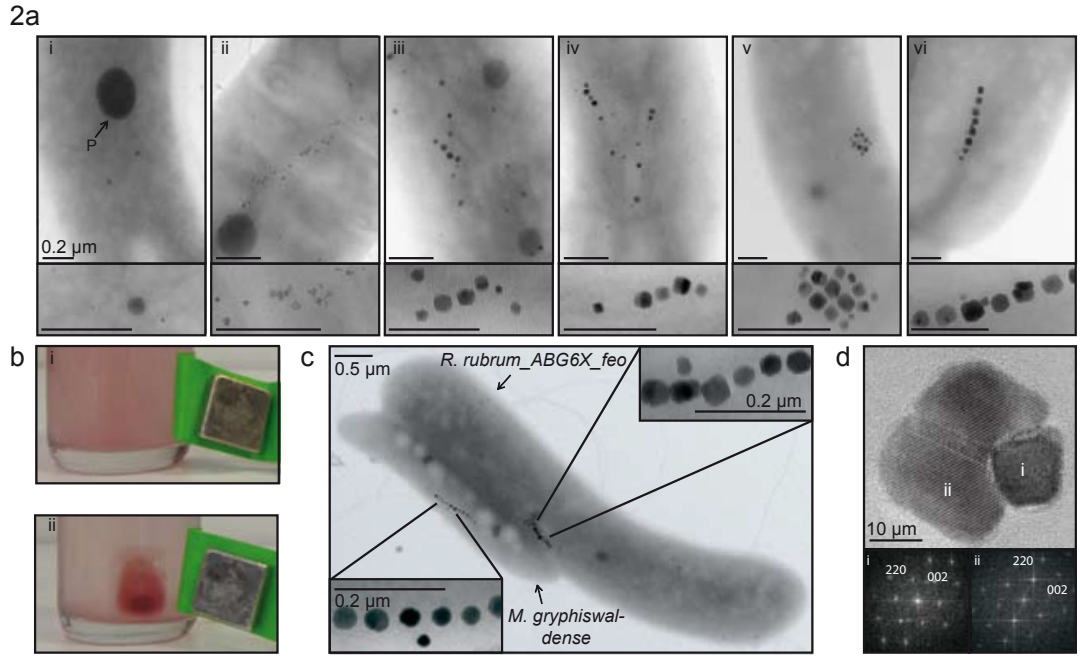

Figure 3.2: **Phenotypes of *R. rubrum* strains expressing different magnetosome gene clusters and auxiliary genes.** a, TEM images: *R. rubrum* wild type (i), containing a larger phosphate inclusion (P) and some small, non-crystalline, electron-dense particles; *R. rubrum_ABG6* (ii); *R. rubrum_ABG6X* (iii); *R. rubrum_ABG6X_ftsZm* (iv); *R. rubrum_ABG6X_dJ* (v); *R. rubrum_ABG6X_feo* (vi). Insets: Magnifications of non-crystalline electron-dense particles (i) or heterologously expressed nanocrystals (ii-vi). All insets are of the same particles\crystals as in their respective main images, except for (v). For further TEM micrographs see Supplementary Fig. 3.10. b, Unlike the untransformed *R. rubrum* wild type, cells of *R. rubrum_ABG6X* accumulated as a visible red spot near the pole of a permanent magnet at the edge of a culture flask. c, TEM micrograph of a mixed culture of the donor *M. gryphiswaldense* and the recipient *R. rubrum_ABG6X_feo*, illustrating characteristic cell properties and magnetosome organization. Insets: Magnifications of magnetosomes from *M. gryphiswaldense* and *R. rubrum_ABG6X_feo*. d, High-resolution TEM lattice image of a twinned crystal from *R. rubrum_ABG6X*, with Fourier transforms (i) and (ii) showing intensity maxima consistent with the structure of magnetite.

The resulting strain *ABG6X* encompassed all 29 relevant genes of the magnetosome island except *ftsZm*. Intriguingly, cells of *ABG6X* exhibited a significant magnetic response (Supplementary Table 3.1) and were 'magnetotactic', that is, within several hours accumulated as a visible pellet near a magnet at the edge of a culture flask (Fig. 3.2b). TEM micrographs revealed the presence of electron dense particles identified as magnetite (Fe_3O_4) (Fig. 3.2d, Supplementary Fig. 3.8 and Table 3.1), which were aligned in short, fragmented chains loosely dispersed within the cell (Fig. 3.2a,iii). Despite their smaller sizes (average, 24 nm) the particles strongly resembled the magnetosomes of the donor strain in terms of their projected outlines and thickness contrast, suggestive of cubooctahedral or octahedral crystal morphologies (Fig. 3.2d). Additional insertion of the *ftsZm* gene under control of the inducible *lac* promoter had no effect on the cellular iron content and the number and size of magnetite crystals in the resulting *R. rubrum_ABG6X_ftsZm* (Fig. 3.2a,iv, Supplementary Table 3.1).

Magnetite biomineralization occurred during microoxic chemotrophic as well anoxic photoheterotrophic cultivation. Medium light intensity, 50 μM iron and 23 °C supported the highest magnetic response (C_{mag}) and robust growth of the metabolically versatile *R. rubrum_ABG6X*, which was indistinguishable from the untransformed wild type (Supplementary Figs 3.4 and 3.5). The magnetic phenotype remained stable for at least 40 generations under non-selective conditions, with no obvious phenotypic changes. To test whether known mutation phenotypes from *M. gryphiswaldense* could be replicated in *R. rubrum*, we constructed variants of expression cassettes in which single genes were omitted from the *mamAB* operon by deletion within the cloning host *Escherichia coli*. The small (77 amino acids) MamI protein was previously implicated in MM vesicle formation and found to be essential for magnetosome synthesis[12].

R. rubrum_ABG6X-dI failed to express magnetosome particles (Supplementary Fig. 3.10), which phenocopied a *mamI* deletion in the related *M. magneticum*[12]. Another tested example was MamJ, which is assumed to connect magnetosome particles to the cytoskeletal magnetosome filament formed by the actin-like MamK[21]. Much as in *M. gryphiswaldense*, deletion of *mamJ* caused agglomeration of magnetosome crystals in 65% of *R. rubrum_ABG6X-dJ* cells (Fig. 3.2a,v, Supplementary Fig. 3.10 and Table 3.1). Together, these observations indicate that magnetosome biogenesis and assembly within the foreign host are governed by very similar mechanisms and structures as in the donor, which are conferred by the transferred genes. As magnetosomes in *R. rubrum_ABG6X* were still smaller than those of *M. gryphiswaldense*, we wondered whether full expression of biomineralization may depend on the presence of further auxiliary functions, possibly encoded outside the canonical magnetosome operons. For instance, deletion of *feoB1* encoding a constituent of a ferrous iron transport system specific for magnetotactic bacteria caused fewer and smaller magnetosomes in *M. gryphiswaldense*[22]. Strikingly, insertion of *feoAB1* into *R. rubrum* strain *ABG6X* resulted in even larger, single-crystalline and twinned magnetosomes and longer chains (440 nm) (Fig. 3.2a,vi, Supplementary Table 3.1). The size (37 nm) of the crystals approached that of the donor, and cellular iron content was substantially increased (0.28% of dry weight) compared with *R. rubrum_ABG6X* (0.18%), although still lower than in *M. gryphiswaldense* (3.5%), partly because of the considerably larger volume of *R. rubrum* cells (Fig. 3.2c).

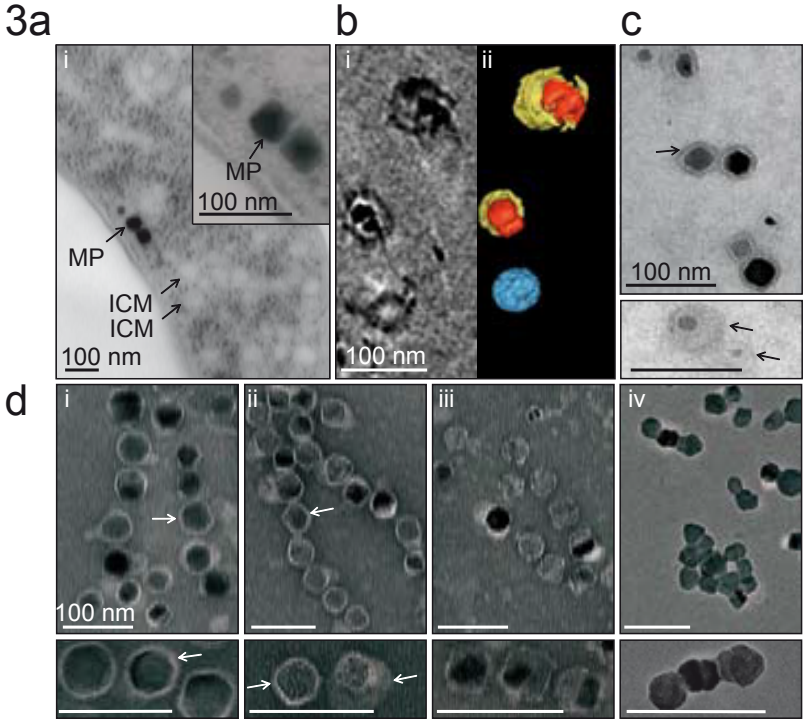

Figure 3.3: **Ultrastructural analysis of *R. rubrum_ABG6X* and isolated crystals.** a, Cryo-fixed, thin-sectioned *R. rubrum_ABG6X* contained intracytoplasmic membranes (ICMs) (93±34 nm, n=95) and magnetic particles (MP). Inset: Magnification of the magnetite crystals. b, Cryo-electron tomography of isolated magnetic particles of *R. rubrum_ABG6X*: x-y slice of a reconstructed tomogram (i) and surface-rendered three-dimensional representation (ii). A membrane-like structure (yellow, thickness 3.4±1.0 nm, n=6) surrounds the magnetic particles (red). (Blue, empty vesicle.) c,d, TEM images of isolated magnetosomes from *R. rubrum_ABG6X* (c and d,ii, iii, iv) and *M. gryphiswaldense* (d,i) negatively stained by uranyl acetate (c) or phosphotungstic acid (d). Insets: Higher-magnification images of magnetic particles; these are of different particles to those shown in the main images, except for (iv). Scale bars, 100 nm. Arrows indicate the magnetosome membrane, which encloses magnetic crystals of *M. gryphiswaldense* (thickness 3.2±1.0 nm, n=103) and *R. rubrum_ABG6X* (thickness 3.6±1.2 nm, n=100). Organic material could be solubilized from magnetite crystals of *R. rubrum_ABG6X* with SDS (sodium dodecyl sulfate, iv) and less effectively also with Triton X-100 (iii).

Magnetosome particles could be purified from disrupted cells by magnetic separation and centrifugation[23]. and formed stable suspensions (Fig. 3.3). Isolated crystals were clearly enclosed by a layer of organic material resembling the MM attached to magnetosomes of *M. gryphiswaldense*. Smaller, immature crystals were surrounded by partially empty vesicles (Fig. 3.3c, inset), which were also seen in thin-sectioned cells (Supplementary Fig. 3.8) and on average were smaller (66+6 nm) than the abundant photosynthetic intracytoplasmic membranes (ICMs) (93+34 nm; Fig. 3.3a, Supplementary Fig. 3.8). Organic material of the putative MM could be solubilized from isolated magnetite crystals of *R. rubrum_ABG6X* by various detergents (Fig. 3.3d), in a similar manner to that reported for MM of *M. gryphiswaldense*[23]. Proteomic analysis of the SDS-solubilized MM revealed a complex composition (Supplementary Fig. 3.6), and several genuine magnetosome proteins (MamKCJAFDMBYOE, Mms6, MmsF) were detected among the most abundant polypeptides (Supplementary Table 3.2). An antibody against MamC, the most abundant protein in the MM of *M. gryphiswaldense*[23], also recognized a promi-

nent band with the expected mass (12.4 kDa) in the MM of *R. rubrum_ABG6X* (Supplementary Fig. 3.6). The subcellular localization of selected magnetosome proteins in *R. rubrum* depended on the presence of further determinants encoded by the transferred genes. For example, MamC tagged with a green fluorescent protein, which is commonly used as magnetosome chain marker in *M. gryphiswaldense*[24] displayed a punctuate pattern in the *R. rubrum* wild type background. In contrast, a filamentous fluorescent signal became apparent in the majority of cells (79%) of the *R. rubrum_ABG6X* background, in which the full complement of magnetosome genes is present (Supplementary Fig. 3.7), reminiscent of the magnetosome-chain localization of these proteins in *M. gryphiswaldense*[24].

Our findings demonstrate that one of the most complex prokaryotic structures can be functionally reconstituted within a foreign, hitherto non-magnetic host by balanced expression of a multitude of structural and catalytic membrane-associated factors. This also provides the first experimental evidence that the magnetotactic trait can be disseminated to different species by only a single event, or a few events, of transfer, which are likely to occur also under natural conditions by horizontal gene transfer as speculated before[18,25,26]. The precise functions of many of the transferred genes have remained elusive in native magnetotactic bacteria, but our results will now enable the dissection and engineering of the entire pathway in genetically more amenable hosts. The approximately 30 transferred magnetosome genes constitute an autonomous expression unit that is sufficient to transplant controlled synthesis of magnetite nanocrystals and their self-assembly within a foreign organism.

However, further auxiliary functions encoded outside the *mam* and *mms* operons are necessary for biomineralization of donor-like magnetosomes. Nevertheless, this minimal gene set is likely to shrink further as a result of systematic reduction approaches in different hosts. Importantly, the results are promising for the sustainable production of magnetic nanoparticles in biotechnologically relevant photosynthetic hosts. Previous attempts to magnetize both prokaryotic and eukaryotic cells by genetic and metabolic means (for example, refs 27,28) resulted in only irregular and poorly crystalline iron deposits. This prompted ideas to borrow genetic parts of the bacterial magnetosome pathway for the synthesis of magnetic nanoparticles within cells of other organisms[4,29]. Our results now set the stage for synthetic biology approaches to genetically endow both uni- and multicellular organisms with magnetization by biomineralization of tailored magnetic nanostructures. This might be exploited for instance in nanomagnetic actuators or *in situ* heat generators in the emerging field of magnetogenetics[30], or for endogenous expression of magnetic reporters for bioimaging[31].

Methods

Bacterial strains, media and cultivation.

The bacterial strains are described in Supplementary Table 3.4. *E. coli* strains were cultivated as previously described[32]. A volume of 1 mM DL-a,e-diaminopimelic acid was added for the growth of auxotrophic strains BW29427 and WM3064. *M. gryphiswaldense* strains were cultivated in flask standard medium (FSM), in liquid or on plates solidified by 1.5% agar, and incubated at 30 °C under microoxic (1% O2) conditions[33]. Cultures of *R. rubrum* strains were grown as specified (Supplementary Fig. 3.3).

Construction of magnetosome gene cluster plasmids and conjugative transfer.

The oligonucleotides and plasmids used in this study are listed in Supplementary Tables 3.4 and 3.5. Red-ET (Lambda red and RecET) recombination was performed as described previously[14]. Briefly, a cloning cassette was amplified by polymerase chain reaction (PCR) and transferred into electrocompetent *E. coli* cells (DH10b) expressing phage-derived recombinases from a circular plasmid (pSC101-BADgbaA). After transfer of the cassette, recombination occurred between homologous regions on the linear fragment and the plasmid. To stitch the magnetosome gene clusters together into a transposon plasmid (Supplementary Fig. 3.1) we used triple recombination[14] and co-transformed two linear fragments, which recombined with a circular plasmid. Recombinants harbouring the correct plasmids were selected by restriction analysis[32]. Conjugations into *M. gryphiswaldense* were performed as described before[33]. For conjugation of *R. rubrum*, cultures were incubated in ATCC medium 112. Approximately 2x10^9 cells were mixed with 1x10^9 *E. coli* cells, spotted on American Type Culture Collection (ATCC) 112 agar medium and incubated for 15 h. Cells were flushed from the plates and incubated on ATCC 112 agar medium supplemented with appropriate antibiotics for 7-10 days (Tc=10 mg ml^{-1}; Km=20 mg ml^{-1}; Gm=10 mg ml^{-1}, where Tc, tetracycline; Km, kanamycin; Gm, gentamicin). Sequential transfer of the plasmids resulted in 1x10^{-6} to 1x10^{-8} antibiotic-resistant insertants per recipient, respectively. Two clones from each conjugation experiments were chosen for further analyses. Characterized insertants were indistinguishable from wild type with respect to motility, cell morphology or growth (Supplementary Fig. 3.5).

Analytical methods.

The optical density of *M. gryphiswaldense* cultures was measured turbidimetrically at 565 nm as described previously[19]. The optical density of *R. rubrum* cultures was measured at 660 nm and 880 nm. The ratio of 880/660 nm was used to determine yields of chromatophores within intact cells (Supplementary Fig. 3.4). Furthermore, *bacteriochlorophyll a* was extracted from cultures with methanol. Absorption spectra (measured in an Ultrospec 3000 photometer, GE Healthcare) of photoheterotrophically cultivated *R. rubrum_ABG6X* cells were indistinguishable from that of the wild type (Supplementary Fig. 3.4).

The average magnetic orientation of cell suspensions (C_{mag}) was assayed with a light scattering assay as described previously[19]. Briefly, cells were aligned at different angles to a light beam by application of an external magnetic field.

Microscopy.

For TEM of whole cells and isolated magnetosomes, specimens were directly deposited onto carbon-coated copper grids. Magnetosomes were stained with 1% phosphotungstic acid or 2% uranyl acetate. Samples were viewed and recorded with a Morgagni 268 microscope. Sizes of crystals and vesicles were measured with ImageJ software. Chemical fixation, high-pressure freezing and thin sectioning of cells were performed as described previously[17]. Processed samples were viewed with an EM 912 electron microscope (Zeiss) equipped with an integrated OMEGA energy filter operated at 80 kV in the zero loss mode. Vesicle sizes were measured with ImageJ software. High-resolution TEM was performed with a JEOL 3010 microscope, operated at 297 kV and equipped with a Gatan Imaging Filter for the acquisition of energy-filtered compositional maps. For TEM data processing and interpretation, DigitalMicrograph and SingleCrystal software were used[20]. Cryo-electron tomography was performed as described previously[21]. Fluorescence microscopy was performed with an Olympus IX81 microscope equipped with a Hamamatsu Orca AG camera using exposure times of 0.12-0.25 s. Image rescaling and cropping were performed with Photoshop 9.0 software.

Acknowledgements

This work was supported by the Human Frontier Science Foundation (grant RGP0052\2012), the Deutsche Forschungsgemeinschaft (grants SCHU 1080\12-1 and 15-1) and the European Union (Bio2MaN4MRI). The authors thank F. Kiemer for expert help with iron measurements and cultivation experiments.

Competing financial interests

I.K. and D.S. (LMU Munich) have filed a patent application on the process described in this work (Production of magnetic nanoparticles in recombinant host cells, EP13193478).

Additional information

Supplementary information is available in the online version of the paper. Reprints and permissions information is available online at www.nature.com\reprints. Correspondence and requests for materials should be addressed to Y.Z. and D.S.

References

1. Prozorov, T., Bazylinski, D. A., Mallapragada, S. K. & Prozorov, R. Novel magnetic nanomaterials inspired by magnetotactic bacteria: topical review. Mater. Sci. Eng. R 74, 133-172 (2013).
2. Baumgartner, J., Bertinetti, L., Widdrat, M., Hirt, A. M. & Faivre, D. Formation of magnetite nanoparticles at low temperature: from superparamagnetic to stable single domain particles. PLoS ONE 8, e57070 (2013).
3. Bazylinski, D. A. & Frankel, R. B. Magnetosome formation in prokaryotes. Nature Rev. Microbiol. 2, 217-230 (2004).
4. Goldhawk, D. E., Rohani, R., Sengupta, A., Gelman, N. & Prato, F. S. Using the magnetosome to model effective gene-based contrast for magnetic resonance imaging. Wiley Interdiscip. Rev. Nanomed. Nanobiotechnol. 4, 378-388 (2012).
5. Murat, D. Magnetosomes: how do they stay in shape? J. Mol. Microbiol. Biotechnol. 23, 81-94 (2013).
6. Lohße, A. *et al*. Functional analysis of the magnetosome island in *Magnetospirillum gryphiswaldense*: the *mamAB* operon is sufficient for magnetite biomineralization. PLoS ONE 6, e25561 (2011).
7. Pollithy, A. *et al*. Magnetosome expression of functional camelid antibody fragments (nanobodies) in *Magnetospirillum gryphiswaldense*. Appl. Environ. Microbiol. 77, 6165-6171 (2011).
8. Staniland, S. *et al*. Controlled cobalt doping of magnetosomes *in vivo*. Nature Nanotech. 3, 158-162 (2008).
9. Jogler, C. & Schüler, D. Genomics, genetics, and cell biology of magnetosome formation. Annu. Rev. Microbiol. 63, 501-521 (2009).
10. Ullrich, S., Kube, M., Schübbe, S., Reinhardt, R. & Schüler, D. A hypervariable 130-kilobase genomic region of *Magnetospirillum gryphiswaldense* comprises a magnetosome island which undergoes frequent rearrangements during stationary growth. J. Bacteriol. 187, 7176-7184 (2005).
11. Raschdorf, O., Müller, F. D., Pósfai, M., Plitzko, J. M. & Schüler, D. The magnetosome proteins MamX, MamZ and MamH are involved in redox control of magnetite biomineralization in *Magnetospirillum gryphiswaldense*. Mol. Microbiol. 89, 872-886 (2013).
12. Murat, D., Quinlan, A., Vali, H. & Komeili, A. Comprehensive genetic dissection of the magnetosome gene island reveals the step-wise assembly of a prokaryotic organelle. Proc. Natl Acad. Sci. USA 107, 5593-5598 (2010).
13. Schübbe, S. *et al*. Transcriptional organization and regulation of magnetosome operons in *Magnetospirillum gryphiswaldense*. Appl. Environ. Microbiol. 72, 5757-5765 (2006).

14. Fu, J. *et al*. Efficient transfer of two large secondary metabolite pathway gene clusters into heterologous hosts by transposition. Nucleic Acids Res. 36, e113 (2008).
15. Martinez-Garcia, E., Calles, B., Arevalo-Rodriguez, M. & de Lorenzo, V. pBAM1: an all-synthetic genetic tool for analysis and construction of complex bacterial phenotypes. BMC Microbiol. 11, 38 (2011).
16. Richter, M. *et al*. Comparative genome analysis of four magnetotactic bacteria reveals a complex set of group-specific genes implicated in magnetosome biomineralization and function. J. Bacteriol. 189, 4899-4910 (2007).
17. Jogler, C. *et al*. Conservation of proteobacterial magnetosome genes and structures in an uncultivated member of the deep-branching *Nitrospira* phylum. Proc. Natl Acad. Sci. USA 108, 1134-1139 (2011).
18. Lefèvre, C. T. *et al*. Monophyletic origin of magnetotaxis and the first magnetosomes. Environ. Microbiol. 15, 2267-2274 (2013).
19. Schüler, D. R., Uhl, R. & Bäuerlein, E. A simple light scattering method to assay magnetism in *Magnetospirillum gryphiswaldense*. FEMS Microbiol. Ecol. 132, 139-145 (1995).
20. Uebe, R. *et al*. The cation diffusion facilitator proteins MamB and MamM of *Magnetospirillum gryphiswaldense* have distinct and complex functions, and are involved in magnetite biomineralization and magnetosome membrane assembly. Mol. Microbiol. 82, 818-835 (2011).
21. Scheffel, A. *et al*. An acidic protein aligns magnetosomes along a filamentous structure in magnetotactic bacteria. Nature 440, 110-114 (2006).
22. Rong, C. *et al*. Ferrous iron transport protein B gene (*feoB1*) plays an accessory role in magnetosome formation in *Magnetospirillum gryphiswaldense* strain MSR-1. Res. Microbiol. 159, 530-536 (2008).
23. Grünberg, K. *et al*. Biochemical and proteomic analysis of the magnetosome membrane in *Magnetospirillum gryphiswaldense*. Appl. Environ. Microbiol. 70, 1040-1050 (2004).
24. Lang, C. & Schüler, D. Expression of green fluorescent protein fused to magnetosome proteins in microaerophilic magnetotactic bacteria. Appl. Environ. Microbiol. 74, 4944-4953 (2008).
25. Jogler, C. *et al*. Comparative analysis of magnetosome gene clusters in magnetotactic bacteria provides further evidence for horizontal gene transfer. Environ. Microbiol. 11, 1267-1277 (2009).
26. Jogler, C. *et al*. Toward cloning of the magnetotactic metagenome: identification of magnetosome island gene clusters in uncultivated magnetotactic bacteria from different aquatic sediments. Appl. Environ. Microbiol. 75, 3972-3979 (2009).
27. Nishida, K. & Silver, P. A. Induction of biogenic magnetization and redox control by a component of the target of rapamycin complex 1 signaling pathway. PLoS Biol. 10, e1001269 (2012).

28. Kim, T., Moore, D. & Fussenegger, M. Genetically programmed superparamagnetic behavior of mammalian cells. J. Biotechnol. 162, 237-245 (2012).
29. Murat, D. *et al*. The magnetosome membrane protein, MmsF, is a major regulator of magnetite biomineralization in *Magnetospirillum magneticum* AMB-1. Mol. Microbiol. 85, 684-699 (2012).
30. Huang, H., Delikanli, S., Zeng, H., Ferkey, D. M. & Pralle, A. Remote control of ion channels and neurons through magnetic-field heating of nanoparticles. Nature Nanotech. 5, 602-606 (2010).
31. Westmeyer, G. G. & Jasanoff, A. Genetically controlled MRI contrast mechanisms and their prospects in systems neuroscience research. Magn. Reson. Imaging 25, 1004-1010 (2007).
32. Sambrook, J. & Russell, D. Molecular Cloning: A Laboratory Manual Vol. 3 (Cold Spring Harbor Laboratory Press, 2001).
33. Kolinko, I., Jogler, C., Katzmann, E. & Schüler, D. Frequent mutations within the genomic magnetosome island of *Magnetospirillum gryphiswaldense* are mediated by RecA. J. Bacteriol. 193, 5328-5334 (2011).

4 Chapter IV

3rd Publication

Genetic dissection of the *mamAB* and *mms6* operons reveals a gene set essential for magnetosome biogenesis in *Magnetospirillum gryphiswaldense*.

Publication state: *Published ahead of print 9 May 2014 in Journal of Bacteriology.*

Abstract

Biosynthesis of bacterial magnetosomes, which are intracellular membrane-enclosed, nano-sized magnetic crystals, is controlled by a set of >30 specific genes. In *Magnetospirillum gryphiswaldense* these are clustered mostly within a large conserved genomic magnetosome island (MAI) comprising the *mms6*, *mamGFDC*, *mamAB* and *mamXY* operons. Here, we demonstrate that the five previously uncharacterized genes of the *mms6* operon have crucial functions in the regulation of magnetosome biomineralization that partially overlap with MamF and other proteins encoded by the adjacent *mamGFDC* operon. While all other deletions resulted in size reduction, elimination of either *mms36* or *mms48* caused the synthesis of magnetite crystals larger than those in the WT. Whereas the *mms6* operon encodes accessory factors for crystal maturation, the large *mamAB* operon contains several essential and non-essential genes involved in various other steps of magnetosome biosynthesis, as shown by single deletions of all *mamAB* genes. While single deletions of *mamL*, *P*, *Q*, *R*, *B*, *S*, *T* and *mamU* showed phenotypes similar to those of their orthologs in a previous study in the related *M. magneticum*, we found *mamI* and *mamN* to be not required for at least rudimentary iron biomineralization in *M. gryphiswaldense*. Thus, only *mamE*, *L*, *M*, *O*, *Q*, and *mamB* were essential for formation of magnetite, whereas a *mamI* mutant still biomineralized tiny particles which, however, consisted of the non-magnetic iron oxide hematite as shown by HRTEM and XANES. Based on this and previous studies we propose an extended model for magnetosome biosynthesis in MSR.

Introduction

Magnetotactic bacteria (MTB) orient along the Earth magnetic field lines to navigate to their growth-favoring microoxic habitats within stratified aquatic sediments (1). This behavior is enabled by the synthesis of ferrimagnetic intracellular organelles termed magnetosomes (2). In the α-proteobacterium

Magnetospirillum gryphiswaldense (in the following referred to as MSR) and related MTB, magnetosomes consist of crystals of the magnetic iron oxide magnetite (Fe_3O_4) enclosed by the magnetosome membrane (MM) that contains a specific set of about 30 proteins (3, 4). The biosynthesis of magnetosomes is a complex process that comprises the (i) invagination of vesicles from the inner membrane (5, 6), (ii) sorting of magnetosome proteins to the MM (7), (iii) iron transport and crystallization of magnetite crystals (8), (iv) crystal maturation (7) and (v) assembly as well as positioning of mature crystals into a linear chain along a filamentous cytoskeletal structure (6, 9).

Each step is under strict genetic control and responsible genes were found to be located mostly within a genomic magnetosome island (MAI) (10, 11), comprising the *mms6* (in the following referred to as *mms6op*), *mamGFDC* (*mamGFDCop*), *mamAB* (*mamABop*), and *mamXY* (*mamXYop*) operons (10-12). These operons were found to be highly conserved also in the closely related *M. magneticum* (in the following referred to as AMB) (13-17). It has been shown that the regions between and flanking the identified magnetosome operons have no functional relevance for magnetosome biosynthesis in MSR and AMB (7, 18). In MSR the *mms6*, *mamGFDC*, *mamAB* and *mamXY* operons are transcribed as single polycistronic messengers under control of the P_{mms6}, P_{mamDC}, P_{mamH}, and P_{mamXY} promoters, respectively (19, 20). A deletion mutant of *mamGFDCop* encoding the most abundant magnetosome proteins retained the ability to form magnetic, although smaller and less regular magnetosomes, while plasmidal overexpression of the entire *mamGFDCop* yielded magnetite particles even larger than those produced by the WT (21). Elimination of the corresponding region R3 in AMB, comprising in addition parts of *mms6op*, caused a severe biomineralization defect, resulting in cells with reduced magnetosome sizes and numbers (7). Deletion of the entire *mamXYop* resulted in smaller and misshaped magnetosome particles in MSR (18), whereas no obvious phenotype was observed for Δ*mamXYop* in AMB (7).

The *mms6op* of MSR comprises the genes *mgr4074*, *mms6*, *mmsF*, *mgr4071* (in the following renamed into *mms36*) and *mgr4070* (renamed into *mms48*; Fig. S4.1), which was previously predicted to encode a TPR-like protein (18). A mutant, in which the entire *mms6op* was deleted (ΔA10), was also severely impaired in the biomineralization of magnetite crystals, which exhibited defects in crystal morphology, size and organization. However, the individual functions of *mgr4074*, *mms6*, *mmsF*, *mms36* and *mms48* as well as their contribution to the strong phenotype of Δ*mms6op* have remained unknown. In AMB, the *mms6* cluster was described to comprise only *amb0955* (*mgr4074*), *amb0956* (*mms6*), *amb0967* (*mmsF*), but to lack homologs of *mms48* and *mms36* (22). Single gene deletions of *mms6* in AMB by different groups revealed inconsistent phenotypes. Whereas Tanaka *et al*. (23), reported an important regulatory function of Mms6 for magnetosome morphology, Murat *et al*. observed only minor effects on magnetosome biosynthesis after deletion of *mms6 in vivo* (22, 24). *In vitro*, the small (12.76 kDa in MSR and 14.69 in AMB) Mms6 protein was shown to be tightly bound to isolated bacterial magnetite crystals as visualized by atomic force microscopy and TEM (25, 26). *In vitro* crystallization experiments suggested that Mms6 and peptides mimicking it have iron-binding activity and affected the formation of cubo-octahedral crystal morphologies (27, 28). In contrast to the smaller accessory oper-

ons, *mamABop* was found to contain genes absolutely essential for magnetosome biosynthesis in MSR and AMB (18, 22). Whereas *mamABop* was found to be sufficient to support at least some rudimentary biomineralization of small magnetite crystals even in the absence of all other magnetosme operons in both strains (18, 22), the *mamXY*, *mamGFDC*, *mms6*, and *mamAB* operons were required altogether for magnetite biomineralization upon their transfer into the foreign host *Rhodospirillum rubrum* (29).

A recent comprehensive genetic dissection of *mamABop* in AMB revealed that *mamH*, *P*, *R*, *S*, and *mamT* encode accessory functions for magnetosome synthesis, since mutants display various biomineralization defects, whereas *mamU* and *mamV* had no obvious magnetosome phenotype (7). As in MSR (see below), *mamK* and *mamJ* were implicated in magnetosome chain assembly, but their loss did not affect biomineralization (30, 31). However, gene deletions of *mamI*, *E*, *L*, *M*, *N*, *O*, and *mamQ* as well as *mamB* (co-deleted with their respective orthologs) fully abolished magnetosome synthesis in AMB (7, 32). Whereas MamI, L, Q and MamB were suggested to be essential for vesicle genesis, MamE, O, M, and MamN were classified to be mainly required only for magnetite crystallization (7). The discovery of a small 'magnetosome islet' in the genome of AMB with further copies of *mamE*, *J*, *K*, *L*, *M*, *F* as well as *mamD* suggested genetic redundancy that has to be clarified with respect to determination of the minimal essential gene set (33). In MSR the 16.4 kb *mamABop* contains 17 genes (*mamH*, *I*, *E*, *J*, *K*, *L*, *M*, *N*, *O*, *P*, *A*, *Q*, *R*, *B*, *S*, *T* and *mamU*) (Fig. 4.3).

Only a few genes of *mamABop* so far were analyzed individually in this organism. The actin-like protein MamK forms a filamentous structure for magnetosome assembly and interacts with the acidic protein MamJ that is involved in connecting magnetosomes to the filament. Both proteins, however, have no or only minor effects on biomineralization (9, 34). Deletion of *mamH* caused a moderate decrease of magnetosome number and size, whereas co-deletion of *mamH* and its partial homologue *mamZ* had a considerably stronger effect with only very few or no regular crystals detectable in the cells (20). Deletion of *mamE*, *O*, *M* and *mamB* resulted in either a total inhibition of crystal nucleation or prevented MM vesicle synthesis (18, 35, 36). However, *mamI*, *L*, *N*, *P*, *A*, *Q*, *R*, *S*, *T*, and *mamU* were not yet analyzed individually by mutagenesis, and it has remained unknown whether they have functions similar or distinct from those of their corresponding orthologs in AMB. Finally, it is not clear, which genes constitute the minimal set of essential determinants for magnetosome biomineralization in MSR.

Here, we analyzed the functional relevance of proteins encoded by *mms6op* and *mamABop* for the biosynthesis of magnetic minerals in MSR. We demonstrate that besides Mms6 and MmsF, *mms6op* of MSR encodes two further important regulators (Mms36 and Mms48) for magnetosome biomineralization. Whereas deletions of *mamA*, *R*, *S*, *T*, and *mamU* resulted in similar phenotypes as those observed for deletion of homologous genes in AMB, we show that other than in AMB, Δ*mamN* and Δ*mamI* still synthesize particles in MSR, thus further shrinking the minimal gene set for iron biomineralization to *mamE*, *L*, *M*, *O*, *Q* and *mamB*. Finally, we propose an extended model for magnetosome biosynthesis.

Material and Methods

Bacterial strains, plasmids, and culture conditions

Bacterial strains and plasmids used in this study are listed in Table S4.1. WT and mutant strains of MSR were grown in liquid modified flask standard medium (FSM) at 30 °C under microaerobic conditions if not otherwise specified (37, 38). Therefore, cells were cultivated in flasks, closed with butyl-rubber stoppers after incubation with a gas mixture of 2% O_2 and 98% N_2 or in purged jars. For anaerobic requirements, O_2 was excluded from the gas mixture, while aerobic conditions were generated through free gas exchange with air. *Escherichia coli* strains were cultivated as previously described (39) and lysogeny broth medium was supplemented with 1 mM DL-α, ε-diaminopimelic acid (DAP) for cultivation of *E. coli* strain BW29427 as well as WM3064. For selection of antibiotic resistant cells, media were supplemented with 25 g/ml kanamycin (Km), 12 g/ml tetracycline (Tet), and 15 g/ml gentamicin (Gm) for *E. coli* strains, and 5 g/ml Km, 5 g/ml Tet, and 20 g/ml Gm for MSR strains, respectively.

Molecular and genetic techniques

Oligonucleotide sequences (Table S4.2) were deduced from the working draft genome sequence of MSR (GenBank accession number No. CU459003) and purchased from Sigma-Aldrich (Steinheim, Germany). Genetic fragments were amplified by standard polymerase chain reaction (PCR) procedures with Phusion polymerase (NEB GmbH, Frankfurt am Main, Germany) and generated plasmids were sequenced with an ABI 3700 capillary sequencer (Applied Biosystems, Darmstadt, Germany), utilizing BigDye Terminator v3.1. Data were analyzed with Software Vector NTI Advance 11.5 (Invitrogen, Darmstadt, Germany) or MacVector 7.2.3 (Oxford Molecular, Oxford, UK).

Generation of unmarked deletion mutants

Markerless single gene deletions within the *mamAB*, *mms6*, and *mamGFDC* operon were partially realized with the pORFM_*galK* plasmid. The vector was digested with BamHI and KpnI to insert the approximately 1 kb downstream and upstream fragments of *mamI*, *L*, *N*, *P*, *Q*, *R*, *S*, *T*, *U*, *mms36*, *mms48*, and *mmsF_mms6*. For integration of homologous regions of *mamA* and *mamL* the plasmid was digested with BamHI/NotI and NsiI/SpeI, respectivaly. Oligonucleotides, used to amplify the 5' and 3' flanking sequence from MSR by PCR are listed in Table S4.3. Both fragments were linked by an overlap PCR with the first and last listed corresponding oligonucleotide, subcloned into pJet1.2/blunt, sequenced and ligated into the digested pORFM_*galK* vectors. Generated plasmids were termed: pAL_ Δ*mamI*, pORΔ*mamL*, pAL_ Δ*mamN*, pAL_ Δ*mamP*, pAL_ Δ*mamA*, pAL_ Δ*mamQ*, pAL_ Δ*mamR*, pAL_ Δ*mamS*, pAL_ Δ*mamT*, pAL_ Δ*mamU*, pAL_ Δ*mms36*, pAL_ Δ*mms48*, and pAL_ Δ*mmsF* Δ*mms6*. Deletion of *mms6*, *mmsF*, *mamF* and double deletion of *mmsF* Δ*mamF* was accomplished by double cross over method. Oligonucleotides for amplification of flanking sections are listed in Table S4.3.

Regions were cloned into pJet1.2/blunt and sequenced. Plasmid pCM184 was digested with ApaI/SacI and 3' end regions were inserted for deletion of *mms6*, *mmsF* and *mamF*. Generated plasmids were digested with EcoRI/NdeI and 5' flanking sequence was inserted, resulting in pCM184_*mms6* 3'5', pCM184_*mmsF* 3'5' and pCM184_*mamF* 3'5'. The generated plasmids were examined by restriction analysis with a set of different enzymes or PCR and transferred into MSR WT by conjugation using *E. coli* BW29427 as donor strain as described elsewhere (18). Genomic insertion mutants were selected on Km plates, cultivated in 100 μl FSM medium over night at 30 °C and scaled up to 1 ml. Proper plasmid integration was verified by PCR and if necessary counter selection was implemented. Positive excision strains were verified by PCR and mutants were termed as: Δ*mamI*, Δ*mamL*, Δ*mamN*, Δ*mamP*, Δ*mamA*, Δ*mamQ*, Δ*mamR*, Δ*mamS*, Δ*mamT*, Δ*mamU*, Δ*mms48*, Δ*mms36*, and Δ*mmsF* Δ*mms6*. Mutants generated by double cross over were cultivated in 10 ml MSR medium and excision of the Km resistance gene was induced after conjugation with the Cre expression plasmid pCM157. Generated strains were termed: Δ*mmsF* and Δ*mms6*. For double deletion of *mmsF* and *mamF*, the plasmid pCM184_*mamF* 3'5' was introduced into Δ*mmsF*, and deletion was verified as described above, resulting in strain Δ*mmsF* Δ*mamF*.

Complementation of generated mutants and GFP localization

For MamC-GFP localization experiments the plasmid pFM323 was integrated into the genome of Δ*mamI*, Δ*mamL*, Δ*mamN*, Δ*mamP*, Δ*mamA*, Δ*mamQ*, Δ*mamR*, Δ*mamS,* and Δ*mamT*. For construction of pAL_*mamI*g, *mamI* was amplified with oligonucleotides AL394/AL395 and inserted into pCL6 after digestion with NdeI/EcoRI. Plasmids for complementation of the other mutant strains were derivatives of pBAM1 and labeled pBAM_*mamL*, *P*, *S*, *T*, *R*, *A*, *N*, *mms48*, *mms36*, and *mgr4074* respectively. Oligonucleotides for amplification of the genes are listed in Table S4.3. Genes were cloned between the NdeI/EcoRI or NdeI/PacI sites (for *mamN*) of pBAM_*GFDC* under control of the P_{mamDC} promoter. Plasmids pBam_*mms36* and pBam_*mms48* were also used for overexpression studies in WT. For complementation of Δ*mmsF*, Δ*mms6*, Δ*mmsF* Δ*mamF*, Δ*mmsF* Δ*mms6*, or ΔA10, corresponding genes were amplified with oligonucleotides listed in Table S4.3. Genes were inserted into pAP150 after digestion with BamHI/NdeI, resulting in pAL_*mmsF*, pAL_*mms6*, pAL_P*mamDC_mms6op*, and pAL_$P_{mamDC_mms6,F,4074}$. The plasmid pBBRMCS2 was digested with NsiI/EcoRI for integration of genes *mms6*, *mmsF* and *mgr4074* after amplification with AL125/AL136, generating pAL_$P_{mms6_mms6,F,4074}$. For transcomplementation assays, the plasmids were transferred to the respective deletion mutant by conjugation. Δ*mmsF_mms6* and Δ*mmsF_mamF* were complemented with pAL_*mms6* and pAL_*mmsF*, respectively. Plasmids pBam_*mgr4074*; pAL_ P_{mamDC_mms6op}; pAL_$P_{mms6_mms6,F,4074}$; pAL_$P_{mamDC_mms6,F,4074}$ were used for complementation studies in ΔA10.

Analytic methods

Optical density and magnetic response (C_{mag}) were analyzed photometrically at 565 nm (40). The applied magnetic field for C_{mag} measurements was about 70 mT, which is able to magnetize very small or irregular magnetosomes within the superparamagnetic state. Intracellular iron concentrations were measured after incubation under anaerobic conditions as described (41).

Phase Contrast and Fluorescence Microscopy

MSR strains with genomic textitegfp were grown in 5 ml FSM in six-well plates for 16 h at 30 °C and 2% O_2 without agitation. Cells were immobilized on agarose pads (FSM salts in H_2O, supplemented with 1% agarose), and imaged with an Olympus BX81 microscope equipped with a 100 UPLSAPO100XO objective (numerical aperture of 1.40) and a Hamamatsu Orca AG camera. The Olympus cell software was used to capture and analyze images.

TEM and HRTEM

Magnetosome phenotypes of cells with respect to size, shape and number per cell were examined by transmission electron microscopy (42), for which cells were concentrated and adsorbed onto carbon-coated copper grids. Cells were imaged with a FEI Morgagni 268 (FEI, Eindhoven, Netherlands) electron microscope at an accelerating voltage of 80 kV. Bright-field TEM images and selected-area electron diffraction (SAED) patterns were recorded on image plates, using a Philips CM20 microscope operated at 200 kV and fitted with a Noran Voyager energy-dispersive X-ray detector. High-resolution transmission electron microscopy (HRTEM) was performed using a JEOL 3010 microscope, operated at 297 kV and equipped with a Gatan Imaging Filter (GIF) for the acquisition of electron energy-loss spectra and energy-filtered compositional maps. For TEM data processing and interpretation the softwares DigitalMicrograph and SingleCrystal were used.

X-ray Absorption Spectroscopy

Bacterial cultures (90-135 mL) were pelleted by centrifugation (5 min at 9,000 x g, 4 °C) and washed 3x by resuspension with 5 mL TBS (pH 7.6) and centrifugation. Pellets were then resuspended in 100 μL TBS + 25 μL glycerol and frozen in liquid nitrogen on sample holders with Kapton film support. Samples were shipped to the European Synchrotron Radiation Facility (ESRF) on dry ice, where they were stored at -80 °C until measurement. Fe K-edge X-ray absorption near edge structure (XANES) spectra were recorded at the undulator beamline ID26 of the ESRF. We used a Si (311) double-crystal monochromator and focusing mirrors giving a beam spot size of ~200x400 μm^2 on the samples. Data were recorded in fluorescence detection mode using a Rowland-type spectrometer equipped with 4 Ge (440) analyzer crystals and a Si-photodiode. During all measurements, samples were cooled to around

10 K using a liquid He cryostat. XANES spectra were recorded with 0.1 eV step from 7100 to 7200 eV. To improve data quality, 10 to 100 XANES scans were recorded for each sample. Samples were moved of few hundreds of microns between each scan in order to minimize radiation damage. Data were averaged using PyMca 4.6.2 after evaluation for iron photo-reduction. Averaged spectra were normalized and fitted using Demeter 0.9.16. As reference materials we used spinach ferredoxin (Sigma Aldrich), hematite (20-60 nm grain size, Alfa Aesar), magnetite, ferrihydrite and phosphate-enriched ferric oxyhydroxides (described earlier in (43)).

Results

Deletion mutagenesis of the *mms6* operon and *mamF*

After reassessment of annotation and correction of the MmsF N-terminus (Figure S4.1), we generated various unmarked in frame single and double deletions of all *mms6op* genes as well as of *mamF* (localized in the adjacent *mamGFDCop*), which is highly similar (61% aa identity) to *mmsF* (see Table 1 and Figure 1 for overview over deletions and resulting phenotypes). We found the hypothetical *mgr4074* to be poorly conserved, and its chromosomal reintegration into Δ*mms6op* (ΔA10) (18) did not alleviate the severe biomineralization defects of the parent strain. We therefore consider *mgr4074* a pseudogene with no role in biomineralization, although further studies are needed to address the expression and putative localization of its gene product.

Strain Δ*mms6* had slightly smaller crystals (30 nm; Wild-type (WT): 36 nm) that were scattered throughout the cell, either aligned in irregularly spaced ”pseudo-chains” (i. e., with <10 crystals per chain) or approximating WT-like chain configurations (Table 4.1; Figure 4.1). Crystals between 30 and 35 nm were predominant (WT: 40-45 nm), but particles larger than 60 nm were absent (WT: <70 nm; Figure S2). The average crystal number per cell was reduced to 30 (WT: 34 particles per cell), and the magnetic response of a Δ*mms6* culture was slightly weaker than that of the WT ($C_{mag(mms6)}$: 1.7±0.1; $C_{mag(WT)}$: 2.0±0.1; Table 4.1). C_{mag} of Δ*mmsF* cells was similar to those of Δ*mms6*. Magnetosomes displayed variable intracellular arrangements, such as one or more short chains, partially scattered crystals, or lacking any chain-like alignment (Figure 4.1). Mean crystal sizes were reduced to <30 nm, whereas the particle number was only slightly lower than in the WT (Table 4.1; Figure S4.2). Since the high similarity of 61% between MmsF and MamF suggested possible functional redundancy, *mamF* was eliminated both alone and in combination with *mmsF*. In Δ*mamF*, MamC encoded downstream of *mamF* in the same operon was found to be properly expressed by immunodetection, indicating that deletion of *mamF* had no polar effect (data not shown). Mean crystal size (34 nm) and number (34 per cell) were similar in Δ*mamF* to WT.

However, the combined excision of both genes within Δ*mmsF* Δ*mamF* resulted in a more drastic decrease in size (25 nm) and number (27 crystals per cell, Figure 4.1; Table 4.1; Figure S4.2).

Thus, loss of MmsF had a more pronounced effect on crystal size, number and alignment than MamF, and the additive effect of their combined deletion suggested that both proteins are involved in size control. Double deletion of *mmsF* and *mms6* reduced size to 24 nm and number to 24 crystals per cell (Table 4.1). However, iron content, size and numbers of magnetite particles as well as C_{mag} (1.6±0.1) of Δ*mmsF* Δ*mms6* were still higher than in the operon deletant ΔA10 (C_{mag} : 1.0±0.1), with particles of 20-25 nm prevailing in both strains (Figure 4.1; Table 4.1; Figure S4.2).

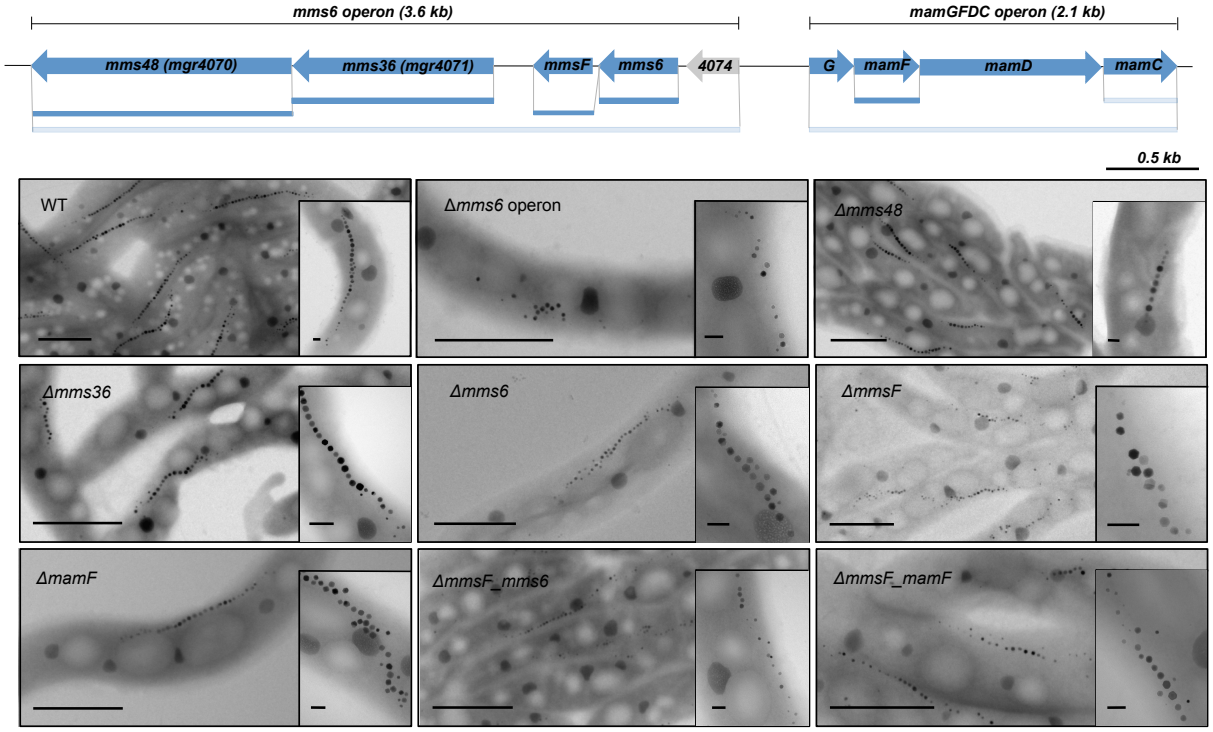

Figure 4.1: **Molecular organization of the *mms6* and *mamGFDC* operons in MSR and TEM micrographs of generated deletion mutants**. Scale bar: 1 μm. Dark blue bars: Indicate extent of gene deletions generated in this study. Light blue bars: Gene deletion mutants generated by (18, 21).

HRTEM images of particles from ΔA12, in which the entire *mms6op* and *mamGFDCop* were deleted together (18), revealed fringes spacing corresponding to magnetite. This indicates that the deleted genes alone do not have a critical role in magnetite formation (Figure 4.2). In contrast to the strong size reduction observed in all other mutant strains, deletions of *mgr4070* and *mgr4071* (renamed into *mms48* und *mms36* according to their predicted protein masses of 48 and 36 kDa, respectively) unexpectedly caused a substantial increase in mean crystal size. Particles synthesized by both strains resembled WT crystals in shape, but were significantly larger in Δ*mms36* (39 nm) and Δ*mms48* (46 nm; Figure 1; Table 4.1; Figure S4.2). This is equivalent to a mean size increase of about 30% compared to WT for the latter strain, in which crystals between 50 and 60 nm were most abundant, with a maximum size of up to 85 nm (Figure S4.2). However, both strains synthesized fewer particles than the WT (Δ*mms36*: 22; Δ*mms48*: 16 per cell), and whereas in WT magnetosome chains of larger particles at midchain are usually flanked by numerous smaller crystals, those characteristic small crystals (15-25 nm) were less

frequent at the chain ends in Δ*mms36* and Δ*mms48* (Figure 4.1; Table 4.1; Figure S4.2). Thus, the predominance of larger (>30 nm) particles partly accounted for the substantially increased mean crystal size. However, despite the reduced particle numbers per cell, overall magnetite biomineralization was increased as evident by the increased iron content of both deletion strains (21% more iron compared to WT).

Genomic expression of additional copies of *mms48* and *mms36* did not significantly change mean particle size (WT::*mms36*: 35 nm; WT::*mms48*: 33 nm; Table 4.1) but the size distribution was shifted towards smaller crystals for both strains. Crystals between 30 and 45 nm were predominant in WT::*mms36* and WT::*mms48*, whereas particles larger than 60 nm were not observed, unlike WT crystals that were most frequently between 40 and 45 nm with a maximum size up to 70 nm (data not shown). Whereas particle number was WT-like for overexpression of Mms36 (32 per cell), crystal number was increased for strain WT::*mms48* (40 per cell; Table 4.1). Interestingly, cells containing double chains were more abundant for WT::*mms48* (WT::*mms48*: 67%; WT::*mms36*: 28%; WT: 32%; Figure S4.3).

In summary, all proteins encoded by *mms6op* are involved in control of magnetosome size or/and number. The previously observed severe biomineralization defects in Δ*mms6op* are thus not due to loss of a single, but several genes, which points towards a cumulative effect on magnetosome synthesis by various proteins encoded by *mms6op.*

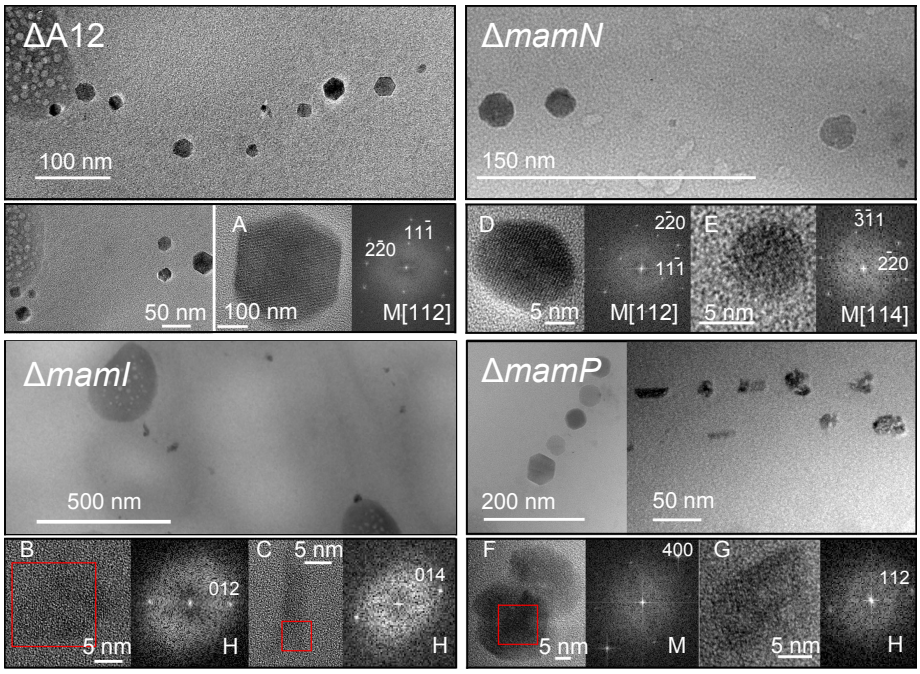

Figure 4.2: **TEM and HRTEM micrographs and their corresponding Fourier transforms of electron dense particles in various generated deletion strains of MSR.** The Fourier transforms were obtained from the images of entire particles or from the boxed areas in each corresponding HRTEM image. The lattice fringe spacings correspond to the strucures of either magnetite (A, D, E, F, G) or hematite (B, C) in the mutants ΔA12, Δ*mamI*, Δ*mamN*, and Δ*mamP*.

Table 4.1: **Characterization of the generated mutants.**

Strain	Deleted Gene/s	Magnetic Response (C_{mag})*	Average Magnetosome Size [nm]	Magnetosome Size [% WT]	Number of Magnetosomes per Cell	Maximum Size [nm]
WT	-	2.0±0.1	35.6±13.0	100	34.3±8.4	69.2
ΔA10	*mms6 operon*	Intermediate	19.7±6.9	55.3	16.8±6.2	39.6
Δ*mms6*	*mms6*	WT	30.4±9.0	85.4	29.7±6.2	57.3
Δ*mmsF*	*mmsF*	Intermediate	28.6±8.0	80.3	30.4±7.4	60.9
Δ*mms48*	*mms48*	WT	46.4±14.8	130.3	16.0±5.6	82.8
Δ*mms36*	*mms36*	WT	39.1±12.9	109.8	22.2±7.3	67.6
Δ*mamF*	*mamF*	WT	33.6±10.4	94.4	33.6±10.4	64.9
Δ*mmsF mamF*	*mmsF, mamF*	WT	25.0±7.4	70.2	26.6±9.3	47.4
Δ*mmsF mms6*	*mmsF, mms6*	Intermediate	24.1±6.4	67.7	24.1±6.8	44.8
WT::*mms36*	-	WT	34.6±9.2	97.2	31.6±10.1	57.2
WT::*mms48*	-	WT	33.2±8.2	93.3	40.2±10.5	58.0
Δ*mamI*	*mamI*	None	14.8±7.1	41.6	9.9±4.3	34.4
Δ*mamL*	*mamL*	None	-	-	-	-
Δ*mamN*	*mamN*	Weak	17.7±7.1	49.7	11.0±7.4	41.3
Δ*mamP*	*mamP*	Intermediate	21.9±15.3	61.5	19.3±10.0	72.8
Δ*mamA*	*mamA*	WT	35.2±13.1	98.9	10.2±4.7	73.4
Δ*mamQ*	*mamQ*	None	-	-	-	-
Δ*mamR*	*mamR*	WT	29.0±11.0	81.5	33.5±10.5	70.2
Δ*mamS*	*mamS*	WT	22.0±7.5	61.8	34.8±12.0	44.2
Δ*mamT*	*mamT*	WT	28.9±10.3	81.2	32.0±8.2	60.1
Δ*mamU*	*mamU*	WT	37.3±13.0	104.8	31.8±8.4	65.3

Deletion analysis of the *mamAB* operon: *mamE*, *L*, *M*, *O*, *Q* and *mamB* are essential for iron biomineralization

First, annotations of all 17 *mamABop* genes were re-assessed. N-termini that were conserved between all three closely related magnetospirilla MSR, AMB and *M. magnetotacticum* were considered the most likely translation starts. Annotations were corrected accordingly for *mamI* and *mamL* (Figure S4.4) and experimentally confirmed by the ability of genes to complement their respective gene deletions. In addition to the previous deletions of the *mamABop* genes, we constructed ten single in frame deletions comprising *mamI*, *L*, *N*, *P*, *A*, *Q*, *R*, *S*, *T*, and *mamU*, respectively. As expected, all resulting deletion strains displayed WT-like growth and morphologies. However, deletion mutants were impaired in mag-

netosome biomineralization to variable extents. Based on their magnetic response mutants either were i) magnetically responsive with variable but significant C_{mag} (Δ*mamN*, *P*, *A*, *R*, *S*, *T*, *mamU*) or ii) entirely non-magnetic without any detectable C_{mag} (Δ*mamI*, *mamQ*, *mamL*; Table 4.1).

TEM analysis confirmed that group (i) strains were still able to synthesize magnetosome-like particles, but displayed various distinct phenotypes with respect to crystal morphology, size, and number per cell (Figure 4.3). Δ*mamU* was hardly distinguishable from WT cells and produced 32 cubo-octahedral crystals per cell with a size of 37 nm. All other mutants showed a drastically decreased magnetosome size, number and/or alignment. Magnetosomes of Δ*mamA* had a WT-like size of 35 nm, but their number was substantially decreased to 10 per cell. Δ*mamS* particles exhibited a widely spaced linear chain-like arrangement within the cell. Whereas the crystal size was strongly decreased (22 nm), they were present in about same numbers as in the WT (35 particles per cell). Δ*mamT* also synthesized irregularly spaced magnetosome chains, whereas in some cells larger magnetosomes appeared at the chain center and formed condensed ”pseudo-chains”. Due to the prevalence of smaller crystals, the mean particle size was decreased to 29 nm, whereas their number was WT-like (32 particles per cell).

Several Δ*mamR* cells showed scattered magnetosomes lacking any chain-like alignment, or short, densely spaced chains flanked by smaller particles with irregular morphologies, or WT chains (average size: 29 nm; number per cell: 34). Δ*mamP* cells at first glance seemed to contain only few (i. e., not more than six magnetosomes, mean three) larger than WT particles (59 nm on average). However, at closer inspection numerous very small and irregularly shaped crystals flanking the larger crystals became apparent with an average size of 16 nm (see arrows in Figure 4.3). In total, Δ*mamP* cells synthesized on average only 19 crystals with a mean size of 22 nm. HRTEM of the two distinct particle types revealed that the lattice fringes for the larger crystals corresponded clearly to magnetite, whereas by contrast the smaller and poorly crystalline particles produced lattice fringes characteristic for hematite (Figure 4.2). The Δ*mamN* mutant showed a very weak, but detectable magnetic response (C_{mag}: 0.1). TEM confirmed the presence of few (11 per cell) tiny, widely spaced crystals with a size of only 18 nm. HRTEM images of these particles and their Fourier-transforms indicated that crystals have the structure of magnetite.

Δ*mamI*, Δ*mamL* and Δ*mamQ* represent the second class of mutants with no detectable magnetic response (C_{mag}: 0). Δ*mamQ* and Δ*mamL* were entirely devoid of any clearly recognizable crystalline electron dense structures (Figure 4.2). In the Δ*mamL* mutant occasionally a few tiny (around 10 nm) structures were observed (not shown), which however, were difficult to discern unambiguously from the cellular body and the background. The relevance and identity of these structures remain to be verified in future studies with higher resolution. Careful analysis of Δ*mamI* cells, however, revealed the presence of a few (10 per cell) electron-dense particles with highly irregular or elongated morphologies and a size of 15 nm (Figure 4.3). As shown by HRTEM, the nuclei within Δ*mamI* were composed of several small grains that formed thin aggregates (Figure 4.2). Lattice fringes were observed in only two particles, and according to the Fourier transforms of the HRTEM images, the spacing between the fringes is very close

to the d(012) and d(014) spacing in hematite. XANES (X-ray Absorption Near Edge Structure) spectra obtained from whole Δ*mamI* and Δ*mamN* cells were clearly distinct from those of pure magnetite as in the WT and suggest that the ferrous compounds are predominantly Fe-S clusters (proteins) that account for around 40% of the total iron content in the cells (Figure S4.5). Magnetite was clearly present in Δ*mamN* cells (around 50% of total iron), whereas the low fit quality for Δ*mamI* did not allow us to reliable determine the structure of the Fe present in the bacteria apart from Fe-S (see supplements for more detailed information). However, the overall line shape appears most consistent with an amorphous or only poorly ordered Fe compound as suggested by HRTEM.

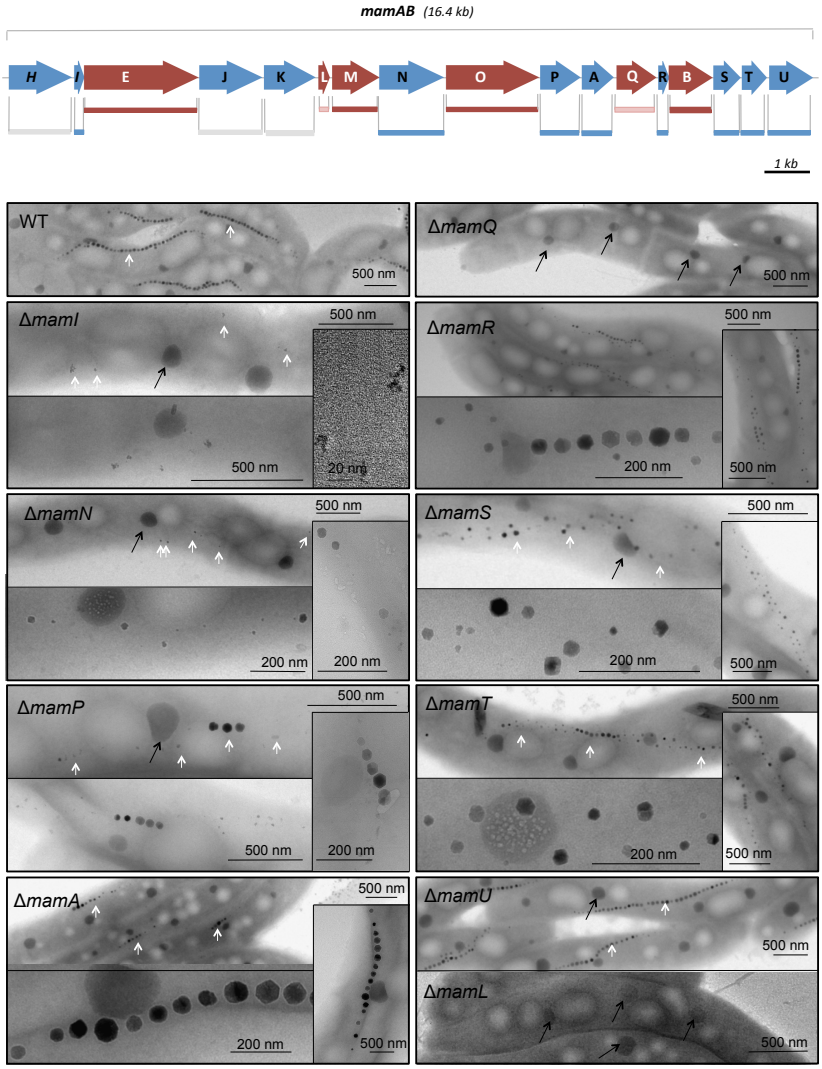

Figure 4.3: **Molecular organization and deletion analysis of the *mamAB* operon of MSR as well as representative TEM micrographs of cells and magnetosome morphologies observed within the generated excision mutants.** The highly conserved *mamAB* operons encodes 17 magnetosome proteins (MamH, I, E, J, K, L, M, N, O, P, A, Q, R, B, S, T, and MamU) in MSR and was found to be essential and sufficient to maintain magnetite biogenesis (18, 22). Red arrows: Genes essential for magnetosome crystal formation. Blue arrows: Genes non-essential for particle formation. Grey bars: Non essential genes, for which deletion strains were previously generated (6, 9, 20). Blue bars: Non-essential genes, (deletions generated in this study). Dark red bars: Essential genes (deletions generated previously (35, 36)). Light red bar: Essential genes (deletions generated in this study). White arrows: magnetosome chains or particles; Black arrows: PHB granules.

Intracellular localization of the magnetosome chain marker MamC-GFP

All mutant strains could be complemented by either genomic reintegration or plasmidal transfer (see supplements). We studied the ability of all mutants to properly localize the abundant MamC magnetosome protein, which served as a marker for magnetosome chain localization in previous studies (6, 36, 44). To this end, MamC was tagged by a chromosomal in-frame EGFP insertion on pFM236 that shows in WT cells a continuous straight-line fluorescence signal (Figure S4.6). Within Δ*mamN*, *P*, *S*, and *mamT* MamC-GFP localized as shorter structures, but still showed a linear localization running along the inner curvature of the cell. Within Δ*mamI* a short, but still elongated fluorescence signal at midcell was observed. Thus MamI, N, P, R, S, and MamT are not required for proper MamC localization. On the contrary, in Δ*mamA*, *mamQ* and *mamL* cells, no defined position of the MamC-GFP signal was detectable, but instead a diffuse spot like accumulation within the cell was predominant (Figure S4.6). In the deletion mutant Δ*mamA* the magnetosome formation was not inhibited, even though MamC is misplaced within this strain, which suggests that MamA may interact with MamC.

Discussion

The Mms6 operon encodes non-essential magnetosome proteins crucial for proper crystal growth

As in AMB (size reduction of crystals by 19%) (22), we observed only minor biomineralization defects upon deletion of *mms6* in MSR (15% size reduction). Only 20% size reduction was also seen after *mmsF* deletion in MSR, which, however, is weaker than its deletion phenotype in AMB (52% size reduction, (22)). However, double deletion of *mms6* and *mmsF* resulted in an almost 32% size reduction, which suggests a certain functional overlap between Mms6 and MmsF. We found functional redundancy between *mmsF* and *mamF* (encoded by the adjacent *mamGFDCop*), since their double deletion exacerbated defects in crystal maturation (30% size reduction). Hence, loss of several genes together contributed to the strong magnetosome defect (45% size reduction) observed after deletion of the entire *mms6op* (ΔA10), which indicates a cumulative regulation of magnetosome biomineralization.

Mms6op of MSR contains two additional genes named *mms36* (*mgr4071*) and *mms48* (*mgr4070*) that are expressed under magnetosome forming conditions (18), but had not yet been studied by deletion analysis in either MSR or AMB. Surprisingly, their deletion caused the synthesis of larger magnetite crystals instead of size reduction. Since no conserved domains or motifs are present in Mms36 and Mms48, apart from weak similarity to proteins involved in porphyrine synthesis (Mms36: 29% to uroporphyrinogen III synthase of *Rhodospirillum rubrum*; Mms48: 28% to HemY-like proteins, possibly involved in porphyrin biosynthesis (45, 46), their precise *in vivo* functions are difficult to infer. They might be itself either inhibitors of crystal growth (32) or recruit other inhibitory proteins to the MM in order to prevent excessive crystal growth.

Genetic analyses of the *mamAB* operon: MamU, T, S, R, A, N and MamI are not essential for iron biomineralization in MSR

We found that deletion of several genes (*mamU, T, S, R, A, P, Q, mamL*) from *mamABop* of MSR essentially phenocopied the deletions of their orthologs in AMB (7). Loss of *mamU*, *T*, *S*, *R*, *A*, *P*, and *mamN* did not entirely abolish biomineralization of magnetite crystals. As in AMB, deletion of MamU did not have any detectable magnetosome phenotype in MSR. MamT of AMB as well as of MSR contains a double cytochrome c motif (CXXCH) referred to as magnetochrome domain necessary for heme-binding (47). It was speculated that MamT therefore transfers electrons to balance the ferric-to-ferrous iron ratio form required for magnetite formation (47). Deletion of *mamT* in MSR resulted in smaller magnetosome particles as in AMB, supporting its previously predicted function in crystal maturation.

As in Δ*mamT*, deletion of *mamR* in MSR resulted in smaller crystals and partially modified chain formation similar to the phenotype observed for Δ*mamR* in AMB. Thus, MamR is involved in controlling particle number and size as also suggested for MamR of AMB (7). We also confirmed a key role of MamS in MSR, which has similarity to the putative serine proteases and magnetochrome domain containing proteins MamE and MamX (20, 32). However, MamS itself lacks a magnetochrome domain, which argues against its direct participation in redox control. The TPR domain-containing protein MamA was speculated to play a role in activation of biomineralization (5). It was suggested that MamA self-assembles through its putative TPR domain and concave site to form a large homooligomeric scaffold surrounding the magnetosomes (48, 49), whereas its convex site interacts with other magnetosome-associated proteins like MamC and several unidentified proteins (48, 49). However, as in AMB the deletion of *mamA* in MSR had only a weak effect (5), suggesting that these interactions are not essential or can be partly compensated by other proteins.

In Δ*mamP* of MSR, particles larger than those synthesized by the WT were flanked by smaller and poorly crystalline particles similar to AMB (50). MamP contains two closely spaced magnetochrome domains and was speculated to interact with MamE, MamX and MamT through its PDZ domain and to somehow regulate the electron transport required for biomineralization of the mixed valence iron oxide magnetite (20, 32, 50). Magnetosomes in Δ*mamP* of MSR show a similar crystallization defect (magnetite crystals flanked by flakes) like the *mamX* mutant of MSR (20) and thus might indicate the involvment in the same step of magnetosome biosynthesis. In contrast, phenotypes of MSR Δ*mamT* (smaller particles) and Δ*mamE* (total loss of electron dense particles) are distinct from the deletion phenotype of Δ*mamP*, suggesting that some or all of the magnetochrome proteins have different or additional functions. However, MamE also contains beside the magnetochrome domains, a protease and double PDZ domains, which might cause the differences between the generated mutants upon their deletion (32). Thus, further analyses are needed to explain the different observed mutant phenotypes, such as the specific deletion of the different magnetochrome domains. MamP from AMB catalyzed the formation of ferrihydrite and magnetite from iron solutions *in vitro*, indicating that MamP binds and oxidizes iron

(50). However, this ability of MamP is not essential *in vivo*, as the Δ*mamP* mutant of MSR continued to biomineralize particles of magnetite. Potentially this might be due to unchecked mineral growth after deletion of a major redox regulator (51) or/and the ability of other magnetochrome proteins like MamX, MamE and MamT to partially compensate the loss of MamP.

In addition to the strong similarities between several AMB and MSR mutants, we also found several striking differences between the two species. MamN was described to be essential for magnetosome biosynthesis, as indicated by the absence of electron dense crystals in AMB (7). However, our TEM, HRTEM and XANES analyses revealed the presence of magnetite particles within Δ*mamN* of MSR. Because of its similarity to the human Permease P that is predicted to regulate the intraorganelle pH of melanosomes together with an ATP-driven proton pump (52), MamN was speculated to regulate pH conditions within the magnetosome vesicles by export of protons released by the precipitation of magnetite ($2Fe^{3+}+Fe^{2+}+4H_2O \rightarrow Fe_3O_4+8H^+$) (38, 53), and thus the observed phenotype of Δ*mamN* might be due to alteration of the intra-magnetosomal pH.

Another gene, which exhibited a strikingly distinct deletion phenotype between AMB and MSR is *mamI*, which encodes a small magnetospirilla-specific magnetosome protein (70 aa) with no significant homology to already characterized proteins. In AMB, MamI was found to be essential for the biosynthesis of both magnetosome membrane vesicles, and consequently, iron biomineralization (7). In contrast, excision of *mamI* in MSR did not entirely abolish the biomineralization of electron dense iron-rich particles, but the mutant still synthesized tiny and poorly crystalline non-magnetic particles, which in some cases were shown to consist of hematite. Recent findings in MSR and AMB indicate that the observed poorly ordered iron (oxyhydr)oxide phases are precursors to the magnetite phase in bacteria (43, 54). In addition, the ability of MamP to precipitate ferrihydrite and magnetite in vitro suggests that magnetite may be formed through a stepwise phase transformation process (50). Such a biosynthetic phase transformation requires a precise control of iron supersaturation, pH, and redox potential levels (55), suggesting that MamI may be involved at an early stage of magnetite nucleation by regulation of proper conditions within the vesicles.

Only MamE, L, M, O, B and MamQ are essential for iron biomineralization in MSR

In addition to the previously identified *mamE* (35), *mamM* (56), *mamO* (35) and *mamB* (56) we also demonstrated *mamQ* and most probably *mamL* to be essential genes for magnetosome synthesis in MSR, since their deletions abolished the biomineralization of clearly distinguishable electron dense particles. MamQ shares homology with the LemA protein, which is conserved in several bacteria but whose function is uncertain (12, 57). MamQ has a high content of α-helices that are somewhat reminiscent to the EFC/BAR domain of Formin Binding Protein 17 (7). BAR domains have the ability to sense and stabilize membrane curvatures (58), and their weak similarity to MamQ might hint towards related functions in MM vesicle genesis of the protein. The small protein MamL has no predicted function, but was shown to be essential for magnetosome membrane genesis in AMB (7). Despite the metabolic and genetic

similarities between AMB and MSR, previous studies already suggested that the function of orthologous genes might be somewhat distinct in these organisms (6, 18, 59). Apart from the possibility that the tiny magnetite and hematite particles in Δ*mamN* and Δ*mamI* of MSR simply had escaped detection in the corresponding mutants of AMB (7), this might possibly due to the different genetic context, with only about 50% of all genes shared by the genomes of these two strains (14). In fact, it can not be excluded that further genes outside of the MAI partially compensate the loss of deleted genes as observed in a recent study, in which a magnetosome islet outside the MAI compensated the deletion of *mamK* in AMB (6, 33).

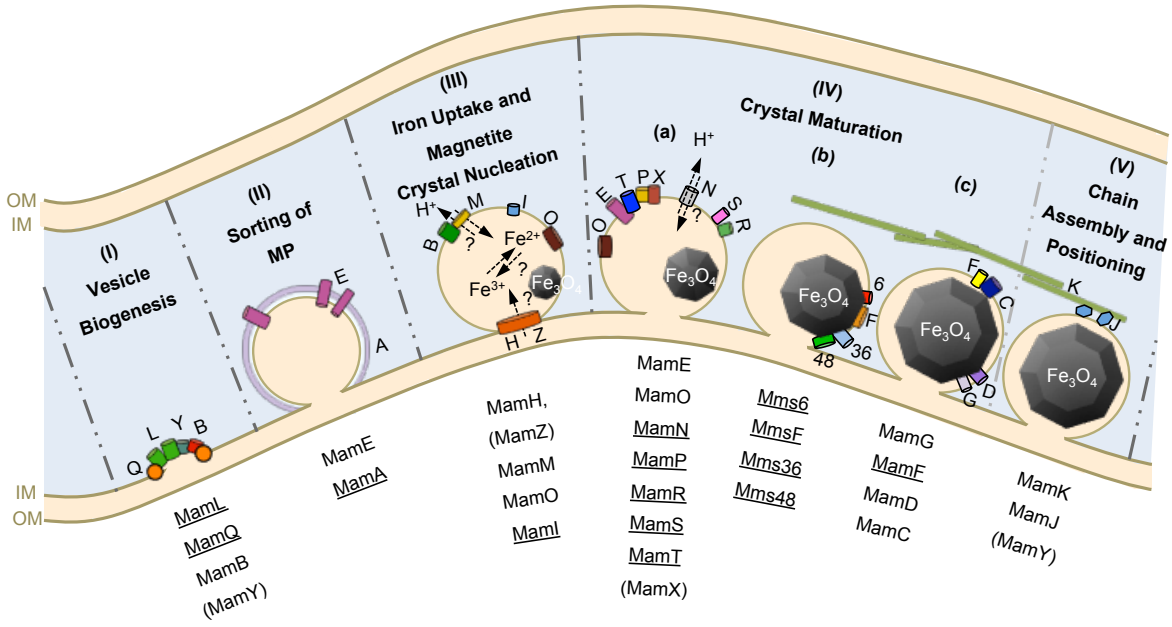

Figure 4.4: **Hypothetical model for magnetosome biosynthesis in MSR.** Magnetosome biosynthesis depends on various steps including various magnetosome proteins. Magnetosome vesicle formation (I) is induced by the proteins MamQ, MamL, and MamB. MamY was found to regulate vesicle shape (23). MamA forms a multiprotein complex surrounding the magnetosome membrane (49) and MamE is involved in localization of magnetosome proteins by a protease independent process (32). The heterodimer of the CDF transporters MamB and MamM transports ferrous iron into the magnetosome vesicles (56) and ferric iron is taken up by MamH and MamZ (20) or formed by oxidation of ferrous iron within the vesicles. MamI is involved in magnetite nucleation. MamO was speculated to be directly involved in precipitation of iron oxide particles (32). The crystal growth is affected by several magnetosome proteins also including MamE that proteolytically remove a/an growth inhibitor/s or activate growth promoting proteins (32). Based on the conserved CXXCH heme-binding motifs within MamE, MamT, MamP and MamX it has been speculated that the proteins form a complex for electron transport to regulate electron flow (20, 47). MamS and MamR control crystal size by an unknown mechanism. MamN exhibits similarity to H^+-translocation proteins and might be involved in crystal growth by regulating intramagnetosomal pH (53). Mms6 is tightly bound to the magnetosome crystals (26, 28) and assembles into coherent micelles for templating crystal growth (60). Mms48 and Mms36 act as inhibitors of crystal growth or recruit inhibiting proteins of particle growth by an unknown mechanism. The small, hydrophobic proteins MamG, MamF, MamD, and MamC control in a cumulative manner the growth of magnetite crystals (21). Magnetosomes were assembled into chains by the interaction of MamJ with the actin-like MamK filament that is also involved in chain positioning (6, 9, 61). OM: outer membrane; IM: inner membrane; MP: magnetosome protein; underlined proteins: analyzed proteins in this study, by single gene deletion of encoding genes. Proteins in brackets: non-essential proteins encoded by the textitmamXYop.

In summary, whereas in AMB eight proteins (MamI, E, L, M, N, O, B, MamQ) were found to be essential for magnetosome biomineralization, in MSR only six proteins (MamE, M, O, B, Q, and most probably MamL) are essential for at least some rudimentary iron biomineralization and, if including MamI, seven proteins for the biosynthesis of magnetite-containing magnetosomes. This leads to an expanded model of magnetosome biosynthesis in MSR (Figure 4.4). However, it remains to be shown whether these essential magnetosome proteins are also sufficient for vesicle formation and crystallization even in the absence of the other factors encoded by the *mamAB* and other magnetosome operons.

Acknowledgement

This work was funded by the Deutsche Forschungsgemeinschaft (grants DFG Schu1080/13-1 and 15-1) and the European Union (Project Bio2MaN4MRI n°245542). AL was supported by the Konrad-Adenauer-Stiftung. We acknowledge the European Synchrotron Radiation Facility for provision of synchrotron radiation facilities. We thank J.-D. Cafun, P. Glatzel, and C. Lapras for assistance in using beamline ID26 at ESRF. We are thankful to R. Susen, A. Hähle, A. Singer, T. Perez Gonzalez and G. Morin for experimental support. The research was further supported by the Max Planck Society and the European Research Council through a Starting Grant to DF (Project MB^2 n°256915).

References

1. Bazylinski D, Lefèvre C, Schüler D. 2013. Magnetotactic Bacteria, p. 453-494. In Rosenberg E, DeLong E, Lory S, Stackebrandt E, Thompson F (ed.), The Prokaryotes. Springer Berlin Heidelberg.
2. Blakemore R. 1975. Magnetotactic bacteria. Science 190:377-379.
3. Schüler D. 2004. Molecular analysis of a subcellular compartment: the magnetosome membrane in *Magnetospirillum gryphiswaldense*. Arch Microbiol 181:1-7.
4. Grünberg K, Müller EC, Otto A, Reszka R, Linder D, Kube M, Reinhardt R, Schüler D. 2004. Biochemical and proteomic analysis of the magnetosome membrane in *Magnetospirillum gryphiswaldense*. Appl Environ Microbiol 70:1040-1050.
5. Komeili A, Vali H, Beveridge TJ, Newman DK. 2004. Magnetosome vesicles are present before magnetite formation, and MamA is required for their activation. Proc Natl Acad Sci U S A 101:3839-3844.
6. Katzmann E, Scheffel A, Gruska M, Plitzko JM, Schüler D. 2010. Loss of the actin-like protein MamK has pleiotropic effects on magnetosome formation and chain assembly in *Magnetospirillum gryphiswaldense*. Mol Microbiol 77:208-224.

7. Murat D, Quinlan A, Vali H, Komeili A. 2010. Comprehensive genetic dissection of the magnetosome gene island reveals the step-wise assembly of a prokaryotic organelle. Proc Natl Acad Sci U S A 107:5593-5598.
8. Faivre D, Böttger LH, Matzanke BF, Schüler D. 2007. Intracellular magnetite biomineralization in bacteria proceeds by a distinct pathway involving membrane-bound ferritin and an iron(II) species. Angew Chem Int Ed Engl 46:8495-8499.
9. Scheffel A, Gruska M, Faivre D, Linaroudis A, Plitzko JM, Schüler D. 2006. An acidic protein aligns magnetosomes along a filamentous structure in magnetotactic bacteria. Nature 440:110-114.
10. Schübbe S, Kube M, Scheffel A, Wawer C, Heyen U, Meyerdierks A, Madkour MH, Mayer F, Reinhardt R, Schüler D. 2003. Characterization of a spontaneous nonmagnetic mutant of *Magnetospirillum gryphiswaldense* reveals a large deletion comprising a putative magnetosome island. J Bacteriol 185:5779-5790.
11. Ullrich S, Kube M, Schübbe S, Reinhardt R, Schüler D. 2005. A hypervariable 130-kilobase genomic region of *Magnetospirillum gryphiswaldense* comprises a magnetosome island which undergoes frequent rearrangements during stationary growth. J Bacteriol 187:7176-7184.
12. Grünberg K, Wawer C, Tebo BM, Schüler D. 2001. A large gene cluster encoding several magnetosome proteins is conserved in different species of magnetotactic bacteria. Appl Environ Microbiol 67:4573-4582.
13. Matsunaga T, Okamura Y, Fukuda Y, Wahyudi AT, Murase Y, Takeyama H. 2005. Complete genome sequence of the facultative anaerobic magnetotactic bacterium Magnetospirillum sp. strain AMB-1. DNA Res 12:157-166.
14. Richter M, Kube M, Bazylinski DA, Lombardot T, Glockner FO, Reinhardt R, Schüler D. 2007. Comparative genome analysis of four magnetotactic bacteria reveals a complex set of group-specific genes implicated in magnetosome biomineralization and function. J Bacteriol 189:4899-4910.
15. Nakazawa H, Arakaki A, Narita-Yamada S, Yashiro I, Jinno K, Aoki N, Tsuruyama A, Okamura Y, Tanikawa S, Fujita N, Takeyama H, Matsunaga T. 2009. Whole genome sequence of *Desulfovibrio magneticus* strain RS-1 revealed common gene clusters in magnetotactic bacteria. Genome Res 19:1801-1808.
16. Jogler C, Kube M, Schübbe S, Ullrich S, Teeling H, Bazylinski DA, Reinhardt R, Schüler D. 2009. Comparative analysis of magnetosome gene clusters in magnetotactic bacteria provides further evidence for horizontal gene transfer. Environ Microbiol 11:1267-1277.
17. Schübbe S, Williams TJ, Xie G, Kiss HE, Brettin TS, Martinez D, Ross CA, Schüler D, Cox BL, Nealson KH, Bazylinski DA. 2009. Complete genome sequence of the chemolithoautotrophic marine magnetotactic coccus strain MC-1. Appl Environ Microbiol 75:4835-4852.

18. Lohße A, Ullrich S, Katzmann E, Borg S, Wanner G, Richter M, Voigt B, Schweder T, Schüler D. 2011. Functional analysis of the magnetosome island in *Magnetospirillum gryphiswaldense*: the *mamAB* operon is sufficient for magnetite biomineralization. PLoS One 6:e25561.
19. Schübbe S, Wurdemann C, Peplies J, Heyen U, Wawer C, Glockner FO, Schüler D. 2006. Transcriptional organization and regulation of magnetosome operons in *Magnetospirillum gryphiswaldense*. Appl Environ Microbiol 72:5757-5765.
20. Raschdorf O, Müller FD, Pósfai M, Plitzko JM, Schüler D. 2013. The magnetosome proteins MamX, MamZ and MamH are involved in redox control of magnetite biomineralization in *Magnetospirillum gryphiswaldense*. Mol Microbiol 89:872-886.
21. Scheffel A, Gardes A, Grünberg K, Wanner G, Schüler D. 2008. The major magnetosome proteins MamGFDC are not essential for magnetite biomineralization in *Magnetospirillum gryphiswaldense* but regulate the size of magnetosome crystals. J Bacteriol 190:377-386.
22. Murat D, Falahati V, Bertinetti L, Csencsits R, Körnig A, Downing K, Faivre D, Komeili A. 2012. The magnetosome membrane protein, MmsF, is a major regulator of magnetite biomineralization in *Magnetospirillum magneticum* AMB-1. Mol Microbiol 85:684-699.
23. Tanaka M, Arakaki A, Matsunaga T. 2010. Identification and functional characterization of liposome tubulation protein from magnetotactic bacteria. Mol Microbiol 76:480-488.
24. Tanaka M, Mazuyama E, Arakaki A, Matsunaga T. 2011. MMS6 protein regulates crystal morphology during nano-sized magnetite biomineralization in vivo. J Biol Chem 286:6386-6392.
25. Arakaki A, Webb J, Matsunaga T. 2003. A novel protein tightly bound to bacterial magnetic particles in *Magnetospirillum magneticum* strain AMB-1. J Biol Chem 278:8745-8750.
26. Oestreicher Z, Valverde-Tercedor C, Chen L, Jimenez-Lopez C, Bazylinski DA, Casillas-Ituarte NN, Lower SK, Lower BH. 2012. Magnetosomes and magnetite crystals produced by magnetotactic bacteria as resolved by atomic force microscopy and transmission electron microscopy. Micron 43:1331-1335.
27. Amemiya Y, Arakaki A, Staniland SS, Tanaka T, Matsunaga T. 2007. Controlled formation of magnetite crystal by partial oxidation of ferrous hydroxide in the presence of recombinant magnetotactic bacterial protein Mms6. Biomat 28:5381-5389.
28. Arakaki A, Masuda F, Amemiya Y, Tanaka T, Matsunaga T. 2010. Control of the morphology and size of magnetite particles with peptides mimicking the Mms6 protein from magnetotactic bacteria. J Colloid Interface Sci 343:65-70.
29. Kolinko I, Lohße A, Borg S, Raschdorf O, Jogler C, Tu Q, Pósfai M, Tompa E, Plitzko JM, Brachmann A, Wanner G, Muller R, Zhang Y, Schüler D. 2014. Biosynthesis of magnetic nanostructures in a foreign organism by transfer of bacterial magnetosome gene clusters. Nat Nanotechnol 9:193-197.

30. Komeili A, Li Z, Newman DK, Jensen GJ. 2006. Magnetosomes are cell membrane invaginations organized by the actin-like protein MamK. Science 311:242-245.
31. Draper O, Byrne ME, Li Z, Keyhani S, Barrozo JC, Jensen G, Komeili A. 2011. MamK, a bacterial actin, forms dynamic filaments in vivo that are regulated by the acidic proteins MamJ and LimJ. Mol Microbiol 82:342-354.
32. Quinlan A, Murat D, Vali H, Komeili A. 2011. The HtrA/DegP family protease MamE is a bifunctional protein with roles in magnetosome protein localization and magnetite biomineralization. Mol Microbiol 80:1075-1087.
33. Rioux JB, Philippe N, Pereira S, Pignol D, Wu LF, Ginet N. 2010. A second actin-like MamK protein in *Magnetospirillum magneticum* AMB-1 encoded outside the genomic magnetosome island. PLoS One 5:e9151.
34. Katzmann E, Scheffel A, Gruska M, Plitzko JM, Schüler D. 2010. Loss of the actin-like protein MamK has pleiotropic effects on magnetosome formation and chain assembly in *Magnetospirillum gryphiswaldense*. Mol Microbiol 77:208-224.
35. Yang W, Li R, Peng T, Zhang Y, Jiang W, Li Y, Li J. 2010. *mamO* and *mamE* genes are essential for magnetosome crystal biomineralization in *Magnetospirillum gryphiswaldense* MSR-1. Res Microbiol 161:701-705.
36. Uebe R, Junge K, Henn V, Poxleitner G, Katzmann E, Plitzko JM, Zarivach R, Kasama T, Wanner G, Pósfai M, Böttger L, Matzanke B, Schüler D. 2011. The cation diffusion facilitator proteins MamB and MamM of *Magnetospirillum gryphiswaldense* have distinct and complex functions, and are involved in magnetite biomineralization and magnetosome membrane assembly. Mol Microbiol 82:818-835.
37. Heyen U, Schüler D. 2003. Growth and magnetosome formation by microaerophilic Magnetospirillum strains in an oxygen-controlled fermentor. Appl Microbiol Biotechnol 61:536-544.
38. Faivre D, Böttger LH, Matzanke BF, Schüler D. 2007. Intracellular magnetite biomineralization in bacteria proceeds by a distinct pathway involving membrane-bound ferritin and an iron(II) species. Angew Chem Int Ed Engl 46:8495-8499.
39. Sambrook J, Russell DW. 2001. Molecular cloning: a laboratory manual, vol. 2. Cold Spring Harbor Laboratory Press, New York.
40. Schüler D, Uhl R, Baeuerlein E. 1995. A simple light-scattering method to assay magnetism in *Magnetospirillum gryphiswaldense* FEMS Microbiol. Lett. 132:139-145.
41. Kolinko I, Jogler C, Katzmann E, Schuler D. 2011. Frequent mutations within the genomic magnetosome island of *Magnetospirillum gryphiswaldense* are mediated by RecA. J Bacteriol 193:5328-5334.

42. Sodhi S, Banda H, Kathyola D, Burciul B, Thompson S, Joshua M, Bateman E, Fairall L, Martiniuk A, Cornick R, Faris G, Draper B, Mondiwa M, Katengeza E, Sanudi L, Zwarenstein M, Schull MJ. 2011. Evaluating a streamlined clinical tool and educational outreach intervention for health care workers in Malawi: the PALM PLUS case study. BMC Int Health Hum Rights 11 Suppl 2:S11.
43. Baumgartner J, Morin G, Menguy N, Perez Gonzalez T, Widdrat M, Cosmidis J, Faivre D. 2013. Magnetotactic bacteria form magnetite from a phosphate-rich ferric hydroxide via nanometric ferric (oxyhydr)oxide intermediates. Proc Natl Acad Sci U S A 110:14883-14888.
44. Lang C, Schüler D. 2008. Expression of green fluorescent protein fused to magnetosome proteins in microaerophilic magnetotactic bacteria. Appl Environ Microbiol 74:4944-4953.
45. Frankenberg N, Moser J, Jahn D. 2003. Bacterial heme biosynthesis and its biotechnological application. Appl Microbiol Biotech 63:115-127.
46. Panek H, O'Brian MR. 2002. A whole genome view of prokaryotic haem biosynthesis. Microbiol 148:2273-2282.
47. Siponen MI, Adryanczyk G, Ginet N, Arnoux P, Pignol D. 2012. Magnetochrome: a c-type cytochrome domain specific to magnetotatic bacteria. Biochem Soc Trans 40:1319-1323.
48. Yamamoto D, Taoka A, Uchihashi T, Sasaki H, Watanabe H, Ando T, Fukumori Y. 2010. Visualization and structural analysis of the bacterial magnetic organelle magnetosome using atomic force microscopy. Proc Nat Ac Sci 107:9382-9387.
49. Zeytuni N, Ozyamak E, Ben-Harush K, Davidov G, Levin M, Gat Y, Moyal T, Brik A, Komeili A, Zarivach R. 2011. Self-recognition mechanism of MamA, a magnetosome-associated TPR-containing protein, promotes complex assembly. Proc Natl Ac of Sci 108:E480-E487.
50. Siponen MI, Legrand P, Widdrat M, Jones SR, Zhang W-J, Chang MCY, Faivre D, Arnoux P, Pignol D. 2013. Structural insight into magnetochrome-mediated magnetite biomineralization. Nature 502:681-684.
51. Rahn-Lee L, Komeili A. 2013. The magnetosome model: insights into the mechanisms of bacterial biomineralization. Front Microbiol 4:352.
52. Brilliant MH. 2001. The mouse p (pink-eyed dilution) and human P genes, oculocutaneous albinism type 2 (OCA2), and melanosomal pH. Pigment Cell Res 14:86-93.
53. Schüler D. 2008. Genetics and cell biology of magnetosome formation in magnetotactic bacteria. FEMS Microbiol Rev 32:654-672.
54. Fdez-Gubieda ML, Muela A, Alonso J, Garcia-Prieto A, Olivi L, Fernandez-Pacheco R, Barandiaran JM. 2013. Magnetite biomineralization in *Magnetospirillum gryphiswaldense*: time-resolved magnetic and structural studies. ACS Nano 7:3297-3305.
55. Bell PE, Mills AL, Herman JS. 1987. Biogeochemical Conditions Favoring Magnetite Formation during Anaerobic Iron Reduction. Appl Environ Microbiol 53:2610-2616.

56. Uebe RJ, K. Henn, V. Poxleitner, G. Katzmann, E. Plitzko, J.M. Zarivach, R. Kasama, T. Wanner, G. Pósfai, M. Böttger, L. Matzanke, B. Schüler, D. 2011. The cation diffusion facilitator proteins MamB and MamM of *Magnetospirillum gryphiswaldense* have distinct and complex functions, and are involved in magnetite biomineralization and magnetosome membrane assembly. Mol Microbiol 82:818Ð835.
57. Lenz LL, Dere B, Bevan MJ. 1996. Identification of an H2-M3-restricted Listeria epitope: implications for antigen presentation by M3. Immunity 5:63-72.
58. McMahon HT, Gallop JL. 2005. Membrane curvature and mechanisms of dynamic cell membrane remodelling. Nature 438:590-596.
59. Richter M, Kube M, Bazylinski DA, Lombardot T, Glockner FO, Reinhardt R, Schüler D. 2007. Comparative genome analysis of four magnetotactic bacteria reveals a complex set of group-specific genes implicated in magnetosome biomineralization and function. J Bacteriol 189:4899-4910.
60. Wang W, Bu W, Wang L, Palo PE, Mallapragada S, Nilsen-Hamilton M, Vaknin D. 2012. Interfacial Properties and Iron Binding to Bacterial Proteins That Promote the Growth of Magnetite Nanocrystals: X-ray Reflectivity and Surface Spectroscopy Studies. Langmuir 28:4274-4282.
61. Katzmann E, Müller FD, Lang C, Messerer M, Winklhofer M, Plitzko JM, Schüler D. 2011. Magnetosome chains are recruited to cellular division sites and split by asymmetric septation. Mol Microbiol 82:1316-1329.

5 Chapter V

4th Publication

Genome engineering of *Magnetospirillum gryphiswaldense* improves magnetosome yield by overexpression of magnetosome operons.

Publication state: *In preparation*.

Introduction

The ability of magnetotactic bacteria (MTB) to orient along the earth's magnetic field is based on specific organelles, the magnetosomes, which are membrane-enveloped crystals of an iron mineral [1]. The model organism *Magnetospirillum gryphiswaldense* (in the following referred to as MSR) synthesizes cuboctahedral magnetite (Fe_3O_4) particles, which are assembled to chain-like nanostructures within the cell. Magnetosome crystals have uniform morphologies [2], a high chemical purity [3], and structural perfection [4], which are mostly unknown from inorganic systems. The unusual characteristics of the crystals, as well as the inherent biocompatibility provided by the magnetosome membrane (MM), inspired numerous ideas for their biotechnological application [5], such as magnetic drug targeting, immunoassays and magnetic resonance imaging [6,7,8,9,10,11].

The biomineralization of magnetite crystals in MTB proceeds in sequential steps including MM vesicle formation, sorting of MM-specific proteins, magnetosomal iron uptake, magnetite crystallization and chain assembly along a cytoskeletal filament [3,12,13,14,15]. We recently discovered genes controlling magnetosome synthesis in MSR to be clustered within a larg (115 kb) genomic magnetosome island, in which they are interspersed by numerous genes of unrelated or unknown functions [16,17]. While the smaller *mamGFDC*, *mms6* and *mamXY* operons have accessory roles in the biomineralization of properly sized and shaped crystals [17,18,19], only the large *mamAB* operon is necessary and sufficient for magnetite biomineralization [17]. In contrast, at least the *mamGFDC*, *mms6*, and *mamAB* operons are needed for formation of poorly crystalline hematite particles in the heterologous host *Rhodospirillum rubrum*, and all four major operons are required for biomineralization of magnetite crystals [20].

Previous studies in MSR and the genetically closely related *M. magneticum* AMB-1 (referred to as AMB) so far focused on genetic dissection of the MAI and the *mam* and *mms* operons by deletion mutagenesis. For instance, a comprehensive analysis of the *mamAB* operon recently revealed that eight proteins (MamI, E, L, M, N, O, B, Q) are essential for magnetosome biomineralization in AMB, whereas in MSR only six proteins (MamE, L, M, O, B, Q) are required for at least some rudimentary iron

biomineralization and, if including MamI, seven proteins for the biosynthesis of magnetite-containing magnetosomes [21,22]. The major magnetosome proteins MamG, F, D, and C, which account for over 35% of all magnetosome-associated proteins, were shown to be involved in size control, since mutant cells formed smaller and less regular magnetite crystals [23,24]. Deletion of the 3.7 kb *mms6* operon resulted in significantly smaller crystals which are aligned in short chains or loosely scattered within the cell [17]. Consistent with this finding, the MTB-specific MmsF and Mms6 proteins are predicted to be major regulators of crystal size and shape in AMB [25,26]. In MSR Mms36 and Mms48 have been shown to influence magnetosome biosynthesis, too and a cumulative effect on biomineralization by various proteins encoded by the *mms6* operon has been suggested [22].

The proteins MamX and MamZ encoded by the *mamXY* operon were shown to be major redox regulators for magnetite biomineralization in MSR [19]. Deletion of the whole operon resulted in size reduction of the crystals as well as in the co-existence of various distinct magnetosome morphologies, including cubo-octahedral magnetite particles flanked by flake-like hematite crystals [17,19].

However, while the impact of gene deletions on magnetosome biomineralization has been studied in different approaches, the effect of overexpression of the *mam* and *mms* genes on magnetosome formation has been poorly investigated so far. This could provide insights in the impact of the *mam* and *mms* protein level on the regulation of biomineralization, and potentially facilitate the genetically controlled overproduction of magnetosomes for various biotechnological applications. For instance, Scheffel *et al*. showed that in trans expression of additional copies of the entire *mamGFDC* operon in the wild type caused the formation of enlarged magnetite particles compared to those produced by the wild type without additional copies [18]. Recently, overexpression of *mms48* resulted in a slight increase in the particle numbers per cell, too [22]. However, due to the lack of an appropriate expression system these first approaches were limited to a gene dosage increase of small operons or single genes. Both studies showed that selective overexpression of single or few magnetosome genes results the synthesis of weakly larger crystals or increased magnetosome numbers in *M gryphiswaldense*. However, the effects of a further gene dosage increase of single operons or even multiplication of all *mam* and *mms* genes on magnetosome formation have not be systematically investigated so far.

Here, we demonstrate the feasibility to enhance magnetite biomineralization in *M gryphiswaldense* by multiplication of single, as well as all major magnetosome operons via transposition. We show that a higher gene dosage of the *mms6* operon results in the formation of larger crystals as well as moderately increased magnetosome numbers per cell. In contrast, overexpression of all major operons specifically enhanced the number of particles by about 117%. This demonstrates that the expression level of different *mam* and *mms* proteins seems to be an important factor in the regulation of crystal formation in *M. gryphiswaldense*. Furthermore, the findings show that genetic engineering by a gene dosage increase of the *mam* and *mms* genes provides a powerful strategy for the precise control of the particle size or numbers.

Results

Overexpression of *mms6* and *mamGFDC* operons

For controlled overexpression of different magnetosome operons, MSR was engineered by mariner or Tn5 transposon driven random chromosomal insertion. This technique has recently also been successfully applied for genetic transfer of the magnetosome biosynthesis pathway into *R. rubrum* [20], expression of recombinant proteins on the magnetosome surface [10], and chromosomal insertion of single magnetosome genes [22]. Transconjugants were obtained at frequencies between 2-5x10^{-7} and chromosomal insertions were stably inherited as indicated by the ability of transformed strains to grow in the presence of kanamycin after 120 generations without antibiotic selection. All insertants essentially displayed WT-like growth (Figure S5.1).

Chromosomal duplication of the *mms6* operon resulted in strain ΔRecA+*mms6* 1x that possesses one native and one inserted *mms6* operon, and remarkably increased magnetosome biomineralization. The merodiploid mutant strain synthesized 36% more crystals per cell (47 compared to 34 magnetosomes per cell within ΔRecA (Table 5.1) with an increased size of 46 nm (ΔRecA=36 nm) and formed a high proportion of multiple chains that were less frequently observed in ΔRecA. Intracellular iron content of ΔRecA+*mms6* 1x was increased by about [14.9±2.9]% (Table S5.1). Insertion of two further *mms6* operons (one native and two inserted *mms6* operons) in strains ΔRecA+*mms6* 2x lead in average (n=1183) to 54 magnetite particles per cell with a size of 48 nm that corresponds to an increase in number by 58%, size by 35%, and intracellular iron content of [34.8±2.5]% compared to ΔRecA (Figure 5.1; Table S5.1). ΔRecA+*mms6* 3x carrying four copies of *mms6* operon produced 58 magnetite crystals per cell with a diameter of 44 nm and an intracellular iron content increased from 2.68% to 3.73% iron per dry weight, which represents only a slight further increase compared to ΔRecA+*mms6* 2x (increase by [38.8±2.5]% compared to ΔRecA (Figure 5.1; Table S5.1). Cultivation under anaerobic conditions with 50 μM or 500 μM iron did not significantly increase iron uptake of ΔRecA+*mms6* 3x compared to cultivation under microaerobic conditions with 50 μM iron (Figure S5.1). Insertion of four additional copies of the *mms6* operon in ΔRecA+*mms6* 4x (5 *mms6* operons in total) did not further increase biomineralization, but on the contrary caused a size reduction of 13% and 6% compared to ΔRecA+*mms6* 2x and ΔRecA+*mms6* 3x, respectively. Cultivation of overproducing strains ΔRecA+*mms6* 2x at higher iron concentrations (250 μM iron) did not further increase magnetosome numbers, although size distributions were slightly shifted towards to larger crystals with maximum sizes up to 85 nm (Figure S5.1).

Within anarobically grown cells of ΔRecA+*mms6* 2x and ΔRecA+*mms6* 3x a variable proportion of enlarged vesicle were visible in cryo electron tomograms (Figure 5.1). These ”giant” vesicles appeared as regularly shaped as in the WT, but their size was increased up to 119 nm (ΔRecA+*mms6* 2x) whereas WT vesicles had a maximum size of 54 nm. However, the ratio between the size of the vesicle and the particle sizes measured from CET tomograms was similar and not significantly increased (ΔRecA+*mms6* 2x: 2.8±0.8, ΔRecA+*mms6* 3x: 2.3±0.9; WT: 2.1±1.4). As reported for the parental strain ΔRecA, all

overexpression strains had a variable proportion of small vibrioid and elongated cells [27] and cells on average became more elongated with increasing copy number of inserted *mms6* operons ([4.53±1.59] μm, [4.56 ±1.46 μm], [5.10±1.95] μm, and [5.3±1.7] μm for ΔRecA+*mms6* 1x, 2x, 3x, and 4x, respectively versus [4.44± 1.26] for ΔRecA (Figure 5.2). Shorter cells (<10 μm) of ΔRecA+*mms6* 2x contained fewer 43 and smaller 43 nm particles, whereas highly elongated cells (>10 μm) had significantly more (53-138 particles, mean: 104; n=572, equivalent to a 206% increase) and larger magnetite crystals (49 nm) with a maximum size of 80 nm.

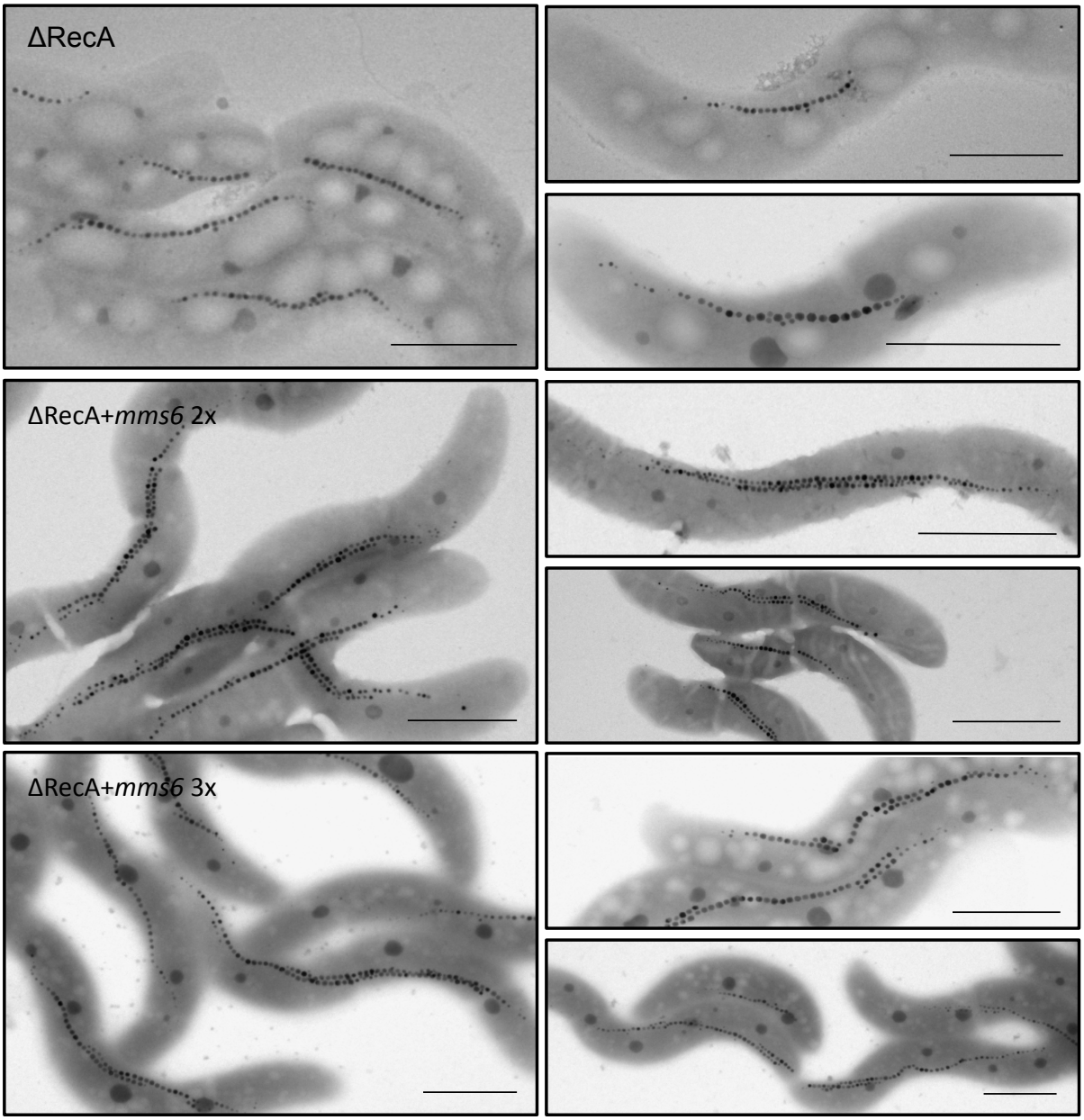

Figure 5.1: **Representative TEM micrographs of magnetosomes found in *mms6* operon overexpression strains and their parent strain ΔRecA.** Whereas ΔRecA synthesizes mostly short and single stranded magnetosome chains, the overexpression strains ΔRecA+*mms6* 2x and ΔRecA+*mms6* 3x produce double chains with increased magnetosome sizes and numbers per cell. Scale bar: 1 μm.

As observed by TEM, in ΔRecA+*mms6* 2x, and 3x cells, the magnetosome chains were persistently located at midcell and split into two subchains during cell division, similar as in the WT [28]. However, we frequently observed that cells of ΔRecA+*mms6* 2x and 3x remained connected by tubular extensions at advanced stages of constriction, which kept the daughter cells attached to each other and hampered their separation immediately after septation before the cells eventually became disconnected. Within these tubular extensions always few (2-10) magnetosome particles were encapsulated and separated from daughter chains (Figure 5.2).

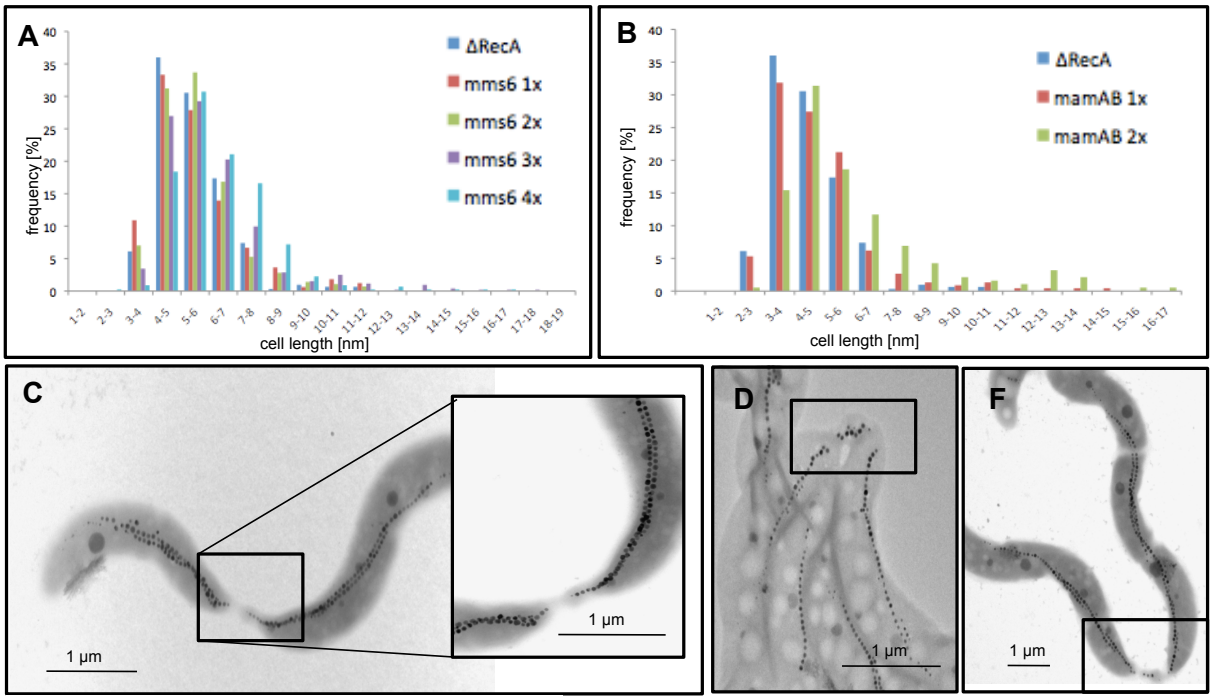

Figure 5.2: **Characterization of overexpression strains.** A: Cell length measurement of overexpression strains. All overexpression strains show an increase in cell length compared to ΔRecA. *mms6* 1x, 2x, 3x, 4x: ΔRecA+*mms6* 1x, 2x, 3x, 4x; *mamAB* 1x, 2x: ΔRecA+*mamAB* 1x, 2x. C, D, F: Tubular extensions found in overexpression strains ΔRecA+*mms6* 2x (C) ΔRecA+*mms6* 3x (D, F).

Next, we explored overexpression of the *mamGFDC* operon, which is adjacent to the *mms6* operon and was previously described to be involved in size control of magnetosomes [18]. While duplication of *mamGFDC* alone had only a weak effect on crystal number per cell (36; n=419), the duplication of both the *mms6* and *mamGFDC* operons (ΔRecA+*mms6*/*GFDC*) caused the synthesis of 32% more crystals per cell (45; n=483) (Table S5.1). Intracellular iron content of ΔRecA+*mamGFDC* was increased by about 7.4%±1.1% and even further 14.1%±1.9% in ΔRecA+*mms6*/*GFDC* (Table S5.1). ΔRecA+*mamGFDC* and ΔRecA+*mms6*/*GFDC* produced 26%, and 27% larger crystals, respectively, compared to ΔRecA (Table S5.1).

In summary, the genomic insertion of up to additional three *mms6* operons enhanced the biosynthesis of magnetosomes with increased sizes and numbers. However, the introduction of either additional *mms6* operon copies or the combined overexpression of *mamGFDC* did not further increase biomineral-

alization, suggesting that magnetosome synthesis was likely limited by different factors encoded elsewhere, which control growth of magnetite particles other than by vesicle sizes, such as iron transport, activation and nucleation of crystals. Therefore, we next attempted to overexpress the large *mamAB* operon that encodes most magnetosome proteins essential and crucial for magnetosome formation.

Genomic multicopy insertion of the *mamAB* operon

Transfer and single-copy chromosomal insertion of the *mamAB* operon was achieved by mariner transposon based gene delivery into random sites with a conjugational efficiency of 10^{-7}-10^{-8} [20]. As with the smaller *mms6* and *mamGFDC* operons, also the *mamAB* operon was stable for 40 generations, after repeated passaging under metabolic stress (cold storage, oxidative stress). ΔRecA+*mamAB* 1x (one native and one inserted *mamAB* operon) showed a similar magnetic response like the parent strain (C_{mag}=0.8±0.2) [27] and the iron content was not significantly increased (+0.4±0.5%; Table S5.1). Cells were slightly elongated ([4.81± 1.82] μm; ΔRecA: [4.44± 1.26] μm; Figure 5.2A) and displayed no obvious morphological abnormalities. However, TEM analyses revealed phenotypic heterogeneity with respect to magnetosome formation with two distinct morphotypes present in variable proportions comprising i) about 47% cells in which the number of regular-sized magnetosomes was increased to 77, ii) 42% cells increased number of magnetosomes (68) with aberrant crystal sizes and intracellular localization, and iii) 10% WT-like cells (Figure 5.3).

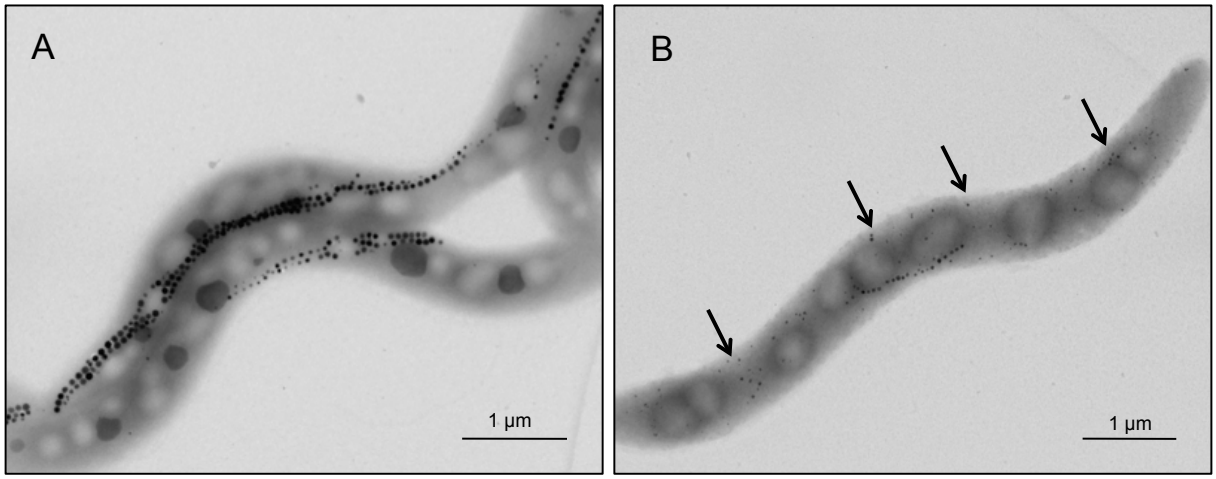

Figure 5.3: **Representative TEM micrographs of *mamAB* overexpression strains.** Phenotypic heterogeneity with respect to magnetosome formation with two distinct morphotypes were found in variable proportions in ΔRecA+*mamAB* 1x and 2x: i) cells with an increased number of regular-sized magnetosomes (A), and ii) cells with aberrant crystal sizes and intracellular localization (B, black arrows) in ΔRecA+*mamAB* 1x.

We next constructed the merotriploid insertion mutant ΔRecA+*mamAB* 2x by transfer of pTps-*mamAB-Gm* into the insertion mutant ΔRecA+*mamAB* 1x. The mutant showed a similar phenotype as observed for ΔRecA+*mamAB* 1x, and the number of magnetosomes did not further increase (68), despite of a slightly increased (by 9.4±0.5%) intracellular iron content. The C_{mag} value of ΔRecA+*mamAB* 2x was even lower than that of the parent strain (C_{mag}= 0.5±0.2), possibly caused by altered cell dimensions

([5.98± 2.58] μm compared to [4.44± 1.26] μm of ΔRecA (Table S5.1; Figure 5.2)). The magnetosome membrane of magnetosome particles isolated from strain ΔRecA+*mamAB* 1x had the same appearance and thickness of (5.4±1.8) nm as ΔRecA (5.2±1.9) nm. Coomassie-stained SDS-PAGE profiles of MM from strains ΔRecA+*mamAB* 1x revealed similar patterns compared to ΔRecA. However in strain ΔRecA+*mamAB* 1x several bands including magnetosome proteins MamA, and MamM, showed higher intensities between 51% and 145%. Western Blot analysis of selected proteins confirmed that MamM and MamA were more abundant within ΔRecA+*mamAB* 1x by about 128% and 145%, respectively, whereas the abundance of MamC was not significantly increased (9%), although the Coomassie-stained MamC band appeared more intense in ΔRecA (Figure S5.2).

In summary, the overexpression of all magnetosome proteins, encoded by the *mamAB* operon, alone did not consistently enhance magnetosome formation and therefore we suggested that further regulators for biogenesis are needed to increase magnetosome yield.

Overexpression of the *mamGFDC*, *mms6*, *mamAB*, and *mamXY* operon

Since all individual four major operons (*mms6*, *mamGFDC*, *mamAB* and *mamXY*) were shown to be implicated in regulation of magnetosome size and number, we next tested whether their combined overexpression may enhance biomineralization even further. Therefore, the *mamAB*, *mms6*, and *mamGFDC* operon were simultaneously integrated into the genome of ΔRecA that was further modified by insertion of the *mamXY* operon using mariner transposon based gene delivery, resulting in strain RecA+*AB6GX* (Figure 5.4).

The intracellular iron content was enormously increased to 3.77% iron per dry weight, which is an increase of about 140.7%±2.4% compared to ΔRecA. TEM revealed that the number of magnetosomes per cell was increased by 117% compared to the parental strain (Table S5.1; Figure 5.4A). About 28% of the cells contained more than 100 magnetosomes whereas ΔRecA did not produce more than 58 particles per cell within the analyzed TEM micrographs. Most cells formed multiple magnetosome chains (2-4), whereas the WT exhibits not more than 2 chains per cell. Beside cells with proper (WT-like) chains localized at the inner convex curvature of the cell, we frequently observed cells with one chain located at the inner convex cell curvature and up to three magnetosome chains at the concave curvature (Figure 5.4B). Additionally, the plentiful particles in some cells lacked a clearly ordered chain-like alignment, but were ”stuffed” into compact bundles or clusters (Figure 5.4C). Interestingly, the mean size of crystals was only slightly increased to 39 nm.

Whereas cells, which were merodiploid for *mamAB* (strain ΔRecA+*mamAB* 1x), showed two distinct magnetosome morphotypes, within strain ΔRecA+*ABG6X* only 12% cells had scattered magnetosomes and aberrant crystal sizes (ΔRecA+*mamAB* 1x: 42%; Figure 5.4D). The magnetic response of ΔRecA+*AB6GX* was not affected by the altered biomineralization phenotype and consistent with the C_{mag} of the parent strain ΔRecA ($C_{magABG6X}$=0.7). In dividing cells we did observe tubular extensions during or after cell division. In contrast to the "giant" MM vesicles observed by CET in strain

ΔRecA+*mms6* 2x and ΔRecA+*mms6* 3x, MM vesicles were not significantly enlarged (Fig. 5.4E-F).

The expression of the FeoAB proteins increased particle size in a heterologous host [20], suggesting that overexpression of these proteins also enhances particle synthesis in MSR. Therefore, the genes *feoA* and *feoB* were inserted into ΔRecA+*AB6GX* by Tn5 transposition. However, crystal sizes were only slightly increased (41 nm instead of 39 nm in ΔRecA+*AB6GX*) in strain ΔRecA+*ABG6X*+*feo*, whereas crystal numbers per cell even slightly decreased (69 particles instead of 74 in strain for ΔRecA+*AB6GX*) (Figure 5.5).

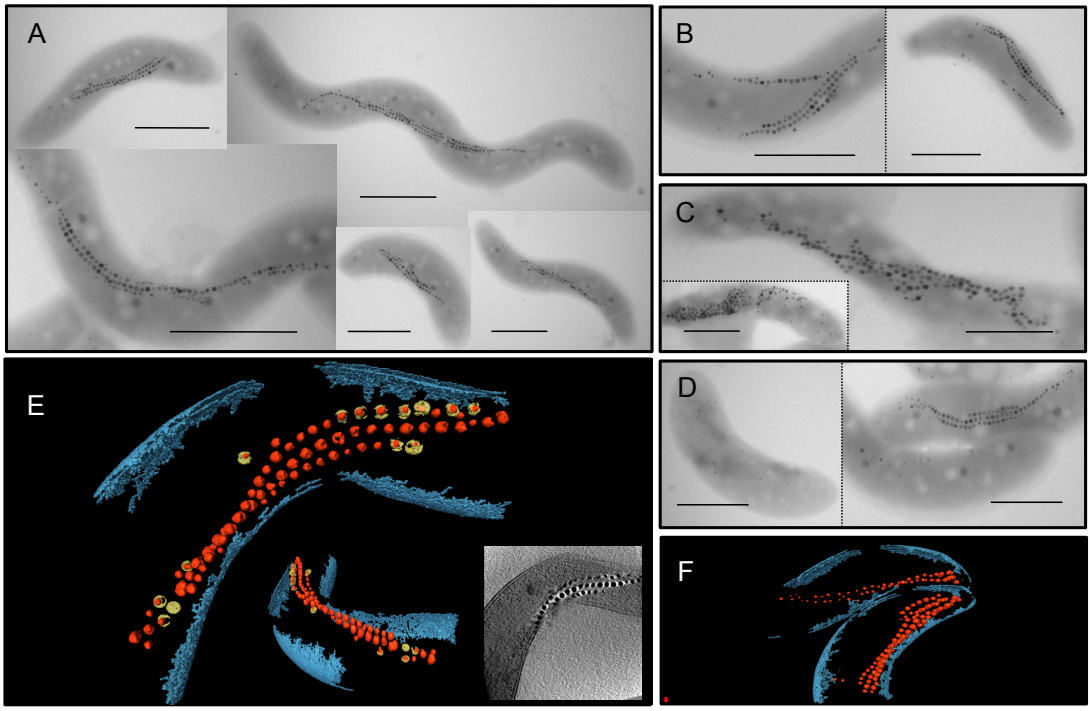

Figure 5.4: **TEM, Cryo-electron micrographs and tomograms of ΔRecA+*ABG6X*.** A, B, C: TEM micrographs of ΔRecA+*ABG6X*. Most cells form multiple magnetosome chains (2-4). Beside cells with proper (WT-like) chains localized at the inner convex curvature of the cell (A), we frequently observed cells with one chain located at the inner convex cell curvature and up to three magnetosome chains at the concave curvature (B). Additionally, the plentiful particles in some cells lack a clearly ordered chain-like alignment, but were "stuffed" into compact bundles or clusters (C). Only few cells contain no or small magnetosomes (D). E, F: Surface rendered volume of ΔRecA+*ABG6X* cells. Depicted are the cell membrane (blue), electron dense particles (red), and magnetosome vesicles (yellow). Insert in E: Cryo-electron micrograph of ΔRecA+*ABG6X*.

Discussion

In this work, we investigated ΔRecA as potential chassis for the construction of various overexpression strains to investigated if magnetosome production in MSR can be enhanced by a gene dosage increase of the *mam* and *mms* operons. In general, overexpression of genes is achieved by placing the target sequence under control of strong promoters for efficient RNA polymerase binding [29]. No stronger promoters than the native magnetosome operon promoters have been identified for *M. gryphiswaldense*

so far [10]. To achieve high product yields, gene cluster amplification via chromosomal insertion has been applied in several studies. For instance, Tang *et al.* recently increased production of the secondary metabolite spinosyn in the native host by partial gene cluster duplication [30]. Using a chemically inducible chromosomal evolution approach, 40 consecutive copies of a poly-3-hydroxybutyrate gene cluster were inserted into the chromosome of *E. coli*, thereby causing a significant increase in the productivity of this biopolymer [31]. In our approach, we inserted additional copies of single, as well as all major magnetosome operons into the chromosome of strain ΔRecA by transposition (Figure 5.5).

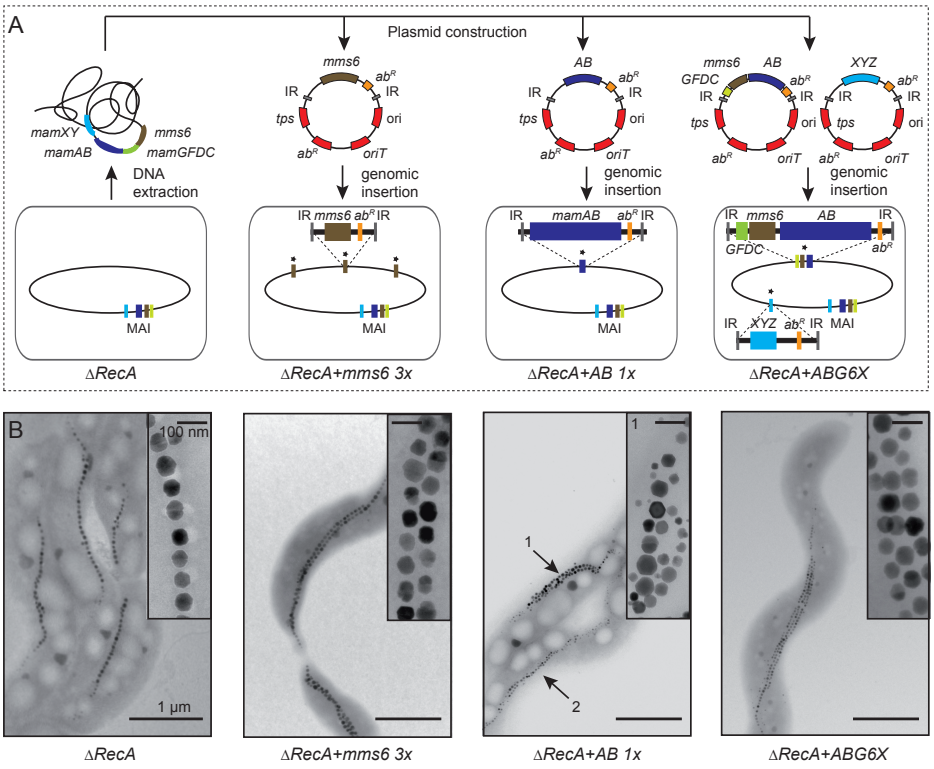

Figure 5.5: **Construction and phenotype of overexpression strains**. A. Strategy for construction of overexpression strains by amplification of different magnetosome operons. Insertional plasmids were constructed based on genomic DNA from *M. gryphiswaldense*. Plasmids contain the magnetosome operons *mamAB* (blue, *AB*), *mamGFDC* (green, *GFDC*), *mms6* (brown) and the *mamXY* operon lacking *ftsZm* (pale blue, *XYZ*). The vector backbone (genes are indicated in red) contains transposase gene (*tps*), inverted repeats (IR), origin of transfer (*oriT*), an R6K or p15A origin of replication (*ori*) and antibiotic resistance cassette (*abR*). After conjugative transfer of the plasmids, the transposase recognizes IR sequences and catalyzes chromosomal insertion of the target sequence. Additional copies of respective magnetosome operons in the chromosome (oval shape) are marked with asterisks. B. TEM analysis of overexpression strains compared to the parental strain ΔRecA. 1 and 2 illustrate the different morphotypes found for ΔRecA+*AB* 1x.

As expected, insertions were stable for at least 40 generations without selection pressure, and no recombination events were observed after serial passaging under physiological stress conditions. Consistent with the finding that the *mms6* operon plays a major role during crystal maturation in *M. gryphiswaldense* [22], its duplication or triplication (strains ΔRecA+*mms6* 2x and 3x) caused magnetosome overproduction of up to 68%. Remarkably, also the mean crystal size was significantly increased (up to 35%). Further copies of the *mms6* operon alone or in combination with the *mamGFDC* operon did not

further augment the overexpression phenotype. Therefore, we speculated that magnetosome biomineralization was limited by the lack of accessory factors encoded in the non-amplified magnetosome operons. Consistent with this hypothesis, overexpression of the large *mamAB* operon alone had pleiotropic phenotypic effects: While some cells contained increased numbers of regularly sized magnetosomes (by 50% compared to ΔRecA), we also detected a morphotype haboring small, aberrantly shaped magnetic nanoparticles. In contrast, overexpression of all magnetosome operons (ΔRecA+*ABG6X*) strongly enhanced magnetosome numbers per cell by 117%, and no heterogeneity among different cells was visible. Altogether, these findings demonstrate that a gene dosage increase of the *mam* and *mms* operons provides an efficient strategy for magnetosome overexpression in *M. gryphiswaldense*.

However, several questions regarding the regulation of magnetosome numbers as well as size in the different overexpression strains still remain elusive. For instance it is unknown, how overexpression of the *mms6* operon alone causes formation of larger crystals. One important factor constraining growth of crystals is the size of magnetosome vesicles. We sometimes found significantly enlarged vesicles in the *mms6* insertion strains by CET. This finding indicates that overexpression of a set of genes might also directly influence the vesicle diameter prior to crystallization, thereby defining the increase in crystal size. This could be caused by accumulation of proteins encoded by the *mms6* operon in the MM, thereby having a marked effect on the vesicle size. In strain ΔRecA+*AB* 1x, we observed that MamM and MamA were enriched in the MM compared to that of strain ΔRecA (by 128% and 125%, respectively). As expected, no changes in the expression level of MamC were detectable in ΔRecA+*AB* 1x. This finding demonstrates that the protein composition of the MM changes by overexpression of only a set of genes.

Besides vesicle biogenesis, also magnetosomal iron uptake into the vesicles plays an essential role in crystal growth. However, none of the proteins encoded by the *mms6* operon shares similarity to known iron transport proteins. Furthermore, overexpression of the *mms6* operon not only resulted in formation of larger crystals, but also the numbers of magnetosomes were increased. These observations suggest that overexpression of a set of magnetosome genes influences the expression or the recruitment of accessory proteins controlling other processes during magnetosome formation, such as magnetosomal iron transport, vesicle biogenesis, or magnetosome chain assembly. In contrast, additional copies of all *mam* and *mms* genes caused the strongest increase in crystal numbers per cell, while the size of the magnetosomes did not change.

Our findings indicate that expression levels of magnetosome proteins seem to be one important factor determining the number and size of magnetite crystals. However, we did not compare the transcript or protein levels of all expressed magnetosome genes in the insertional mutants with that of the ΔRecA control. Therefore, it is unknown whether a gene dosage increase of the *mam* and *mms* operons results in uniform overexpression of all amplified magnetosome genes. Our findings also raise the question, which accessory factors encoded outside the *mam* and *mms* operons might limit the number or size of magnetosomes in the overexpression strains as well as in the WT. For instance, the extracellular iron

concentration is known to be linked to crystal formation in *M. gryphiswaldense* [32]. In the WT, iron concentrations of 100 μM have been shown to support highest cell yield and magnetism [32]. Since the intracellular iron content was enhanced in overexpression strains (by up to 141%) magnetosome biosynthesis might be further increased by higher iron concentrations in the medium. However, incubation of insertion mutants in medium supplemented with 250 μM ferric citrate (instead of 50 μM) did not result in a further increase in magnetosome numbers or size. This might indicate that the intracellular iron supply was already saturated for lower iron concentrations in the medium. This finding could hint towards an insufficient expression of additional iron transport proteins, which might limit further magnetosomal iron uptake.

The *feoAB1* operon encoding a ferrous uptake system has been found to play a role in magnetosome formation in *M. gryphiswaldense* [33]. However, its chromosomal duplication in ΔRecA+*ABG6X* had only minor effects on the crystal size. Insufficient expression of non- amplified genes encoding components of other iron uptake systems, such as the ferrous uptake protein FeoB2 [34], might prevent further accumulation of iron in the cell. Furthermore, the regulator protein Fur is involved in global iron homeostasis in *M. gryphiswaldense* [35], and has been found to control expression of all identified iron uptake proteins, such as components of ferrous (FeoAB) and ABC ferric ion transport systems. Therefore, this protein could also be indirectly involved in limiting the numbers and size of magnetosomes by regulating the transcription of genes encoding components of iron uptake systems. However, deletion of *fur* had only minor effects on biomineralization in *M. gryphiswaldense* [35]. Therefore, this protein likely plays only a minor role in controlling magnetosome formation in the WT as well as in the overexpression strains. Besides the intracellular iron supply, which constrains magnetosome formation, other factors encoded outside the *mam* and *mms* operons might limit magnetosome biosynthesis in *M. gryphiswaldense*. Several enzymes participating in denitrification (nitrate reductase Nap, nitrite reductase Cd_1) [36,37], aerobic respiration (cytochrome c oxidase Cbb_3) [38], and the oxygen sensor Fnr [39] have been found to poise optimal redox conditions during magnetite biomineralization. Consequently, the corresponding proteins could also indirectly limit the number or size of magnetite crystals by regulation of the intracellular redox balance. However, a more comprehensive genetic analysis will be necessary in the future to elucidate whether accessory, yet-unknown factors control magnetosome formation in the WT as well as in the overexpression strains.

In summary, our approach demonstrates that it is possible to specifically engineer *M. gryphiswaldense* for enhanced magnetosome production. The constructed strains could be used for the high and stabilized production of magnetosomes, which are functionalized by genetic fusion with fluorescent markers or other recombinant proteins [40,41]. Furthermore, overexpression of selected magnetosome genes by chromosomal engineering might be exploited for the design of size-controlled nanocrystals that display altered magnetic properties. This could be of particular interest in applications, which depend on specific magnetic properties of the particles such as magnetic resonance imaging [42] or hyperthermal treatment of tumors [43].

Material and Methods

Bacterial strains, plasmids, and culture conditions

MSR and its mutant strains (Table S5.1) were grown in liquid modified flask standard medium (FSM) or low iron medium (LIM) at 30 °C under microaerobic condition if not otherwise specified [2,44]. Therefore, cells were cultivated in gased flasks with a mixture of 2% O_2 and 98% N_2 or in purged jars. For anaerobic cultivation, O_2 was excluded from the gas mixture, while aerobic conditions were generated through free gas exchange to air. Single colonies, were transferred into 100 μl FSM medium in 96-deep-well plates (Eppendorf, Hamburg, Germany) and incubated in anaerobic jars for 5 to 6 days. The liquid cultures were scaled up to an final volume of 10 ml. Culture conditions for *Escherichia coli* strains (Table S5.2) were as previously described [45] and for strains BW29427 and WM3064 lysogeny broth medium was supplemented with 1 mM DL-α, ε-diaminopimelic acid (DAP). For selection of antibiotic resistant strains the following antibiotics concentrations were used: 25 g/ml kanamycin (Km), 12 g/ml tetracycline (Tet), and 15 g/ml gentamicin (Gm) for *E. coli* strains, and 5 g/ml (Km), 5 g/ml (Tet), and 20 g/ml (Gm) for MSR strains, respectively. Magnetosomes were isolated as previously after microaerobic cultivation of 5 L cultures. Optical density and magnetic response (C_{mag}) were analyzed photometrical at 565 nm [46].

Molecular and genetic techniques

Total DNA from all strains were isolated as described previously [47,48]. Oligonucleotide sequences for Amplification of DNA fragments (Tabel S5.3) were deduced from the working draft genome sequence of *M. gryphiswaldense* (GenBank accession number No. CU459003) and were purchased from Sigma-Aldrich (Steinheim, Germany). Standard polymerase chain reaction (PCR) procedures were used to amplify genetic fragments and plasmids were sequenced using BigDye Terminator v3.1 chemistry on an in-house ABI 3700 capillary sequencer (Applied Biosystems, Darmstadt, Germany). Sequences were analyzed with Software Vector NTI Advance 11.5 (Invitrogen, Darmstadt, Germany). For genomic sequencing of over expression strains tagged libraries (about 200-300 bp insert size) were constructed from 1 ng of genomic DNA with the Nextera XT DNA kit (Illumina) according to the manufacturer's protocol. The eight libraries were sequenced in multiplex format using the Illumina MiSeq technology and 2x 150 nt paired-end reads with an error rate of 0.47%, as determined by an internal phiX control. The obtained sequences were assembled de novo as well as to the reference genome with the commercial software, CLC Genomics Workbench 5.5.

Analytical methods

Iron content of magnetosomes or whole cells was measured three times in triplicates by ferrozine assay [49]. After 16 hours of cultivation cells were washed with 20 mM Tris-HCl, 5 mM EDTA, pH 7.4 to remove extracellular iron. 1 ml cultures were centrifuged for 1 min at 11,000 rpm and resuspended in 90 μl

HNO_3 (65%) for 3 h at 99 °C. Afterwards, the lysate was cleared by centrifugation and resuspended in 1 ml H_2O and ferrozine assay was performed as previously described [44].

Construction of plasmids for overexpression

Plasmids pTps-*AB* and pTps-*XYZ* were constructed in a previous study by Kolinko *et al*., 2014 [20]. For cloning of plasmid *Gm*-pTps-*AB*, the *Km* resistance gene on plasmid pTps-*AB* was exchanged by *gentamicin* via recombinogenic cloning. To this end a cloning cassette comprising the *gentamicin* gene and the respective promoter was PCR-amplified (oligonucleotides IB173/IB174) and transferred into electrocompetent *E. coli* cells (DH10b+pTps-*AB*) expressing phage derived recombinases from a circular plasmid (pSC101-BAD-*gbaA*). After transfer of the cassette, recombination between homologous regions on the linear fragment and the plasmid pTps-*AB* occurred. For overexpression of the *mms6* and *mamGFDC* operons, a modified pBam-1 vector was designed. To this end *gfp* was integrated into pBam-1 after digestion with KpnI and EcoRI, resulting in pBam-*gfp*. The *mamGFDC* and *mms6* operons were amplified by PCR from the genome of MSR (*mamGFDC* operon: IKa/IKb; *mms6* operon: AL179/AL301) and were inserted into the XbaI-KpnI digested pBam-*gfp*, resulting in pBam-*mamGFDC* and pBam-*mms6* 1x, respectively with a C-terminal fusion to *mamC* or *mgr4070* of *gfp*. For generation of pBam-*mms6* 2x and pBam-*GFDC*/*mms6*, the *mms6* operon of pBam-*mms6* 1x was amplified with oligonucleotides AL377/AL379 and integrated into pBam-*mamGFDC* as well as pBam-*mms6* 1x after digestion with EcoRI. Gentamycin gene, flanked by a *lox71* and *lox66* sequence was generated by amplification with oligonucleotides AL300/AL303 from pBBR-MCS5 and cloned into the SanDI/AatII side of pBam-*mamGFDC*, resulting in pBam-*GFDC*/*Gm*. The *mms6* operon was inserted after digestion of pBam-*GFDC*/*Gm* with XbaI/KpnI, generating pBam-*mms6*/*Gm*. Generated plasmids were examined by restriction analysis with a set of different enzymes or PCR and transferred into different recipients via conjugation as described elsewhere [16].

Fluorescence microscopy

For localization studies with GFP and cell length measurement, generated mutant strains of *M. gryphiswaldense* were immobilized on agarose pads (FSM salts in H_2O, supplemented with 1% agarose), and analysed with an Olympus BX81 microscope provided with a 100 UPLSAPO100XO objective (numerical aperture of 1.40) and a Hamamatsu Orca AG camera. Data were evaluated with the Olympus cell software.

TEM and CET

Cells or magnetosomes were concentrated and adsorbed onto carbon-coated copper grids for TEM analyses. Isolated magnetosomes were treated with 1% v/v uranylacetat for staining of magnetosome membrane. Cells and vesicles were imaged with a FEI Morgagni 268 (FEI, Eindhoven, Netherlands)

at an accelerating voltage of 200 kV. For CET analysis, cell were cultivated anaerobically in FSM or aerobically in LIM and treated with formaldehyde (Fluka, Switzerland) to a final concentration of 0.1% v/v after 16 h of cultivation. A FEI Tecnai F30 Polara transmission electron microscope (FEI; Eindhoven, the Netherlands), equipped with a 300 kV field emission gun, a Gatan GIF 2002 Post-Column Energy Filter, and a 2048 pixel Gatan CCD Camera (Gatan; Pleasanton, CA) was used for data generation, whereby all measurements were performed at 300 kV, with the energy filter operated in the zero-loss mode (slit width of 20 eV) and tilt series were processed with the Serial EM (Mastronarde, 2005) and FEI's Explore 3D software. Sample preparation and tilt record was implemented as described previously [50].

Cell fractionation

Mutant strain ΔRecA, ΔRecA+*mamAB* 1x and ΔRecA+*mms6* 3x were grown in 5 L FSM under microaerobic conditions. After centrifugation at 9,200 g, cells were resuspended in 20 mM Tris-HCl, pH 7.4, 5 mMEDTA and stored at 4 °C. Procedures for cell fractionation and magnetosomes isolation was executed as described elsewhere [8,24].

Gel electrophoresis and Western blot experiments

The BCA-Protein Micro assay kit (Pierce) was used for determination of protein concentrations, according to the manufacturer's recommendation. Either whole cells or the magnetosome membrane fraction was used for one-dimensional SDS-PAGE based on procedure of Laemmli [51]. To this end an OD of 10 was adjusted for whole cell preparation or 6.5 mg of protein was suspended in electrophoresis sample buffer supplemented with 2% (wt/wt) SDS and 5% (wt/vol) 2-mercaptoethanol. Samples were incubated for 5 min at 98 °C and loaded onto polyacrylamide gels containing 15% polyacrylamid. After 1.5 h at 100 V the gel was stained with Coomassie, whereby unstained gels were used for Western blot experiments, which were performed as explained previously [52].

Acknowledgement

This work was funded by the Deutsche Forschungsgemeinschaft (grants DFG Schu1080/13-1 and 15-1) and the European Union (Project Bio2MaN4MRI n°245542). AL was supported by the Konrad-Adenauer-Stiftung.

References

1. Bazylinski DA, Frankel RB (2004) Magnetosome formation in prokaryotes. Nat Rev Microbiol 2: 217-230.
2. Faivre D, Böttger LH, Matzanke BF, Schüler D (2007) Intracellular magnetite biomineralization in bacteria proceeds by a distinct pathway involving membrane-bound ferritin and an iron(II) species. Angew Chem Int Ed Engl 46: 8495-8499.
3. Faivre D, Schüler D (2008) Magnetotactic bacteria and magnetosomes. Chem Rev 108: 4875-4898.
4. Coker VS, Pearce CI, Lang C, van der Laan G, Pattrick RAD, *et al*. (2007) Cation site occupancy of biogenic magnetite compared to polygenic ferrite spinels determined by X-ray magnetic circular dichroism. Europ J Mineral 19: 707-716.
5. Lang C, Schüler D (2006) Microbial Bionanotechnology: Biological Self-Assembly Systems and Biopolymer- Based Nanostructures. In: Rehm B, editor. Microbial Bionanotechnology: Biological Self-Assembly Systems and Biopolymer- Based Nanostructures. Wymondham: Horizon Scientific Press. pp. 107.
6. Sun J-B, Duan J-H, Dai S-L, Ren J, Guo L, *et al*. (2008) Preparation and anti-tumor efficiency evaluation of doxorubicin-loaded bacterial magnetosomes: Magnetic nanoparticles as drug carriers isolated from *Magnetospirillum gryphiswaldense*. Biot Bioengin 101: 1313-1320.
7. Lang C, Schüler D, Faivre D (2007) Synthesis of magnetite nanoparticles for bio- and nanotechnology: genetic engineering and biomimetics of bacterial magnetosomes. Macromol Biosci 7: 144-151.
8. Ohuchi S, Schüler D (2009) *In Vivo* Display of a Multisubunit Enzyme Complex on Biogenic Magnetic Nanoparticles. Appl Environ Microbiol 75: 7734-7738.
9. Lang C, Schüler D (2008) Expression of green fluorescent protein fused to magnetosome proteins in microaerophilic magnetotactic bacteria. Appl Environ Microbiol 74: 4944-4953.
10. Borg S, Hofmann J, Pollithy A, Lang C, Schüler D (2014) New vectors for chromosomal integration enable high-level constitutive or inducible magnetosome expression of fusion proteins in *Magnetospirillum gryphiswaldense*. Appl Environ Microbiol. doi: 10.1128/AEM.00192-14
11. Westmeyer GG, Jasanoff A (2007) Genetically controlled MRI contrast mechanisms and their prospects in systems neuroscience research. Magnetic resonance imaging 25: 1004-1010.
12. Schüler D (2008) Genetics and cell biology of magnetosome formation in magnetotactic bacteria. FEMS Microbiol Rev 32: 654-672.
13. Katzmann E, Scheffel A, Gruska M, Plitzko JM, Schüler D (2010) Loss of the actin-like protein MamK has pleiotropic effects on magnetosome formation and chain assembly in *Magnetospirillum gryphiswaldense*. Mol Microbiol 77: 208-224.

14. Scheffel A, Gruska M, Faivre D, Linaroudis A, Plitzko JM, *et al*. (2006) An acidic protein aligns magnetosomes along a filamentous structure in magnetotactic bacteria. Nature 440: 110-114.
15. Uebe R, Voigt B, Schweder T, Albrecht D, Katzmann E, *et al*. (2010) Deletion of a *fur-like* gene affects iron homeostasis and magnetosome formation in *Magnetospirillum gryphiswaldense*. J Bacteriol 192: 4192-4204.
16. Ullrich S, Kube M, Schübbe S, Reinhardt R, Schüler D (2005) A hypervariable 130-kilobase genomic region of *Magnetospirillum gryphiswaldense* comprises a magnetosome island which undergoes frequent rearrangements during stationary growth. J Bacteriol 187: 7176-7184.
17. Lohße A, Ullrich S, Katzmann E, Borg S, Wanner G, *et al*. (2011) Functional analysis of the magnetosome island in *Magnetospirillum gryphiswaldense*: the *mamAB* operon is sufficient for magnetite biomineralization. PLoS One 6: e25561.
18. Scheffel A, Gardes A, Grünberg K, Wanner G, Schüler D (2008) The major magnetosome proteins MamGFDC are not essential for magnetite biomineralization in *Magnetospirillum gryphiswaldense* but regulate the size of magnetosome crystals. J Bacteriol 190: 377-386.
19. Raschdorf O, Müller FD, Pósfai M, Plitzko JM, Schüler D (2013) The magnetosome proteins MamX, MamZ and MamH are involved in redox control of magnetite biomineralization in *Magnetospirillum gryphiswaldense*. Mol Microbiol 89: 872-886.
20. Kolinko I, Lohße A, Borg S, Raschdorf O, Jogler C, *et al*. (2014) Biosynthesis of magnetic nanostructures in a foreign organism by transfer of bacterial magnetosome gene clusters. Nat Nanotechnol 9: 193-197.
21. Murat D, Byrne M, Komeili A (2010) Cell biology of prokaryotic organelles. Cold Spring Harb Perspect Biol 2: a000422.
22. Lohße A, Borg S, Raschdorf O, Kolinko I, Tompa E, *et al*. (2014) Genetic dissection of the *mamAB* and *mms6* operons reveals a gene set essential for magnetosome biogenesis in *Magnetospirillum gryphiswaldense*. J Bacteriol. doi: 10.1128/JB.01716-14.
23. Scheffel A, Schüler D (2007) The acidic repetitive domain of the *Magnetospirillum gryphiswaldense* MamJ protein displays hypervariability but is not required for magnetosome chain assembly. J Bacteriol 189: 6437-6446.
24. Grünberg K, Müller EC, Otto A, Reszka R, Linder D, *et al*. (2004) Biochemical and proteomic analysis of the magnetosome membrane in *Magnetospirillum gryphiswaldense*. Appl Environ Microbiol 70: 1040-1050.
25. Tanaka M, Mazuyama E, Arakaki A, Matsunaga T (2011) MMS6 protein regulates crystal morphology during nano-sized magnetite biomineralization *in vivo*. J Biol Chem 286: 6386-6392.

26. Murat D, Falahati V, Bertinetti L, Csencsits R, Körnig A, *et al*. (2012) The magnetosome membrane protein, MmsF, is a major regulator of magnetite biomineralization in *Magnetospirillum magneticum* AMB-1. Mol Microbiol 85: 684-699.
27. Kolinko I, Jogler C, Katzmann E, Schüler D (2011) Frequent mutations within the genomic magnetosome island of *Magnetospirillum gryphiswaldense* are mediated by RecA. J Bacteriol 193: 5328-5334.
28. Katzmann E, Müller FD, Lang C, Messerer M, Winklhofer M, *et al*. (2011) Magnetosome chains are recruited to cellular division sites and split by asymmetric septation. Mol Microbiol 82: 1316-1329.
29. Cebolla A, Royo JL, De Lorenzo V, Santero E (2002) Improvement of recombinant protein yield by a combination of transcriptional amplification and stabilization of gene expression. Appl Environ Microbiol 68: 5034-5041.
30. Tang Y, Xia L, Ding X, Luo Y, Huang F, *et al*. (2011) Duplication of partial spinosyn biosynthetic gene cluster in *Saccharopolyspora spinosa* enhances spinosyn production. FEMS Microbiol Lett 325: 22-29.
31. Tyo KE, Ajikumar PK, Stephanopoulos G (2009) Stabilized gene duplication enables long-term selection-free heterologous pathway expression. Nature Biotechnol 27: 760-765.
32. Schüler D, Baeuerlein E (1996) Iron-limited growth and kinetics of iron uptake in *Magnetospirillum gryphiswaldense*. Arch Microbiol 166: 301-307.
33. Rong C, Huang Y, Zhang W, Jiang W, Li Y, *et al*. (2008) Ferrous iron transport protein B gene (*feoB1*) plays an accessory role in magnetosome formation in *Magnetospirillum gryphiswaldense* strain MSR-1. Res Microbiol 159: 530-536.
34. Rong C, Zhang C, Zhang Y, Qi L, Yang J, *et al*. (2012) FeoB2 Functions in magnetosome formation and oxidative stress protection in *Magnetospirillum gryphiswaldense* strain MSR-1. J Bacteriol 194: 3972-3976.
35. Uebe R, Voigt B, Schweder T, Albrecht D, Katzmann E, *et al*. (2010) Deletion of a *fur-like* gene affects iron homeostasis and magnetosome formation in *Magnetospirillum gryphiswaldense*. J Bacteriol 192: 4192-4204.
36. Li YJ, Katzmann E, Borg S, Schüler D (2012) The Periplasmic Nitrate Reductase Nap Is Required for Anaerobic Growth and Involved in Redox Control of Magnetite Biomineralization in *Magnetospirillum gryphiswaldense*. J Bacteriol 194: 4847-4856.
37. Li YJ, Bali S, Borg S, Katzmann E, Ferguson SJ, *et al*. (2013) Cytochrome cd_1 Nitrite Reductase NirS Is Involved in Anaerobic Magnetite Biomineralization in *Magnetospirillum gryphiswaldense* and Requires NirN for Proper d_1 Heme Assembly. J Bacteriol 195: 4297-4309.
38. Li Y, Raschdorf O, Silva KT, Schüler D (2014) The terminal oxidase Cbb3 functions in redox control of magnetite biomineralization in *Magnetospirillum gryphiswaldense*. J Bacteriol. doi: 10.1128/JB.01652-14.

39. Li Y (2014) Oxygen regulation and redox control of magnetosome biomineralization in *Magnetospirillum gryphiswaldense*. Munich: Ludwig-Maximilians-Universität München.
40. Borg S, Hofmann J, Pollithy A, Lang C, Schüler D (2014) New vectors for chromosomal integration enable high-level constitutive or inducible magnetosome expression of fusion proteins in *Magnetospirillum gryphiswaldense*. Appl Environ Microbiol. doi: 10.1128/AEM.00192-14.
41. Lang C, Schüler D (2006) Biogenic nanoparticles: production, characterization, and application of bacterial magnetosomes. J Phys: Condens Matter 18: 2815-2828.
42. Sun C, Lee JS, Zhang M (2008) Magnetic nanoparticles in MR imaging and drug delivery. Adv Drug Deliv Rev 60: 1252-1265.
43. Hergt R, Hiergeist R, Zeisberger M, Schüler D, Heyen U, *et al*. (2005) Magnetic properties of bacterial magnetosomes as diagnostic and therapeutic tools. J Magn Magn Mater 293: 80-86.
44. Heyen U, Schüler D (2003) Growth and magnetosome formation by microaerophilic Magnetospirillum strains in an oxygen-controlled fermentor. Appl Microbiol Biotechnol 61: 536-544.
45. Sambrook J, Russell DW (2001) Molecular cloning: a laboratory manual. New York: Cold Spring Harbor Laboratory Press.
46. Schüler D, Uhl R, Baeuerlein E (1995) A simple light-scattering method to assay magnetism in *Magnetospirillum gryphiswaldense* FEMS Microbiol Lett 132: 139-145.
47. Marmur J (1961) A procedure for the isolation of deoxyribonucleic acid from micro-organisms. J Mol Biol 3: 208-IN201.
48. Grünberg K, Wawer C, Tebo BM, Schüler D (2001) A large gene cluster encoding several magnetosome proteins is conserved in different species of magnetotactic bacteria. Appl Environ Microbiol 67: 4573-4582.
49. Stookey LL (1970) Ferrozine-a new spectrophotometric reagent for iron. Anal Chem 42: 779-781.
50. Katzmann E, Scheffel A, Gruska M, Plitzko JM, Schüler D (2010) Loss of the actin-like protein MamK has pleiotropic effects on magnetosome formation and chain assembly in *Magnetospirillum gryphiswaldense*. Mol Microbiol 77: 208-224.
51. Laemmli UK (1970) Cleavage of structural proteins during the assembly of the head of bacteriophage T4. Nature 227: 680-685.
52. Uebe RJ, K. Henn, V. Poxleitner, G. Katzmann, E. Plitzko, J.M. Zarivach, R. Kasama, T. Wanner, G. Pósfai, M. Böttger, L. Matzanke, B. Schüler, D. (2011) The cation diffusion facilitator proteins MamB and MamM of *Magnetospirillum gryphiswaldense* have distinct and complex functions, and are involved in magnetite biomineralization and magnetosome membrane assembly. Mol Microbiol 82: 818-835.

6 Chapter VI

Discussion

Magnetosome biomineralization within magnetotactic bacteria (MTB) is a complex process under control of a specific set of proteins, which direct the formation of highly ordered crystals enclosed by a phospholipid membrane. These proteins were found to be encoded within a conserved genomic region, known as magnetosome island (MAI). In this doctoral thesis, deletion mutagenesis was combined with analyses of protein expression profiles and bioinformatic predictions to identify, which genes within the MAI are important for magnetite biosynthesis in *M. gryphiswaldense*. The phenotypic characterization of generated mutants was used to elucidate the encoded protein functions and to determine the minimal essential gene set for magnetosome formation. Finally, overexpression of the most important regulators was successfully applied to enhance magnetosome production.

6.1 Only less than 25% of MAI genes are associated with magnetosome biomineralization

The comprehensive investigation of the MAI of *M. gryphiswaldense* (*mgr4026* to *mgr4174*) by combined bioinformatic and proteomic analysis revealed that with the exception of *mgr4041* and *mgr4106*, which are *M. gryphiswaldense*-specific, all other genes from the 115 kb core region, which were found expressed are also highly conserved in magnetospirilla or even all MTB (Figure 6.1). Most expressed proteins (26 of 33) were found to be encoded by the magnetosome operons *mms6*, *mamGFDC*, *mamAB*, and *mamXY* that were also the only regions, which displayed a magnetosome phenotype upon their deletion. Using a modified Cre-*lox* method, which allows the efficient excision of large fragments, it was observed that all other regions have no functional relevance for biomineralization under analyzed conditions and corresponding genes might just represent genetic ”junk”, or remnants from previous transfer events of the MAI. It remains possible that some deletion strains could show a phenotype under different growth conditions, or at least only in combination with other deletions.

The largest single deletion strain ΔA7 comprised 53 kb (deletion of *mgr4106* to *mgr4174* including the *mamXY* operon) that resembled the phenotype of the Δ*mamXY* operon mutant (Figure 6.1). The modified Cre-*lox* method further enabled the construction of strains bearing multiple unmarked deletions by sequential rounds of insertions and excisions. The combined deletion of all regions without obvious effects on magnetosome formation upon their excisions resulted in strain ΔA345 (deletion of *mgr4079* to *mgr4088*, *mgr4106* to *mgr4146*, and *mgr4151* to *mgr4174*; 81 ORFs; 50% of the MAI). About 78% of all transposase genes of the MAI were eliminated in this strain and cells were able to synthesize wildtype-like magnetic particles (Figure 6.1).

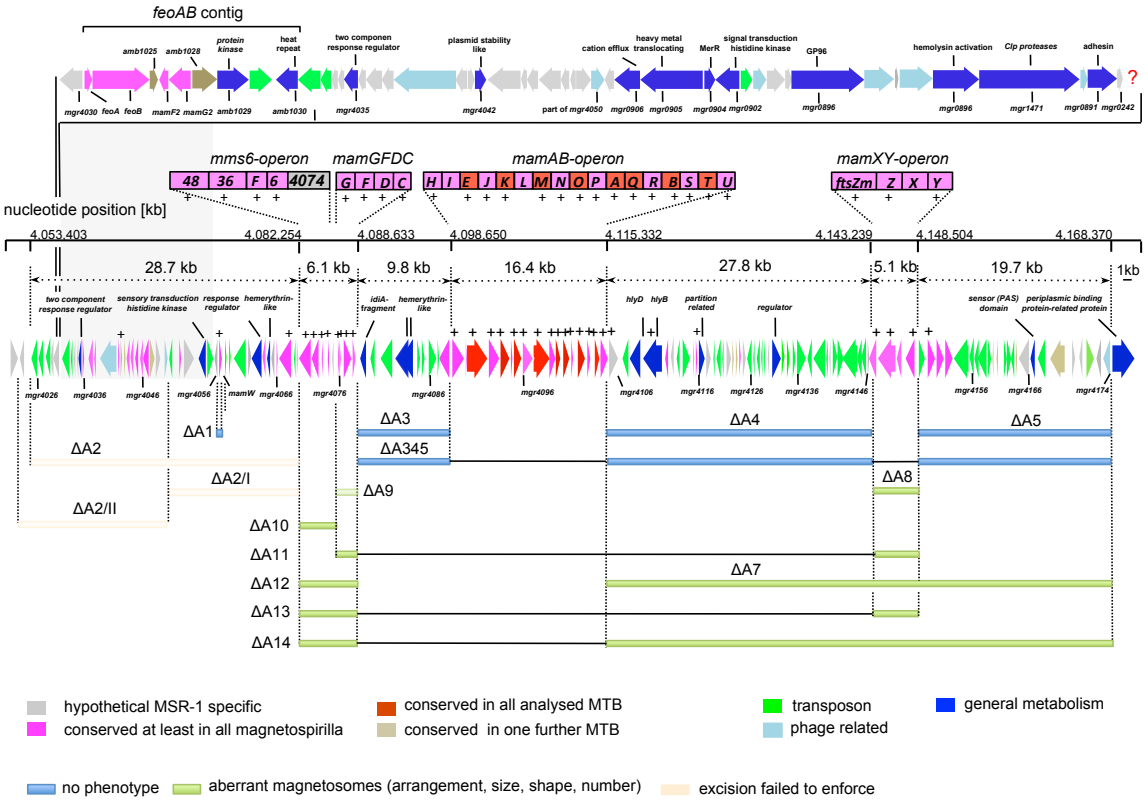

Figure 6.1: **Molecular organization and characteristics of the MAI of *M. gryphiswaldense***. Extensions of deletions are shown by bars of different colors indicating the general phenotype. For an overview, strains generated in previous studies are shown in transparent. Degree of gene conservation is highlighted by different colors. Genes found expressed by proteomic analysis are indicated with "+". A misassembly (grew block) of the A2 region was detected by Illumina sequencing (MiSeq) and a region of uncertain length, including the *feoAB* contig was detected.

However, genetic stability of the MAI within strain ΔA345 was not increased compared to the wildtype and prolonged cultivation, induced by several rounds of excision, rather resulted in more unmagnetic cells. This is also seen in the wildtype during subcultivation in the laboratory after several rounds of passaging, cold storage or oxidative stress, as the MAI undergoes frequent rearrangements [1,2].

Targeted deletion of the 28.7 kb large A2 region (*mgr4026* to *mgr4069*; 44 ORFs) either alone or in various combinations with other regions of the MAI as well as excision of the whole MAI (*mgr4026* to *mgr4174*) failed upon numerous altering sequences within the genome of *M. gryphiswaldense*. It was revealed that the organization of the MAI between *mgr4030* (hypothetical gene) and *mgr4056* (hypothetical gene) is deviating from the original assembly and a region of uncertain length interrupts the A2 region (for details see Figure 6.1). In addition, this lead to the discovery of a so far unidentified gene cluster, referred to as *feoAB* contig, which encodes a second copy of the Feo iron uptake system FeoAB1 (Figure 6.1). This contig also comprises a further copy of the magnetosome genes *mamD* (namely *mamD2*) and *mamF* (namely *mamF2*), which were shown to be involved in magnetosome formation by their deletion with the homologues of *mamF2*, *mmsF* and *mamF* located within the *mms6* and *mamGFDC* operon, respectively but are not essential for magnetosome biosynthesis (Uebe et al., in preperation). However, these genes are not existing within the official working draft sequence of *M. gryphiswaldense*, but were

described to be located upstream of the *mamXY* operon in the previously completed genome sequence, in which several rearrangements were identified compared to the draft sequence, indicating the high genomic flexibility of the MAI [3,4]. The region contains further genes, which are available within the official working draft sequence of *M. gryphiswaldense*, but were not aligned as one single contig, including *mgr4043-4050*, *mgr0907-0890*, and *mgr1471* as well as *mgr0242*. Since proper assembly of the MAI is complicated by the presence of numerous identical repeats, it has to be determined whether the insert sequence (i) interrupts the A2 region, which increases the size of the MAI of *M. gryphiswaldense* or (ii) is located elsewhere within the genome.

Among the deleted regions of the MAI with no obvious phenotype are several of the magnetospirilla-specific genes, such as *mgr4067*, *mgr4109*, *mgr4115*, *mgr4152*, and *mgr4057* (*mamW*), which had been previously implicated in magnetosome biosynthesis because of its magnetosome expression. No phenotypes were detected for the two hemerythrin-like genes harbored within the deleted A3 region, too (Figure 6.1). Because of their MAI localization and the known functions of hemerythrins from other organisms in sensing or transport of oxygen and iron, it was speculated that these proteins may play a role in magneto-aerotaxis and magnetosome formation. However, it cannot be excluded that their loss can be compensated by numerous homologues (e.g. 23 further hemerythrin-like genes) encoded elsewhere in the genome. Altogether, whereas more than 50% of the MAI seems to have no obvious functions for magnetosome biosynthesis, less than 25% of the MAI regions could be associated with magnetosome formation, which are confined to the *mms6*, *mamGFDC*, *mamAB*, and *mamXY* operons as predicted.

6.2 The *mms6*, *mamGFDC* and *mamXY* operons encode several important regulators with accessory functions for magnetosome biosynthesis

Single-operon deletion of the *mms6* operon (ΔA10) comprising *mgr4074*, *mms6*, *mmsF*, *mms36* and *mms48* significantly decreased magnetic response due to defects in crystal morphology, size and organization (Figure 6.1). Mms6 and MmsF were suggested to be major regulators for magnetosome crystal biomineralization in *M. magneticum* in several studies [5,6,7,8,9]. However, gene deletion of *mms6* or *mmsF* in *M. gryphiswaldense* caused minor biomineralization defects and only double deletion of both genes resulted in an almost 32% size reduction, which suggests a certain functional overlap between Mms6 and MmsF. While most deletions resulted in size reduction, elimination of either *mms36* or *mms48* caused the synthesis of magnetite crystals larger than those in the wildtype. Since no conserved domains or motifs are present in Mms36 and Mms48 their precise *in vivo* functions are difficult to predict. Mms36 and Mms48 might be itself either inhibitors of crystal growth [10] or recruit other inhibitory proteins to the MM in order to prevent excessive crystal growth. In conclusion, only the loss of several genes of the *mms6* operon together contributed to the strong magnetosome defect (45% size reduc-

tion) observed after deletion of the entire *mms6* operon, which indicates a cumulative regulation of all encoded proteins for magnetosome biomineralization.

Co-deletion of the *mms6* operon together with the *mamGFDC* operon in strain ΔA12 resulted in a further reduction of shape regularity and alignment of crystals, but only in a slight decrease of size, whereas the number of particles per cell was similar to strain ΔA10 (Figure 6.1). This argues for a certain functional overlap between the two operons, which is consistent with the high similarity between some of the encoded proteins: such as MmsF and MamF, which share a 61% identity, and Mms6, which contains a conspicuous LG-rich motif like in MamG and MamD. A redundant function for MmsF and MamF was revealed, as deletion of *mmsF* in the ΔmamF background had a stronger effect on magnetosome size (30% reduction of the wildtype crystal size) as described for single gene deletions.

Deletion of the *mamXY* operon, which contains several magnetotaxis signature genes, and for which a key role in magnetosome biosynthesis was predicted mainly based on comparative genome analysis, had a crucial influence on magnetite biomineralization in *M. gryphiswaldense*. Within Δ*mamXY* cells the co-existence of various distinct magnetosome morphologies was observed with regular crystals flanked by poorly crystalline and elongate particles (Figure 6.1). These findings were consistent with the results of the previously reported single gene deletions of *mamX* and *mamZ* in *M. gryphiswaldense* with mutants producing tiny misshaped hematite particles flanking regular magnetite crystals as shown by HRTEM. However, a delocalization of magnetosome chains was observed in Δ*mamXY* cells. In contrast to the wildtype, in which crystals form a straight line located at the convex side of the cell, the mutants formed chains at the outer concave site, caused by *mamY* deletion. Hence MamY is likely to be important for chain localization (Raschdorf *et al.*, in preparation).

In summary, it was demonstrated that proteins encoded by the *mamGFDC*, *mms6* and *mamXY* operons of *M. gryphiswaldense* have important and additive functions for the maturation of functional magnetite crystals that are large enough to interact with the weak geomagnetic field but are not essential for biosynthesis of magnetosomes.

6.3 The *mamAB* operon is sufficient for magnetite biomineralization in *M. gryphiswaldense* and encodes the minimal essential gene set of MamE, L, M, O, B and MamQ for iron biomineralization

Intriguingly, even in mutants, in which the *mms6*, *mamGFDC*, and *mamXY* operons were deleted in triple (ΔA14 and ΔA13; Figure 6.1), magnetite formation was not entirely abolished and cells still weakly aligned in magnetic fields. Crystal sizes were further decreased and both strains only synthesized tiny misshapen electron dense crystallites. Hence the *mamAB* operon is the only region of the MAI, which is necessary and sufficient to maintain magnetite biomineralization in *M. gryphiswaldense* even in the

absence of the *mamGFDC*, *mms6*, and *mamXY* clusters. Whereas the *mamAB* operon is sufficient to support at least some rudimentary biomineralization of small magnetite crystals even in the absence of all other magnetosme operons, the *mamXY*, *mamGFDC*, *mms6*, and *mamAB* operons are required altogether for magnetite biomineralization upon their transfer into the foreign host *Rhodospirillum rubrum* [11]. However, consistent with observations for *M. magneticum*, only the *mamAB* operon contains both non-essential and essential genes for magnetosome formation in *M. gryphiswaldense* (Figure 6.2). Besides the genes *mamH*, *mamJ*, and *mamK*, which were previously shown to be not essential for particle synthesis, single gene deletions of *mamU*, *mamT*, *mamS*, *mamR*, *mamA*, *mamP*, *mamN*, and *mamI* generated in this study, did not entirely inhibit particle synthesis and mutants still formed electron dense particles. Whereas, MamN and MamI are described to be essential for both crystal formation and vesicle synthesis in *M. magneticum* [12], MamN and MamI are not required for at least rudimentary iron biomineralization in *M. gryphiswaldense*. TEM, HRTEM and XANES revealed the presence of tiny magnetite crystals within Δ*mamN* and the synthesis of poorly crystalline unmagnetic hematite particles in Δ*mamI*. In addition to the previously identified *mamE*, *mamO* [13], *mamM* and *mamB* [14] we also found *mamQ* and *mamL* to be essential genes for magnetosome synthesis in *M. gryphiswaldense*, since their deletions abolished the biomineralization of electron dense particles (Figure 6.2). However, previously in Δ*mamL* mutant occasionally a few tiny (around 10 nm) structures were observed, which however, were difficult to discern unambiguously from the cellular body and the background. The relevance and identity of these structures remain to be verified in future studies with higher resolution.

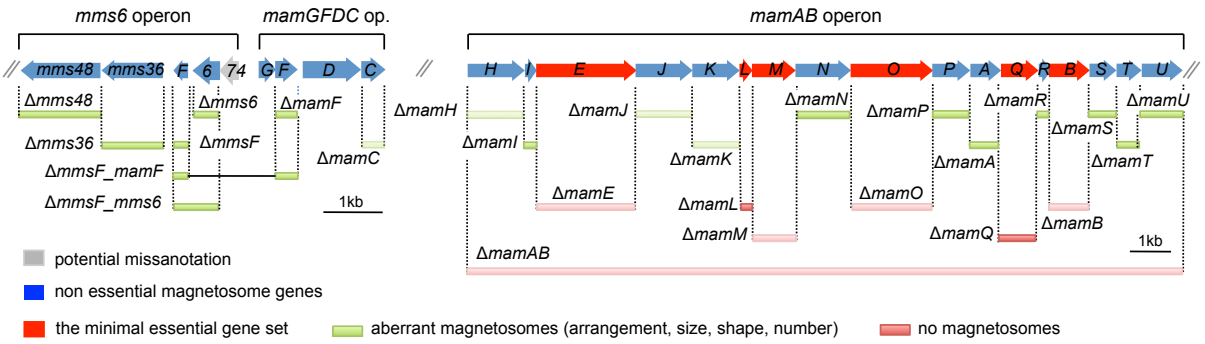

Figure 6.2: **Molecular organization and deletion analysis of the *mms6*, *mamGFDC* and *mamAB* operons of *M. gryphiswaldense***. Gene deletion within the *mms6* operon (*mms48*, *mms36*, *mmsF*, *mms6*) and *mamGFDC* operon (*mamG*, *mamF*, *mamD*, *mamC*) led to severe defects in morphology, size and organization of magnetite crystals without abolishing magnetosome biosynthesis. The highly conserved *mamAB* operon encodes non-essential (MamH, I, J, K, N, P, A, R, S, T, and MamU) and essential (MamE, M, O, Q, B and most probably MamL) magnetosome proteins for magnetite biosynthesis in *M. gryphiswaldense*. Bars, indicate extent of gene deletions. Transparent bars: strains were previously generated [13,15,16,17,18].

To confirm their essential role for particle synthesis in *M. gryphiswaldense*, the genes were cloned together on different synthetic operons. However, chromosomal reintegration of neither *mamE*, *L*, *M*, *O*, *Q*, and *mamB*, nor in combinations with *mamI* or with *mamI* and *mamN* had any detectable phenotypic effect on the non-magnetic Δ*mamAB* operon mutant. Genomic insertion of all cassettes into the un-

magnetic single gene deletion strains fully or partially restored magnetosome biomineralization in nearly all strains except of Δ*mamI* and Δ*mamE*, indicating that MamL, M, N, Q, and MamB were properly expressed from the synthetic operons. As no mutations within the plasmids were observed by sequencing, the failed restoration within Δ*mamI* and Δ*mamE* might be due to the exchange of the native ribosomal binding sites (RBS) that cause diminished gene and protein expression.

In summary, whereas in *M. magneticum* eight proteins (MamI, E, M, N, O, B, Q, and most probably MamL) were found to be essential for magnetosome biomineralization, in *M. gryphiswaldense* only six proteins (MamE, M, O, B, Q, and most probably MamL) are essential for at least some rudimentary iron biomineralization and, if including MamI, seven proteins are necessary for the biosynthesis of magnetite-containing magnetosomes. Further studies are necessary to show whether these essential magnetosome proteins are also sufficient for vesicle formation and crystallization even in the absence of other factors encoded by the *mamAB* and other magnetsome operons.

6.4 The controlled overexpression of the *mms6*, *mamGFDC*, *mamAB* and *mamXY* magnetosome operons enhance magnetosome formation in *M. gryphiswaldense*

In this work, mutagenesis has proven to be an effective tool not only to identify underlying mechanisms of magnetosome biosynthesis, but also to engineer modified magnetosome features, i.e. for generating variable particle sizes. Comparable experiments in other bacteria have shown that both deletion and overexpression of gene clusters are extremely powerful tools in genome engineering, mainly applied in optimized biotechnological processes or for elucidation of protein functions [19,20,21,22]. Whereas deletion of the *mms6* operon resulted in magnetosomes size and number reduction of 45% and 51%, respectively, the expression of the *mms6* operon genes within ΔA10 from the stronger P_{mamDC} promoter restored biomineralization even beyond the wildtype level resulting in cells synthesizing larger and more magnetosomes. This prompted us to study the effect of controlled overexpression of all magnetosome operons either alone or in various combinations. In a joined study conducted together with Isabel Kolinko (LMU Munich), we systematically i) investigated effects of overproducing strains and deduced potential functions of overexpressed proteins and ii) analyzed whether overexpression results in magnetosome overproduction by increasing magnetosome size and number. To reduce the risk of homologous recombination, an isogenic RecA deficient strain of *M. gryphiswaldense* [2] served as a chassis, which produces similar magnetosome sizes and numbers compared to the wildtype.

Chromosomal duplication or triplication of the *mms6* operon increased magnetosome number up to 69% and yielded magnetite particles even larger than those produced by the wildtype (35%), confirming the role of all proteins encoded by the *mms6* operon for regulation of crystal growth. Integration of a fourth *mms6* operon into ΔRecA (in total five *mms6* operons) or combined expression with the adjacent

mamGFDC operon that was previously reported to affect magnetosome size [23] did not further enhance particle formation. Overexpression of Mms48 alone highly increased magnetosome number and cells frequently contained multiple chains, which were also observed within the *mms6* operon overexpression strains (Figure 6.3). Thus, Mms48 may interact or recruit other magnetosome proteins important for vesicle biogenesis and/or iron uptake. Genomic expression of additional copies of *mms48* and *mms36* did not further decrease mean particle size (as suggested from deletion analyses described above) but size distributions were slightly shifted towards smaller particles. This might indicate that inhibition of particle growth is not directly caused by Mms48 and Mms36 and might depend on further recruited proteins, which interact with Mms48 and Mms36.

Overexpression of the large *mamAB* operon alone had pleiotropic phenotypic effects, and while some cells contained increased numbers of regularly sized magnetosomes, also a morphotype habouring small, aberrantly shaped magnetic nanoparticles was observed. The two distinct morphotypes might be due to the lack of accessory factors encoded in the *mms6*, *mamGFDC* and *mamXY* operons. Consistent with this hypothesis, the overexpression of all magnetosome operons in ΔRecA+*ABG6X* highly enhanced magnetosome production by increasing the number of particles about 117% compared to the wildtype.

We found that cells were longer in all overexpression strains, potentially related to a minor cell division phenotype of the mutants: cells often remained connected by tubular extensions at advanced stages of constriction, which kept the daughter cells attached to each other. During cell division, the magnetosome chain has to be split and separated from the cohesive forces caused by magnetostatic interactions within the chains. A physical model demonstrated that the magnetic attraction significantly increases in a two-stranded chain [24]. This was frequently observed in the overexpression strains of the *mms6* or *mamAB* operon and even increased to three or more chains within the ΔRecA+*ABG6X* strain (Figure 6.3).

Whereas the mutant ΔRecA+*mamAB* 1x showed no significant increase in intracellular iron content, mutants ΔRecA+*mms6* 3x and ΔRecA+*ABG6X* produced 39% and 141% more iron compared to ΔRecA, respectively. Several questions regarding the regulation of magnetosome numbers as well as size in the different overexpression strains still remain unknown. For instance it is unknown, how overexpression of the *mms6* operon alone causes formation of larger crystals. One important factor constraining growth of crystals is the size of magnetosome vesicles. In some cases we found significantly enlarged vesicles in the *mms6* insertion strains by CET. This finding indicates that overexpression of a set of genes might also directly influence the vesicle diameter prior to crystallization and defines the increase in crystal size. This could be caused by accumulation of proteins encoded by the *mms6* operon in the magnetosome membrane, thereby having a marked effect on vesicle size.

Overexpression of the *mms6* operon not only resulted in formation of larger crystals, but also the number of magnetosomes was increased, which suggests that proteins encoded by the *mms6* operon might be itself involved in vesicle biogenesis and/or magnetosomal iron transport or recruit accessory

proteins controlling those processes during magnetosome formation. However, whereas none of the *mms6* operon encoded proteins shares similarity to known iron transports or were shown to be involved in vesicle genesis by deletion analyses, the *mamAB* operon encodes several factors involved in vesicle biogenesis (MamL, MamB and MamQ) and iron transport (MamB and MamM). Thus, observations might hint towards interactions and/or recruitment between/of proteins encoded by the *mms6* and *mamAB* operons.

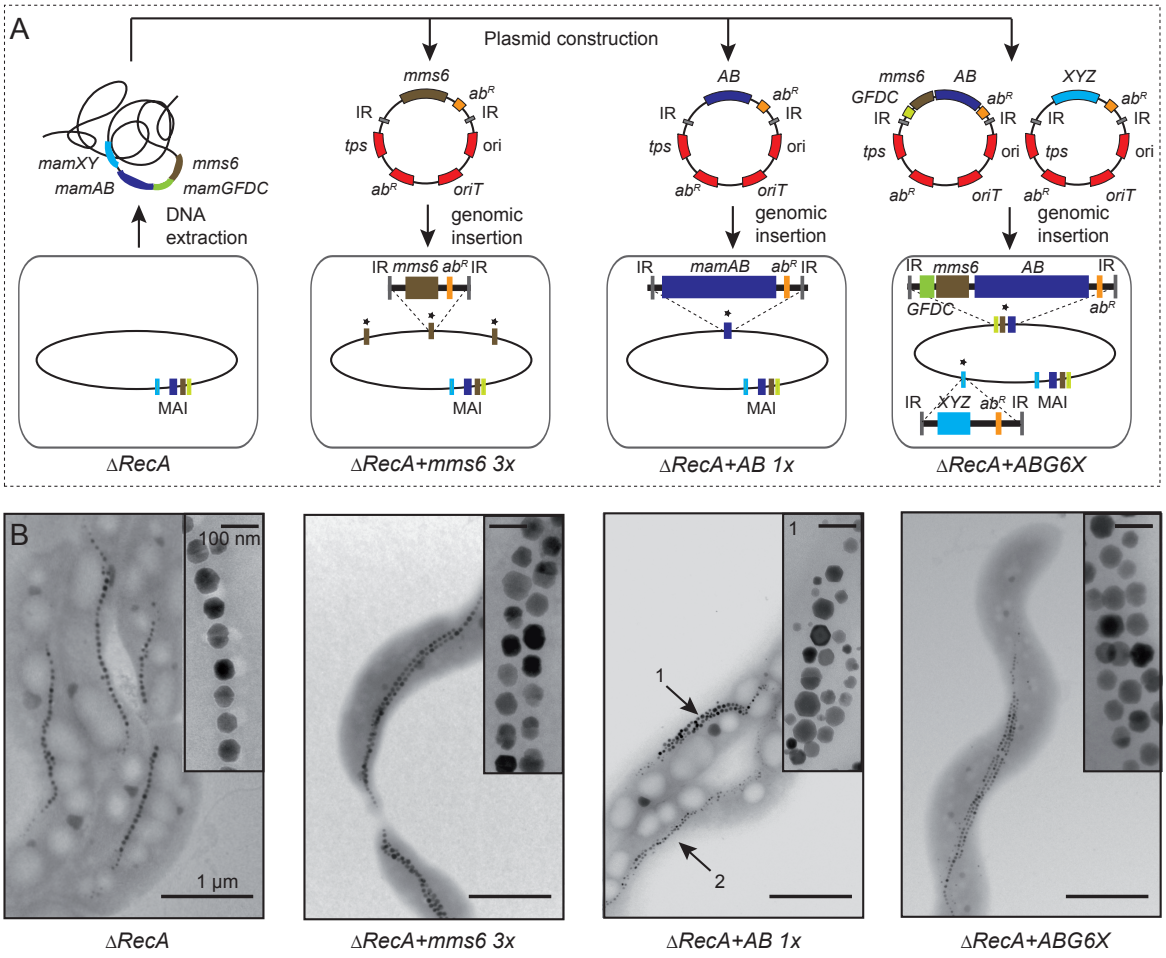

Figure 6.3: **Construction and phenotype of overexpression strains.** A. Strategy for construction of overexpression strains by amplification of different magnetosome operons. Insertional plasmids were constructed based on genomic DNA from *M. gryphiswaldense*. Plasmids contain the magnetosome operons *mamAB* (blue, *AB*), *mamGFDC* (green, *GFDC*), *mms6* (brown) and the *mamXY* operon lacking *ftsZm* (pale blue, *XYZ*). The vector backbone (genes are indicated in red) contains transposase gene (*tps*), inverted repeats (IR), origin of transfer (*oriT*), an R6K or p15A origin of replication (*ori*) and antibiotic resistance cassette (*abR*). After conjugative transfer of the plasmids, the transposase recognizes IR sequences and catalyzes chromosomal insertion of the target sequence. Additional copies of respective magnetosome operons in the chromosome (oval shape) are marked with asterisks. B. TEM analysis of overexpression strains compared to the parental strain ΔRecA. 1 and 2 illustrate the different morphotypes found for ΔRecA+*AB* 1x.

Our findings also raise the question, which accessory factors encoded outside the *mam* and *mms* operons might limit the number or size of magnetosomes in the overexpression strains as well as in the wildtype. The *feoAB1* operon encoding a ferrous uptake system has been found to play a role in magne-

tosome formation in *M. gryphiswaldense* [33]. However, its chromosomal duplication in ΔRecA+*ABG6X* had only minor effects on the crystal size. Insufficient expression of non- amplified genes encoding components of other iron uptake systems, such as the ferrous uptake protein FeoB2 [34], might prevent further accumulation of iron in the cell. Furthermore, the regulator protein Fur is involved in global iron homeostasis in *M. gryphiswaldense* [35], and has been found to control expression of all identified iron uptake proteins, such as components of ferrous (FeoAB) and ABC ferric ion transport systems. Therefore, this protein could also be indirectly involved in limiting the numbers and size of magnetosomes by regulating the transcription of genes encoding components of iron uptake systems.

Besides the intracellular iron supply, which constrains magnetosome formation, further factors might limit magnetosome biosynthesis in *M. gryphiswaldense*. Several enzymes participating in denitrification (nitrate reductase Nap, nitrite reductase Cd_1) [36,37], aerobic respiration (cytochrome c oxidase Cbb_3) [38], and the oxygen sensor Fnr [39] have been found to poise optimal redox conditions during magnetite biomineralization. Consequently, the corresponding proteins could also indirectly limit the number or size of magnetite crystals by regulation of the intracellular redox balance. However, a more comprehensive genetic analysis will be necessary in the future to elucidate whether accessory, yet-unknown factors control magnetosome formation in the wildtype as well as in the overexpression strains.

In summary, higher gene dosage of the magnetosome operons induces an increase in crystal production within the native hosts by unknown mechanism. While duplication or triplication of the *mms6* operon alone caused formation of larger crystals and a moderate increase in crystal numbers, amplification of all *mam*- and *mms* gene clusters specifically enhanced magnetosome numbers per cell.

6.5 Model for magnetosome biosynthesis: The step-wise formation of magnetic organelles

Based on results obtained by this thesis and all other previous studies of magnetosome proteins an extended model for magnetosome biosynthesis in *M. gryphiswaldense* was finally proposed (Figure 6.3). Within the last years it became clear that magnetosome biogenesis relies on five major steps: (i) vesicle biogenesis, (ii) magnetosome protein sorting, (iii) iron uptake and magnetite crystal nucleation, (iv) crystal maturation and (v) chain assembly as well as positioning [12]. To generate intracellular magnetic mineral phases, cells must create and maintain a highly curved membrane compartment [25] that includes MamB, MamQ, and most propably MamL.

Both MamB (described below) and the small protein MamL, which has no predicted function, were shown to be essential for magnetosome membrane genesis in *M. magneticum* [12] and *M. gryphiswaldense* by a so far unknown mechanism [Raschdorf *et al*., in preparation; 14]. However, the relevance and identity of magnetosome-like structures within Δ*mamL* remain to be verified in future studies with higher resolution. MamQ shares homology with the LemA protein, which is conserved in several bacte-

ria but whose function is uncertain [26,27]. MamQ has a high content of α-helices that are somewhat reminiscent to the EFC/BAR (Fes-CIP4-homology/Bin-Amphiphysin-Rvs) domain of the Formin Binding Protein 17 [12]. BAR domains have the ability to sense and stabilize membrane curvatures [28,29], and their weak similarity to MamQ might hint towards related functions in MM vesicle genesis of the protein. However, we revealed a minor number of empty vesicles by CET within Δ*mamQ* cells, which were randomly organized. Previously, it was suggested that some magnetosome proteins are sorted prior to the vesicle formation and accumulate on the inner membrane as protein-protein-lipid complexes that leads to a natural invagination without a special protein support and might explain random formation of vesicles within Δ*mamQ* cells [30].

A further important step for magnetosome formation is the sorting of magnetosome proteins, which was shown to be regulated by MamA and MamE, whereas MamA, a TPR (tetratricopeptide repeat) domain-containing protein was speculated to play a role in activation of biomineralization [29]. MamA self-assembles through its putative TPR domain and concave site to form a large homooligomeric scaffold surrounding the magnetosomes [31,32], while its convex site interacts with other magnetosome-associated proteins like MamC and several unidentified proteins [31,32]. The HtrA/DegP family protease MamE is involved in magnetosome protein localization by a protease independent process since the proteins MamA and MamJ are delocalized within Δ*mamE* of *M. magneticum* and a protease-deficient variant of MamE still supports the formation of small magnetite crystals [10].

MamO, a further magnetosome-associated protease, probably acts as localization determinant for magnetosome proteins, as anion transporter or is directly involved in precipitation of iron oxide particles [10]. MamB and MamM were implicated in magnetosome-directed iron transport according to their similarity to members of the cation diffusion facilitator (CDF) family [27,33,34]. Additionally, MamB and MamM are involved in magnetite nucleation, and establishment of proper environments for magnetite synthesis [13,14]. Further proteins involved in iron uptake and magnetite nucleation are MamZ, MamX and MamH that were proposed to form an iron oxidoreductase and transport complex in *M. gryphiswaldense* [15]. The small magnetosome protein MamI (70 aa) has no significant homology to already characterized proteins. Δ*mamI* still synthesized tiny and poorly crystalline non-magnetic particles, which consist of hematite. Recent findings in *M. gryphiswaldense* and *M. magneticum* indicate that the observed poorly ordered iron (oxyhydr)oxide phases are precursors to the magnetite phase in bacteria [35,36]. In addition, the ability of MamP to precipitate ferrihydrite and magnetite *in vitro* (discussed below) suggests that magnetite may be formed through a stepwise phase transformation process [37]. Such a biosynthetic phase transformation requires a precise control of iron supersaturation, pH, and redox potential levels [38]. Hence MamI may be involved in an early stage of magnetite nucleation by regulation of proper conditions within the vesicles.

The proteins MamN, P, S, T, and MamR are most likely involved in maturation of magnetosomes, since deletion of corresponding genes resulted in defects in crystal size, number and morphology. Due to similarity of MamN to the human Permease P that regulates the intraorganelle pH of melanosomes together

with an ATP-driven proton pump [39], MamN presumably regulates pH conditions within the magnetosome vesicles by export of protons released by the precipitation of magnetite ($2Fe^{3+} + Fe^{2+} + 4H_2O \rightarrow Fe_3O_4 + 8H^+$) [40,41]. Thus the observed phenotype of Δ*mamN* might be due to alteration of the intra-magnetosomal pH. MamP contains a double cytochrome c motif (CXXCH), referred to as magnetochrome domain that is necessary for heme-binding [42] and seems to interact with the magnetochrome domain containing proteins MamE, MamX and MamT through its PDZ domain to somehow regulate the electron transport required for biomineralization of the mixed valence iron oxide magnetite [10,15,37]. Magnetosomes in Δ*mamP* of *M. gryphiswaldense* show a similar crystallization defect (magnetite crystals flanked by flakes) like the *mamX* mutant of *M. gryphiswaldense* [15] and thus might indicate the involvment in same steps of magnetosome biosynthesis. In contrast, phenotypes of *M. gryphiswaldense* Δ*mamT* (smaller particles) and Δ*mamE* (total loss of electron dense particles) are distinct from the deletion phenotype of Δ*mamP*, suggesting that some or all of the magnetochrome proteins have different or additional functions. Isolated MamP from *M. magneticum* catalyzed the formation of ferrihydrite and magnetite from iron solutions *in vitro*, indicating that MamP binds and oxidizes iron [37].

MamR contains a HTH-17 domain mainly occurring in excisionases (Xis) that is known to interact through its α-helix with integrases and promotes recombination by helping integrases to bind dsDNA [43]. MamR also contains two α-helices that might evoke interactions with other crucial magnetosome proteins and thus, controlling particle number and size as suggested for MamR of *M. magneticum* [12]. MamS, which has similarity to the putative serine proteases and magnetochrome domain containing proteins MamE and MamX, plays a key role for crystal maturation, too [10,15]. However, MamS itself lacks a magnetochrome domain, which argues against its direct participation in redox control. The protease activity of MamE and MamO is assumedly important for crystal growth, too, and MamE presumably removes growth inhibitors proteolytically or activates growth promoting proteins to regulate crystal size [10]. Furthermore, proteins encoded by the *mms6* and *mamGFDC* operons [23] are key regulators for magnetite crystal growth (as discussed above). Finally, the assembly and midcell positioning of nascent magnetosome chains is coordinated by the actin-like MamK and the acidic MamJ protein [16,17,44,45].

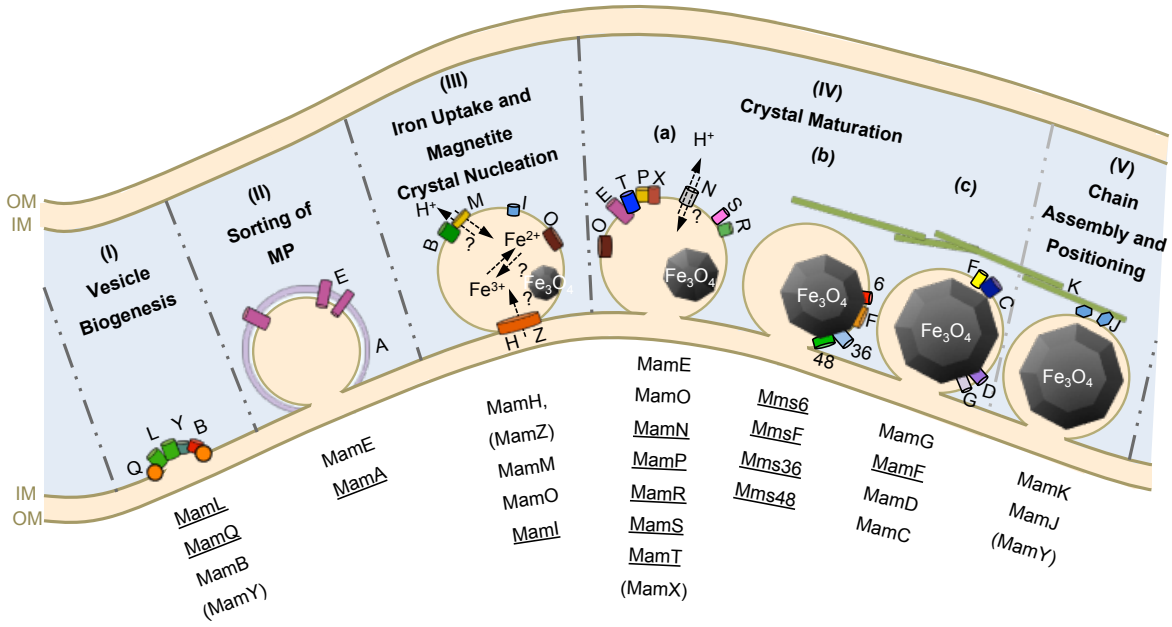

Figure 6.4: **Hypothetical model for magnetosome biosynthesis in *M. gryphiswaldense***. Magnetosome biosynthesis depends on various steps including various magnetosome proteins. (I) Magnetosome vesicle formation is induced by the proteins MamQ, MamL, and MamB. MamY regulates vesicle shape [46]. (II) MamA forms a multiprotein complex surrounding the magnetosome membrane [32] and MamE is involved in localization of magnetosome proteins by a protease independent process [10]. (III) The heterodimer of the CDF transporters MamB and MamM transport ferrous iron into the magnetosome vesicles [14] and ferric iron is taken up by MamH and MamZ [15] or formed by oxidation of ferrous iron within the vesicles. MamI is involved in magnetite nucleation. MamO most likely is involved in precipitation of iron oxide particles [10]. (IV) Crystal growth is affected by several magnetosome proteins also including MamE that removes growth inhibitors proteolytically or activates growth promoting proteins [10]. Based on the conserved CXXCH heme-binding motif within MamE, MamT, MamP and MamX proteins presumably form a complex for electron transport to regulate electron flow [15,42]. MamS and MamR control crystal size by an unknown mechanism. MamN exhibits similarity to H^+-translocation proteins and might be involved in crystal growth by regulating intramagnetosomal pH [39]. Mms6 is tightly bound to the magnetosome crystals [7,47] and assembles into coherent micelles for templating crystal growth [48]. Mms48 and Mms36 act as inhibitors of crystal growth or recruit inhibiting proteins of particle growth by an unknown mechanism. The small, hydrophobic proteins MamG, F, D, and MamC control in a cumulative manner the growth of magnetite crystals [23]. Magnetosomes are assembled into chains by the interaction of MamJ with the actin-like MamK filament that is also involved in chain positioning [16,17,24]. MamY plays a crucial role in proper magnetosome chain localization [Raschdorf *et al.*, in preparation]. OM: outer membrane; IM: inner membrane. Underlined proteins: analyzed proteins in this study, by single gene deletion of encoding genes. Proteins in brackets: non-essential proteins encoded by the *mamXY* operon.

References

1. Ullrich S, Kube M, Schübbe S, Reinhardt R, Schüler D (2005) A hypervariable 130-kilobase genomic region of *Magnetospirillum gryphiswaldense* comprises a magnetosome island which undergoes frequent rearrangements during stationary growth. J Bacteriol 187: 7176-7184.
2. Kolinko I, Jogler C, Katzmann E, Schuler D (2011) Frequent mutations within the genomic magnetosome island of *Magnetospirillum gryphiswaldense* are mediated by RecA. J Bacteriol 193: 5328-5334.
3. Rong C, Zhang C, Zhang Y, Qi L, Yang J, *et al*. (2012) FeoB2 Functions in magnetosome formation and oxidative stress protection in *Magnetospirillum gryphiswaldense* strain MSR-1. J Bacteriol 194: 3972-3976.
4. Wang X, Wang Q, Zhang W, Wang Y, Li L, *et a*l. (2014) Complete Genome Sequence of *Magnetospirillum gryphiswaldense* MSR-1. Genome Announc 2.
5. Arakaki A, Webb J, Matsunaga T (2003) A novel protein tightly bound to bacterial magnetic particles in *Magnetospirillum magneticum* strain AMB-1. J Biol Chem 278: 8745-8750.
6. Amemiya Y, Arakaki A, Staniland SS, Tanaka T, Matsunaga T (2007) Controlled formation of magnetite crystal by partial oxidation of ferrous hydroxide in the presence of recombinant magnetotactic bacterial protein Mms6. Biomat 28: 5381-5389.
7. Arakaki A, Masuda F, Amemiya Y, Tanaka T, Matsunaga T (2010) Control of the morphology and size of magnetite particles with peptides mimicking the Mms6 protein from magnetotactic bacteria. J Colloid Interface Sci 343: 65-70.
8. Prozorov T, Mallapragada SK, Narasimhan B, Wang L, Palo P, *et al*. (2007) Protein-Mediated Synthesis of Uniform Superparamagnetic Magnetite Nanocrystals. Adv Funct Mat 17: 951-957.
9. Murat D, Falahati V, Bertinetti L, Csencsits R, Körnig A, *et al*. (2012) The magnetosome membrane protein, MmsF, is a major regulator of magnetite biomineralization in *Magnetospirillum magneticum* AMB-1. Mol Microbiol 85: 684-699.
10. Quinlan A, Murat D, Vali H, Komeili A (2011) The HtrA/DegP family protease MamE is a bifunctional protein with roles in magnetosome protein localization and magnetite biomineralization. Mol Microbiol 80: 1075-1087.
11. Kolinko I, Lohße A, Borg S, Raschdorf O, Jogler C, *et al*. (2014) Biosynthesis of magnetic nanostructures in a foreign organism by transfer of bacterial magnetosome gene clusters. Nat Nanotechnol 9: 193-197.
12. Murat D, Quinlan A, Vali H, Komeili A (2010) Comprehensive genetic dissection of the magnetosome gene island reveals the step-wise assembly of a prokaryotic organelle. Proc Natl Acad Sci U S A 107: 5593-5598.

13. Yang W, Li R, Peng T, Zhang Y, Jiang W, et al. (2010) *mamO* and *mamE* genes are essential for magnetosome crystal biomineralization in M*agnetospirillum gryphiswaldense* MSR-1. Res Microbiol 161: 701-705.
14. Uebe RJ, K. Henn, V. Poxleitner, G. Katzmann, E. Plitzko, J.M. Zarivach, R. Kasama, T. Wanner, G. Pósfai, M. Böttger, L. Matzanke, B. Schüler, D. (2011) The cation diffusion facilitator proteins MamB and MamM of *Magnetospirillum gryphiswaldense* have distinct and complex functions, and are involved in magnetite biomineralization and magnetosome membrane assembly. Mol Microbiol 82: 818-835.
15. Raschdorf O, Müller FD, Pósfai M, Plitzko JM, Schüler D (2013) The magnetosome proteins MamX, MamZ and MamH are involved in redox control of magnetite biomineralization in *Magnetospirillum gryphiswaldense*. Mol Microbiol 89: 872-886.
16. Katzmann E, Scheffel A, Gruska M, Plitzko JM, Schüler D (2010) Loss of the actin-like protein MamK has pleiotropic effects on magnetosome formation and chain assembly in *Magnetospirillum gryphiswaldense*. Mol Microbiol 77: 208-224.
17. Scheffel A, Gruska M, Faivre D, Linaroudis A, Plitzko JM, *et al*. (2006) An acidic protein aligns magnetosomes along a filamentous structure in magnetotactic bacteria. Nature 440: 110-114.
18. Uebe R, Junge K, Henn V, Poxleitner G, Katzmann E, *et al*. (2011) The cation diffusion facilitator proteins MamB and MamM of *Magnetospirillum gryphiswaldense* have distinct and complex functions, and are involved in magnetite biomineralization and magnetosome membrane assembly. Mol Microbiol 82: 818-835.
19. Yanai K, Murakami T, Bibb M (2006) Amplification of the entire kanamycin biosynthetic gene cluster during empirical strain improvement of *Streptomyces kanamyceticus*. Proc Natl Acad Sci U S A 103: 9661-9666.
20. Tyo KE, Ajikumar PK, Stephanopoulos G (2009) Stabilized gene duplication enables long-term selection-free heterologous pathway expression. Nat Biotechnol 27: 760-765.
21. Kikuchi Y, Itaya H, Date M, Matsui K, Wu LF (2009) TatABC overexpression improves *Corynebacterium glutamicum* Tat-dependent protein secretion. Appl Environ Microbiol 75: 603-607.
22. Jung K, Jung H, Colacurcio P, Kaback HR (1995) Role of glycine residues in the structure and function of lactose permease, an *Escherichia coli* membrane transport protein. Biochem 34: 1030-1039.
23. Scheffel A, Gardes A, Grünberg K, Wanner G, Schüler D (2008) The major magnetosome proteins MamGFDC are not essential for magnetite biomineralization in *Magnetospirillum gryphiswaldense* but regulate the size of magnetosome crystals. J Bacteriol 190: 377-386.
24. Katzmann E, Müller FD, Lang C, Messerer M, Winklhofer M, *et al*. (2011) Magnetosome chains are recruited to cellular division sites and split by asymmetric septation. Mol Microbiol 82: 1316-1329.

25. Rahn-Lee L, Komeili A (2013) The magnetosome model: insights into the mechanisms of bacterial biomineralization. Front Microbiol 4: 352.
26. Lenz LL, Dere B, Bevan MJ (1996) Identification of an H2-M3-restricted Listeria epitope: implications for antigen presentation by M3. Immunity 5: 63-72.
27. Grünberg K, Wawer C, Tebo BM, Schüler D (2001) A large gene cluster encoding several magnetosome proteins is conserved in different species of magnetotactic bacteria. Appl Environ Microbiol 67: 4573-4582.
28. McMahon HT, Gallop JL (2005) Membrane curvature and mechanisms of dynamic cell membrane remodelling. Nature 438: 590-596.
29. Komeili A, Vali H, Beveridge TJ, Newman DK (2004) Magnetosome vesicles are present before magnetite formation, and MamA is required for their activation. Proc Natl Acad Sci U S A 101: 3839-3844.
48. Nudelman H, Zarivach R (2014) Structure prediction of magnetosome-associated proteins. Front Microbiol 5. doi: 10.3389/fmicb.2014.00009
31. Yamamoto D, Taoka A, Uchihashi T, Sasaki H, Watanabe H, *et al*. (2010) Visualization and structural analysis of the bacterial magnetic organelle magnetosome using atomic force microscopy. Proc Nat Ac Sci 107: 9382-9387.
32. Zeytuni N, Ozyamak E, Ben-Harush K, Davidov G, Levin M, *et al*. (2011) Self-recognition mechanism of MamA, a magnetosome-associated TPR-containing protein, promotes complex assembly. Proc Nat Ac Sci 108: E480-E487.
33. Grünberg K, Müller EC, Otto A, Reszka R, Linder D, *et al*. (2004) Biochemical and proteomic analysis of the magnetosome membrane in *Magnetospirillum gryphiswaldense*. Appl Environ Microbiol 70: 1040-1050.
34. Nies DH (2003) Efflux-mediated heavy metal resistance in prokaryotes. FEMS Microbiol Rev 27: 313-339.
35. Baumgartner J, Morin G, Menguy N, Perez Gonzalez T, Widdrat M, *et al*. (2013) Magnetotactic bacteria form magnetite from a phosphate-rich ferric hydroxide via nanometric ferric (oxyhydr)oxide intermediates. Proc Natl Acad Sci U S A 110: 14883-14888.
36. Fdez-Gubieda ML, Muela A, Alonso J, Garcia-Prieto A, Olivi L, *et al*. (2013) Magnetite biomineralization in *Magnetospirillum gryphiswaldense*: time-resolved magnetic and structural studies. ACS Nano 7: 3297-3305.
37. Siponen MI, Legrand P, Widdrat M, Jones SR, Zhang W-J, *et al*. (2013) Structural insight into magnetochrome-mediated magnetite biomineralization. Nature 502: 681-684.
38. Bell PE, Mills AL, Herman JS (1987) Biogeochemical Conditions Favoring Magnetite Formation during Anaerobic Iron Reduction. Appl Environ Microbiol 53: 2610-2616.
39. Brilliant MH (2001) The mouse p (pink-eyed dilution) and human P genes, oculocutaneous albinism type 2 (OCA2), and melanosomal pH. Pigment Cell Res 14: 86-93.

40. Schüler D (2008) Genetics and cell biology of magnetosome formation in magnetotactic bacteria. FEMS Microbiol Rev 32: 654-672.
41. Faivre D, Böttger LH, Matzanke BF, Schüler D (2007) Intracellular magnetite biomineralization in bacteria proceeds by a distinct pathway involving membrane-bound ferritin and an iron(II) species. Angew Chem Int Ed Engl 46: 8495-8499.
42. Siponen MI, Adryanczyk G, Ginet N, Arnoux P, Pignol D (2012) Magnetochrome: a c-type cytochrome domain specific to magnetotatic bacteria. Biochem Soc Trans 40: 1319-1323.
43. Cho EH, Gumport RI, Gardner JF (2002) Interactions between Integrase and Excisionase in the Phage Lambda Excisive Nucleoprotein Complex. J Bacteriol 184: 5200-5203.
44. Katzmann JA, Snyder MR, Rajkumar SV, Kyle RA, Therneau TM, *et al*. (2011) Long-term biological variation of serum protein electrophoresis M-spike, urine M-spike, and monoclonal serum free light chain quantification: implications for monitoring monoclonal gammopathies. Clin Chem 57: 1687-1692.
45. Komeili A, Li Z, Newman DK, Jensen GJ (2006) Magnetosomes are cell membrane invaginations organized by the actin-like protein MamK. Science 311: 242-245.
46. Tanaka M, Arakaki A, Matsunaga T (2010) Identification and functional characterization of liposome tubulation protein from magnetotactic bacteria. Mol Microbiol 76: 480-488.
47. Oestreicher Z, Valverde-Tercedor C, Chen L, Jimenez-Lopez C, Bazylinski DA, *et al*. (2012) Magnetosomes and magnetite crystals produced by magnetotactic bacteria as resolved by atomic force microscopy and transmission electron microscopy. Micron 43: 1331-1335.
48. Wang W, Bu W, Wang L, Palo PE, Mallapragada S, *et al*. (2012) Interfacial Properties and Iron Binding to Bacterial Proteins That Promote the Growth of Magnetite Nanocrystals: X-ray Reflectivity and Surface Spectroscopy Studies. Langmuir 28: 4274-4282.

Future directions

The complex process of magnetosome formation requires a high number of different magnetosome proteins to form highly crystalline magnetite particles in *M. gryphiswaldense*. Results of this work provide new insights into the functional diversity of magnetosome proteins encoded by the *mms6*, *mamGFDC*, *mamAB* and *mamXY* operons and how these operons can be used to enhance magnetosome formation.

This will be, for example useful for future genome reduction approaches in MTB. By removal of unnecessary or problematic genomic regions, strains of *M. gryphiswaldense* can be engineered for the production of magnetosome particles with increased genetic stability due to the elimination of repeats and transposases. Instead of repeated, deletion of MAI regions that led to highly instable phenotypes the deletion of the entire MAI and reintegration of important magnetosome genes is a promising method. However, it will be indispensable to obtain a complete and gap-free closed *M. gryphiswaldense* genome, especially to identify the real organization of the A2 region within the MAI.

Despite the identification of essential and non-essential proteins for magnetite formation as well as their importance for the various steps of magnetosome biosynthesis, the functions of most MM proteins still remain unknown and several detailed analyses are required. It remains to be shown whether the identified essential magnetosome proteins are also sufficient for magnetosome biosynthesis in *M. gryphiswaldense* in the absence of other factors encoded by the *mamAB* operon and other magnetosome operons. Therefore, a synthetic construct encoding MamE, L, M, O, Q and MamB (and MamI) should be expressed in the absence of *mms6*, *mamGFDC*, *mamAB* and *mamXY* operon to verify the minimal essential gene set.

The transfer of modified magnetosome operons based on results obtained from this thesis will be useful to genetically endow unicellular and multicellular organisms with magnetization by biosynthesis of tailored magnetic nanoparticles.

Additionally, the modular expression or overexpression of various magnetosome genes and operons can be used for the production of engineered magnetic nanoparticles with tailored properties in *M. gryphiswaldense*. For example elimination of Mms48 and Mms36 from the overexpression strains might further enhance particle size, since both proteins seem to be involved in crystal growth inhibition.

Overexpression of a selected set of magnetosome genes could be exploited for the design of size-controlled nanoparticles that display altered magnetic features or display various functionalized magnetosome proteins. The constructed strains will be useful for high and steady magnetosome production for several nanotechnological and biotechnological applications.

Acknowledgement

I am deeply grateful to my supervisor Prof. Dr. D. Schüler for giving me the opportunity to work in his laboratory on magnetotactic bacteria and for his guidance and support throughout this thesis.

I am also very grateful to Prof. Dr. H. Jung, Prof. Dr. A. Böttger, Prof. Dr. U. C. Vothknecht, Prof. Dr. C. N. David and Dr. T. Ott for their interest in my studies, their support during preparation for examination and evaluation of my work.

Moreover, I also like to thank Prof. Dr. G. Wanner and Dr. A. Brachmann (LMU Munich), Prof. Dr. T. Schweder and Dr. B. Voigt (EMAU Greifswald), Dr. M. Richter (MPI for Marine Microbiology Bremen), Prof. Dr. M. Pśfai and Dr. É. Tompa (University of Pannonia Hungary), Dr. D. Faivre and Dr. J. Baumgartner (MPI of Colloids and Interfaces Potsdam) for the close and successful collaborations.

I wish to extend my warmest thanks to all those in the "Magnetolab" who gave me support while doing my research, for many inspiring discussions and the friendly atmosphere in the lab. Especially, I want to thank Dr. Emanuel Katzmann, Dr. René Uebe, Dr. Yingjie Li, Dr. Karen Tavares, Felix Popp and Isabelle Mai - it has been a lot of fun to work with you in the lab. I am also thankful to Isabel Kolinko for the fruitful collaboration. Many thanks to "my" practicum students Rosa Susen and Andreas Haehle for your help. Espacially, thanks to Andreas Singer, because now we all now that blue tips do not fit into yellow boxes.

I very much appreciate the financial support from the Konrad Adenauer Foundation e.V. that enabled me to perform this work, to meet a lot of interesting people and to expand my horizon also behind scientific research.

Special thanks obtains the most important person in the lab Sarah Borg. I never had managed this work without you. Thank you for many encouraging words, plenty of fun and excellent comments on this thesis ("Saranna for ever").

I sincerely thank my parents Silke and Axel Loh§e and my sisters Juliane, Sophia and Helena for their support and patience. I am deeply grateful to my mother, who has always believed in me.

My deepest gratitude goes to Carlo, my "Dickes" and father of our little "Moahn" Bruno. Thank you for many scientific and non-scientific discussions. Each day with you, Carlo and Bruno, is wonderful and perfect. Thank you for all: the endless inspirations, wonderful moments, sleepless nights, the unlimited patience and support, and the endless fun. I love you.

Curriculum vitae

Persönliche Informationen

GEBURTSTAG	03. Dezember 1986
GEBURTSORT	Schlema, Deutschland
NATIONALITÄT	deutsch
FAMILIENSTAND	ledig, ein Sohn
WOHNHAFT	Höfestieg 7 in 37077 Göttingen
TELEFON	(+49) 151 20620713
E-MAIL ADRESSE	alohsse@gmx.de

Wissenschaftlicher Werdegang

02/2009 - 05/2014	**Diplomandin**/ **Doktorandin** Molekulare Mikrobiologie	
MIT DIRK SCHÜLER	Biozentrum, Ludwig-Maximilians-Universität	München
04/2008 - 02/2009	**Hilfswissenschafter** Angewandte Biotechnologie	
MIT PETRA RADEHAUS	Hochschule Mittweida	Mittweida
09/2007 – 03/2008	**Forschungspraktikantin** Proteomics/ Immunologie	
MIT MARTIN V. BERGEN	Helmholtz-Zentrum für Umweltforschung	Leipzig

Schulische und akademische Ausbildung

11/209 – 05/2014	**Promotion** (Dr. rer. nat.) Molekular-/ Mikrobiologie	
PROMOTION	Biozentrum, Ludwig-Maximilians-Universität	München
VOLLSTIPENDIUM	**Konrad Adenauer Stiftung e.V.**	Sankt Augustin
09/2005 – 10/2009	**Dipl.-Ing. (FH)** Umwelttechnik/ Biotechnologie (Note: 1.6)	
INGENIEURSSTUDIUM	Hochschule Mittweida	Mittweida
08/1997 – 06/2005	**Allgemeine Hochschulreife** (Abitur) (Note: 2.0)	
SEKUNDARSTUFE II	Georgius-Agricola Gymnasium	Glauchau

....

München, den Anna Lohße

Supplement: Chapter II

Functional analysis of the magnetosome island in *Magnetospirillum gryphiswaldense*: The *mamAB* operon is sufficient for magnetite biomineralization.

Publication state: published in PLoS One. 2011;6(10):e25561.

Materials and Methods

Construction of integrative plasmids and deletion mutagenesis

Downstream and upstream sequences of the deletion targets (AL01-AL03; AL05-AL08; AL11; Fig. S2.2) were amplified by PCR using *M. gryphiswaldense* chromosomal DNA and oligonucleotides listed in Table S2.3. PCR products were subcloned into pJet1.2 vector, sequenced and finally ligated into the mobilizable suicide plasmids. The basic suicide vector, pAL01 was constructed by amplifying homologous region AL01 by PCR using the primer pair AL33/AL34, containing the *lox71* sequence. AL01 was digested with EcoRI-SalI and inserted into the corresponding site of pK19mobGII [1], resulting in pAL01. After digestion with EcoRI and NotI the plasmid was used for constructing vectors pAL05 and pAL07. The homologous regions were amplified with primers AL42/AL43 and AL48/AL49, respectively. Moreover, the multiple cloning site (MCS) from pBBR-MCS5 plasmid was amplified by PCR with AL115/AL116 primers. The fragment was digested with EcoRI-NotI and ligated into the same position of pAL01, creating pAL01_MCS1. Consequently, the homologous region AL03, amplified with primers AL107/AL108, was integrated after digestion with ClaI and NotI, resulting in pAL03. The basic vector pAL02/2 was constructed amplifying the homologous sequence AL02/2 by PCR using the primer pair AL19/AL20, containing the *lox66* site. The 2148-bp fragment was cut with SalI-HindIII and cloned into pT18mob2. The resulting plasmid was designated pT18mob2_AL02/2. Gene for gentamicin resistance (Gm) was amplified by PCR from pBBR-MCS5 plasmid with primers AL81/AL82, and was inserted after digestion with EcoRI-SalI, resulting in pAL02/2_Tet. Tetracycline resistance gene was destructed by

digestion with PstI and the blunted and self-ligated vector was named pAL02/2. The MCS from pBBR-MSC5 was amplified with primers AL113/AL114 and the fragment was cut with HindIII-BamHI. Thus, the following plasmids were generated by using the following primer pairs and restriction endonucleases: pAL06 (AL121/AL122; XhoI-PvuI) as well as pAL08 (AL92/93; BamHI- NotI). Due to plasmid instability a terminator sequence was inserted into pAL02/2_MCS2 after amplification with primers AL152/AL153 from plasmid pAP150 and digestion with *KspI*, resulting in pAL02/2_term. The plasmid was used to construct pAL11_term, whereby homologous sequences were amplified with primer pair AL94/95 and digested with BamHI-NotI. Excisions of the *mms6* operon and *mamXY* operon were conducted by double cross-over mutagenesis as described previously [2,3]. Consequently, pCM184 [4] derivate were generated, whereby following oligonucleotides and restriction endonucleases were used to amplify and insert corresponding downstream and upstream fragments: pCM184_*mms6*_5'3' WT ([AL352/AL353; MfeI-NdeI], [AL354/AL355; ApaI-SacI]); pCM184_*mms6*_5'3' GFDC ([AL352/AL353; MfeI-NdeI], [AL132/AL133; MluI-SacI]); pCM184_*mamXY*_5'3' ([AL190/AL191; MfeI-NcoI], [AL188/AL189; ApaI-SacI]) and pCM184_*mamXY*_5'3'SU ([SU88/Su89; EcoRI-SmaI], [SU422/423; ApaI-ClaI*I*). While pCM184_*mamXY*_5'3' was used in the ΔA12 background, pCM184_*mamXY*_5'3'SU was employed in wildtype and Δ*GFDC* [2]. For Single gene excision of the *mamW* gene, upstream fragment was PCR amplified using primer pairs SU304/SU305 and SU306/SU307 for downstream region. Constructs were digested with MunI-NdeI or ApaI-SacI and ligated into pCM184, resulting in pCM184_*mamW*_3'5'. After conjugation of the final integrative plasmids into *M. gryphiswaldense* strains, single or double insertion mutants were selected with corresponding antibiotics and verified by direct cell PCR. The excision of large genomic segments was induced after conjugation with the Cre expression plasmid pCM157 [4]. Original lac promotor was exchanged by a native *M. gryphiswaldense* promotor (generated by Y. Le, unpublished data). To obtain marker-less mutants after double crossover occurred, the vector was also used for deletion of the inserted *Km* gene from pCM184. Specific gene replacements were verified by PCR and sequencing. ΔA19 was designed as previously reported [5] using MSR-1B as parent strain and the plasmids pSUMAI13_5' (pK19mobGII

derivate) and pSUMAI13_3' (pAS200 derivate) generated with following primer pairs and matching restriction endonucleases: [SU510/SU511; BamHI/XbaI] and [SU488/SU489; SalI/HindIII]. Plasmid pK19mobGII_*mamJKL*_3'5' for deletion of genes *mamJ, mamK, mamL* was generated by inserting 1 kb fragments upstream and downstream of *mamJ* and *mamK* (amplified with primer pairs EK1_*JKL* u_f/ EK1_*JKL* u_r and EK_JKL d_f/ EK_*JKL* d_r) into pK19mobGII after digestion with *XmaI-SpeI* and *SmaI*, respectively.

Conjugation experiments

Plasmid transfer via conjugation was performed with *E. coli BW29427* as donor strain and *M. gryphiswaldense* R3/S1 or its descendants as acceptor strains. Conjugation procedure was performed as described previously [3,5] with following modifications for genomic plasmid insertion: After the first plasmid transfer and 2h cultivation in liquid media, cells of single insertion mutants were grown in 100 ml FSM under selective conditions. *E. coli BW29427* containing the second insertion plasmid, was added after 32h of incubation. The concentrated suspension was spotted onto FSM agar dishes containing DAP, incubated for 8h and flushed from agar surface. After incubation of 2h in liquid FSM, cells were grown on selective agar plates containing X-Gluc. Blue colonies were transferred in 100 µl FSM as well as scaled up to 10 ml after positive testing for plasmid integration via PCR. Double integration mutants were subjected to excision by conjugation with pCM157 [5].

For *trans*-complementation, plasmid pCDS52_*mms6_mmsF* containing *mmsF*, *mms6*, *mgr4074* and the native *mms6* promoter (P_{mms6}) was constructed. The 1,448 bp fragment was digested with NsiI-EcoRI, and inserted into the same sites of pBBR-MCS2. Plasmid pmamXYop was constructed by PCR amplification of the *mamXY* operon with primer pairs AL200/AL201, which was inserted into pBBR-MCS2 after digestion with NdeI and XbaI. Other mutants could not be complemented because of their large sizes between 6 and 68 kb.

Supplementary tables

Table S1. Strains and plasmids used in this study.

Strains and plasmids	Description	References
M. gryphiswaldense strains		
MSR-1 R3/S1	Rif^r Sm^r, spontaneous mutant	[3]
MSR-1B	Spontaneous mutant, lacking 40,385 kb genomic region	[6]
ΔmamAB#K7	Δ*mamAB*	[5]
MSR-1B *mgr4058tomgr4146*	MSR-1B range of excision from *mgr4058* to *mgr4146*	[5]
MSR_SU12	Δ*mamAB* with deletion to *mgr4029*	[5]
Δ*GFDC*	Δ*mamGFDC*	[2]
Δ*mamJKL*	Δ*mamJKL*	this study
MSR+pAL01	MSR-1 R3/S1 (pAL01), Km^r	this study
MSR+pAL01+pAL02/2	MSR-1 R3/S1 (pAL01, pAL02/2), Km^r, Gm^r	this study
MSR+pAL01+pAL11_term	MSR-1 R3/S1 (pAL01, pAL11_term), Km^r, Gm^r	this study
MSR+pAL03	MSR-1 R3/S1 (pAL03), Km^r	this study
MSR+pAL03+pAL06	MSR-1 R3/S1 (pAL03, pAL06), Km^r, Gm^r	this study
MSR+pAL03+pAL08	MSR-1 R3/S1 (pAL03, pAL08), Km^r, Gm^r	this study
MSR+pAL05	MSR-1 R3/S1 (pAL05), Km^r	this study
MSR+pAL05+pAL02/2	MSR-1 R3/S1 (pAL02/2, pAL05), Km^r, Gm^r	this study
MSR+pAL07	MSR-1 R3/S1 (pAL07), Km^r	this study
MSR+pAL07+pAL08	MSR-1 R3/S1 (pAL07, pAL08), Km^r, Gm^r	this study
ΔA2	MSR-1 R3/S1 range of excision from *mgr4026* to *mgr4069*	this study
ΔA3	MSR-1 R3/S1 range of excision from *mgr4079* to *mgr4088*	this study
ΔA4	MSR-1 R3/S1 range of excision from *mgr4106* to *mgr4146*	this study
ΔA5	MSR-1 R3/S1 range of excision from *mgr4151* to *mgr4174*	this study

ΔA7	MSR-1 R3/S1 range of excision from *mgr4106* to *mgr4174*	this study
ΔA8	Δ*mamXY*	this study
ΔA10	Δ*mms6* operon	this study
ΔA11	Δ*mamXY,* Δ*mamGFDC*	this study
ΔA12	Δ*mms6* operon*,* Δ*mamGFDC*	this study
ΔA13	Δ*mms6* operon*,* Δ*mamGFDC,* Δ*mamXY*	this study
ΔA14	Δ*A7* with deletion of *mms6* and *mamGFDC* operon	this study
ΔA19	MSR-1B with deletion from *mgr4151* to *mgr4175*	this study
ΔA10_*pCDS52_mms6_mmsF*	Δmms6 operon (p*CDS52_mms6_mmsF*), Km^r	this study
ΔA10_pBBR-MCS2	Δ*mms6* operon (pBBR-MCS2), Km^r	this study
ΔA8_p*mamXY*	Δ*mamXY* (pmamXY), Km^r	this study
MSR-1_p*mamXY*	MSR-1 R3/S1 (pmamXY), Km^r	this study
E. coli strain		
E. coli BW29427	*thrB1004 pro thi rpsL hsdS lacZDM15 RP4-1360D(araBAD)567DdapA*	Datsenko and Wanner (unpublished)
E. coli DH5a	*1341::[erm pir(wildtype)]trahsdR17recA1-endA1gyrA96thi-1relA1*	Invitrogen
Plasmids		
pJet1.2	Ap^r, *eco47IR*, *rep* (pMB-1)	Fermentas
pT18mob2	Tet^r, pK18*mob*2 derivate	[7]
pK19mobGII	Km^r, pMB-1 replicon, *gusA*, *lacZα*	[1]
pCM184	Km^r, Ap^r, Tet^r	[4]
pCM157	Tet^r, Cre expression vector	[4]
pBBR-MCS2	Km^r, *lacZa*	[8]
pBBR-MCS5	Gm^r, *lacZa*	[8]
pAP150	pBBR-MCS2, $P_{mamDC45}$, *gfp2*, terminator sequence from pUC18R6K	[9]
pAS200	Gm^r, ColE1 ori, *sacB* of Bacillus subtilis	[4]
pAL01	pK19mobGII digested with SalI and EcoRI, insertion of *lox71* and homologous sequence AL01	this study
pAL01_MCS1	pAL01, digested with EcoRI and NotI, insertion of MCS from pBBR-MCS5	this study

pT18mob2_AL02/2	pT18*mob*2 digested with SalI and HindI, insertion of the *lox66* and homologous sequence AL02/2	this study
pAL02/2_Tet	pT18*mob*2_AL02/2 digested with SalI and EcoRI, insertion of gentamicin gene from pBBR-MCS5	this study
pAL02/2	pAL02/2_Tet digested with PstI, blunted and self-ligated	this study
pAL02/2_MCS2	pAL02/2 digested with HindIII and BamHI, insertion of MCS from pBBR-MCS5	this study
pAL02/2_term	pAL02/2_MCS2 digested with KspI, insertion of terminator sequence	this study
pAL03	pAL01_MCS1 digested with ClaI and NotI, insertion of homologous sequence AL03	this study
pAL05	pAL01 digested with EcoRI and NotI, insertion of homologous sequence AL05	this study
pAL06	pAL02/2_MCS2 digested with PvuI and XhoI, insertion of homologous sequnce AL06	this study
pAL07	pAL01 digested with EcoRI and NotI, insertion of homologous sequence AL07	this study
pAL08	pAL02/2 digested with BamHI and NotI, insertion of homologous sequence AL08	this study
pAL11_term	pAL02/2_term digested with BamHI and NotI, insertion of homologous sequence AL11	this study
pCM184_*mms6*_5' WT	pCM184 digested with MfeI and NdeI, insertion downstream fragment of *mgr4070*	this study
pCM184_*mms6*_5'3' WT	pCM184_mms6_5' WT digested with ApaI and SacI, insertion upstream fragment of *mgr4074*	this study
pCM184_*mms6*_5'3' GFDC	pCM184_mms6_5' WT digested with MluI and SacI, insertion downstream fragment of *mamC*	this study
pCM184_*mamXY*_5'	pCM184 digested with MfeI and NcoI, insertion downstream fragment of *ftsZm*	this study
pCM184_*mamXY*_5'3'	pCM184_mamXY_5' digested with ApaI	this study

pCM184_*mamXY*_5'3'	pCM184_mamXY_5' digested with ApaI and SacI, insertion upstream fragment of *mamX*	this study
pCM184_*mamXY*_5'SU	pCM184 digested with EcoRI and SmaI, insertion downstream fragment of *ftsZm*	this study
pCM184_*mamXY*_5'3'SU	pCM184 digested with ApaI and ClaI, insertion upstream fragment of *mamX*	this study
pCM184_*mamW*_5'	pCM184 digested with MnuI and NdeI, insertion upstream fragment of *mamW*	this study
pCM184_*mamW*_5'3'	pCM184_*mamW*_5' gigested with ApaI and SacI, insertion downstream fragment of *mamW*	this study
pSUMAI13_3'	pAS200 digested with SalI and HindIII, insertion upstream fragment of *mgr4174*	this study
pSUMAI13_5'	pKmobGII digested with BamHI and XbaI, insertion upstream fragment of *mgr4151*	this study
pK19mobGII_*mamJKL*_3'	pK19mobGII digested with XbaI and SpeI, insertion of upstream fragment of *mamJ*	this study
pK19mobGII_*mamJKL*_3'5'	pK19mobGII_*mamJKL*_3' digested with SmaI, insertion of downstream fragment of *mamL*	this study
pCDS52_*mms6_mmsF*	pBBR-MCS2 digested with NsiI and EcoRI, insertion *mmsF*, *mms6* and *mgr4074*	this study
p*mamXY*	pBBR-MCS2 digested with NsiI and EcoRI, insertion of *mamXY* operon,	this study

Table S2. DNA oligonucleotides used in this work.

Name	Sequence
AL019	5'-ATTGTCGACATAACTTCGTATAGCATACATTATACGAACGG
	TAGGATCCGGCATCCTGATCGGTAGGCGAT
AL020	5'-AAGCTTAGAAGGGTTACGACGCCGGT
AL033	5'-GAATTCGGCTGTTCGGCACCTCTGTT
AL034	5'-AATGTCGACTCTAGACTCGAGATAACTTCGTATAATGTATG
	CTATACGAACGGTAGCGGCCGCTGATCTCGGGATCACTCGGT
AL042	5'-GAATTCGCCACCTTGACAGAAATTGATATC
AL043	5'-GCGGCCGCTCTTCCAACGAAATTGTGCG
AL048	5'-GAATTCTTACCGCTCTTCGGCATCCACGCC
AL049	5'-GCGGCCGCGGCAGCCTCATTTAAACATTCAGG
AL081	5'-GAATTCACACCGTGGAAACGGATGAAGGCAC
AL082	5'-GTCGACGCGCCTGAAGCCCGTTCTGG
AL092	5'-GGATCCATGCCGGCGGACAGCAGATGCT
AL093	5'-GCGGCCGCGCACGGAGACTCTCATAGTG
AL094	5'-GGATCCACGCCTTCATCCTTGAACCA
AL095	5'-GCGGCCGCTGGACATCAACGAAAAGGCA
AL107	5'-ATCGATGTTCGATATCCGTCTGCGC
AL108	5' - GCGGCCGCCTCTTCGGGGCAACGTGAA
AL113	5'-GGATCCATAAGAATGCGGCCGCCCGCTCGAGCCCGGGCT GCAGGAATTCGA
AL114	5'-AAGCTTTGGGTTCGTGCCTTCATCCG
AL115	5'-GAATTCGGATCCGATATCAAGCTTATCGATACCGTCGACC
AL116	5'-GCGGCCGCTGGGTTCGTGCCTTCATCCGTT
AL121	5'-CTCGAGTATCGCCACCTTATGGGGAG
AL122	5'-CGATCGATGCTGTCGGCCATCATCAT
AL125	5'-GAATTCCTGATCTCCGGCAAGTGTAT
AL132	5'-ACGCGTTGAAATATTGGGCTGGTTCACG
AL133	5'-GAGCTCTGCTGCTGCCAATATCGTCG
AL136	5'-ATGCATTCACCCGAGGCCGAACCTCA
AL152	5'-TATACCGCGGGGCGGATTTGTCCTACTCAGG
AL153	5'-GACTCCGCGGGACTCCTGTTGATAGATCCAGTAATGAC
AL178	5'-GGATCCTTCATGTACTGCGGAACAGTCG
AL179	5'-CATATGTTGGGCTTGTGGTTTTGGCGG
AL188	5'-GGGCCCAAGGGCTGCTCCCGTGGTGG
AL189	5'-GAGCTCCCCACGCATGTACACAGCCATA
AL190	5'-CAATTGCTCGCTAAAAATGTGGGTTTCCG
AL191	5'-CCATGGGCCGCTCCGGAAGAATCAAGC
AL352	5'-CAATTGTGGCCCCGGTCAAGTCAACT
AL353	5'-CATATGTACATGAGGGCATCGCGTTG '
AL354	5'-GGGCCCAATTGTCGACAAATCCCAAAGA
AL355	5'-GAGCTCCCAAAGCAAAGGACTCCG
SU88	5'-GAATTCTAAAAATGTGGGTTTCCG

SU89	5'-CCCGGGTGAGCCGCTCCGGAAGAAT
SU304	5'-CAATTGATTGCCAGATGATCTTGATCATGTC
SU305	5'-CATATGCATGGCCGCTTTCCAAACAGGTGA
SU306	5'-GGGCCCTGAGGGAGTGGGGACTGCGAAGTA
SU307	5'-GAGCTCAGCCGAACCGACCAAATACTGG
SU422	5'-ATCGATCACAAGGGATAGATATGGC
SU423	5'-GGGCCCCTAACCTTGATCCCCG
SU488	5'-GTCGACATGCCGGCGGACAGCAGATGCT
SU489	5'-AAGCTTGCACGGAGACTCTCATAGTG
SU510	5'-GGATCCTTACCGCTCTTCGGCATCCACGCC
SU511	5'-TCTAGACAAGGCAGCCTCATTTAAACATTCAGG
EK1 JKL u_f	5'-TCTAGAGCAGCCGGTCCGATCGCCTTTGG
EK_JKL u_r	5'-CCCGGGATTGCTAACTAGTTATCCCGCTCCACCCTCAAAGAA
EK_JKL d_f	5'-ACTAGTCGCATTCCATGCTCCGTCGGAGC
EK2_JKL d_r	5'-CCCGGGGGATCCCCGACGAAAATGGTTACGCCCG

Supplementary figures

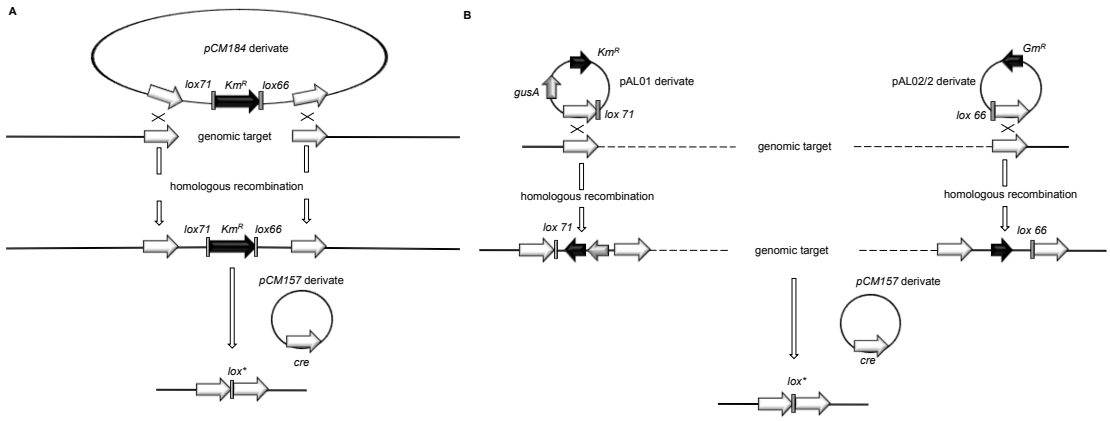

Figure S1. Schematic illustration of methods for generation of deletions within the MAI. (A) Allelic replacement of target genes using double cross-over followed by removal of selection marker with Cre-*lox* mediated excision. (B) Cre-*lox* recombination using the modified sequences *lox71* and *lox66* for specific excision of large chromosomal regions and construction of marker-less mutant strains. After excision the modified lox* sequence remains in the genome, but is poorly recognized by Cre recombinase making multiple recombination events possible.

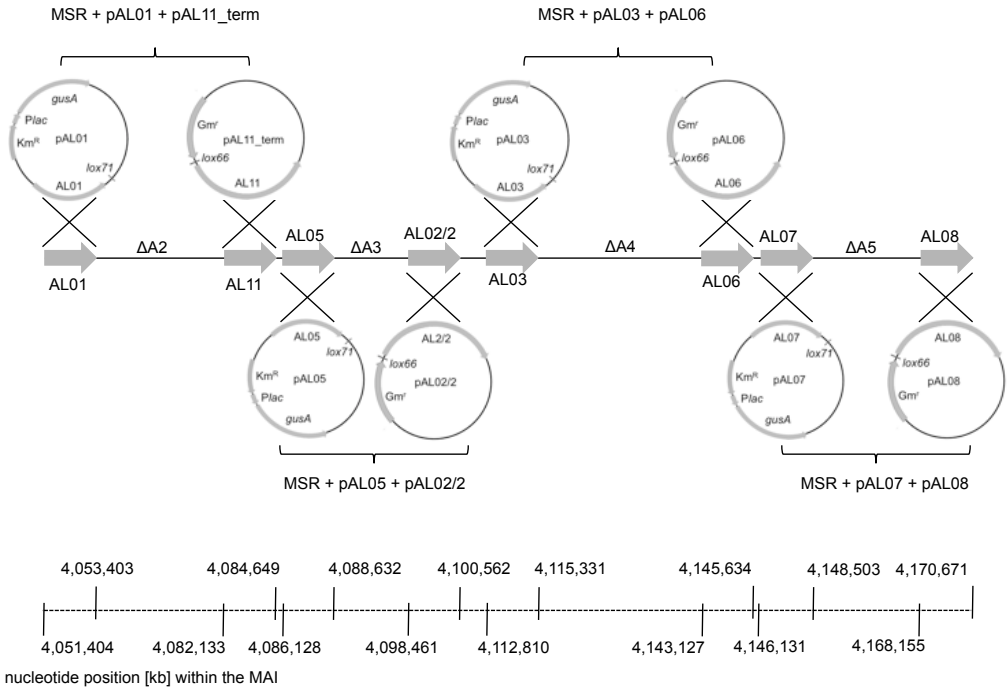

Figure S2. Constructed suicide plasmids (pAL01 to pAL11_term) for integration of modified *lox* sequences. Regions (AL01 to AL11) within the MAI of *M. gryphiswaldense* used for site-specific plasmid insertion via homologous recombination to enable subsequent excision between *lox* sites of double insertions.

References

1. Katzen F, Becker A, Ielmini MV, Oddo CG, Ielpi L (1999) New mobilizable vectors suitable for gene replacement in gram-negative bacteria and their use in mapping of the 3' end of the Xanthomonas campestris pv. campestris gum operon. Appl Environ Microbiol 65: 278-282.
2. Scheffel A, Gardes A, Grünberg K, Wanner G, Schüler D (2008) The major magnetosome proteins MamGFDC are not essential for magnetite biomineralization in *Magnetospirillum gryphiswaldense* but regulate the size of magnetosome crystals. J Bacteriol 190: 377-386.
3. Schultheiss D, Schüler D (2003) Development of a genetic system for *Magnetospirillum gryphiswaldense*. Arch Microbiol 179: 89-94.
4. Marx CJ, Lidstrom ME (2002) Broad-host-range *cre-lox* system for antibiotic marker recycling in gram-negative bacteria. Biotechniques 33: 1062-1067.
5. Ullrich S, Schüler D (2010) Cre-*lox*-based method for generation of large deletions within the genomic magnetosome island of *Magnetospirillum gryphiswaldense*. Appl Environ Microbiol 76: 2439-2444.
6. Schübbe S, Kube M, Scheffel A, Wawer C, Heyen U, *et al*. (2003) Characterization of a spontaneous nonmagnetic mutant of *Magnetospirillum gryphiswaldense* reveals a large deletion comprising a putative magnetosome island. J Bacteriol 185: 5779-5790.
7. Tauch A, Kirchner O, Löffler B, Götker S, Pühler A, *et al*. (2002) Efficient electrotransformation of corynebacterium diphtheriae with a mini-replicon derived from the *Corynebacterium glutamicum* plasmid pGA1. Curr Microbiol 45: 362-367.
8. Kovach ME, Elzer PH, Hill DS, Robertson GT, Farris MA, *et al.* (1995) Four new derivatives of the broad-host-range cloning vector pBBR1MCS, carrying different antibiotic-resistance cassettes. Gene 166: 175-176.
9. Pollithy A, Römer T, Lang C, Müller FD, Helma J, *et al*. (2011) Magnetosome expression of functional camelid antibody fragments (nanobodies) in *Magnetospirillum gryphiswaldense.* Appl Environ Microbiol.
10. Grünberg K, Wawer C, Tebo BM, Schüler D (2001) A large gene cluster encoding several magnetosome proteins is conserved in different species of magnetotactic bacteria. Appl Environ Microbiol 67: 4573-4582.
11. Grünberg K, Müller EC, Otto A, Reszka R, Linder D, *et al*. (2004) Biochemical and proteomic analysis of the magnetosome membrane in *Magnetospirillum gryphiswaldense*. Appl Environ Microbiol 70: 1040-1050.
12. Ullrich S, Kube M, Schübbe S, Reinhardt R, Schüler D (2005) A hypervariable 130-kilobase genomic region of *Magnetospirillum gryphiswaldense* comprises a

magnetosome island which undergoes frequent rearrangements during stationary growth. J Bacteriol 187: 7176-7184.

13. Uebe R, Voigt B, Schweder T, Albrecht D, Katzmann E, *et al.* (2010) Deletion of a *fur-like* gene affects iron homeostasis and magnetosome formation in *Magnetospirillum gryphiswaldense*. J Bacteriol 192: 4192-4204.

Table S3. Annotation and characteristics of MAI genes of *M. gryphiswaldense.*

Genomic Location	Length [bp]	Annotation	Blastp hits for AMB/MS/MC/RS/MV*	Hits outside MTB (E-value / Organism)*	Protein expression/ Reference
mgr4024	496	hypothetical protein	- / - / - / - / nf	/	-
mgr4025	266	hypothetical protein	- / - / - / - / nf	/	-
mgr4029	170	hypothetical protein	- / - / - / - / nf	/	-
mgr4030	283	hypothetical protein	- / 7e-09 / 1e-153 / 5e-39	7e-09 / *Thermomicrobium roseum* DSM 5159	-
mgr4033	77	hypothetical protein	- / - / - / - / nf	/	-
mgr4034	71	hypothetical protein	- / - / - / - / nf	/	-
mgr4035	163	two-component response regulator	4e-23 / 1e-19 / 3e-09 / 7e-09 / nf	1e-15 / *Caulobacter crescentus* NA1000	-
mgr4036	106	hypothetical protein	1e-08 / 2e-15 / - / - / nf	2e-20 / *Pseudomonas putida* BIRD-1	-
mgr4037	199	hypothetical protein	3e-77 / 4e-75 / - / - / 5e-92	2e-9 / *Polaromonas sp*. JS666	-
mgr4038	145	structural protein	7e-77 / 8e-76 / - / - / nf	5e-34 / *Desulfovibrio vulgaris str. Hildenborough*	-
mgr4039	766	phage-related	0.0 / 0.0 / - / 1e-34 / 0.0	2e-164 / *Methylobacillus flagellatus* KT	-
mgr4040	144	hypothetical protein	6e-74 / 3e-74 / -/ - / 2e-41	4e-38 / *Burkholderia vietnamiensis* G4	-
mgr4041	82	hypothetical protein	- / - / - / - / nf	2e-18 / *Candidatus* Accumulibacter phosphatis clade IIA str. UW-1	+ [d]
mgr4042	137	plasmid	- / 3e-6 / - / - / nf	8e-41/ *Polaromonas sp.* JS666	-

		stability like			
mgr4043	200	hypothetical protein	5e-97 / 4e-96 / - / - / 4e-47	8e-58 / *Burkholderia vietnamiensis* G4	-
mgr4044	72	hypothetical protein	1e-14 / 3e-15 / - /- / nf	/	-
mgr4045	136	hypothetical protein	6e-73 / 2e-71 / - / - / nf	/	-
mgr4046	270	hypothetical protein	9e-27 / 3e-25 / 3e-15 / - / nf	3e-31 / α-proteobacterium BAL199	-
mgr4047	102	hypothetical protein	4e-13/ 9e-19 / - / - / nf	1e-08 / *Rhodospirillum centenum* SW	-
mgr4048	67	hypothetical protein	- / 4e-17 / - / - / nf	2e-21 / α-proteobacterium BAL199	-
mgr4049	138	hypothetical protein	- / - / - / - / nf	/	-
mgr4050	186	phage-related	- / 1e-35 / 5e-14 / - / nf	9e-64 / α-proteobacterium BAL199	-
mgr4052	116	hypothetical protein	3e-51 / 2e-51 / - / - / nf	/	-
mgr4053	410	hypothetical protein	- / - / - / - / nf	3e-140 / *Mesorhizobium loti* MAFF303099	-
mgr4054	340	sensory transduction histdine kinase	1e-75 / 3e-73 /- / - / nf	7e-61 / δ-proteobacterium MLMS-1	-
mgr4056	378	hypothetical protein	- / - / - / - / nf	/	-
mgr4057	138	MamW	1e-44 / 7e-45 / - / - / nf	/	+ [b, c, d]
mgr4061	342	hypothetical protein	- / - / - / - / nf	/	-
mgr4062	421	two-component response regulator	e-122 / 2e-63 / - / - / nf	1e-13 / *Asticcacaulis excentricus* CB 48	-
mgr4063	161	hypothetical protein	2e-30 / 4e-31 / - / - / nf	/	-
mgr4064	159	hemerythrin-	5e-58 / 8e-59/ 1e-10 / 1e-8 / nf	3e-12 / *Candidatus* Methanoregula boonei	-

mgr4064	159	hemerythrin-like	5e-58 / 8e-59/ 1e-10 / 1e-8 / nf	3e-12 / *Candidatus* Methanoregula boonei 6A8	-
mgr4065	55	hypothetical protein	- / - / - / - / nf	/	-
mgr4066	109	hypothetical protein	7e-13 / 5e-13 / - / - / nf	/	-
mgr4067	503	pentapeptide repeat containing protein	1e-172 / 1e-173 / - /- / nf	5e-27 / *Anaerotruncus colihominis* DSM 17241S101	+
mgr4069	85	hypothetical protein	- / - / - / - / nf	/	-
mgr4070	449	TPR-like protein	1e-136 / 1e-135 / - / - / nf	2e-22 / *Rhodospirillum rubrum* ATCC 11170	+
mgr4071	347	hypothetical protein	1e-86 / 2e-10 / - / - / nf	4e-5 / *Starkeya novella* DSM 506	+
mgr4072	124	MmsF	7e-44 / 1e-44 / 4e-21 / - /8e-27	1e-5 / *Clostridium scindens* ATCC 35704	+ [b, d]
mgr4073	136	Mms6	2e-16/ 2e-16/ - / - / >1e-5	/	+ [b, d]
mgr4074	90	hypothetical protein	- / - / - / - / nf	/	-
mgr4075	111	MamG	6e-9 / 1e-7 / - / - / nf	/	+ [b]
mgr4076	111	MamF	1e-42 / 1e-42 / 8e-20 / - / 9e-25	1e-5 / *Blautia hydrogenotrophica* DSM 10507	+ [b, d]
mgr4077	314	MamD	2e-89 / 5e-90 / 7e-14 / - / 7e-5	/	+ [a, b, d]
mgr4078	125	MamC	5e-21 / 5e-21 / 3e-07 / - / 1e-6	/	+ [a, b, d]
mgr4079	278	IdiA-fragment	1e-82 / 1e-82 / - / - /nf	1e-87 / *Synechococcus sp*. JA-2-3B'a(2-13)	-
mgr4082	524	hemerythrin-like	6e-83/ e-105/ 7e-09 / 3e-10/ nf	8e-13 / *Colwellia psychrerythraea* 34H	-
mgr4083	150	hemerythrin-like	2e-83/ 1e-83 / 1e-11 / 2e-10/ nf	3e-14 / *Candidatus Koribacter versatilis Ellin345*	-
mgr4088	415	hypothetical protein	0.0 / 0.0 / - / - / nf	2e-64 / *Bradyrhizobium sp.* BTAi1	-
mgr4089	428	MamH	0.0 / 3e-87 / 1e-116 / - /1e-141	1e-36 / *Chlorobium luteolum* DSM 273	+
mgr4090	77	MamI	3e-15 / 3e-15 /3e-11 / - / 2e-09	/	-
					+ [a, b, d]

mgr4092	426	MamJ	2e-74 / 2e-74 / - / - / nf	/	+ [b, d]
mgr4093	360	MamK	0.0 / 0.0 / 3e-99 / 1e-65 / 1e-101	3e-92 / *Desulfurivibrio alkaliphilus* AHT2	+ [d]
mgr4094	123	MamL	8e-32 / 1e-19 /- / - / nf	/	-
mgr4095	318	MamM	1e-173 / 1e-173 / 1e-75 / 3e-35 / 1e-95	7e-33 / *Thermoanaerobacter sp*. X514	+ [b, d]
mgr4096	437	MamN	0.0 / 0.0 / - / - / 4e-99	4e-46 / *Clostridium botulinum* H04402 065	+ [b]
mgr4097	632	MamO	0.0 / 0.0 / 1e-78 / 3e-13 / e-148	4e-13 / *Acidimicrobium ferrooxidans* DSM 10331	+ [b, d]
mgr4098	270	MamP	1e-108 / 1e-108 / 8e-34 / - / 2e-57	3e-4 / *Legionella pneumophila str. Corby*	+
mgr4099	217	MamA	1e-113 / 1e-113 / 3e-37 / 1e-09 / 2e-49	2e-15 / *Microscilla marina* ATCC 23134	+ [a, b, d]
mgr4100	272	MamQ	1e-111 / 1e-110 / 1e-37 / 2e-53 / 2e-48	1e-17 / *Bacillus sp*. NRRL B-14911	+ [b, d]
mgr4101	72	MamR	1e-30 / 6e-31 / - / - / 3e-07	/	+ [b, d]
mgr4102	297	MamB	e-159 / e-159 / 2e-79 / 2e-36 / 2e-92	8e-44 / Natranaerobius thermophilus JW/NM-WN-LF	+ [a, b, d]
mgr4103	180	MamS	4e-60 / 2e-60 / 5e-13 / - / 5e-27	/	+ [b, d]
mgr4104	174	MamT	2e-86/ 2e-82 /4e-26 / 9e-05 / 1e-40	/	+ [b, d]
mgr4105	297	MamU	1e-114 / 1e-116 / - / - / nf	2e-36 / *Azospirillum sp.* B510	+
mgr4106	411	hypothetical protein	- / - / - / - / nf	/	+
mgr4108	458	HlyD secretion protein	4e-38 / 1e-44 / 5e-67 / 5e-32 / 7e-60	1e-77 / *Bradyrhizobium japonicum* USDA 110	-
mgr4109	738	HlyB secretion protein	1e-72 / e-133 / 0.0 / e-128	0.0 / *Pseudomonas aeruginosa*	+ [d]
mgr4110	168	Gp28	8e-04/ 2e-04 / - / - / nf	4e-14 / *Polaromonas sp.* JS666	-
mgr4111	161	hypothetical protein	- / - / - / - / nf	/	-
mgr4114	69	hypothetical protein	- / 7e-10 / - / - / nf	/	-
mgr4115	115	hypothetical protein	2e-09/ 2e-08 / - / - / nf	/	+ [d]
mgr4116	250	partition-related protein	2e-13 / 1e-15 / 2e-06 / 5e-06 / nf	1e-82 / *Azospirillum sp*. B510	-
mgr4117	216	hypothetical protein	- / - / - / - / nf	9e-50 / *Azospirillum sp*. B510	-

mgr4121	58	hypothetical protein	- / - / - / - / nf	/	-
mgr4122	140	hypothetical protein	- / - / 2e-43 / - / nf	1e-37 / *Aromatoleum aromaticum* EbN1	-
mgr4123	74	hypothetical protein	- / - / 4e-25 / - / nf	8e-22 / *Chlorobium phaeobacteroides* DSM 266	-
mgr4124	130	hypothetical protein	2e-50 / 3e-51 / 1e-40 / - / nf	3e-28 / *Pseudomonas fluorescens* WH6	-
mgr4125	155	hypothetical protein	- / - / - / - / nf	/	-
mgr4131	77	hypothetical protein	- / - / - / - / nf	1e-20 / *Rhodoferax ferrireducens* T118	-
mgr4132	398	regulator protein	1e-130 / e-132 / - / - / nf	2e-07 / *Hirschia baltica* ATCC 49814	-
mgr4140	93	hypothetical protein	- / - / - / - / nf	/	-
mgr4146	98	hypothetical protein	- / - / - / - / nf	/	-
mgr4147	323	FtsZm	e-124 / e-124 / 6e-82 / 2e-79 / nf	1e-119 / *Candidatus* Puniceispirillum marinum IMCC1322	+ [d]
mgr4148	661	MamZ	0.0 / 0.0 / 1e-163 / - / 1e-128	4e-35 / *Variovorax paradoxus* EPS	+
mgr4149	269	MamX	1e-117 / 1e-117 / 3e-34 / - / 3e-14	/	-
mgr4150	371	MamY	1e-139 / e-140 / - / - / 2e-17	/	+ [d]
mgr4152	326	hypothetical protein	1e-154 / 1e-156 / - / - / 2e-111	7e-51 / *Chthoniobacter flavus* Ellin428	+
mgr4153	308	hypothetical protein	1e-141 / 1e-143 / - / - / 7e-63	1e-19 / *Spirosoma linguale* DSM 74	-
mgr4154	299	hypothetical protein	1e-140 / 1e-139 / 5e-134 / - / 9e-76	/	-
mgr4160	115	hypothetical protein	3e-17 / - / - / - / nf	/	-
mgr4161	87	hypothetical protein	- / 6e-47 / - / - / nf	/	-
mgr4165	58	hypothetical protein	3e-10 / - / - / - / nf	/	-

mgr4166	422	hypothetical protein	2e-74 / 2e-63 / - / - / nf	5e-14 / α-proteobacterium BAL199	-
mgr4167	165	sensor (PAS) domain	4e-58 / 3e-43 / 4e-12 / 7e-07 / nf	2e-45 / Roseibium sp. TrichSKD4	-
mgr4169	699	hypothetical protein	1e-112 / - / - / - /nf	3e-58 / Cellvibrio japonicus Ueda107	-
mgr4170	133	hypothetical protein	- / - / - / - / nf	/	-
mgr4171	112	hypothetical protein	- / - / - / - / nf	2e-15 / Hoeflea phototrophica DFL-43	-
mgr4173	273	hypothetical protein	- / - / - / - / nf	/	-
mgr4174	190	phage-related protein	1e-21 / 5e-30 / 6e-07 / 6e-17 / nf	8e-37 / Paracoccus denitrificans PD1222	-

*Homologs in magnetotactic or non magnetotactic bacteria were identified by NCBI database search engine with an e-value threshold of <1e-05.

[a] [10], [b] [11], [c] [12], [d] [13]

Supplement: Chapter III

Biosynthesis of magnetic nanostructures in a foreign organism by transfer of bacterial magnetosome gene clusters.

Publication state: published in Nature Nanotechnology. 2014 Mar;9(3):193-7.

Supplementary methods

Construction of Tn5 transposon plasmids

For construction of translational (C-terminal) gene fusions, the *mamDC* promoter (XbaI, BamHI restriction sites added) was cloned in front of either the *mamGFDC* operon or the *mamJ* gene (NdeI, KpnI), which were followed by the *egfp* gene (KpnI, EcoRI). The resulting construct was cloned into pBAM1[1] modified by a tetracycline resistance cassette (exchange of km^R against tc^R with SanDI and AatII). The replicative plasmid pFM211 (Frank Müller, unpublished) harboring *ftsZm* with a *mCherry* fusion under control of an inducible lac promoter was recombined with pBAM1 to construct pBAM-ftsZm_mcherry. The resident km^R was replaced by tc^R using ET-recombination. For construction of pBAM_feoAB1, a fragment with P_{mamH} and *feoAB1* was amplified by PCR from pRU1feoAB (XbaI, EcoRI) and cloned into Tet-pBAM1.

Intracellular iron measurements

Cellular iron contents were determined after incubation under photoheterotrophic conditions in 10 ml Hungate tubes using a modified version of the ferrozine assay[2]. To this end, 4 ml cultures were centrifuged for 1 min at 11.000 rpm, resuspended in 90 µl HNO_3 (65%) and incubated for 3 h at 99 °C.

Sequencing

For whole genome sequencing of strain *R. rubrum_ABG6X* a genomic DNA library was generated with the Nextera Kit (Illumina). Sequencing (1.25 Mio clusters, 2x 250 bp) was performed with a MiSeq sequencer (Illumina). Data analysis with CLC Genomics Workbench (CLCbio) confirmed single-site integration of both expression cassettes without mutations, except for a spontaneous deletion (aa 169-247) within the hypervariable non-essential CAR domain of *mamJ* which was shown to be irrelevant for protein function[3].

Magnetosome isolation, electrophoresis and immuno-chemical detection

For magnetosome isolation and expression analysis, cultures of *R. rubrum* were grown photoheterotrophically in sealed 5 liter flasks illuminated by white light, 1000 lux intensity. Cells were harvested, washed and resuspended into HEPES buffer[4]. Cell suspensions were lysed by sonication

and cellular debris was removed by low-speed centrifugation. Magnetic separation of magnetosome particles, solubilization of the enclosing organic layer and fractionation of non-magnetic membrane fraction and soluble proteins were performed as previously described[5,6]. Polyacrylamide gels were prepared according to the procedure of Laemmli[7]. Protein samples from different cellular fractions (magnetosome membrane, soluble fraction, non-magnetic membrane fraction) were resuspended in electrophoresis sample buffer and denatured at 98 °C for 5 min[8]. 10 µg of protein extracts were separated on a 15% SDS-polyacrylamide gel. Protein bands were visualized by Coomassie brilliant blue staining. Western blot analysis for detection of MamC was performed as previously described[6].

Mass spectrometry

For mass spectrometry 25 µg solubilised proteins were tryptically in-gel digested as described previously[9]. The resulting fragments were separated on a C18 reversed-phase column and analyzed by nano-electrospray ionization-LC tandem MS (ESI-LC-MS/MS), recorded on an Orbitrap mass spectrometer[9]. Spectra were analyzed via Mascot™ software using the NCBI nr Protein Database and a database from *M. gryphiswaldense*[10].

References

1 Martinez-Garcia, E., Calles, B., Arevalo-Rodriguez, M. & de Lorenzo, V. pBAM1: an all-synthetic genetic tool for analysis and construction of complex bacterial phenotypes. *BMC Microbiol.* **11**, 38 (2011).

2 Viollier, E., Inglett, P. W., Hunter, K., Roychoudhury, A. N. & Van Cappellen, P. The ferrozine method revisited: Fe(II)/Fe(III) determination in natural waters. *Appl. Geochem.* **15**, 785-790 (2000).

3 Scheffel, A. & Schüler, D. The acidic repetitive domain of the *Magnetospirillum gryphiswaldense* MamJ protein displays hypervariability but is not required for magnetosome chain assembly. *J. Bacteriol.* **189**, 6437-6446 (2007).

4 Uebe, R. *et al.* The cation diffusion facilitator proteins MamB and MamM of *Magnetospirillum gryphiswaldense* have distinct and complex functions, and are involved in magnetite biomineralization and magnetosome membrane assembly. *Mol. Microbiol.* **82**, 818-835, doi:10.1111/j.1365-2958.2011.07863.x (2011).

5 Grünberg, K. *et al.* Biochemical and proteomic analysis of the magnetosome membrane in *Magnetospirillum gryphiswaldense*. *Appl. Environ. Microbiol.* **70**, 1040-1050 (2004).

6 Lang, C. & Schüler, D. Expression of green fluorescent protein fused to magnetosome proteins in microaerophilic magnetotactic bacteria. *Appl. Environ. Microbiol.* **74**, 4944-4953 (2008).

7 Laemmli, U. K. Cleavage of structural proteins during the assembly of the head of bacteriophage T4. *Nature* **227**, 680-685 (1970).

8 Uebe, R. *et al.* The cation diffusion facilitator proteins MamB and MamM of *Magnetospirillum gryphiswaldense* have distinct and complex functions, and are involved in magnetite biomineralization and magnetosome membrane assembly. *Mol. Microbiol.* **82**, 818-835 (2011).

9 Klein, A. *et al.* Characterization of the insertase for beta-barrel proteins of the outer mitochondrial membrane. *J. Cell biol.* **199**, 599-611 (2012).

10 Richter, M. *et al.* Comparative genome analysis of four magnetotactic bacteria reveals a complex set of group-specific genes implicated in magnetosome biomineralization and function. *J. Bacteriol.* **189**, 4899-4910 (2007).

Supplementary tables

Table S1: Summary of magnetic responses ("C_{mag}"), intracellular iron content and crystal size and number of various strains (median values, ± = standard deviation). If not indicated otherwise, cells were grown in the presence of 50 µM ferric citrate. Magnetic response and total iron content measurements were performed with (n) biological replicates under identical conditions (see also material & methods). For determination of crystal size and number per cell, cells of one clone were analyzed by TEM (n=sample size). The Mann-Whitney test (http://elegans.som.vcu.edu/~leon/stats/utest.html) was performed for crystal size comparison of *R. rubrum_ABG6X* and *R. rubrum_ABG6X_feo*: the difference was highly significant (p<0.001, two tailed test). Crystal size comparison of *R. rubrum_ABG6X_feo* and *M. gryphiswaldense* revealed no significant difference (p≥0.05, two tailed test).

Strain	Magnetic response ("C_{mag}")	Iron content (% dry weight)	Crystal size (nm)	Crystal number per cell
M. gryphiswaldense MSR-1	1.4 ± 0.2 (n=3)	3.5 (n=3)	36 ± 9 (n=310)	24 ± 8 (n=52)
M. gryphiswaldense Δ*mamAB_AB*	1.2 ± 0.2 (n=3)	n.d.	37 ± 10 (n=112)	23 ± 7 (n=24)
M. gryphiswaldense MSR-1B_*AB*	0.2 (n=3)	n.d.	17 ± 6 (n=112)	16 ± 6 (n=20)
M. gryphiswaldense MSR-1B_*ABG*	0.6 ± 0.1, (n=3)	n.d.	25 ± 6 (n=104)	13 ± 6 (n=20)
M. gryphiswaldense MSR-1B_*ABG6*	0.9± 0.2 (n=3)	n.d.	35 ± 8 (n=103)	18 ± 8 (n=22)
R. rubrum ATCC 11170	-	0.07 ± 0.04 (n=3)	-	-
R. rubrum_AB	-	0.08 (n=3)	-	-
R. rubrum_ABG	-	0.10 ± 0.01 (n=3)	-	-
R. rubrum_ABG6	-	0.17 (n=4)	12 ± 6 (n=304)	26 ± 10 (n=50)
R. rubrum_ABG6X	0.3 ± 0.2 (n=3)	0.17 ± 0.02 (n=4)	24 ± 7 (n=307)	10 ± 4 (n=50)
R. rubrum_ABG6X 500 µM ferric citrate	0.3 (n=4)	n. d.	25 ± 7 (n=301)	11 ± 5 (n=51)
R. rubrum_ABG6X 100 µM ferrous sulfate	0.2 (n=4)	n.d.	24 ± 8 (n=312)	10 ± 5 (n=52)
R. rubrum_ABG6X_ftsZm	0.6 ± 0.1* (n=3)	0.18 ± 0.03 (n=3)	26 ± 9 (n=300)	11 ± 4 (n=51)
R. rubrum_ABG6X_dJ	0.2 (n=3)	0.18 ± 0.01 (n=3)	27 ± 9 (n=300)	9 ± 4 (n=50)**
R. rubrum_ABG6X_dI	-	0.09 ± 0.07 (n=3)	-	-
R. rubrum_ABG6X_feo	0.8 ± 0.1 (n=3)	0.28 ± 0.07 (n=3)	37 ± 10 (n=300)	10 ± 4 (n=52)

*The slightly increased C_{mag} is likely due to effects of the genuine cell division protein FtsZm on cell morphology, as no difference in iron content and crystal size or number per cell was detectable.

**64% of mutant cells (n=32) harbored clustered magnetosomes, whereas 36% still showed a chain-like alignment of magnetosomes (n=18).

Table S3: Strains and plasmids used in this study. Km^R= kanamycin resistance, Tc^R= tetracycline resistance, Ap^R= ampicillin resistance, BSD^R= blasticidin S resistance, Cm^R= chloramphenicol resistance, Gm^R= gentamicin resistance, $Spec^R$= spectinomycin resistance.

Strain or plasmid	Characteristics	Reference(s) or source
Magnetospirillum gryphiswaldense strains		
M. gryphiswaldense MSR-1	Wild-type (wt)	DSM-6361,[15]
M. gryphiswaldense MSR-1B	spontaneous unmagnetic mutant lacking parts of the MAI	[16]
M. gryphiswaldense Δ*mamAB*	*mamAB* deletion mutant	[17]
M. gryphiswaldense Δ*mamAB* _*AB*	Km^R, transposon mutant with inserted *mamAB* operon	This study
M. gryphiswaldense MSR-1B_*AB*	Km^R, transposon mutant with inserted *mamAB* operon	This study
M. gryphiswaldense MSR-1B_*ABG*	Km^R, $Spec^R$, transposon mutant with inserted *mamAB and mamGFDC* operon	This study
M. gryphiswaldense MSR-1B_*ABG6*	Km^R, Cm^R, transposon mutant with inserted *mamAB, mamGFDC* and *mms6* operon	This study
Rhodospirillum rubrum strains		
R. rubrum ATCC 11170	wt	[18] (kindly provided by H. Grammel, Magdeburg)
*R. rubrum*_*AB*	Km^R, transposon mutant with inserted *mamAB* operon	This study
*R. rubrum*_*ABG*	Km^R, $Spec^R$, transposon mutant with inserted *mamAB and mamGFDC* operon	This study
R. rubrum _*ABG6*	Km^R, Cm^R, transposon mutant with inserted *mamAB, mamGFDC* and *mms6* operon	This study
*R. rubrum*_*ABG6X*	Km^R, Cm^R, Gm^R transposon mutant with inserted *mamAB, mamGFDC, mms6* and *mamXY* operon (without *ftsZm*)	This study
*R. rubrum*_*ABG6X_dJ*	Km^R, Cm^R, Gm^R, Ap^R transposon mutant with inserted *mamAB* (*mamJ* deletion)*, mamGFDC, mms6* and *mamXY* operon (without *ftsZm*)	This study
*R. rubrum*_*ABG6X_dI*	Km^R, Cm^R, Gm^R, Ap^R	This study

	transposon mutant with inserted *mamAB* (*mamI* deletion)*, mamGFDC, mms6* and *mamXY* operon (without *ftsZm*) Km^R, Cm^R, Gm^R, Tc^R	
R. rubrum_ABG6X_ftsZm	transposon mutant with inserted *mamAB, mamGFDC, mms6* and *mamXY* operon (without *ftsZm*) and *ftsZm* under control of an inducible lac promoter Km^R, Cm^R, Gm^R, Tc^R	This study
R. rubrum_ABG6X_feo	transposon mutant with inserted with inserted *mamAB, mamGFDC, mms6, mamXY* and *feoAB1* operon	This study
R.rubrum_GFDC-EGFP	Tc^R transposon mutant with inserted *mamGFDC-EGFP* Km^R, Cm^R, Gm^R, Tc^R	This study
R.rubrum_ABG6X_GFDC-EGFP	transposon mutant with inserted *mamAB, mamGFDC, mms6* and *mamXY* operon (without *ftsZm*) and *mamGFDC-EGFP*	This study
R. rubrum_J-EGFP	Tc^R transposon mutant with inserted *mamGFDC-EGFP* Km^R, Cm^R, Gm^R, Tc^R	This study
R. rubrum_ABG6X_J-EGFP	transposon mutant with inserted *mamAB, mamGFDC, mms6* and *mamXY* operon (without *ftsZm*) and *mamJ-EGFP*	This study
Escherichia coli strains		
DH10b	*F– mcrA Δ(mrr-hsdRMS-mcrBC) Φ80lacZΔM15 ΔlacX74 recA1 endA1 araD139 Δ(ara leu) 7697 galU galK rpsL nupG λ– dap* auxotroph derivative of *E. coli* strain B2155	Invitrogen
BW29427		K. Datsenko and B. L. Wanner, unpublished
WM3064	*thrB1004 pro thi rpsL hsdS lacZΔM15 RP4-1360 Δ(araBAD)567 ΔdapA1341::[erm pir]*	W. Metcalf, kindly provided by J. Gescher, KIT Karlsruhe
Plasmids		
pSC101-BAD-gbaA	Tc^R, replicative plasmid containing redα/redβ recombinases under the control of a L-Arabinose inducible promoter, temperature sensitive origin of replication	[19]
p15A-Tps-oriT-Km	Km^R, BSD^R, oriT, p15A origin of replication, mariner tps, cloning cassette	[20]
pSSK18 (BAC_*mamAB*)	BAC containing the	[16]

	mamAB operon from *M. gryphiswaldense*	
pTps_AB	Km^R, BSD^R, mariner tps vector containing *mamAB* operon	This study
pTps_ABG	$Spec^R$, Km^R, BSD^R, mariner tps vector with *mamAB* and *mamGFDC* operon	This study
pTps_ABG6	Cm^R, Km^R, BSD^R, mariner tps vector with *mamAB*, *mamGFDC*, and *mms6* operon	This study
pTps_XYZ	Gm^R, BSD^R, mariner Tps vector with *mamY*, *mamX* and *mamZ*	This study
pTps_ABG6_dJ	Cm^R, Km^R, BSD^R, Ap^R, mariner tps vector with *mamAB*, *mamGFDC*, and *mms6* operon, (*mamJ* deletion)	This study
pTps_ABG6_dI	Cm^R, Km^R, BSD^R, Ap^R, mariner tps vector with *mamAB*, *mamGFDC*, and *mms6* operon, (*mamI* deletion)	This study
pBAM1	Km^R, Ap^R, γR6K origin of replication, oriT, Tn5 vector	[21]
Tet-pBAM1	Tc^R, Ap^R, γR6K origin of replication, oriT, Tn5 vector	This study
Tet-pBam_mamGFDC-EGFP	Tc^R, Ap^R, *mamGFDC* operon under control of $P_{mamDC}$with a C-terminal EGFP fusion, Tn5 vector	This study
Tet-pBam_MamJ-EGFP	Tc^R, Ap^R, *mamJ* under control of P_{mamDC} with a C-terminal EGFP fusion, Tn5 vector	This study
pRU-1feoAB	Km^R, broad host range pBBRMCS2, *feoAB1* operon under the control of P_{mamH}	R. Uebe, unpublished
Tet-pBam_feoAB1	Tc^R, Ap^R, *feoAB1* operon under the control of P_{mamH}, Tn5 vector	This study
Tet-pBam-ftsZm_mCherry	Tc^R, Ap^R, *ftsZm, lacI* with a C-terminal mCherry fusion under control of inducible P_{lac}, Tn5 vector	This study
pFM211	Km^R, broad host range pBBRMCS2, lacI, *ftsZm* with C-terminal *mCherry* fusion, *mamK* with N-terminal EGFP fusion	F. Müller, unpublished

Table S4: Oligonucleotides used in this study.

Primer	Nucleotide sequence (5'-3')[a]	Product
Mam-tps5	AATTCGCACGGACTATAGCAACGAATCGAGGTCGGTTGAC	p15A-Tps-oriT-Km, ET-recombination with BAC_*mamAB,* pTps_AB
Mam-tps3	AAGCCATAAATCAGAAGAACTCGTCAAGAAGGC GAACGAAGATGAGACAGAAATCCGTGGCGCCGAGCGTAA GCATCCGGTGAGAACCTCATTCCCTCATGATACAG	
mamGFC3	TATCATGAGGGAATGAGGTTCTCACCGGATGCTTACGCTC	*mamGFDC* operon, ET-recombination with pTps_AB
mamGFC5	GGCGCCAGAGCACATCGGGGTGAATGACGAC CGCTAGCTGCGGGTTATTCGCATTTGC	
spectMam3	TCAAAACCCGCGCAGAGGCAAATGCGAATAACCCGCAGCT	Spectinomycin resistance cassette, ET-recombination with pTps_AB
spectMam5	AGCGTTATAATTTTTTTAATCTGTTATT TGATCCGCTATGGTAAGCGCATCATGTCCGGATCCCATGG CGTTCCGCTCGTAACGTGACTGGCAAGAGATATT	
mms6cm5	TACTGCGATGAGTGGCAGGGCGGGGCGTAAGCTTACAATT	*mms6* operon, ET-recombination with pTps_ABG
mms6mam3	TCCATTCGCCATTC GTGCTTCGCTGTGTCCACAAGAACC	
cm-mms6-3	TGGCGAATGGAAATTGTAAGCTTACGCCCCGCCCTGCCAC TC	Chloramphenicol resistance cassette, ET-recombination with pTps_ABG
cm-mms6-5	TGATCCGCTATGGTAAGCGCATCATGTCCGGATCCCATGG CGTTCCGCTCGTCCTGGTGTCCCTGTTGATACC	
IK097	TCTAGAGGGCCCCAACTTTTTCGCTTTACTAGCTCTTAGTT CTCCAATAAATTCCCTGCGTCGA	P_{mamDC} in pBAM1
IK098	CATATGCTGATCTCCGGCAAGTGTATGCACGATTCCCTCTC TGCCCCTTAAAATCGACGCAGGGAAT	
IK107	CATATGATCAAGGGCATCGCGGG	*mamGFDC* operon in pBAM1
IK101	GGTACCGGCCAATTCTTCCCTCAGAA	
IK102	GGTACCGGAGGCGGAGGCGGT	*egfp* in pBAM1
IK103	GAATTCTTACTTGTACAGCTCGTCCATG	
IK163	GAATTCTTAGCCGATTCGCAG	*mamXY*-operon (without ftsZm), ET-recombination with p15A-Tps-oriT-Gm
IK164	GAGCTCGGCAGCCTCATTTAAA	
IK173	CCGGAATTGCCAGCTGGGGCGCCCTCTGGTAAGGTTGGG AAGCCCTGCAACGTATAATATTTGCCCATG	Gentamicin resistance cassette, ET-Recombination with p15A-Tps-oriT-Km
IK174	AGGCGATAGAAGGCGATGCGCTGCGAATCGGGAGCGGCG ATACCGTAAAGCGATCTCGGCTTGAA	
IK208	CCCGGTACCCAGCTTTTGTTCCCTTTAGTGAGGGTTAATTG CGCGCTTGGCCTCATTCCCTCATGATACAGAGAC	p15A-Tps-oriT-Gm, ET-recombination with *mamXY*
IK209	GGCGTTACCCAACTTAATCGCCTTGCAGCACATCCCCCTTT CGCCAGCTGTCTCGGCTTGAACGAATTG	
IK213	GACGTCGAGCCACGGCGG	Tetracycline resistance cassette in pBAM1
IK214	GGGTCCCTCAGGTCGAGGTGGC	
IK215	TCTAGACTACAAGAATGTCCCGC	*feoAB1* operon+P_{mamH} in pBAM1
IK216	GAATTCGGCATCCTGATCGGT	
IK217	CATATGATGGCAAAAAACCGG	*mamJ* in pBAM1
IK218	GGCGGTACCTTTATTCTTATCTTCAGCATCAC	
IK235	GGGTGGAGCGGGATAATGGCAAAAAACCGGCGTGATCGC GGCACGGCTAAATACATTCAAATATGTATCC	Ampicillin resistance cassette insertion into *mamJ* of pTps_ABG6
IK236	CTATTTATTCTTATCTTCAGCATCACATTTCGGCGATGAACA ACTACCTTACCAATGCTTAATCAGTG	
IK239	CGCCGCTTGTGTTCTGTATCAAGACTGGAGAACGTTTATG CCAACTAAATACATTCAAATATGTATCC	Ampicillin resistance cassette Insertion into *mamI* of pTps_ABG6
IK240	TCAACCATCGATGTTAGGGTCTGAGTTCGCCCTCTTACCG GCAGGTTACCAATGCTTAATCAGTG	
IK251	AAACCGCCCAGTCTAGCTATCGCCATGTAAGCCCACTGCA AGCTACCTGCCCTCATTCCCTCATGATACA	Tet-pBAM1, ET-recombination with recombination with pFM211
IK252	CAGCACATCCCCCTTTCGCCAGCTGGCGTAATAGCGAA GAGGCCCGCACCGGATTTTGAGACACAAGACGTC	

References

1 Richter, M. *et al.* Comparative genome analysis of four magnetotactic bacteria reveals a complex set of group-specific genes implicated in magnetosome biomineralization and function. *J. Bacteriol.* **189**, 4899-4910 (2007).

2 Katzmann, E. *et al.* Magnetosome chains are recruited to cellular division sites and split by asymmetric septation. *Mol. Microbiol.* **82**, 1316-1329 (2011).

3 Draper, O. *et al.* MamK, a bacterial actin, forms dynamic filaments *in vivo* that are regulated by the acidic proteins MamJ and LimJ. *Mol. Microbiol.* **82**, 342-354 (2011).

4 Scheffel, A., Gardes, A., Grünberg, K., Wanner, G. & Schüler, D. The major magnetosome proteins MamGFDC are not essential for magnetite biomineralization in *Magnetospirillum gryphiswaldense* but regulate the size of magnetosome crystals. *J. Bacteriol.* **190**, 377-386 (2008).

5 Scheffel, A. *et al.* An acidic protein aligns magnetosomes along a filamentous structure in magnetotactic bacteria. *Nature* **440**, 110-114 (2006).

6 Zeytuni, N. *et al.* Self-recognition mechanism of MamA, a magnetosome-associated TPR-containing protein, promotes complex assembly. *Proc. Natl. Acad. Sci. U S A* **108**, E480-487 (2011).

7 Komeili, A., Vali, H., Beveridge, T. J. & Newman, D. K. Magnetosome vesicles are present before magnetite formation, and MamA is required for their activation. *Proc. Natl. Acad. Sci. U S A* **101**, 3839-3844, doi:10.1073/pnas.0400391101 (2004).

8 Arakaki, A., Webb, J. & Matsunaga, T. A novel protein tightly bound to bacterial magnetic particles in *Magnetospirillum magneticum* strain AMB-1. *J. Biol. Chem.* **278**, 8745-8750 (2003).

9 Prozorov, T. *et al.* Protein-Mediated Synthesis of Uniform Superparamagnetic Magnetite Nanocrystals. *Adv. Funct. Mater.* **17**, 951–957 (2007).

10 Uebe, R. *et al.* The cation diffusion facilitator proteins MamB and MamM of *Magnetospirillum gryphiswaldense* have distinct and complex functions, and are involved in magnetite biomineralization and magnetosome membrane assembly. *Mol. Microbiol.* **82**, 818-835 (2011).

11 Murat, D. *et al.* The magnetosome membrane protein, MmsF, is a major regulator of magnetite biomineralization in *Magnetospirillum magneticum* AMB-1. *Mol. Microbiol.* (2012).

12 Tanaka, M., Arakaki, A. & Matsunaga, T. Identification and functional characterization of liposome tubulation protein from magnetotactic bacteria. *Mol. Microbiol.* **76**, 480-488 (2010).

13 Yang, W. *et al. mamO* and *mamE* genes are essential for magnetosome crystal biomineralization in *Magnetospirillum gryphiswaldense* MSR-1. *Res. Microbiol.* **161**, 701-705 (2010).

14 Quinlan, A., Murat, D., Vali, H. & Komeili, A. The HtrA/DegP family protease MamE is a bifunctional protein with roles in magnetosome protein localization and magnetite biomineralization. *Mol. Microbiol.* **80**, 1075-1087 (2011).

15 Schleifer, K. *et al.* The genus *Magnetospirillum* gen. nov., description of *Magnetospirillum gryphiswaldense* sp. nov. and transfer of *Aquaspirillum magnetotacticum* to *Magnetospirillum magnetotacticum c*omb. nov. *Syst. Appl. Microbiol.* **14**, 379–385 (1991).

16 Schübbe, S. *et al.* Characterization of a spontaneous nonmagnetic mutant of *Magnetospirillum gryphiswaldense* reveals a large deletion comprising a putative magnetosome island. *J. Bacteriol.* **185**, 5779-5790 (2003).

17 Lohsse, A. *et al.* Functional analysis of the magnetosome island in *Magnetospirillum gryphiswaldense*: the *mamAB* operon is sufficient for magnetite biomineralization. *PLoS One* **6**, e25561 (2011).

18 Pfenning, N. & Trüper, H. G. Type and Neotype Strains of the Species of Phototrophic Bacteria Maintained in Pure Culture. *Int. J. Syst. Bacteriol.* **21**, 19-24 (1971).

19 Wang, J. *et al.* An improved recombineering approach by adding RecA to lambda Red recombination. *Mol Biotechnol* **32**, 43-53 (2006).

20 Fu, J. *et al.* Efficient transfer of two large secondary metabolite pathway gene clusters into heterologous hosts by transposition. *Nucleic Acids Res.* **36**, e113 (2008).

21 Martinez-Garcia, E., Calles, B., Arevalo-Rodriguez, M. & de Lorenzo, V. pBAM1: an all-synthetic genetic tool for analysis and construction of complex bacterial phenotypes. *BMC Microbiol.* **11**, 38 (2011).

Supplementary figures

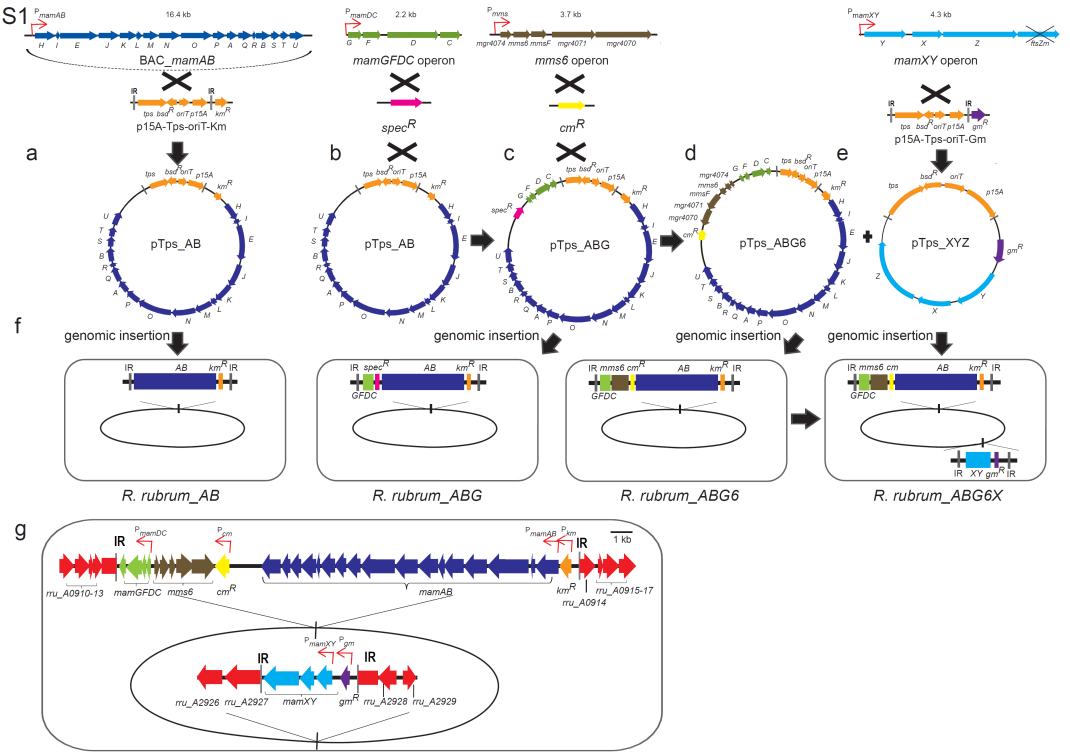

Fig. S1: Construction scheme of insertion cassettes for modular expression of the *mam* and *mms* operons. (**a**) Recombineering of a BAC containing the *mamAB* operon (blue) and a vector backbone (Km-p15A-Tps-oriT-Km, orange) harboring a MycoMar transposase gene (*tps*), inverted repeats (IR), origin of transfer (*oriT*), p15A origin of replication (*p15A*) and a *kanamycin*^{R} cassette (*km*^{R}, orange). (**b**) Insertion of a *spectinomycin*^{R} cassette (*spec*^{R}, pink) and the *mamGFDC* operon (green) into pTps_AB by triple recombination. (**c & d**) Stitching of pTps_ABG by insertion of the *mms6* operon and a *chloramphenicol*^{R} cassette. (**e**) pTps_XYZ consisting of a Tps vector backbone (orange), *mamXYZ* (pale blue) and a *gentamicin*^{R} gene (*gm*^{R}, purple) was constructed. (**f**) Plasmids were transferred by conjugation into *R. rubrum*. Transposition of the DNA-fragments within the IR sequences occurred at random positions at TA dinucleotide insertion sites by a “cut and paste” mechanism[1]. (**g**) Chromosomal insertion sites of the transposed constructs in *R. rubrum_ABG6X* are shown with adjacent genes (red) as revealed by whole genome sequencing performed with a MiSeq sequencer (Illumina) (accession number of *R. rubrum* ATCC 11170: NC_007643). pTps_ABG6 inserted within a gene encoding a putative aldehyd dehydrogenase (YP_426002), and pTps_XYZ inserted within rru_A2927, encoding a putative acriflavin resistance protein (protein accession number YP_428011). Sequences of inserted magnetosome operons matched those of the donor (*M. gryphiswaldense*) with no detectable mutations, except for a deletion (aa 169-247) within the hypervariable non-essential CAR domain of *mamJ,* which was shown to be irrelevant for protein function[2]

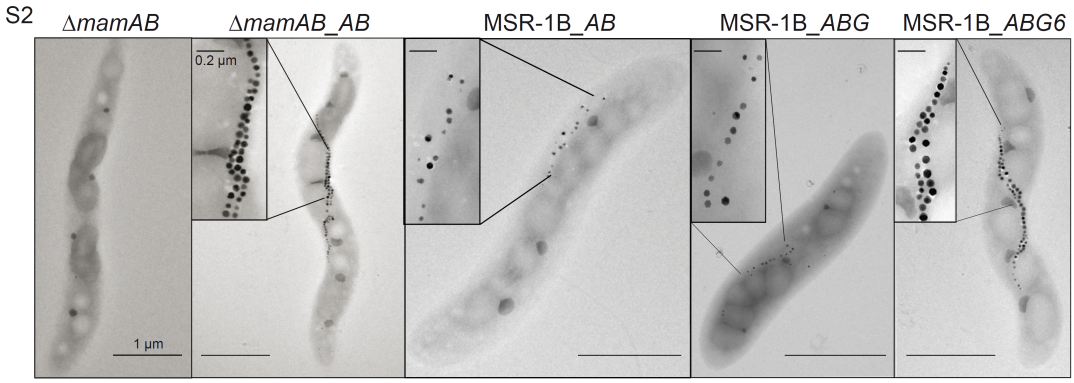

Fig. S2: Transmission electron micrographs of MSR mutants expressing various insertional transposon constructs. The plasmids pTps_AB, pTps_ABG and pTps_ABG6 were transferred into the non-magnetic *M. gryphiswaldense* mutants Δ*mamAB*[3] and MSR-1B, the latter lacking most of the magnetosome genes except of the *mamXY* operon[3,4]. After transfer of pTps_AB, a wt-like phenotype was restored in *ΔmamAB_AB* as revealed by C_{mag} (1.2 ± 0.2) and measured crystal sizes (37 ± 10 nm) in comparison with *M. gryphiswaldense* wt (36 ± 9 nm, C_{mag}=1.4 ± 0.2) (see also Table S1). Mutant MSR-1B was only partly complemented after insertion of pTps_AB and pTps_ABG, that is, C_{mag} and crystal sizes were still lower than in the wt (Table S1). Transfer of pTps_ABG6 restored nearly wt-like magnetosome formation in MSR-1B (35 ± 8 nm, C_{mag}=0.9± 0.1). ±= s.d. Scale bar: 1 µm, insets: 0.2 µm.

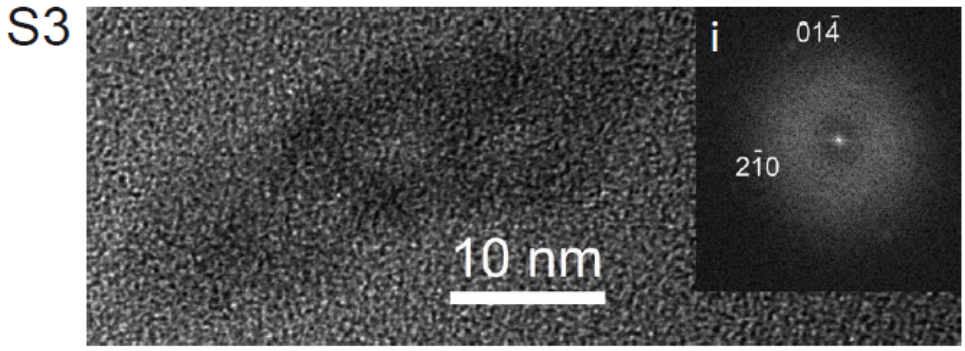

Fig. S3: HRTEM lattice image of a crystal from *R. rubrum_ABG6* with the corresponding Fourier transform (i) that shows intensity maxima consistent with the structures of hematite.

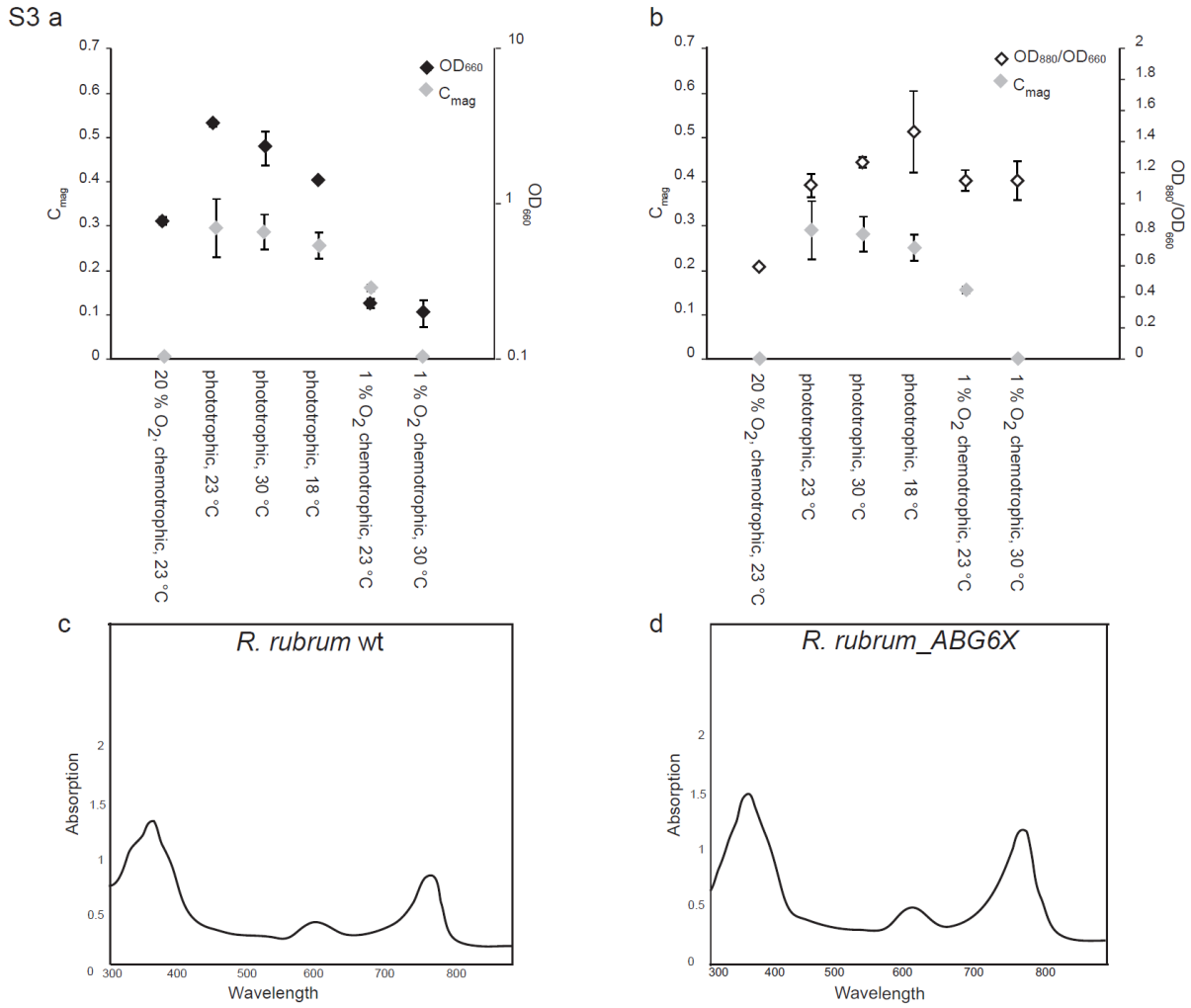

Fig. S4: Growth, magnetic response and ICM/Bchl a production of *R. rubrum_AGB6X*. (**a & b**) Cells were grown in ATCC 112 (chemotrophic, 20% O_2), Sistrom A (phototrophic, anoxygenic) and M2SF (chemotrophic, 1%O_2) medium for 3 (30 °C), 4 (23 °C) or 10 (18 °C) days. Optical density at 660 nm (black diamonds) and 880 nm and magnetic response (grey diamonds) were measured. The ratio OD_{880}/OD_{660} (white diamonds) correlates with the amount of chromatophores produced in the cells (median values n=3, error bars indicate s.d.). No C_{mag} was detectable under aerobic and microaerobic conditions at 30 °C. (**c & d**) Absorption spectra of extracted bacteriochlorophylls from *R. rubrum* wt (**c**) and *R. rubrum*_ABG6X (**d**) (phototrophic growth, 30 °C).

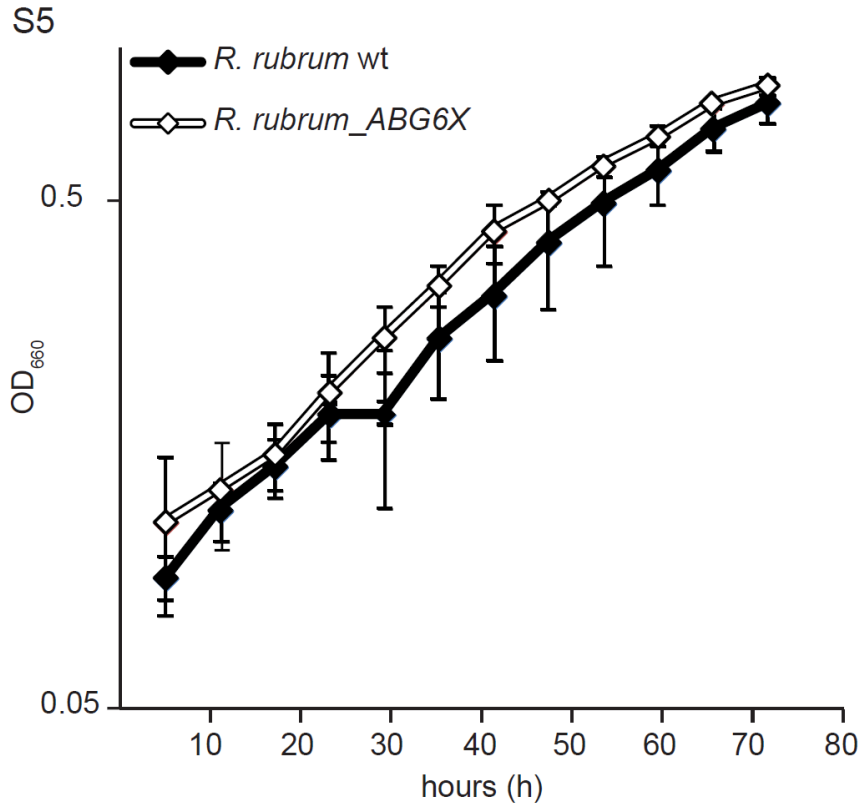

Fig. S5: Growth of *R. rubrum* wt and *R. rubrum_ABG6X* (OD_{660}). Cells of *R. rubrum* were incubated in Sistrom A medium (1000 lux) for 3 days at 23 °C under anaerobic conditions. No growth defects of mutant strain *ABG6X* (median values n=3, error bars indicate s.d.) were detectable compared to the untransformed wt (n=3).

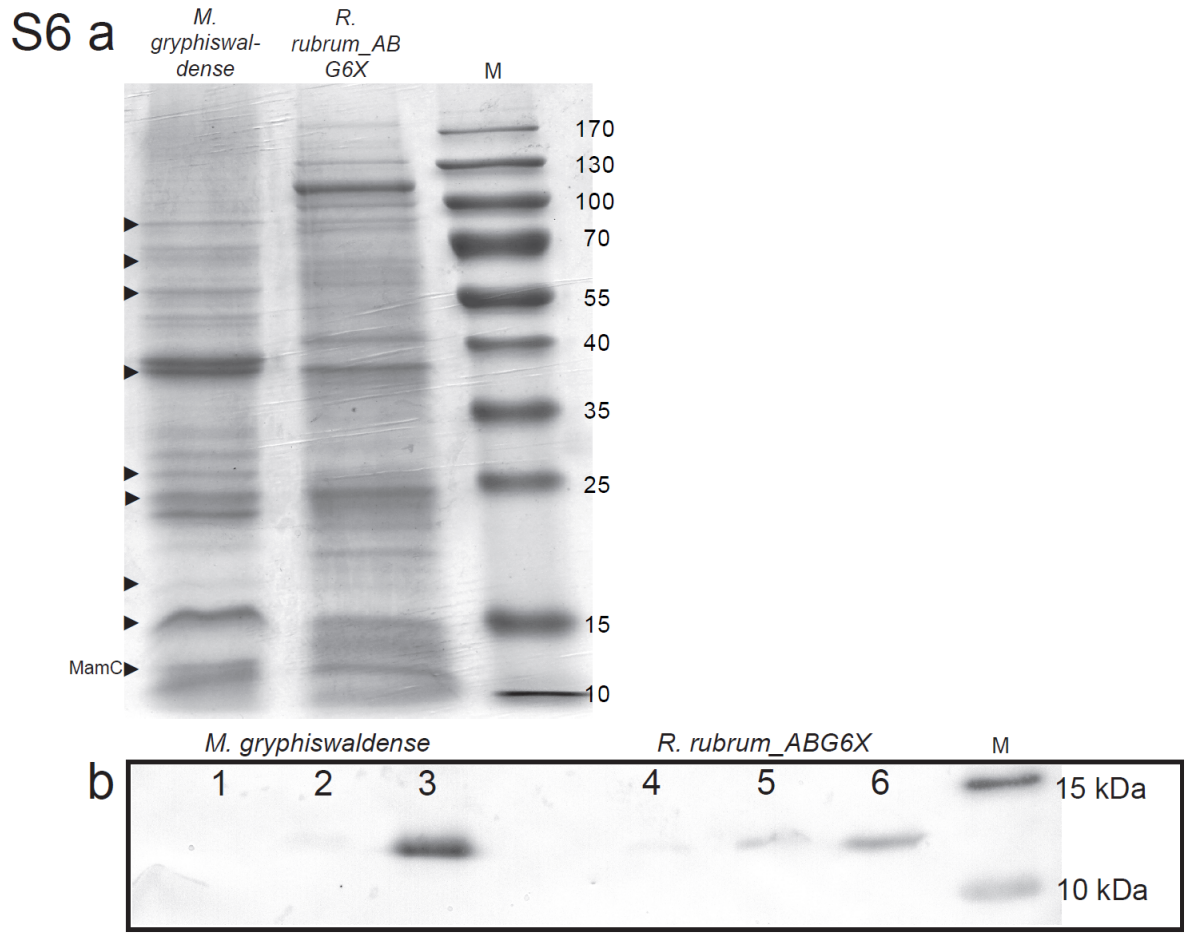

Fig. S6: Proteomic analysis of magnetosomes from *R. rubrum_ABG6X*. (**a**) 1D SDS-PAGE of Coomassie blue stained proteins solubilized from isolated magnetosome particles of *M. gryphiswaldense* and *R. rubrum_ABG6X*. Bands of the same size are indicated (arrowheads). (**b**) Immunodetection of MamC (12.4 kDa) in blotted fractions of *M. gryphiswaldense* and *R. rubrum_ABG6X* using an anti-MamC antibody[5]. A signal for MamC was detectable in the magnetic membrane fraction of *R. rubrum_ABG6X* (6), which was absent from the soluble fraction, but faintly present also in the non-magnetic membrane fraction (5), possibly originating from empty membrane vesicles or incomplete magnetic separation during isolation. Protein extracts from *M. gryphiswaldense*: 1. soluble fraction, 2. non-magnetic membrane fraction, 3. magnetosome membrane. Protein extracts from *R. rubrum_ABG6X*: 4. soluble fraction, 5. non-magnetic membrane fraction, 6. magnetic ("magnetosome") membrane fraction. M: Marker.

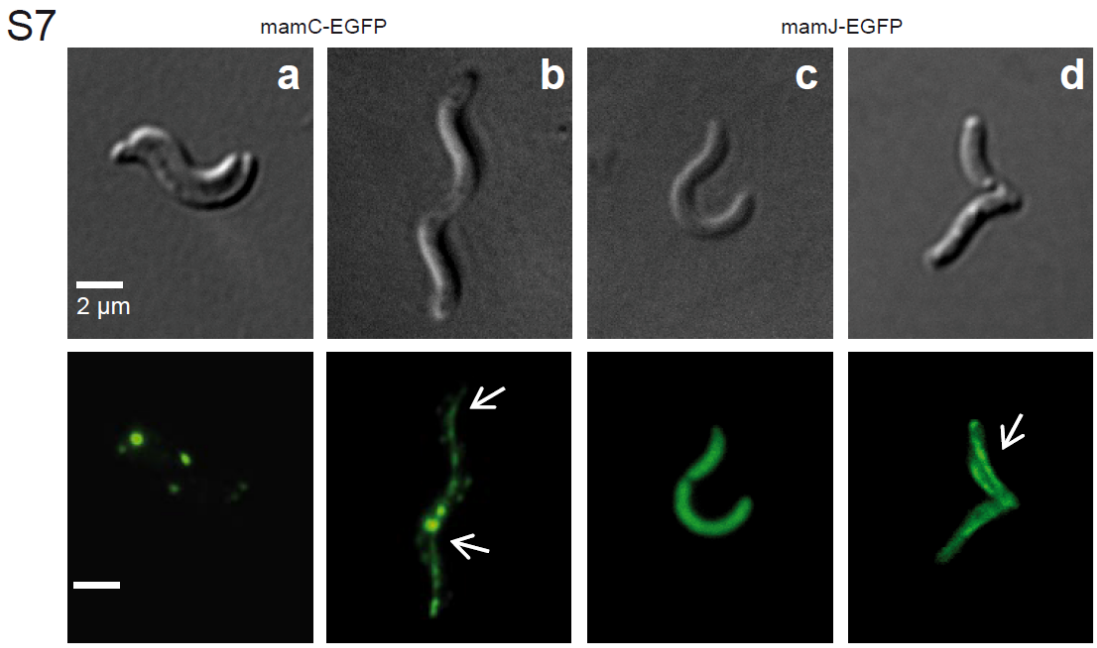

Fig. S7: Fluorescence microscopy of *R. rubrum* wt and *R. rubrum_ABG6X* cells expressing different EGFP-tagged magnetosome proteins. For localization studies of fluorescently labeled magnetosome proteins, strains were cultivated in ATCC medium overnight at 30 °C with appropriate antibiotics (Table S3). (**a & b**) MamGFDC with a C-terminal MamC-EGFP fusion expressed in *R. rubrum* wt (n=151) (**a**), and *R. rubrum_ABG6X* (n=112) (**b**). In the transformed strain, a filamentous structure is visible for 79% of the cells (n=89). **c & d**, MamJ-EGFP expressed in *R. rubrum* wt (n=109) (**c**), and in *R. rubrum_ABG6X* (n=89) displaying a chain-like fluorescence signal in 63% of the cells (n=56) (**d**). Scale bar: 2µm.

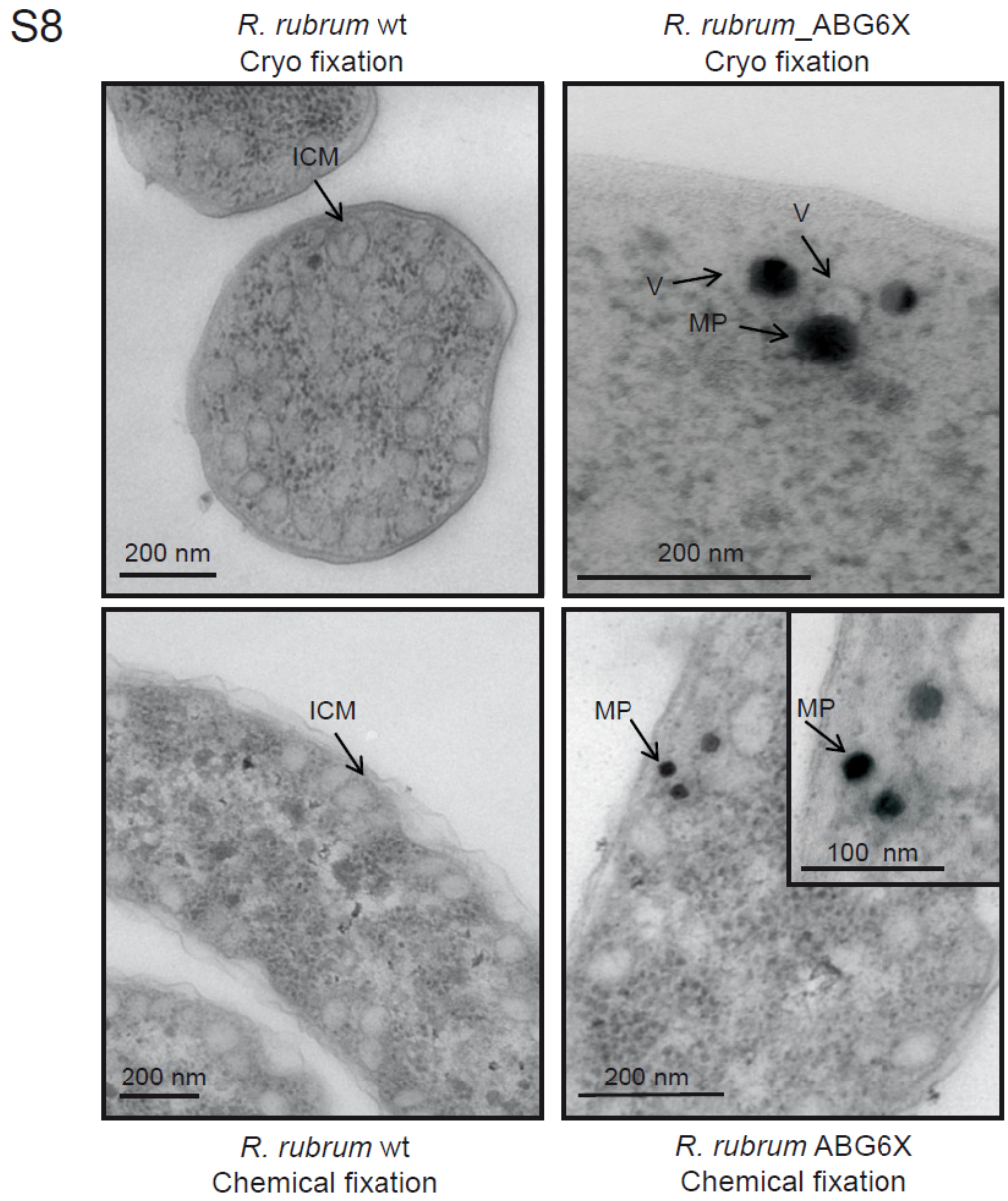

Fig. S8: TEM of cryo- or chemically fixed, thin sectioned *R. rubrum* strains. Cells were cultivated under photoheterotrophic conditions. ICM sizes of cryo fixed *R. rubrum* wt (93 ± 34 nm, n=95) and vesicles surrounding immature magnetosomes of cryo fixed *R. rubrum_ABG6X* (66 ± 6 nm, n=6) were measured.

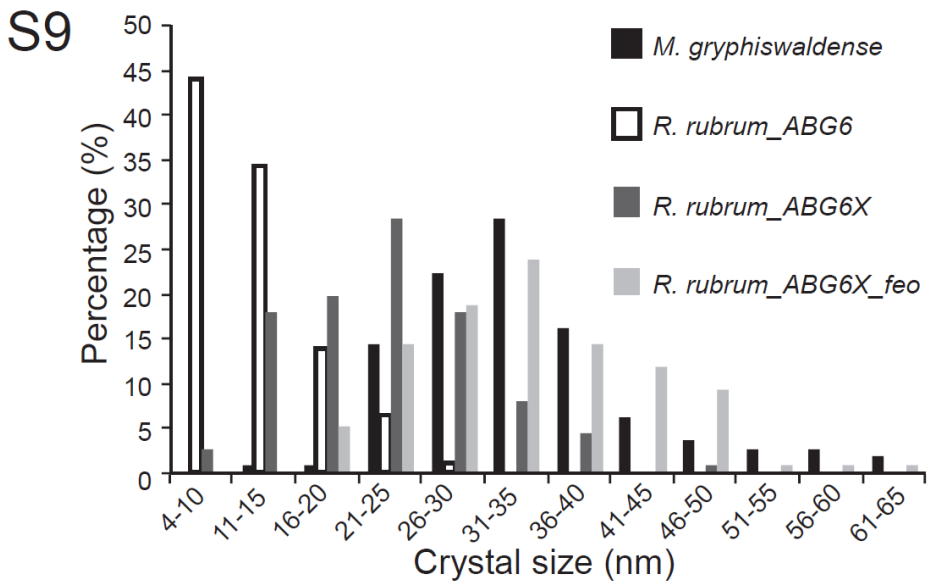

Fig. S9: Size distribution of magnetosome crystals in *M. gryphiswaldense* and different *R. rubrum* strains. Whereas crystals of *R. rubrum_ABG6* (n=303) and *R. rubrum_ABG6X* (n=306) were smaller than those of the donor *M. gryphiswaldense* (n=310), crystal sizes of *R. rubrum_ABG6X_feo* (n=301) were significantly larger, approaching those of the donor strain (see also Table S1).

S10

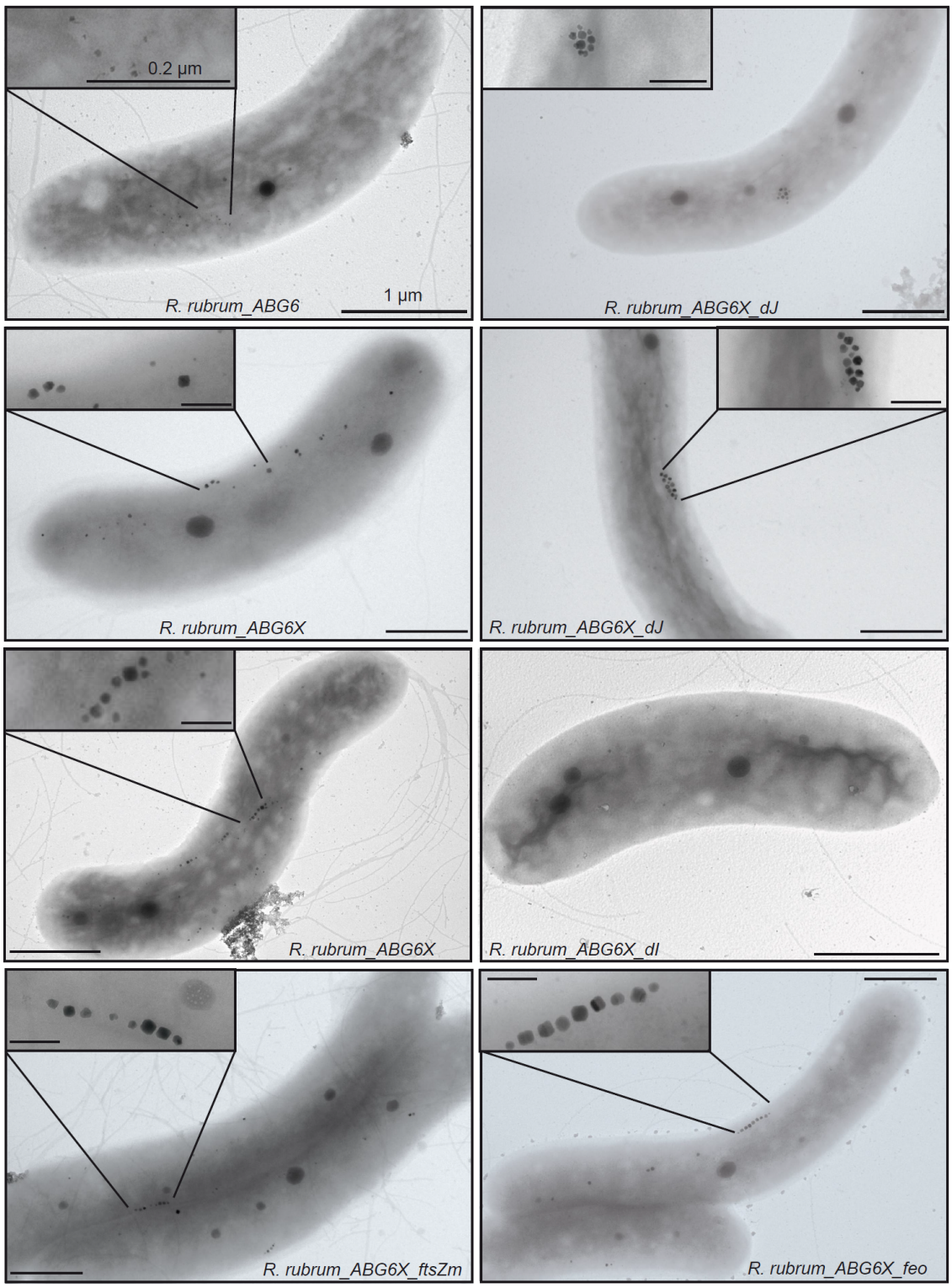

Figure S10: Transmission electron micrographs of whole cells of different *R. rubrum* strains expressing magnetosome gene clusters. Scale bar: 1 µm, inset: 0.2 µm.

References

1 Rubin, E. J. *et al. In vivo* transposition of *mariner*-based elements in enteric bacteria and mycobacteria. *Proc. Natl. Acad. Sci. U S A* 96, 1645-1650 (1999).

2 Scheffel, A. & Schüler, D. The acidic repetitive domain of the *Magnetospirillum gryphiswaldense* MamJ protein displays hypervariability but is not required for magnetosome chain assembly. *J. Bacteriol.* 189, 6437-6446 (2007).

3 Lohsse, A. *et al.* Functional analysis of the magnetosome island in *Magnetospirillum gryphiswaldense*: the *mamAB* operon is sufficient for magnetite biomineralization. *PLoS One* 6, e25561 (2011).

4 Schübbe, S. *et al.* Characterization of a spontaneous nonmagnetic mutant of *Magnetospirillum gryphiswaldense* reveals a large deletion comprising a putative magnetosome island. *J. Bacteriol.* 185, 5779-5790 (2003).

5 Lang, C. & Schüler, D. Expression of green fluorescent protein fused to magnetosome proteins in microaerophilic magnetotactic bacteria. *Appl. Environ. Microbiol.* 74, 4944-4953 (2008).

Table S2: Magnetosome proteins identified in the MM of strain *R. rubrum_ABG6X* by nano-electrospray ionization-LC tandem MS (ESI-LC-MS/MS). Spectra were analyzed via Mascot™ software using the NCBI nr Protein Database and a database from *M. gryphiswaldense*[1] (asterisks). Proteins are listed in the order of their exponentially modified protein abundance index (emPAI). The data have been deposited to ProteomeXchange with identifier PXD000348 (DOI 10.6019/PXD000348).

Protein	Accession number	Coverage (%)	No. of spectrum matches	No. of sequence peptides	Molecular weight (kDa)	Calculated pI	emPAI	Putative function
MamK	MGR_4093	57	9	9	39.6	5.4	1.51	Magnetosome chain assembly/positioning [2,3]
MamC	MGR_4078	32	4	3	12.4	5.1	1.01	Crystal size and shape control [4]
MamJ	MGR_4092	32	10	6	48.6	4.0	0.76	Magnetosome chain assembly [5]
MamA	MGR_4099	37	1	1	23.9	5.7	0.65	TPR-like protein associated with the magnetosome membrane [6,7]
MamF	MGR_4076	17	1	1	12.4	9.1	0.60	Magnetosome size and shape control [4]
Mms6	MGR_4073	19	1	1	12.7	9.5	0.58	Magnetosome crystallization [8,9]
MamD	MGR_4077	20	3	3	30.2	9.8	0.49	Crystal size and shape control [4]
MamM*	MGR_4095	15	3	3	34.7	5.8	0.42	Iron transport/MM assembly [10]
MmsF*	MGR_4072	8	2	1	13.9	9.3	0.23	Crystal size and shape control [11]
MamB*	MGR_4102	7	1	1	32.1	5.4	0.21	Iron transport/MM assembly [10]
MamY*	MGR_4150	18	2	2	40.9	4.8	0.16	Tubulation and magnetosome membrane formation [12]
MamO*	MGR_4097	6	3	3	65.3	6.5	0.15	Magnetosome crystallization [13,14]
MamE	MGR_4091	4	2	2	78.3	8.1	0.08	Magnetosome crystallization [13,14]

Supplement: Chapter IV

Genetic dissection of the *mamAB* and *mms6* operons reveals a gene set essential for magnetosome biogenesis in *Magnetospirillum gryphiswaldense.*

Publication state: published in Journal of Bacteriology. Ahead of print 9 May 2014

Materials and Methods

HRTEM of mutants Δ*mamI* and Δ*mamN*

As shown by HRTEM, the nuclei within Δ*mamI* were composed of several small grains that formed thin aggregates (Figure 4.2). In most particles, the incipient nuclei did not show lattice fringes in HRTEM images and lacked a visible crystalline structure. This might be caused by either (i) no close orientation of these particles to a crystallographic zone axis, or (ii) an amorphous structure, which seems more likely because of the weak diffraction contrast of the nuclei. Lattice fringes were observed in only two particles, and according to the Fourier transforms of the HRTEM images, the spacing between the fringes was ~3.71 Å (Figure 4.2B), which is very close to the d(012) spacing in hematite, whereas no other iron oxide has a d-spacing close to this value. For a second highly elongated particle only part of the crystal produced fringes with a distance of 2.72 Å, and showed again a value very close to that of hematite (d(014) = 2.70 Å) (Figure 4.2C). Thus, the few tiny electron dense particles seem to consist of hematite.

Complementation of mutant strains

Mutants carrying the respective insertion plasmids showed WT-like magnetosome biomineralization (Figure S4.3). Expression of WT alleles of *mms6* and *mmsF* from replicative plasmids pAL_*mms6* and pAL_*mmsF* was sufficient to restore phenotypes of Δ*mms6* and Δ*mmsF* at least in a significant fraction of cells (Figure S4.3). Complementation of ΔA10 with *mms6*, *mmsF* and *mgr4074* together (p*mmsF_mms6_4074*) led to crystals with 37 nm and 38

nm in size, but only 23 and 18 crystals per cell under control of the P_{mms6} and P_{mamDC} promoter, respectively. Only the entire *mms6* operon was able to fully restore both numbers and crystal size back to WT dimensions (Figure S4.3). Conjugative transfer of pAL_*mamIg* and pOR086 into mutants Δ*mamI* and Δ*mamQ* resulted in restoration of particle synthesis in 83% and 66% of cells, respectively. However, strain Δ*mamQ*_ pOR086 synthesized fewer particles than WT.

Table S1. Strains and plasmids used in this study.

Strains and plasmids	Description	References
MSR strains		
MSR-1 R3/S1	Rif^r Sm^r, spontaneous mutant	(1)
Δ*mamAB*	Δ*mamAB*	(2)
ΔA13	Δ*mms6* operon*,* Δ*mamGFDC,* Δ*mamXY*	(3)
ΔA12	Δ*mms6* operon*,* Δ*mamGFDC,*	(3)
ΔA10	Δ*mms6* operon	(3)
Δ*mamI*	deletion of *mgr4090*	this study
Δ*mamL*	deletion of *mgr4094*	this study
Δ*mamN*	deletion of *mgr4096*	this study
Δ*mamP*	deletion of *mgr4098*	this study
Δ*mamA*	deletion of *mgr4099*	this study
Δ*mamQ*	deletion of *mgr4100*	this study
Δ*mamR*	deletion of *mgr4101*	this study
Δ*mamS*	deletion of *mgr4103*	this study
Δ*mamT*	deletion of *mgr4104*	this study
Δ*mamU*	deletion of *mgr4105*	this study
Δ*mms48*	deletion of *mgr4070*	this study
Δ*mms36*	deletion of *mgr4071*	this study
Δ*mmsF*	deletion of *mgr4072*	this study
Δ*mms6*	deletion of *mgr4073*	this study
Δ*mmsF_mms6*	deletion of *mgr4072 and mgr4073*	this study
Δ*mmsF_mamF*	deletion of *mgr4072 and mgr4076*	this study
Δ*mamI::mamI*	Δ*mamI*+pAL*_mamIg,* Km^r	this study
Δ*mamL::mamL*	Δ*mamL*+pOR*mamL*	this study
Δ*mamN*::*mamN*	Δ*mamN*+pBam*_mamN,* Km^r	this study
Δ*mamP*::*mamP*	Δ*mamP*+pBam*_mamP,* Km^r	this study
Δ*mamA*::*mamA*	Δ*mamA*+pBam*_mamA,* Km^r	this study
Δ*mamQ*::*mamQ*	Δ*mamQ*+pOR86, Km^r	this study
Δ*mamR*::*mamR*	Δ*mamR*+pBam*_mamR,* Km^r	this study
Δ*mamS*::*mamS*	Δ*mamS*+pBam*_mamS,* Km^r	this study
Δ*mamT*::*mamT*	Δ*mamT*+pBam*_mamT,* Km^r	this study
Δ*mms48*::*mms48*	Δ*mms48*+pBam*_mms48,* Km^r	this study
Δ*mms36*::*mms36*	Δ*mms36*+pBam*_mms36,* Km^r	this study
Δ*mmsF*::*mmsF*	Δ*mmsF+pAL_mmsF,* Km^r	this study
Δ*mms6*::*mms6*	Δ*mms6+pAL_mms6,* Km^r	this study
Δ*mmsF_mms6*::*mms6*	Δ*mmsF_mms6+pAL_mms6,* Km^r	this study

Δ*mmsF_mamF::mmsF*	Δ*mmsF_mamF+pAL_mmsF,* Km^r	this study
ΔA10::P_{mms6}*_mmsF,6,4074*	ΔA10+P_{mms6}*_mmsF,6,4074*+ pAL_P_{mms6}*_mmsF,6,4074*, Km^r	this study
ΔA10::P_{mamDC}*_mmsF,6,4074*	ΔA10+P_{mamDC}*_mmsF,6,4074*+ pAL_P_{mamDC}*_mmsF,6,4074,* Km^r	this study
ΔA10::*mms6op*	ΔA10+pAL_P_{mamDC}*_mms6op,* Km^r	this study
Δ*mamI::mamCgfp*	Δ*mamI, gfp* fused to the chromosomal *mamC*	this study
Δ*mamN::mamCgfp*	Δ*mamN, gfp* fused to the chromosomal *mamC*	this study
Δ*mamP::mamCgfp*	Δ*mamP, gfp* fused to the chromosomal *mamC*	this study
Δ*mamA::mamCgfp*	Δ*mamA, gfp* fused to the chromosomal *mamC*	this study
Δ*mamQ::mamCgfp*	Δ*mamQ, gfp* fused to the chromosomal *mamC*	this study
Δ*mamR::mamCgfp*	Δ*mamR, gfp* fused to the chromosomal *mamC*	this study
Δ*mamS::mamCgfp*	Δ*mamS, gfp* fused to the chromosomal *mamC*	this study
Δ*mamT::mamCgfp*	Δ*mamT, gfp* fused to the chromosomal *mamC*	this study
WT::*mms36*	MSR-1, chromosomal integration of *mms36*	this study
WT::*mms48*	MSR-1, chromosomal integration of *mms48*	this study
***E. coli* strains**		
BW29427	*thrB1004 pro thi rpsL hsdS lacZDM15 RP4-1360D(araBAD)567DdapA*	Datsenko and Wanner, unpublished data
DH5a	*1341::[erm pir(WT)]trahsdR17 recA1-endA1gyrA96thi-1relA1*	Invitrogen
S17-1*λpir*	RPA-2, Tc::Mu-Km::Tn7 (λpir)	(4)
WM3064	*thrB1004 pro thi rpsL hsdS lacZDM15 RP4-1360D(araBAD) 567DdapA*::[*erm pir*]	(5)
Plasmids		
pJet1.2	Ap^r, *eco47IR*, *rep* (pMB-1)	Fermentas

pCM184	Km^r, Ap^r, Tet^r	(6)
pBam1	*ori*R6K, Km^r, Ap^r	(7)
pBam_*mamGFDC*	pBam1, inserted mamGFDC operon	Lohße, Kolinko *et al*., in preparation
pBBR1MCS2	Mobilizable broad-host-range vector, Km^r	(8)
pCL6	pBBR1MCS2, 10-glycine linker, *egfp,* Km^r	(9)
pAP150	pBBR1MCS2, 10-glycine linker, *egfp*, Km^r	(10)
pORFM_*galK*	suicide vector, Km^r	Raschdorf *et al*., submitted for publication
pFM236	integrative plasmid, *gfp,* Km^r	Raschdorf *et al*., submitted for publication
pAL_*mamI* 3'5'	pORFM_*galK*, upstream and downstream fragments of *mamI*, Km^r	this study
pOR_Δ*mamL*	pORFM_*galK*, upstream and downstream fragments of *mamL,* Km^r	this study
pAL_*mamN* 3'5'	pORFM_*galK*, upstream and downstream fragments of *mamN,* Km^r	this study
pAL_*mamP* 3'5'	pORFM_*galK*, upstream and downstream fragments of *mamP,* Km^r	this study
pAL_*mamA* 3'5'	pORFM_*galK*, fragments of *mamA,* Km^r	this study
pAL_*mamQ* 3'5'	pORFM_*galK*, insertion of upstream and downstream fragments of *mamQ,* Km^r	this study
pAL_*mamR* 3'5'	pORFM_*galK*, upstream and downstream fragments of *mamR,* Km^r	this study
pAL_*mamS* 3'5'	pORFM_*galK*, upstream and downstream fragment of *mamS,* Km^r	this study
pAL_*mamT* 3'5'	pORFM_*galK*, upstream and downstream fragments of *mamT,* Km^r	this study
pAL_*mamU* 3'5'	pORFM_*galK*, upstream and	this study

pAL_*mamU* 3'5'	pORFM_*galK*, upstream and downstream fragments of *mamU,* Km^r	this study
pAL_*mamAB* 3'5'	pORFM_*galK*, upstream fragments of *mamH* and downstream fragment of *mamU,* Km^r	this study
pAL_*mmsF*_*mms6* 3'5'	pORFM_*galK*, downstream fragments of *mmsF* and upstream fragment of *mms6,* Km^r	this study
pCM184_*mmsF* 3'5'	pCM184, downstream and upstream fragment of *mmsF,* Km^r	this study
pCM184_*mms6* 3'5'	pCM184, downstream and upstream fragments of *mms6,* Km^r	this study
pCM184_*mamF* 3'5'	pCM184, downstream and upstream fragments of *mamF,* Km^r	this study
pAl_*mamIg*	pCL6, *mamI*, Km^r	this study
pBam_*mamN*	pBam_*GFDC*, *mamN*, Km^r	this study
pBam_*mamP*	pBam_*GFDC*, *mamP*, Km^r	this study
pBam_*mamA*	pBam_*GFDC*, *mamA,* Km^r	this study
pBam_*mamR*	pBam_*GFDC*, *mamR*, Km^r	this study
pBam_*mamS*	pBam_*GFDC*, *mamS*, Km^r	this study
pBam_*mamT*	pBam_*GFDC*, *mamT,* Km^r	this study
pOR086	pBBR1MCS2, *mamQ*, Km^r	this study
pBam_*mgr4074*	pBam_*GFDC*, *mgr4074,* Km^r	this study
pAL*g*	pAP150, 10-glycine linker, *egfp,* Km^r	this study
pAL_*mmsF*	pAP150, *mmsF,* Km^r	this study
pAL_*mms6*	pAP150, *mms6,* Km^r	this study
pAL_P$_{mamDC}$_*mms6op*	pAP150, *mms6* operon, P_{mamDC}, Km^r	this study
pAL_ P$_{mms6}$_*mms6,F,4074*	pAP150, *mms6, mmsF, mgr4074,* P_{mms6}, Km^r	this study
pAL_ P$_{mamDC}$_*mms6,F,4074*	pAP150, *mms6, mmsF, mgr4074,*	this study

Table S2. DNA oligonucleotides used in this work.

Name	Sequence
AL251	GGATCCGGTTGGCGGAGCCTCCATT
AL252	CATAAACGTTCTCCAGTCTTGAT
AL253	ATCAAGACTGGAGAACGTTTATGCCTAACATCGATGGTTGATGAC
AL254	GGTACCACTTCATCCAGTGCGAAAAGG
AL255	GGATCCATTAAGCGCTGACATTCCATGC
AL256	CACCTAGTTATCCACCTTGGA
AL257	CCAAGGTGGATAACTAGGTGATCGCCGTTCTCGCAGGATG
AL258	GGTACCCATGGCCACAGTTTGGGCCG
AL259	GGATCCGGGCATGAATGTGGTGCAAG
AL260	CATTCCCGGCTAATCCCAAAAC
AL261	GTTTTGGGATTAGCCGGGAATGGAAGCTTGCCACGTGATAAATT
AL262	GGTACCGGGCATCCTCGTACATGGTG
AL263	GGATCCGGTGCTTATGTTGGCGGCAT
AL264	CATACTGTTCTCCAAAATCCCA
AL265	TGGGATTTTGGAGAACAGTATGGATGAACGTTCGGCCGTCTA
AL266	GCGGCCGCGCTATAGATGCGGTGCGGCAG
AL267	GGATCCTAAGGACAACCGTCCCGGCA
AL268	CATATCCGCCTCGTTGCTATC
AL269	ATAGCAACGAGGCGGATATGCATTCGCAGGAATCCAAGAATTG
AL270	GGTACCTATCGAACTGCACGTCCTCG
AL271	GGATCCGCAATCGCGTACAGCTACGA
AL272	GGTCATCAAGGCACTTCCCT
AL273	AGGGAAGTGCCTTGATGACCTGGAATACATGAACCGATGAAG
AL274	GGTACCCAGAATCAAGACTAGAGCGCC
AL275	GGATCCTGCAGGTGCTTGAGATGGTC
AL276	CATGATTCCCCTCTCCTGATC
AL277	ATCAGGAGAGGGGAATCATGTGGATGACCGTGCAGTGAG
AL278	GGTACCAACGATCATTGACCCGTCCC
AL279	GGATCCCGAGGACGTGCAGTTCGATA
AL280	CATGTTCACCCTCTCTGTCC
AL281	GGACAGAGAGGGTGAACATGGGCATTAAATGGCTGTTGTAAGC
AL282	GGTACCGCCATCCATCCGTTCACG
AL283	GGATCCTACCCGTGGGGAAGGCAAGA
AL284	CATCTTCCACACAGCCCCTG
AL285	CAGGGGCTGTGTGGAAGATGTCCATACTGGTTCCGAAATACG
AL286	GGTACCCGAGGCTACGGGCTTTTTCC

AL287	GGATCCCCGTCAATGGTTTCGTGAAGG
AL288	CATTCCCGTCACAATTCACCT
AL289	AGGTGAATTGTGACGGGAATGTCCATACTGGTTCCGAAATACG
AL364	GGATCCATTTCTGAACGGCAAAGGCA
AL365	TGATCCATGCTATTACGCCT
AL366	AGGCGTAATAGCATGGATCACGGTGCCTTTTCGTTGATGT
AL367	GGTACCACTACTTGATTGCTAAGGAGAA
AL368	GGATCCTAGCGCGCAGCAAAGTTGC
AL369	TGAGGGCATCGCGTTGTTTG
AL370	CAAACAACGCGATGCCCTCACAGGACGATCAGGCGTAATA
AL371	GGTACCGGTCCTGGTTCTGTATCTGG
AL372	GGATCCCTCGGTGCGTCTGATCAATA
AL373	TGAGGTTCGGCCTCGGGTGA
AL374	TCACCCGAGGCCGAACCTCAGGTTCCGACCGGAACCC
AL375	GGTACCCAAAATAGTCTCGGCCATTG
AL202	GAATTCCCATCGCCGACAATTCAGAC
AL203	CATATGCTGAGGTTCGGCCTCGGGTGATT
AL204	GGGCCCTTCATGTCCCCCCCCCCCCGTTCA
AL205	GAGCTCGCCTCAGCCTGCGCTTTGCG
AL208	GAATTCCGCGTTCCATTTCACCCAGG
AL209	CATATGTGCTTTGCCCTCGCTTAAGC
AL210	GGGCCCCGGCGAGCGATCTAACGGAC
AL211	GAGCTCAAACATCGGGAGCGCCATGG
AL240	GAATTCGCCTCCAGCCAGGGTTGGA
AL241	CATATGGCGACGCGCTGTCCTGAAC
AL242	GGGCCCCATTCCGTTGGCGATCTGAG
AL243	GAGCTCACTGACGAGACCGTCGCCGT
AL244	ATATGGAATTCGGAGGCGGAGGCGGTGGCGGAGGTGGCGGAGTGAGCAAGG GCGAGGAG
AL245	GGATCCTTACTTGTACAGCTCGTC
AL236	CATATGATGGTTTGCCCCCCTGGGGT
AL250	GAATTCGGACAGCGCGTCGCGCAG
AL398	CATATGATGAATAGCAAACTCGTCCT
AL464	GAATTCCTAATTTATCACGTGGCAAG
AL402	CATATGATGGACTTTCGGCCTGATCA
AL465	GAATTCTCACTGCACGGTCATCCAC
AL404	CATATGATGGGTACGCCAGGGGG
AL466	GAATTCTTACAACAGCCATTTAATGCC
AL406	CATATGATGACCTTTGTTCAGGGCG

AL467	GAATTCTCATCGGTTCATGTATTCCA
IB302	GGCGGTACCATGTCTAGCAAGCCG
IB303	GGCTCTAGATTAGACGGCCGAAC
AL414	CATATGGTGGTTGGATTTATCACCCT
AL469	TTAATTAATCATCCTGCGAGAACGGC
AL417	CATATGATGCTATTACGCCTGATCGT
AL487	GAATTCTCATGTACTGCGGAACAGTC
AL488	GAATTCTCACTCGTCTCGAGACGA
AL489	CATATGATGGACATCAACGAAAAGGC
AL499	GAATTCTCAAGTAGTGCGGGACTGAA
AL500	CATATGTTGGGCTTGTGGTTTTGGCG
AL220	GGATCCTCAGATCCGGTCGGCCACC
AL221	CATATGATGGTTGAAGCAATCCTTCGGA
AL134	GGATCCTCAGGACAGCGCGTCGCG
AL135	CATATGATGGTTTGCCCCCCTGGGGT
AL178	GGATCCTTCATGTACTGCGGAACAGTCG
AL179	CATATGTTGGGCTTGTGGTTTTGGCGG
AL234	GGATCCTCACCCGAGGCCGAACCTCA
AL394	CATATGATGCCAAGCGTGATTTTCGG
AL395	GAATTCACCATCGATGTTAGGGTCTG
OR252	GACAATGCATTGCTCAGCGAGATCAGTGACC
OR253	GTCAGCGCTTAATGACGATGTTTCCGATCACTCTTACCATACCAATG
OR254	CATTGGTATGGTAAGAGTGATCGGAAACATCGTCATTAAGCGCTGAC
OR255	ACTCACTAGTGTTCTGCACCGCCTCACC

Table S3. Oligonucleotides for amplification of sequences and genes important for gene deletions or complementation experiments.

Amplified region	Oligonucleotides
5' flanking sequence of *mamI*	AL251/AL252
3' flanking sequence of *mamI*	AL253/AL254
5' flanking sequence of *mamL*	OR252/OR253
3' flanking sequence of *mamL*	OR254/OR255
5' flanking sequence of *mamN*	AL255/AL256
3' flanking sequence of *mamN*	AL257/AL258
5' flanking sequence of *mamP*	AL259/AL260
3' flanking sequence of *mamP*	AL261/AL262
5' flanking sequence of *mamA*	AL263/AL264
3' flanking sequence of *mamA*	AL265/AL266
5' flanking sequence of *mamQ*	AL267/Al268
3' flanking sequence of *mamQ*	AL269/Al270
5' flanking sequence of *mamR*	AL271/AL272
3' flanking sequence of *mamR*	AL273/AL274
5' flanking sequence of *mamS*	AL275/AL276
3' flanking sequence of *mamS*	AL277/AL278
5' flanking sequence of *mamT*	AL279/AL280
3' flanking sequence of *mamT*	AL281/AL282
5' flanking sequence of *mamU*	AL283/AL284
3' flanking sequence of *mamU*	AL285/AL286
5' flanking sequence of *mms36*	AL364/AL365
3' flanking sequence of *mms36*	AL366/AL367
5' flanking sequence of *mms48*	AL368/AL369
3' flanking sequence of *mms48*	AL370/AL371
5' flanking sequence of *mmsF_mms6*	AL372/AL373
3' flanking sequence of *mmsF_mms6*	AL374/AL375
5' flanking sequence of *mmsF*	AL202/AL203

3’ flanking sequence of *mmsF*	AL204/AL205
5’ flanking sequence of *mamF*	AL208/AL209
3’ flanking sequence of *mamF*	AL210/Al211
5’ flanking sequence of *mms6*	AL240/AL241
3’ flanking sequence of *mms6*	AL374/AL375
mamP	AL398/AL464
mamS	AL402/AL465
mamT	AL404/AL466
mamR	AL406/AL467
mamA	IB302/IB303
mamN	AL414/AL469
mms36	AL488/Al489
mms48	AL417/AL487
mgr4074	AL499/AL500
mmsF	AL220/AL221
mms6	AL134/AL135
mms6 operon	AL178/AL179
mms6, mmsF, mgr4074	AL179/AL234

Supplementary figures

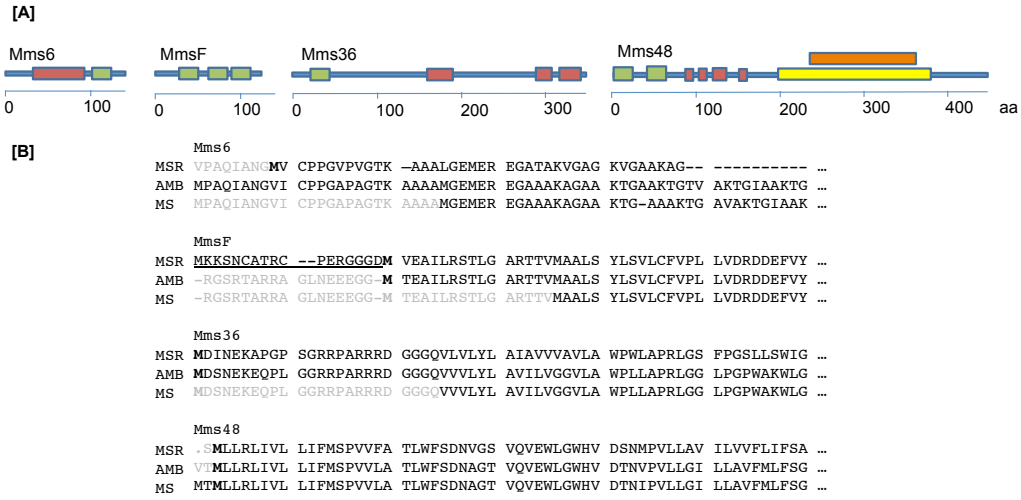

Figure S4.1. Domain structures and protein sequence analysis of proteins encoded by the *mms6* operon of MSR.

A: Predicted domain structure of Mms6, MmsF, Mms36 and Mms48 (11, 12). All proteins contain transmembrane domains (13), and except for MmsF the proteins have predicted regions of low complexity (red). Mms48 has a predicted C-terminal TPR-HemY domain (yellow), and a PEP-TPR domain (orange).

B: Protein sequence comparison of magnetosome proteins encoded by the *mms6* operon of MSR, AMB, and MS. Black letters correspond to previous protein annotations; Bold letters mark the supposed start sequence; Grey letters illustrate sequences in front of previously annotated proteins; Underlined amino acids demonstrate potential false annotated sequences within the previous annotations of MSR.

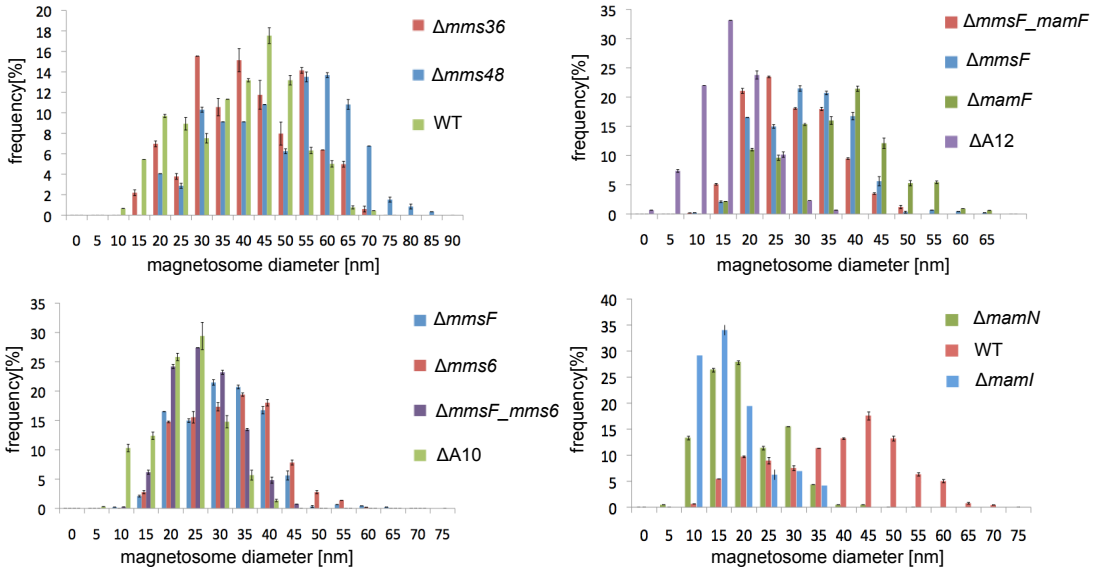

Figure S4.2. Magnetosome size distribution of various generated deletion strains of MSR. Magnetosome size distributions of electron dense particles within the mutants ΔA10, Δ*mms6*, Δ*mmsF*, Δ*mmsF_mms6,* Δ*mamF,* Δ*mmsF_mamF*, Δ*A12,* Δ*mms36*, Δ*mms48,* and WT.

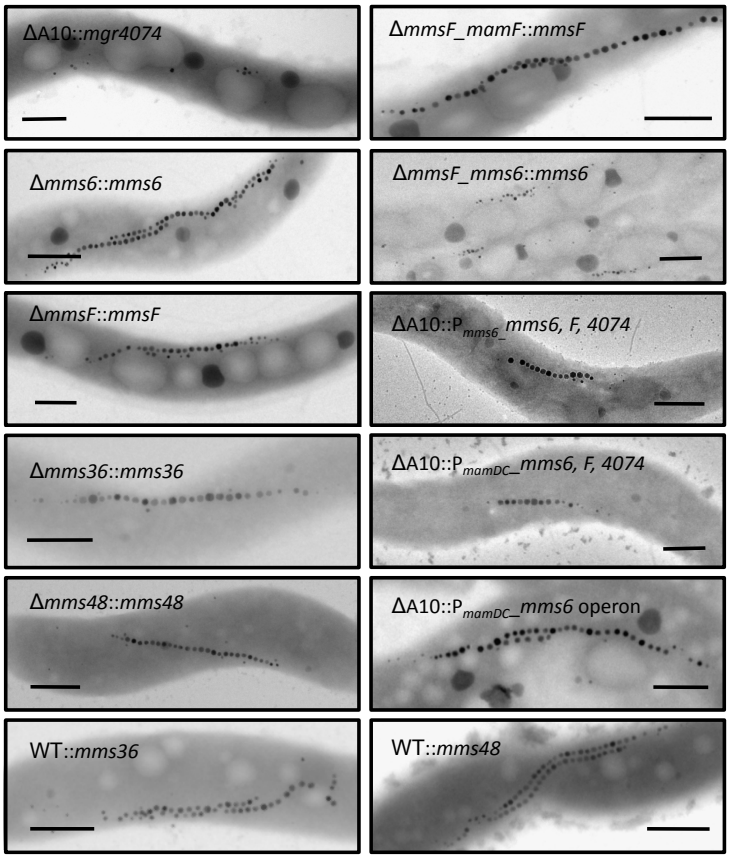

Figure S4.3. Overview about complementation experiments of various generated deletion strains of MSR and overexpression strains. TEM micrographs of ΔA10, Δ*mms6*, Δ*mmsF*, Δ*mms36*, Δ*mms48, ΔmmsF_mamF, and ΔmmsF_mms6* cells with indicated gene complementations and overexpression strains WT::*mms36* and WT::*mms48*. Scale bars: 500 nm.

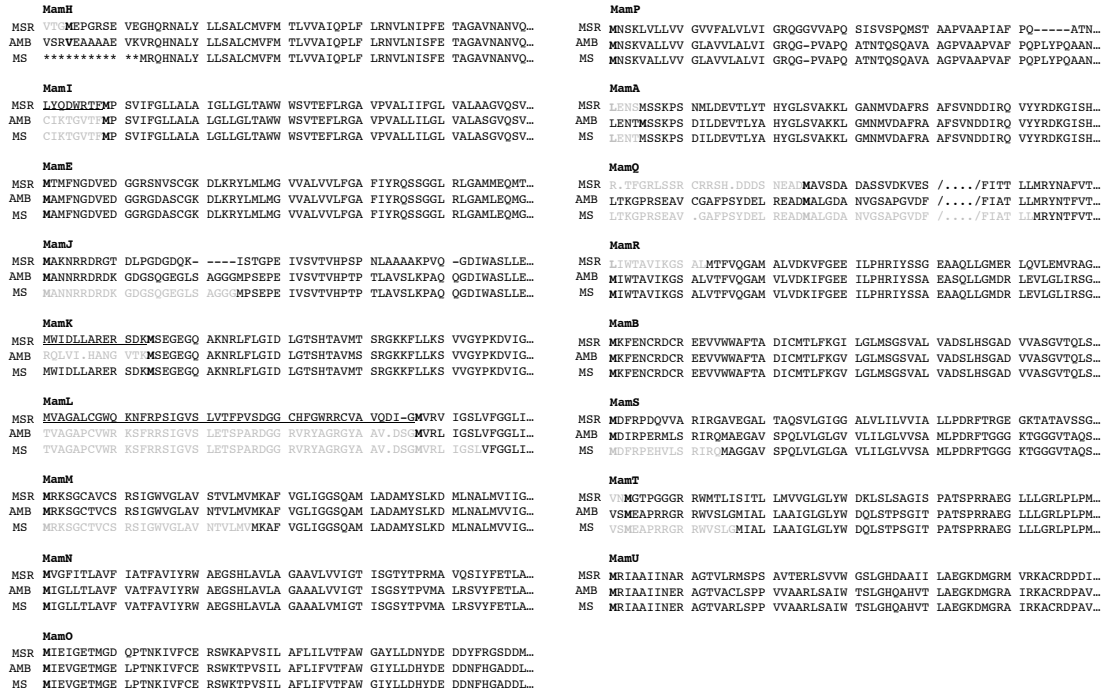

Figure S4.4. Protein sequence alignments of magnetosome proteins encoded by the *mamAB* operon of *M. gryphiswaldense* (MSR), *M. magneticum* (AMB), and *M. magnetotacticum* (MS). Asterisks mark amino acids that not part of the published geneome sequence; Black letters correspond to previous protein annotations; Bold letters mark the likely start codon; Grey letters indicate amino acids in front of previous protein annotations; Underlined amino acids demonstrate false sequences within the previous annotations of MSR.

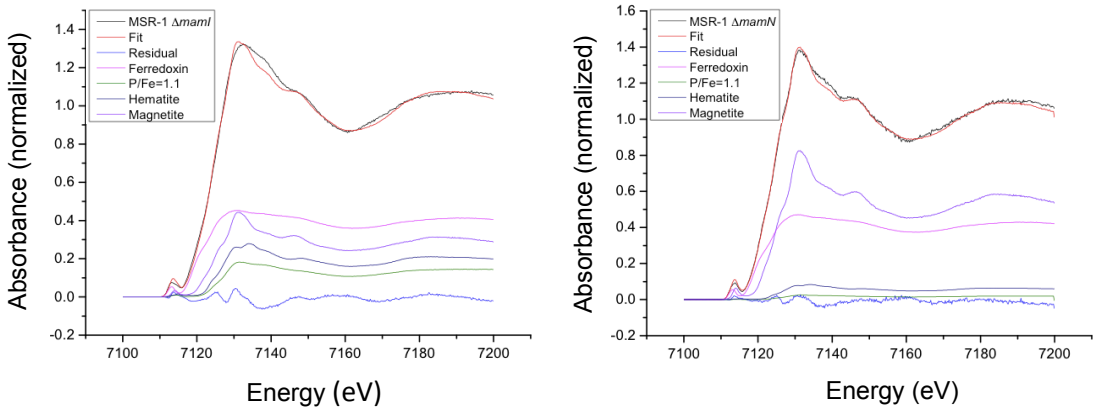

Figure S4.5: XANES (X-ray Absorption Near Edge Structure) analysis of mutants Δ*maml* and Δ*mamN*. XANES spectra obtained from Δ*maml* (A) and Δ*mamN* (B) are clearly distinct from those of pure magnetite as in the WT or phosphate-rich ferric hydroxides as observed in the early mineralization stages in induction experiments with MSR or AMB (14, 15). For both mutants the pre-edge peak and the low energy part of the edge are shifted towards lower energies with respect to a magnetite reference spectrum, which indicates the presence of higher ratios of ferrous iron in the cells than in the WT (33% Fe(II), 67% Fe(III)). Linear combination fitting with reference compounds (magnetite, hematite, ferrihydrite, phosphate-enriched ferric hydroxides, ferrous hexaphosphate, spinach ferredoxin) suggest that the ferrous compounds are predominantly Fe-S clusters (proteins) and account for around 40% of the total iron content in the cells. Magnetite is clearly present in the Δ*mamN* mutant (around 50% of total iron), whereas the low fit quality for Δ*maml* (large residue) does not allow us to reliable determine the structure of the Fe present in the bacteria apart from Fe-S. However, the overall line shape appears most consistent with an amorphous or only poorly ordered Fe compound as suggested by HRTEM.

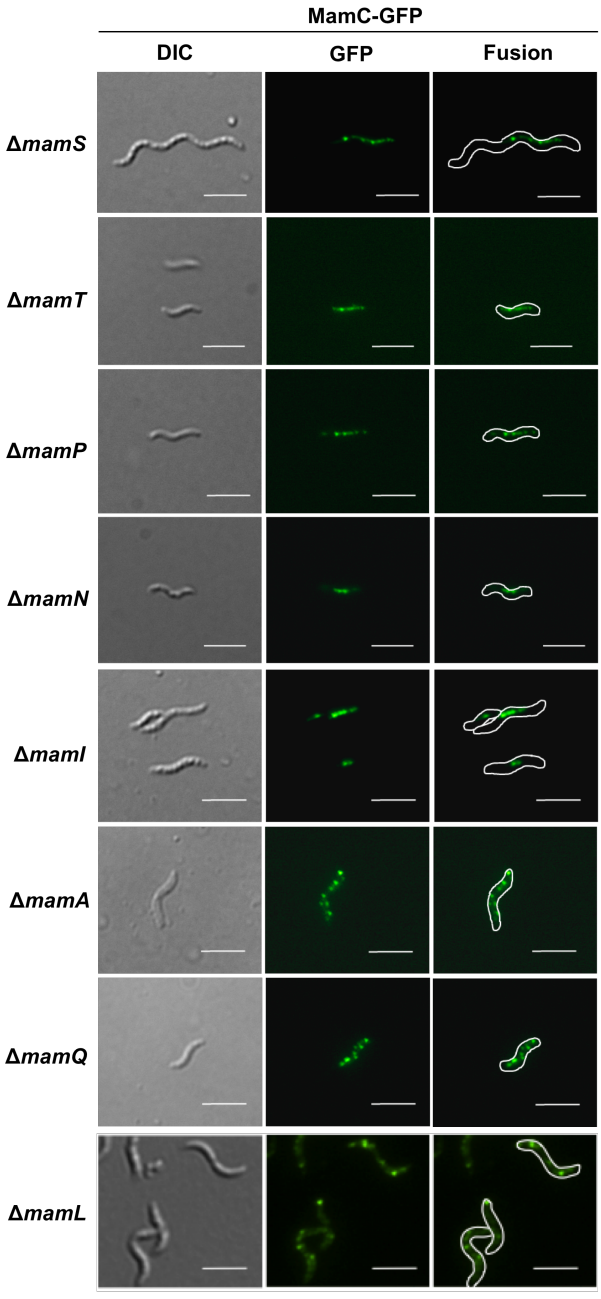

Figure S4.6. Fluorescence micrographs of MSR WT and various deletion strains expressing different MamC-GFP fusions. Scale bar: 1

References

1. **Schultheiss D, Schüler D.** 2003. Development of a genetic system for Magnetospirillum gryphiswaldense. Arch Microbiol **179:**89-94.
2. **Ullrich S, Schüler D.** 2010. Cre-*lox*-based method for generation of large deletions within the genomic magnetosome island of *Magnetospirillum gryphiswaldense*. Appl Environ Microbiol **76:**2439-2444.
3. **Lohße A, Ullrich S, Katzmann E, Borg S, Wanner G, Richter M, Voigt B, Schweder T, Schüler D.** 2011. Functional analysis of the magnetosome island in *Magnetospirillum gryphiswaldense*: the *mamAB* operon is sufficient for magnetite biomineralization. PLoS One **6:**e25561.
4. **Simon R, Priefer U, Puhler A.** 1983. A Broad Host Range Mobilization System for *In Vivo* Genetic Engineering: Transposon Mutagenesis in Gram Negative Bacteria. Nat Biotech **1:**784-791.
5. **Saltikov CW, Newman DK.** 2003. Genetic identification of a respiratory arsenate reductase. Proceedings of the National Academy of Sciences **100:**10983-10988.
6. **Marx CJ, Lidstrom ME.** 2002. Broad-host-range *cre-lox* system for antibiotic marker recycling in gram-negative bacteria. Biotechniques **33:**1062-1067.
7. **Martinez-Garcia E, Calles B, Arevalo-Rodriguez M, de Lorenzo V.** 2011. pBAM1: an all-synthetic genetic tool for analysis and construction of complex bacterial phenotypes. BMC Microbiology **11:**38.
8. **Kovach ME, Elzer PH, Hill DS, Robertson GT, Farris MA, Roop RM, 2nd, Peterson KM.** 1995. Four new derivatives of the broad-host-range cloning vector pBBR1MCS, carrying different antibiotic-resistance cassettes. Gene **166:**175-176.
9. **Lang C, Schüler D.** 2008. Expression of green fluorescent protein fused to magnetosome proteins in microaerophilic magnetotactic bacteria. Appl Environ Microbiol **74:**4944-4953.
10. **Pollithy A, Romer T, Lang C, Müller FD, Helma J, Leonhardt H, Rothbauer U, Schüler D.** 2011. Magnetosome expression of functional camelid antibody fragments (nanobodies) in *Magnetospirillum gryphiswaldense*. Appl Environ Microbiol.
11. **Schultz Jr, Milpetz F, Bork P, Ponting CP.** 1998. SMART, a simple modular architecture research tool: Identification of signaling domains. Proceedings of the National Academy of Sciences **95:**5857-5864.
12. **Letunic I, Doerks T, Bork P.** 2012. SMART 7: recent updates to the protein domain annotation resource. Nucleic Acids Research **40:**D302-D305.
13. **Bolivar F, Rodriguez R, Greene P, Betlach M, Heyneker H, Boyer H, Crosa J, Falkow S.** 1977. Construction and characterization of new cloning vehicles. II. A multipurpose cloning system. Gene **2:**95 - 113.
14. **Fdez-Gubieda ML, Muela A, Alonso J, Garcia-Prieto A, Olivi L, Fernandez-Pacheco R, Barandiaran JM.** 2013. Magnetite biomineralization in *Magnetospirillum*

gryphiswaldense: time-resolved magnetic and structural studies. ACS Nano **7:**3297-3305.

15. **Baumgartner J, Morin G, Menguy N, Perez Gonzalez T, Widdrat M, Cosmidis J, Faivre D.** 2013. Magnetotactic bacteria form magnetite from a phosphate-rich ferric hydroxide via nanometric ferric (oxyhydr)oxide intermediates. Proc Natl Acad Sci U S A **110:**14883-14888.

Supplement: Chapter V

Genome engineering of *Magnetospirillum gryphiswaldense* improves magnetosome yield by overexpression of magnetosome operons.

Publication state: *In preparation*.

Supplementary table

Table S5.1: Characteristic of generated overexpression strain.

Strain	Genotype	Crystal Size	Increased size [%] compared to WT	Crystal number per cell	Increased number [%] compared to WT	Iron content [%] compared to ΔRecA	Cell length [µm]
WT	1x MAI	35.6±13.0	-	34.3±8.4	-	-	-
ΔRecA	1x MAI	36.2±11.0	1.7	33.9±10.3	-1.2	100	4.44± 1.26
ΔRecA+ *mamGFDC*	2x *mamGFDC* operon	44.9±13.5	26.1	36.3±12.4	5.8	7.4±1.1	-
ΔRecA+ *mms6* 1x	2x *mms6* operon	45.7±14.2	28.4	46.5±14.3	35.6	14.9±2.9	4.53±1.59
ΔRecA+ *GFDC/mms6*	2x *mms6* 2x *mamGFDC* operon	45.1±12.2	26.7	45.1±14.3	31.5	14.1±1.9	-
ΔRecA+ *mms6* 2x	3x *mms6* operon	47.9±12.8	34.6	54.3±29.9	58.3	34.8±2.5	4.56 ±1.46
ΔRecA+ *mms6* 3x	4x *mms6* operon	44.4±13.2	24.7	57.8±26.9	68.5	38.8±2.5	5.10 ±1.95
ΔRecA+ *mms6* 4x	5x *mms6* operon	41.9±12.0	17.7	46.0±14.8	34.1	-	5.30±1.70
ΔRecA+ *mamAB* 1x	2x *mamAB* operon	34.0±17.6	-4.5	73.4±43.1	114.0	0.4±0.5	4.81± 1.82
ΔRecA+ *ABG6X*	2x *mamGFDC* 2x *mms6* 2x *mamAB* 2x *mamXY* operon	38.7±11.9	8.7	74.5±34.9	117.2	140.7±2.4	

Supplementary figures

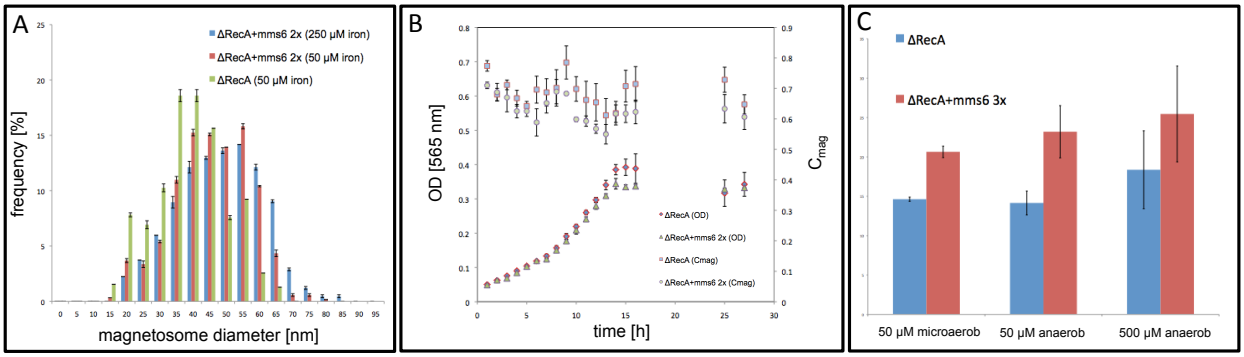

Figure S1: Characterization of *mms6* operon overexpression strains. A: Cultivation of overproducing strain ΔRecA+*mms6* 2x at higher iron concentrations (250 µM iron) did not further increase magnetosome numbers, although size distribution were slightly shifted towards to larger crystals with maximum sizes up to 85 nm compared to ΔRecA. B: Growth curve and C_{mag} measurements of ΔRecA and ΔRecA+*mms6* 2x. C: Cultivation under anaerobic conditions with 50 µM or 500 µM iron did not significantly increase iron uptake of ΔRecA+*mms6* 3x compared to cultivation under microaerobic conditions with 50 µM iron.

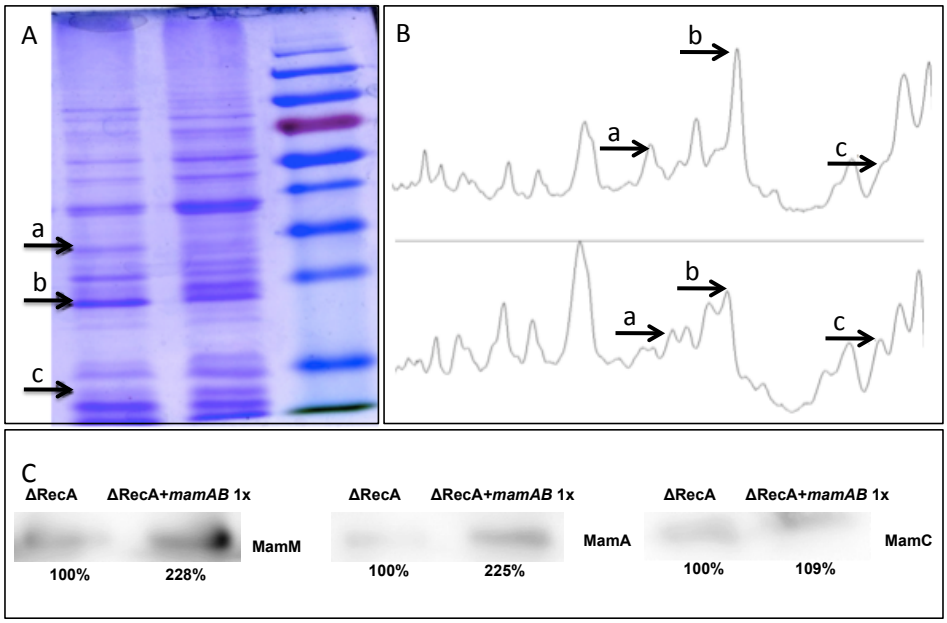

Figure S2: Proteomic characterization of the *mamAB* overexpression mutants.
A: SDS-PAGE of the magnetosome membrane of ΔRecA and RecA+*mamAB* 1x. Comassie-stained SDS-PAGE profiles of MM from strains ΔRecA+*mamAB* 1x revealed similar patterns compared to ΔRecA.
B: Image J analysis was performed to quantitatively compare band intensities correlating with different proteins. In strain ΔRecA+*mamAB* 1x several bands including magnetosome proteins MamM (a), and MamA (b), showed higher intensities. MamC showed a higher intensity within the membrane of ΔRecA (c).
C: Quantitative protein analysis was performed for the magnetosome membrane of ΔRecA and ΔRecA+*mamAB* 1x. Western Blot analysis of selected proteins confirmed that MamM and MamA were more abundant within ΔRecA+*mamAB* 1x by about 128% and 125%, respectively, whereas the abundance of MamC was not significantly increased (9%), although the Coomassie-stained MamC band appeared more intense in ΔRecA.